Development of an *in vitro* model for Non-Replicating Persistent *Mycobacterium tuberculosis*, and an investigation of the novel phenotype

Savannah Ellen Ramshaw Gibson

B.Sc Hons Microbiology and Immunology

A thesis submitted for examination for the award of the degree of

Doctor of Philosophy

Aston University

March 2021

Development of an *in vitro* model for Non-Replicating Persistent *Mycobacterium tuberculosis,* and an investigation of the novel phenotype

Savannah Ellen Ramshaw Gibson

Doctor of Philosophy

2021

Tuberculosis is the primary cause of global death by a single infectious agent. This widespread infection is assisted by the existence of a large reservoir of disease in the form of Latent Tuberculosis which is thought to infect over ¼ of the world's population. Latent Tuberculosis is caused when an existing *Mycobacterium tuberculosis* infection is encapsulated within a granuloma and the bacilli adapt their physiology to cope with this hostile environment known as the Non-Replicating Persistent (NRP) state. The background of Tuberculosis, Latent Tuberculosis and scientific modelling of these states is discussed in Chapter 1. The first results chapter of this thesis, Chapter 2, sets out a novel multi-stress *in vitro* model of Latent Tuberculosis to create a more physiologically relevant *M. tuberculosis* NRP phenotype. Chapter 3 uses the *in vitro* model proposed in Chapter 2, along with a control *in vitro* model to conduct widespread antimicrobial testing against a variety of antimicrobials; from frontline, second line and antibiotics in clinical trials to novel compound libraries. This uncovered an exceptionally antibiotic tolerant phenotype, not previously seen in less physiologically relevant models of Latent Tuberculosis. Chapter 4 is an investigation into the mechanism of action of the sole antibiotic hit from Chapter 3, Dapsone. An assessment of the previously proposed drug target, FolP1, revealed an alternative target, the formally defined "inactive ortholog", FolP2. Through a range of biochemical techniques, FolP2 activity in the cholesterol catabolism pathway was established, revealing a new, previously unreported and druggable aspect of latent *M. tuberculosis* physiology. Chapter 5 utilises the *in vitro* model proposed in Chapter 2 to establish the presence of the NRP state in the opportunistic pathogen *Mycobacterium abscessus*. It was identified that *M. abscessus* shared the same drug-indifferent phenotype

that has been observed for *M. tuberculosis,* proposing a further hypothesis for the poor treatment outcomes of this infection. Overall, this thesis has provided a physiologically relevant model of a global infection that revealed a highly drug resistant phenotype with the subsequent discovery of an established antimicrobial agent that could be repurposed for latent tuberculosis chemotherapy. This novel contribution to the knowledge will invariably catalyse future drug discovery into this neglected area of tuberculosis research and has the potential to change the way we treat latent *M. tuberculosis* infection.

Publications associated with this thesis

Gibson, S. E. R., Harrison, J. and Cox, J. A. G. (2018) 'Modelling a silent epidemic: A review of the *in vitro* models of latent tuberculosis', Pathogens. doi: 10.3390/pathogens7040088.

Gibson, S. E. R., Harrison, J. and Cox, J. A. G. (2021) 'Drug susceptibility screening using *in vitro* models of hypoxic non-replicating persistent mycobacteria.' Mycobacteria Protocols, Springer [Accepted, in press]

Table of Contents

List of Figures

List of Tables

Acknowledgements

I would like to thank Dr. Jonathan Cox for giving me the opportunity to do this PhD. Thank you for the support and guidance given throughout the last four years. Special thanks has to be given for the superhuman effort to make this thesis the best it could be. I would also like to thank Aston University for funding me through my PhD. I would like to thank Dr. James Harrison and Rose Lopeman for their assistance in providing aerobic results for Chapter 5.

Special thanks has to be given to Dr. James Harrison for his sage advice and instructions on how to lab. I wish I had followed you around with a pen and paper. Thank you for making me laugh whilst teaching me how to clone and picking me up after the umpteenth failed protein preparation. Also thank you for all of the buffers. To Rose, Federica, Bella, Victoria, Kat and everyone in Lab 327, thank you for three years of help, laughter and karaoke.

To Bebiana, you have been my friend, mentor, therapist and teacher for all things mass spectrometry. Your friendship has been one of the best parts of my PhD. Thank you for always being there for me, no matter the circumstance. Thank you for all the laughter, adventures, dancing and food, it was amazing.

To Dr. Gary Gibson, my wonderful Dad, thank you. Every time I desperately needed support, you were there. Thank you for telling me that everything was going to be ok. Turns out you were right again!

To the Loose Cannons, thank you for providing me a sanctuary of friendship, where I could be a girl going adventuring with friends despite whatever was happening in the real world.

Finally, to James without whom I would have quit a long time ago. Thank you for all the support you have given me and all the sacrifices you made to keep me going. Thank you for sticking it out and being my anchor. Thank you for always seeing me and everything that was happening and staying by my side. I could not have done this without you.

List of Abbreviations

% - Percent

µL – microlitre

Acr – alpha crystallin

ADC – Bovine Serum Albumin, Dextrose, Catalase

ANOVA – Analysis of Variance Assay

BCE – Before Common Era

BCG – Bacille Calmette Guerin

BSA – Bovine Serum Albumin

CFU/mL – Colony Forming Units per millilitre

CoA – Coenzyme A

DHFR – Dihydrofolate Reducatase

DHPS - 7,8-dihydropteroate synthase

DNA – Deoxyribonucleic acid

DOTS – Direct Observed Treatments

FolP1 – Folate protein 1

FolP2 – Folate protein 2

HIV – Human Immunodeficiency Virus

HSR - Head Space Ratio

HTS – High Throughput Screen

HyRRA – Hypoxic Resazurin Reduction Assay

LC – Liquid Chromatography

LORA – Low Oxygen Recovery Assay

LPS – Lipopolysaccharide

LTBI – Latent Tuberculosis Infection

MBC - Minimum Bactericidal Concentration

MDR-TB – Multi-Drug Resistant Tuberculosis

MIC – Minimum Inhibitory Concentration

mL – millilitre

MS – Mass Spectrometry

MS, Cholesterol model – Multi- Stress, Cholesterol model

NO – Nitric Oxide

NRP – Non-Replicating Persistence

OADC – Oleic Acid, Bovine Serum Albumin, Dextrose, Catalase

OD – Optical Density

PBS – Phosphate Buffered Saline

PCR – Polymerase Chain Reaction

pH – power of hydrogen

REMA – Resazurin Microtitre Assay

RLU – Relative Light Units

RNA – Ribonucleic Acid

RPF – Resuscitation Promoting Factors

SDG – Sustainable Development Goal

TCA cycle – Tricarboxylic Acid cycle

TST – Tuberculin Skin Test

TB - Tuberculosis

WHO – World Health Organisation

XDR-TB – Extremely Drug Resistant Tuberculosis

Chapter 1:

General Introduction

Chapter 1 Introduction

1.1 Tuberculosis

1.1.1 The History of Tuberculosis

Tuberculosis, caused by the bacterium *Mycobacterium tuberculosis,* has been a deadly threat to humanity since the origin of our species. This pathogen became so well adapted to humanity that it shows remarkably low genetic variance (Gutierrez et al., 2005). This low genetic variance can allow researchers to amplify ancient DNA to prove *M. tuberculosis'* presence and track its passage through time. *M. tuberculosis* is estimated to be approximately 3 million years old, making it older than other ancient diseases such as *Yersinia pestis* (causative agent of the Plague) (Achtman et al., 1999; Gutierrez et al., 2005).

The first definitive evidence of *M. tuberculosis* infection in humans comes from the Old Kingdom of Ancient Egypt. In the early 19th Century, during excavations of the necropolis British explorers found mummies presenting with a distinctive curvature of the spine, commonly known as Pott's disease and is a symptom of extrapulmonary Tuberculosis (Zink et al., 2001). Further study showed that all of the subjects who were presenting with skeletal TB had amplifiable *M. tuberculosis* DNA within their preserved skeletal tissues; interestingly, many of the mummies studied who did not show signs of skeletal TB also contained amplifiable *M. tuberculosis* DNA (Zink et al., 2001). One particularly fascinating case is Granville's mummy. Investigative studies of this mummy have dated it to c. 600 BCE and is the remains of a woman called Irtyersenu who was 50 years old (Granville, 1825; Hedges et al., 1997). Granville originally determined that the cause of death was ovarian "dropsy" or cancer (Granville, 1825). A later study showed that the cysts on her ovaries proved to be completely benign and would not have been the cause of death (Nunn & Tapp, 2000; Strouhal, 1976). The cause of death was determined by taking pulmonary exudate from the lungs and a sample of the femur and examining the above tissue for *M. tuberculosis.*

Moving forward to Ancient Greece, Hippocrates described TB, which he called Phthisis frequently in his medical writing. In his famous medical text, 'The Aphorisms of Hippocrates', there are some particular selected aphorisms *"Phthisis manifests itself, for the most part, between the eighteenth and the thirty fifth year*" (Hippocrates, 1708).

The Renaissance revolutionised the archaic ideologies of the Middle ages, bringing about a fresh approach to medicine. One of the most notable doctors of the time was René Laënnec, the man who invented the stethoscope (Bishop, 1981). Laënnec was the scientist who made the first argument that Phthisis should be renamed Tuberculosis. He rightly argued that the 12 different forms of Phthisis all stemmed from the same causative agent and were all linked, despite being found in different organs in the body (Bishop, 1981). His book was the first to describe Tuberculosis fully and identify Pulmonary and extra Pulmonary disease.

Laënnec's work was built upon by Robert Koch who made his major breakthrough in understanding Tuberculosis disease when he isolated the causative agent, *M. tuberculosis,* for the first time (Koch, 1882). His work was the first to argue that Tuberculosis was a disease caused by bacteria and could be mainly isolated from tubercules in the lungs and brain of infected individuals (Koch, 1882). He also identified and isolated tuberculin, which would go on to be used in the diagnostic test, the tuberculin skin test (TST). This diagnostic test, also called the Mantoux test is still used today. This was not Koch's only contribution to the field as he was also the first person to link *M. tuberculosis* (TB) and *Mycobacterium leprae* (Leprosy).

1.1.2 *Mycobacterium tuberculosis*

Mycobacteria constitute a group of non-motile, non-sporulating, Gram-indeterminate rod-shaped bacilli from the Actinomycete family (Parish & Stoker, 1999). This group ranges from harmless soil microorganisms such as *Mycobacterium smegmatis* to true pathogens such as *M. tuberculosis* and *Mycobacterium leprae.*

M. tuberculosis, the causative agent of Tuberculosis in humans, has been pandemic for thousands of years and remains the primary cause of mortality caused by a single infectious agent. Generally, *M. tuberculosis* bacilli are approximately 1-4 μm in length and 0.3-0.6 μm in width (Schoonmaker et al., 2014). *M. tuberculosis* replicates slowly; approximately once every 12-24 hrs (Delogu et al., 2013). It has a comparatively large genome with 4,411,529 base pairs coding for an approximated 4,000 genes (Cole et al., 1998).

M. tuberculosis is a particularly complex microorganism with a unique cell wall, an arsenal of virulence factors and methods of survival when faced with extreme environmental pressures (Barry, 2001; Forrellad et al., 2013; D. E. Minnikin et al., 2002; Wayne & Sohaskey, 2001).

As *M. tuberculosis* is the causative agent of Tuberculosis, throughout this thesis the bacterium will be referred to as *M. tuberculosis* and the disease will be referred to as Tuberculosis (TB)

1.1.3 Mycobacterial Cell Wall

Arguably, one of the most important components of a prokaryotic cell is the cell wall. In all bacteria, the cell wall serves a multitude of functions. It serves as protection against inhospitable environments - for example, extremes of pH or immune system activity - and provides essential resistance to osmotic pressure. In addition to these protective qualities, the bacterial cell wall can also act as multiple virulence factors with components such as lipopolysaccharide (LPS) and pili which is a demonstrable antigen (Takeuchi et al., 1999)

In the 1880s, Hans Christian Gram discovered that bacterial cells could be divided into two distinct groups by Gram staining with crystal violet, iodine, ethanol/acetone and carbol fushcin. This process became known as the Gram stain. Whilst the broad class of prokaryotes can be classified by the Gram stain as either Gram positive or Gram negative, mycobacteria have a unique cell wall that does not fit into either category and is commonly referred to as Gram indeterminate (Figure 1.1). The mycobacterial cell wall encapsulates the inner cell membrane in a thick layer of peptidoglycan – similarly to a Gram-positive cell wall (Jankute et al., 2015). This peptidoglycan retains the basic core shared by all bacteria with a glycan backbone with peptide side chains. However, certain modifications in binding are made in *Mycobacteria* that allow the peptidoglycan to become stronger and as well as decreasing the cells susceptibility to lysozyme (Mahapatra et al., 2005; Raymond et al., 2005). Nevertheless, the similarities to the typical Gram positive/negative walls stop here as throughout the peptidoglycan layer is a covalently bound macromolecule called arabinogalactan (Figure 1.1) (Mikušová et al., 1996). Arabinogalactan is composed of galactose and arabinose sugar molecules with branched arabinose molecules connected to a galactose chain (McNeil et al., 1987). The peptidoglycan-bound arabinogalactan has mycolic acids bound its arabinose branches (Jankute et al., 2015) (Figure 1.1).

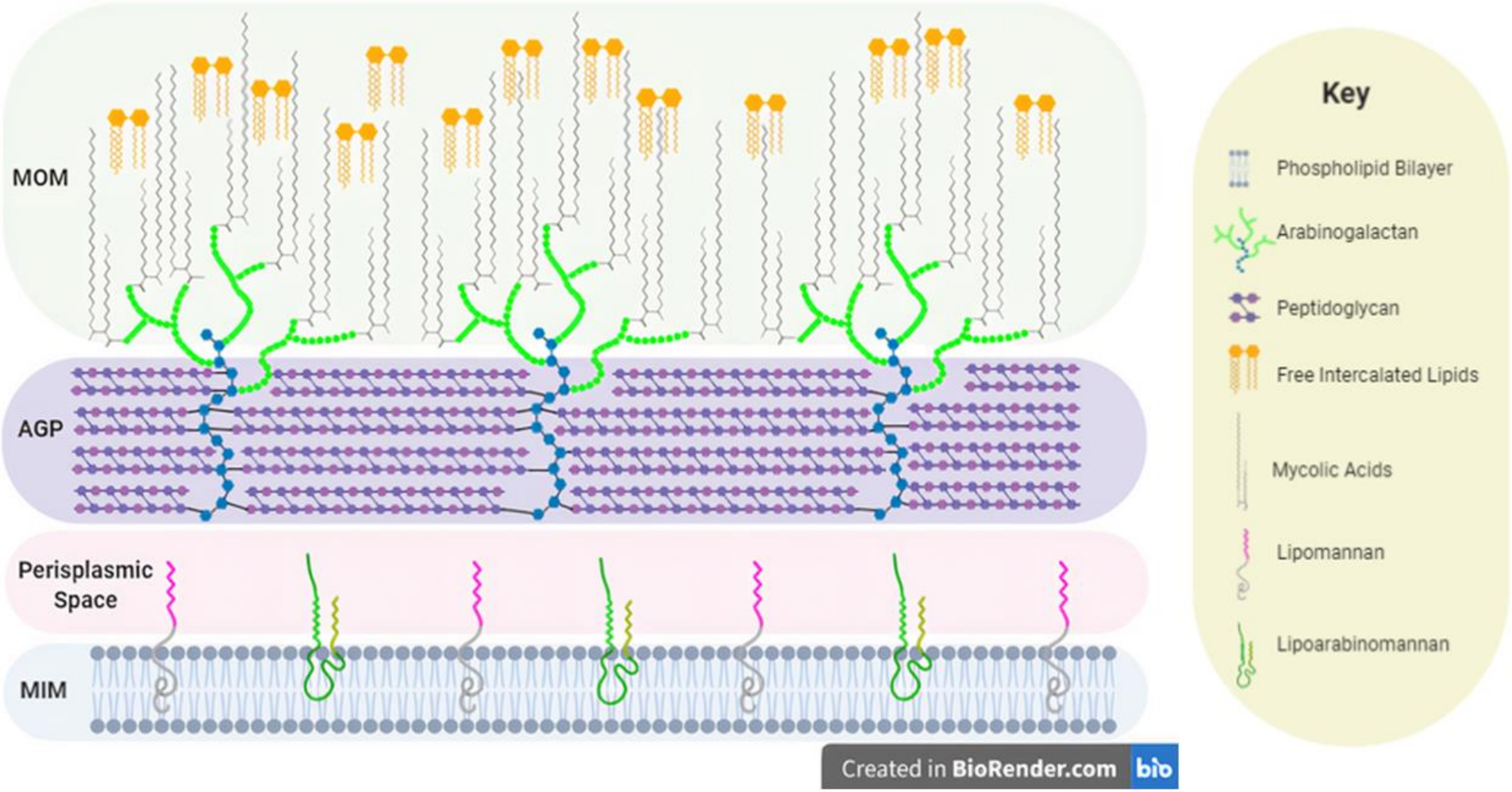

Figure 1.1 **Summary Diagram of the Mycobacterial Cell Wall** as currently elucidated. This diagram is based on the Minnikin model of the cell wall, albeit reduced to provide a summary(Minnikin, 1982). The cell wall starts with the Mycobacterial Inner Membrane (MIM), which is followed by the Periplasmic Space. Preceeding that is the Arabinogalactan Peptidoglycan (AGP). The outer-most layer of the cell wall isthe Mycobacterial Outer Membrane (MOM)

These mycolic acids make up the majority of the outer membrane (Figure 1.1). Mycolic acids or 2-alkyl, 3-hydroxy long chain fatty acids, appear in three major formations: α, methoxy- and keto (Marrakchi et al., 2014). These mycolic acids often have other free lipids associated with them to form a dense, lipid rich outer membrane (D. E. Minnikin et al., 2002). This uniquely structured cell wall with an outer membrane composed of mycolic acids and other free lipids was first proposed by Minnikin in 1982 and is one of the foremost methods of virulence of *M. tuberculosis* (D. Minnikin, 1982; Niederweis et al., 2010). It is partly, this lipid rich or "waxy" and mostly impermeable outer layer that allows *Mycobacteria* to survive in hostile environments and makes them difficult to treat (D. E. Minnikin et al., 2002).

1.1.4 Epidemiology of Tuberculosis

Tuberculosis (TB) is a global disease with that is believed to have infected over ¼ of the global population and remains one of the top 10 leading causes of mortality worldwide (Houben & Dodd, 2016). Since 2007, is primary cause of death due to a single infectious agent (WHO, 2020). In 2018, the World Health Organisation (WHO) reported approximately 10 million people were new incidences of TB (WHO, 2020) (Figure 1.2).

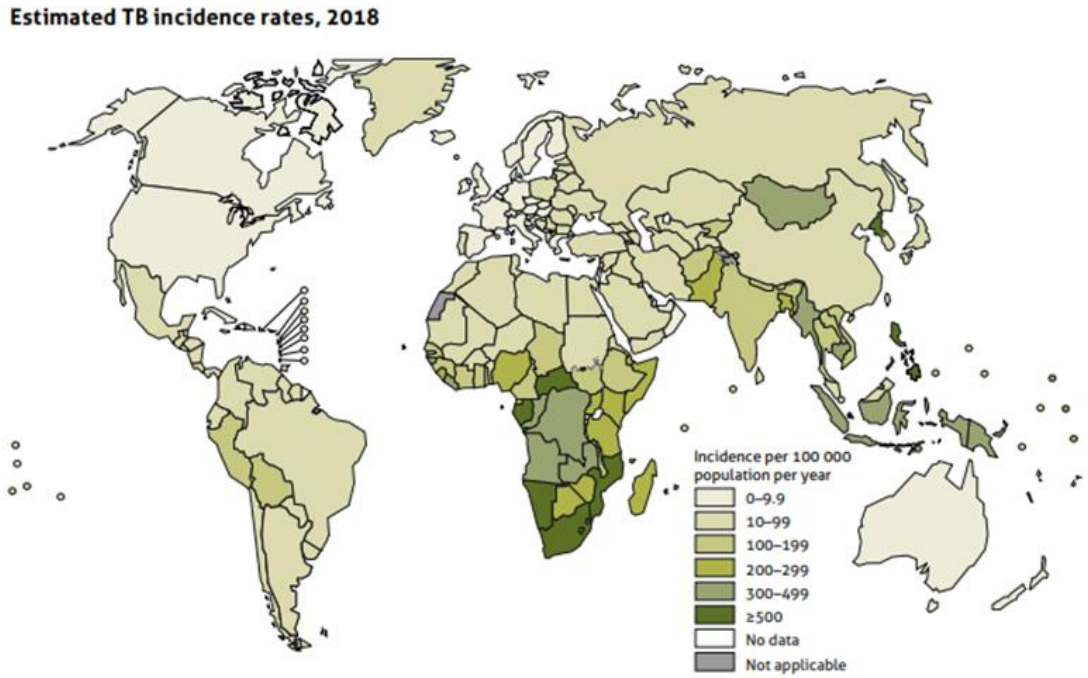

Figure 1.2 **Incidence of Tuberculosis infection** in 2018 as reported in the Global Tuberculosis Report 2019. Incidence as reported as per 100,000 to normalise the data for differing population size.

In 2015, a worldwide initiative called the END-TB programme was launched and set an ambitious target of of decreasing incidence rates by 20% and a 35% reduction in deaths by 2020 (Houben & Dodd, 2016; World Health Organization, 2015). Despite multinational efforts, TB incidence rate has only decreased by 6.3% since 2015 falling short of the 2020 milestone of 20%. The highest incidence of TB cases are found in South East Asia (44% of worldwide cases) and Africa (24%). Europe was found to have the lowest TB incidence rate of 2.4%. The country with the highest disease burden was found to be India with 27% of worldwide cases (Figure 1.2). This incidence rate is decreasing in some high burden countries; for example,

Russia saw incidence fall by 5.4% per year meaning that it is on track to reach the END-TB milestone of a 20% reduction (WHO, 2020). Nevertheless, other countries, despite international aid have seen an increase in incidence rate, resulting in a low decrease in worldwide incidence.

In 2018, there were an estimated 1.2 million deaths in HIV negative patients and an additional 251,000 deaths in HIV positive patients. The effects of poverty on the spread and treatment of TB are most evident when looking at the distribution of deaths caused by the disease. 83% of TB deaths (that are HIV-negative) were in South East Asia and Africa. India alone, in 2018, accounted for 35% of global TB deaths with an estimated 440,000 deaths (WHO, 2020). The worldwide mortality rate has decreased by 46% between 2000 and 2018; the number of absolute TB deaths has decreased 27% between 2000 and 2018. Whilst, this impressive reduction demonstrates great international cooperation, the elimination of TB is proving a challenge as the END-TB 2020 milestone was for absolute TB deaths to decrease by 35% which we are not on target to reach (World Health Organization, 2015).

Men bear a higher burden of TB disease compared women and children. Worldwide in 2018, men accounted for 57% of all cases, whereas women and children accounted for 32% and 11% respectively. Part of WHO's initiative is to fight TB is to meet "sustainable development goals" or SDGs. These SDGs include: "End poverty" and "End hunger" (WHO, 2020).These goals are certainly commendable and would likely help reduce the burden of disease on the most vulnerable groups in society. Nevertheless, the achievement of these goals remains far off, so the focus would likely yield better short and medium term results. Novel methods of diagnosis and treatment are imperative if we are to eradicate this deadly disease.

Overall, Tuberculosis has proved to be a growing problem that is seemingly unencumbered by international initiatives and effort (Figure 1.2). There is a clear need for a change in approach to the international view of Tuberculosis to fund research and initiatives to combat spread.

1.1.5 Aetiology of Tuberculosis

Tuberculosis is an airborne disease spread, by the exhalation of droplet nuclei from an infected individual, commonly through coughing but also by talking and sneezing (Knechel, 2009). Droplet nuclei are 1-5 μm in diameter, containing 1-10 TB bacilli and have been found to last for several hours after expectoration (S. H. Lee, 2016; Loudon et al., 1969). These droplet nuclei can be inhaled by an uninfected person and can progress down into the lungs (Frieden et al., 2003).

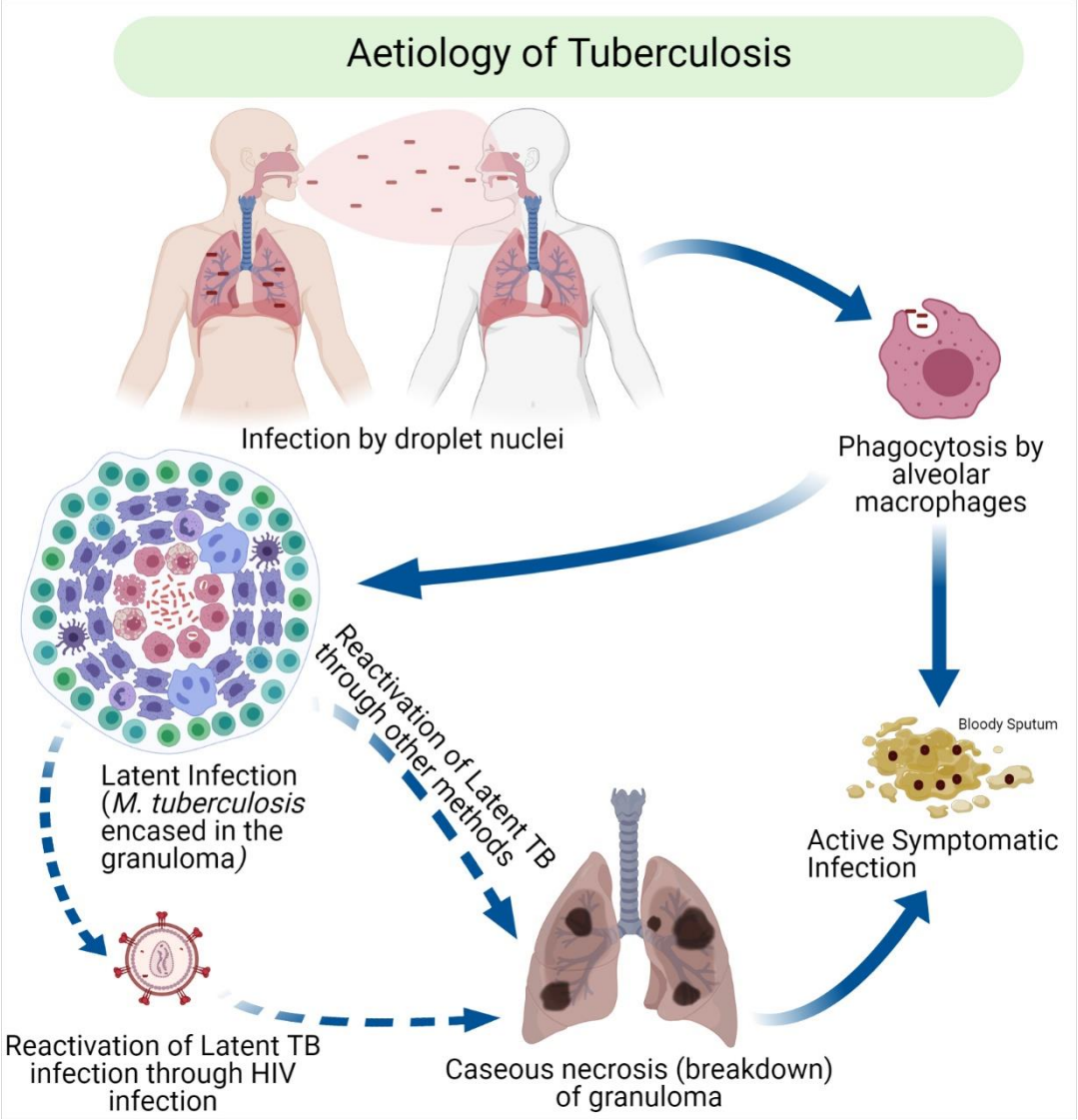

Figure 1.3 **The Aetiology of Tuberculosis** showing the path of Tuberculosis infection, from contact with an infectious individual through to active disease. The patient in some cases progresses straight to active disease (25 %) but in the majority of cases (75%), the infection is contained by the immune system in a granuloma. If the immune system becomes compromised, either through HIV infection or another means, the granuloma will break down and allow the encapsulated *M. tuberculosis* to resuscitate back to active infection.

Once these droplet nuclei have been inhaled and successfully manage to evade the pulmonary mucosal system, they are phagocytosed largely by resident alveolar macrophages (Figure 1.3). Phagocytosis by resident alveolar macrophages and subsequently by dendritic cells is the innate immune system's primary method of defence and it is successful in many microorganisms. Over millennia, *M. tuberculosis* has adapted to evade these mechanisms. Once within the phagosome, *M. tuberculosis* utilises the lipoarabinomannan (LAM) bound to its cell wall to block phagosome maturation by inhibiting Ca_{2+} release and blocking the Phosphatidylinositol-3-Kinase (PI3K) pathway (Chua et al., 2004). With the phagosome no longer a threat, *M. tuberculosis* begins to replicate inside the phagocyte (Figure 1.3). In addition, to lysosome evasion, *M. tuberculosis* begins to block TNF-a signals by expressing virulence factor type-I NADH dehydrogenase and thus inhibits host cell apoptosis to maintain the safe environment of the phagosome (Miller et al., 2010; Velmurugan et al., 2007). *M. tuberculosis* also promotes the host cell's recruitment of other professional phagocytes to the site of infection (Figure 1.3). The recruitment of neutrophils and dendritic cells in most other infections would be a strategic move from the immune system, but in the case of TB it simply exacerbates the problem as *M. tuberculosis* can also take up residence in varying other phagocytes, such as neutrophils and dendritic cells (Wolf et al., 2007).

The infection slowly gains ground and can spread to other parts of the body via the bloodstream, resulting in extrapulmonary TB (*see* **section 1.1.6**). Approximately 42 days after exposure, an adaptive immune response begins (Figure 1.3). Activated CD4 and CD8 T cells start to migrate towards the localised site of infected phagocytes. These cells will limit the replication and spread of the bacteria, by encapsulating the infected phagocytes and bacteria to form a granuloma. There is no vascularisation through the granuloma, which causes the centre becomes hypoxic and nutrient deficient. This hostile environment leads to the death of most bacteria; however, *M. tuberculosis* can enter a protective state referred to as non-replicating persistence (NRP) which allows them to survive (Figure 1.3) (Wayne & Sohaskey,

2001). Whilst the granuloma is maintained, the bacteria become quiescent and the patient does not exhibits symptoms of disease; the disease is now called Latent Tuberculosis (Dutta & Karakousis, 2014).

If the immune system can maintain the granuloma around the *M. tuberculosis,* the infected individual could be latently infected for the duration of their life. Nevertheless, if the patient becomes immunosuppressed, even mildly, this can lead to an impairment of granuloma maintenance, resulting in the granuloma becoming progressively caseous and necrotised, eventually leading to bacterial release resulting in a secondary infection. Human Immunodeficiency Virus (HIV) infects CD4+ T cells, leading to an overall drop in cell mediated immunity (Figure 1.3). If co-infected with *M. tuberculosis*, in a lack of proinflammatory cytokines promoting the maintenance the granuloma and leads to the reactivation of disease (Ehlers & Schaible, 2012; J. D. Ernst, 2012; Vla et al., 1998). The reactivation of TB has many other co-factors. Of these, uncontrolled diabetes mellitus stands out as it causes a decline in cell mediated immunity, preventing the patient from tolerating anti-mycobacterial therapy (Dooley & Chaisson, 2009).

1.1.6 Clinical Manifestation of Tuberculosis

For most immunocompetent people, the primary infection of TB is mostly asymptomatic with patients experiencing mild flu like symptoms if any (Knechel, 2009; S. H. Lee, 2016). If the immune system is able to effectively contain the infection within a granuloma, the disease progresses into the Latent stage of Tuberculosis infection (*see* **section 1.2**). If the patient is unable to form a granuloma at the point of initial infection (i.e. immunocompromised patient due to HIV), or at some point the patient can no longer maintain the integrity of the granuloma (i.e. due to the onset of diabetes mellitus), the infection can reactivate and progress to the secondary stage of infection (Figure 1.3).

The secondary stage of infection is characterised by early non-specific symptoms such as chills, night sweats, fever, malaise, and progressive fatigue (Knechel, 2009) (Figure 1.4). Another symptom is wasting where the patient loses weight due to a lack of appetite (Figure 1.4). Wasting is, perhaps, the classic non-specific symptom of Tuberculosis; several characters in literature are described as "*pale and waifish when suffering from consumption*" (T. M. Daniel, 2006).

Tuberculosis can present in two separate ways: a pulmonary disease and an extrapulmonary disease with the former being the most common (Figure 1.4). A persistent cough is the most common symptom of pulmonary tuberculosis. This cough generally produces a purulent, bloody sputum (Knechel, 2009). As the pulmonary infection progresses, the patient will exhibit a high fever, pleuritic chest pain and shortness of breath (dyspnea) (Figure 1.4).

Extrapulmonary tuberculosis occurs in approximately 20% of patients and is where the disease expresses outside the lungs. Tuberculosis can spread to any other part of the body but is most dangerous when it presents in the brain (Knechel, 2009). Whilst in the brain, the infection can progress to tuberculoid meningitis which, even with treatment often proves fatal. Other common location for extrapulmonary tuberculosis include: the urinary tract, the joints and bones and the meninges (Ehlers, 2009; S. H. Lee, 2016).

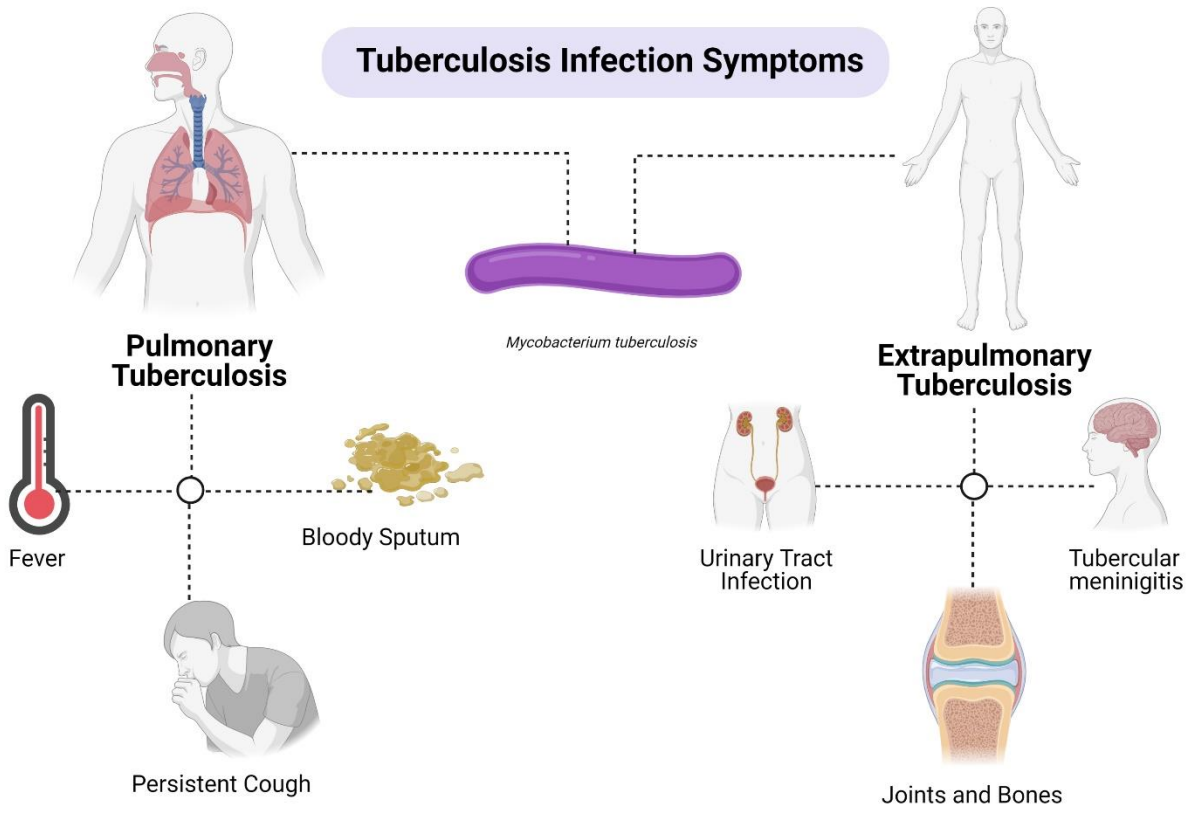

Figure 1.4: **Summary Figure of the common symptoms of Tuberculosis.** created in biorender.com

1.1.7 Current Treatment of Tuberculosis

Tuberculosis is a complicated infection that can prove difficult to treat, even in an immunocompetent patient. The current recommended treatment for drug susceptible TB is a four-part combination therapy of Isoniazid (INH), Rifampicin (RIF), Ethambutol (ETH) and Pyrazinamide (PYZ) (Dawson et al., 2015; McKenna & Furin, 2019). Initially, the first phase of treatment – which lasts for two months – is a combination of all four drugs administered daily. After the initial phase of treatment for two months, the treatment regimen progresses to the continuation phase. The continuation phase consists of INH and RIF being taken three times a week for a further four months (WHO, 2017).

Due to the intensive nature of this drug regimen, the patient compliance has proved problematic. So, WHO recommended their new initiative, DOTS – or Direct Observed Treatments – where patients are monitored taking each dose and given support (e.g. mental health support) where applicable (World Health Organization, 1999).

1.1.7.1 Isoniazid

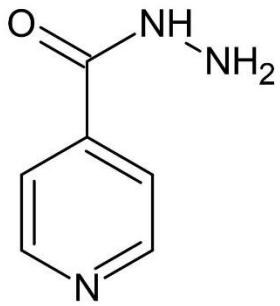

Figure 1.5: **Chemical Structure of Isoniazid**. Isoniazid is a part of the frontline HRZE therapy

Isoniazid is one of four frontline drugs for *M. tuberculosis* treatment (Figure 1.6); it was discovered in 1952 by Roche. Currently, it is prescribed for six months as part of the HRZE TB regimen (WHO, 2017). It is also one part of the two component Latent Tuberculosis therapy, administered for six months. INH is a prodrug that, before activation, has no antimicrobial effects (Figure 1.5). It is activated by KatG, a catalase-peroxidase, by peroxidation to produce several damaging products (Ng et al., 2004; Zhang et al., 1992). These products constitute INH's mechanism of action (Timmins & Deretic, 2006).

The most commonly used method of inhibition by INH is the direct inhibition of InhA. This inhibition occurs when INH is oxidised by KatG in the presence of NADH. This product then forms a covalently linked INH-NADH adduct (Rozwarski et al., 1998). The INH-NADH adduct strongly inhibits an enoyl acyl carrier protein reductase, InhA. InhA forms a part of the fatty acid synthesis (FAS) II system, which is responsible for fatty acid elongation, a crucial constituent of mycolic acid synthesis (Banerjee et al., 1994; Dessen et al., 1995). Mycolic acids form an essential part of the mycobacterial cell wall, thus inhibiting synthesis causes a downstream synthetic lethality to the cell (Jankute et al., 2015).

If INH is activated by KatG in the presence of NADP, instead of NADH, a different active adduct forms: INH-NADP (Rozwarski et al., 1998). It has been demonstrated *in vitro* that this INH-NADP adduct can inhibit key folic acid biosynthesis protein, dihydrofolate reductase (DHFR) (Argyrou et al., 2006). This inhibition ceases the production of folate which has a severe

downstream effect on many intracellular processes including nucleic acid biosynthesis and consequently causes a downstream synthetic lethality.

Resistance to INH was observed quickly after its introduction and remains a growing threat (Middlebrook, 1954; Slayden & Barry, 2000). Despite this, resistance to INH is relatively complicated due to its complex mechanism of action.

There are two distinct mechanistic routes that result in INH resistance (da Silva & Palomino, 2011). Firstly, a mutation in either *katG* (the gene for activator protein, KatG) or *inhA* (the target gene, InhA) that results in an INH loss of function (Hazbón et al., 2006). The most common method of resistance is a mutation in *katG* which prevents the protein from activating INH (Zhang et al., 1992). There are over 100 different mutations in *katG* that have been shown to alter function of KatG and reduce the activity of INH. The most common mutation is Ser315Thr which produces a form of KatG that is able to produce an INH product but one that is unable to form an adduct with NAD and thus blocks activity (Vilchèze & Jacobs, Jr., 2007). Mutations can also be found in *inhA* and again reduce activity of INH by preventing the binding of the INH adducts (Leung et al., 2006).

Alternatively, a mutation in the promoter region can cause a downregulation in expression of either *inhA* or *katG* respectively (Ando et al., 2011; Dalla Costa et al., 2009). The downregulation of either gene results in a more resistant phenotype towards INH.

1.1.7.2 Rifampicin

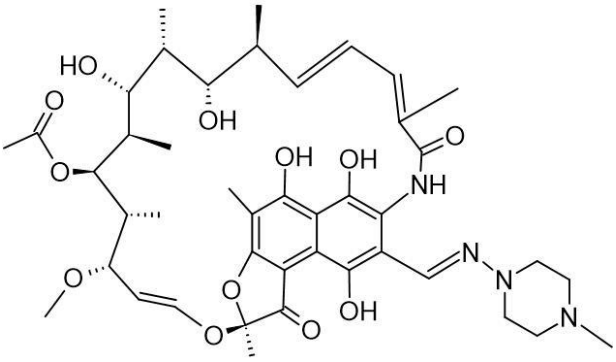

Figure 1.6: **Chemical Structure of Rifampicin**. Rifampicin is a part of the frontline HRZE therapy.

Rifampicin is a fast acting antituberculous drug that was introduced in 1966 (Maggi et al., 1966). RIF is also used for the treatment of other mycobacterial diseases such as Leprosy (*M. leprae*) and *M. avium* complex (Figure 1.6).

The primary mechanism of action for RIF is blocking RNA synthesis by inhibiting bacteria RNA polymerase (McClure & Cech, 1978). RNA polymerase is responsible for the transcription of DNA to RNA, thus making it an attractive drug target (Maggi et al., 1966). Experiments utilising radiolabelled rifampicin showed that RIF binds tightly to RNA polymerase and blocks any other molecule from binding due to its high affinity for the protein (Handschin & Wehrli, 1976; Wehrli et al., 1968). RNA polymerase is a large protein formed of five subunits: ααββ'σ. RIF has been found to bind to the β subunit (Wehrli, 1983). This binding causes RNA synthesis to abort after the first phosphodiester bond in a process called abortive initiation (Wehrli, 1983).

Furthermore, in addition to inhibiting the β subunit of RNA polymerase, RIF causes a reduction in the binding affinity of RNA polymerase for nucleotide triphosphates (ATP, GTP etc.) (McClure & Cech, 1978).

Resistance to RIF has been increasing year on year and it was estimated that in 2018, over half a million people fell ill with rifampicin-resistant TB (WHO, 2020). *M. tuberculosis* becomes resistant to RIF through mutations to the β subunit of RNA polymerase. The β subunit is coded

for by the gene *rpoB* and the relevant mutations occur mainly between codons 504-533; a region called the rifampicin resistance determining region (RRDR) (Somoskovi et al., 2001; Telenti et al., 1993). Approximately 96% of resistant strains have a mutation in the RRDR and the most common mutation affecting between 65-86% of strains are either His526Asp or in Ser531Leu. These are also the most effective mutations giving the strain the highest MIC to RIF. Other mutations of key residues within the RRDR to give some resistance to RIF but are not the equal of the former two mutations (Moghazeh et al., 1996; Ohno et al., 1996).

Around 4% of RIF resistant strains contain mutations within *rpoB* that are outside the RRDR (Somoskovi et al., 2001). The two mutations associated with these strains are Val146Phe and Ile572Phe (Siu et al., 2011). Both mutations are close to the binding pocket of RNA polymerase and thus prevent the binding of RIF to RNA polymerase (Siu et al., 2011).

1.1.7.3 Ethambutol

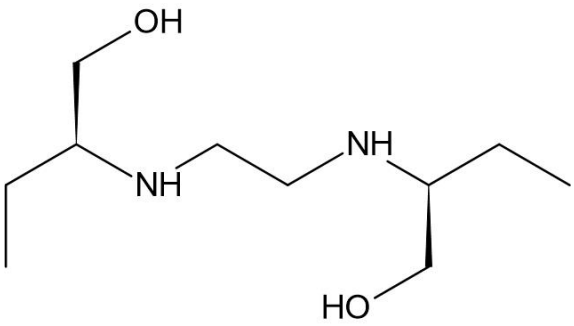

Figure 1.7: **Chemical Structure of Ethambutol**. Ethambutol is a part of the frontline HRZE therapy.

Despite being introduced in 1961 and forming one part of the main Tuberculosis combination therapy, the mechanism of action for Ethambutol (ETH) is still relatively undeciphered (Telenti et al., 1997) (Figure 1.7). The main theory as to the mechanism of action is that ETH blocks the polymerisation of arabinose into cell wall arabinogalactan (Takayama & Kilburn, 1989). It has also been shown that upon treatment with ETH, the lipid carrier decaprenol phosphoarabinose starts to accumulate, which in high concentrations can be toxic (Sreevatsan et al., 1997). Decoprenol phophoarabinose is a major intermediate in arabinan biosynthesis and its accumulation mid-way through the biosynthetic pathway suggests that ETH blocks the transfer of arabinose to the cell wall acceptor. This led to the inference that the target of ETH is a set of arabinotransferases: EmbA, EmbB and EmbC (Telenti et al., 1997). Resistance to ETH in clinical isolates has exceeded 4% and is increasing (Goude et al., 2009; Sreevatsan et al., 1997; WHO, 2017).

1.1.7.4 Pyrazinamide

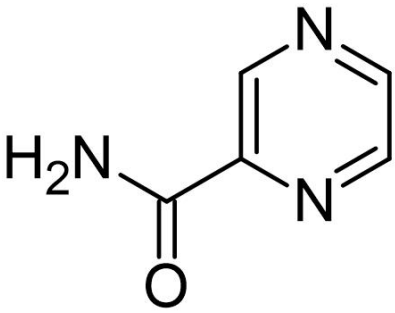

Figure 1.8: **Chemical Structure of Pyrazinamide**. Pyrazinamide is a part of the frontline HRZE therapy.

Pyrazinamide (PYZ) is one part of the HRZE combination therapy used to treat active tuberculosis (Figure 1.8) (WHO, 2017). It was introduced into active TB therapy in 1949, although the mechanism of action took a while longer to elucidate and is still not fully understood (Zhang et al., 2003). PYZ, like INH, is a pro-drug that is activated by a bacterial nicotinamadase/pyrazinamidase (PYase) to form pyrazinoic acid.

PYZ is unusual as for the drug to have activity against *M. tuberculosis,* the pH has to be specific (Zhang et al., 2003). A neutral pH, such as in an *in vitro* culture, results in PYZ having little to no activity. The best antimicrobial activity is found at an acidic pH, which is consistent with active disease (McDermott & Tompsett, 1954). It is believed that this acidic pH converts the pyrazinoic acid into a highly protonated form of the acid. This acid can then readily diffuse through the membrane and start to accumulate intracellularly. This diffusion across the cell membrane can disrupt the membrane potential, which contributes to the antimicrobial effects of PYZ (Zhang et al., 2015).

It has also been shown that the accumulation of pyrazinoic acid can inhibit protein and RNA synthesis. The accumulation can also prevent the transports of essential bases and amino acids such as uracil and methionine (Zhang et al., 2003, 2015).

1.1.8 Antimicrobial Resistance and Tuberculosis

Over the last century, tuberculosis (TB) has shown a great deal of antimicrobial resistance. After the discovery of Streptomycin in 1945 turned TB into a treatable disease, treatment has advanced to comprehensive combination therapies such as the HRZE (*see* **section 1.1.7**). Resistance to these frontline antibiotics began to appear consistently within the next 30 years. By the turn of the century, multi-drug resistant TB (MDR-TB) infection became a problem of increasing complexity. Long, multi-drug regimens started to be prescribed; most of which had severe associated side effects.

Multi-Drug Resistant TB (MDR-TB) is described by the WHO as TB that is resistant to both RIF and INH and therefore requires a more extensive treatment (WHO, 2020). The current advisory treatment for a case of MDR-TB can last between 15-20 months (World Health Organization, 2019). The latest WHO recommended antibiotic therapy – as per 2019 – consists of: Moxifloxacin/Levofloxacin, Bedaquiline, Linezolid with the addition of either clofazimine or cycloserine (World Health Organization, 2019). If resistance is seen to any of the above, the following should be added on a case by case basis: Ethambutol, Delamanid, Pyrazinamide, Imipenem-Cilastatin, Meropenem, Amikacin, Streptomycin, Ethionamide/Prothionamide, *p*-aminosalicyclic acid (Pontali et al., 2019; World Health Organization, 2019)**.** Despite this intensive antibiotic regimen, global treatment success rates have remained low at 56%.

MDR-TB is becoming more prevalent despite efforts to halt its progress (Figure 1.9). The WHO estimates that in 2018 there were 484,000 MDR-TB cases. A limitation of data is the wide confidence interval caused by the lack of testing for this figure is wide (417,000-556,000); this

is due to a lack of testing for MDR upon a positive TB diagnosis. There have been several hotspots of MDR-TB disease flagged, particularly in Russia and South East Asia (Figure 1.10).

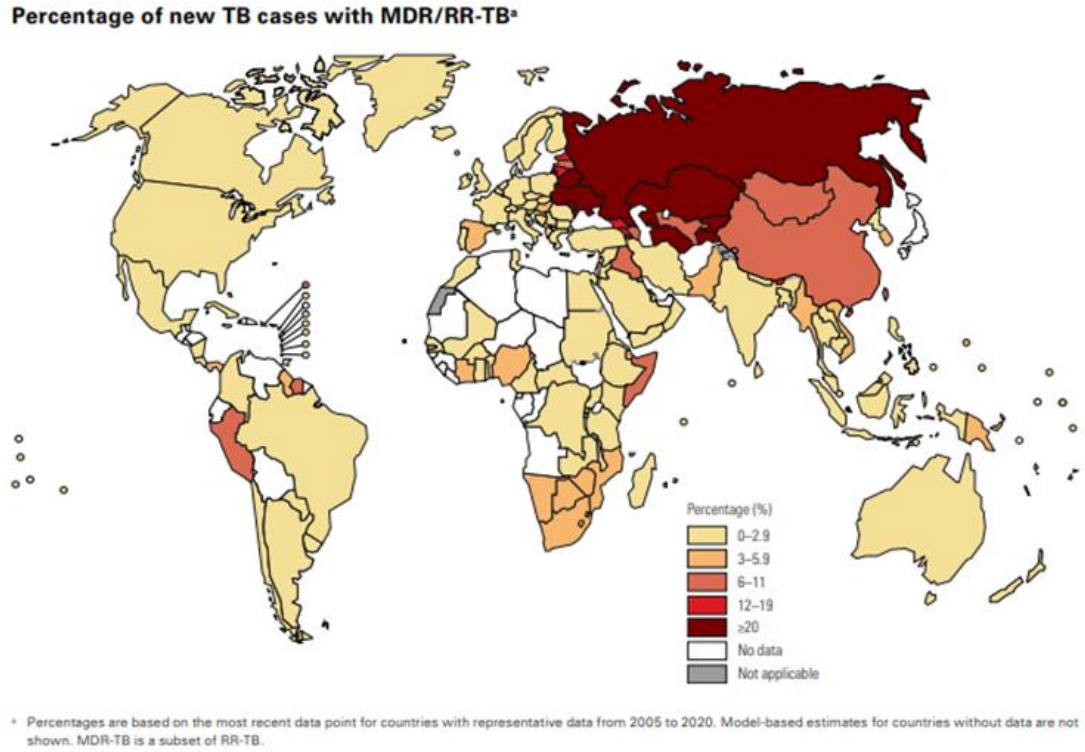

Figure 1.9: **Global Map showing the percentage incidence of Multi-Drug Resistant Tuberculosis (MDR-TB) arising in newly infected cases** (WHO, 2020)

An even greater concern is Extremely Drug Resistant TB (XDR-TB), which is defined as resistance to both RIF and INH as well as a fluoroquinolone (e.g Moxifloxacin) and a second line injectable (e.g Kanamycin) (Migliori et al., 2007; Prasad, 2010). It was estimated that in 2016, 6.2% of MDR-TB cases could be classified as XDR-TB.

In 2018, 3.5% of new global TB infections were classified as MDR-TB, with the highest burden on the former Soviet Union with roughly 25% of all new TB cases classified as MDR-TB (Figure 1.9) (Migliori et al., 2012; WHO, 2020).

The issue of MDR-TB is not limited to new cases of TB, the statistics for “previously treated” TB are truly striking (Figure 1.11). Previously treated means cases that were confirmed positive, were treated, and then tested culture or smear negative for *M. tuberculosis* (Zignol et al., 2007). Patients then develop a secondary TB infection. 18% of these previously treated infections were categorised as MDR-TB. Figure 1.11 thoroughly demonstrates the link between previously treated cases and MDR. The former Soviet Union demonstrates a particularly high burden with 50% of all previously treated cases is classified as MDR in 2018 (WHO, 2020) (Figure 1.10). These statistics give a clear link between previously treated infection and the emergence of MDR (Zignol et al., 2006)

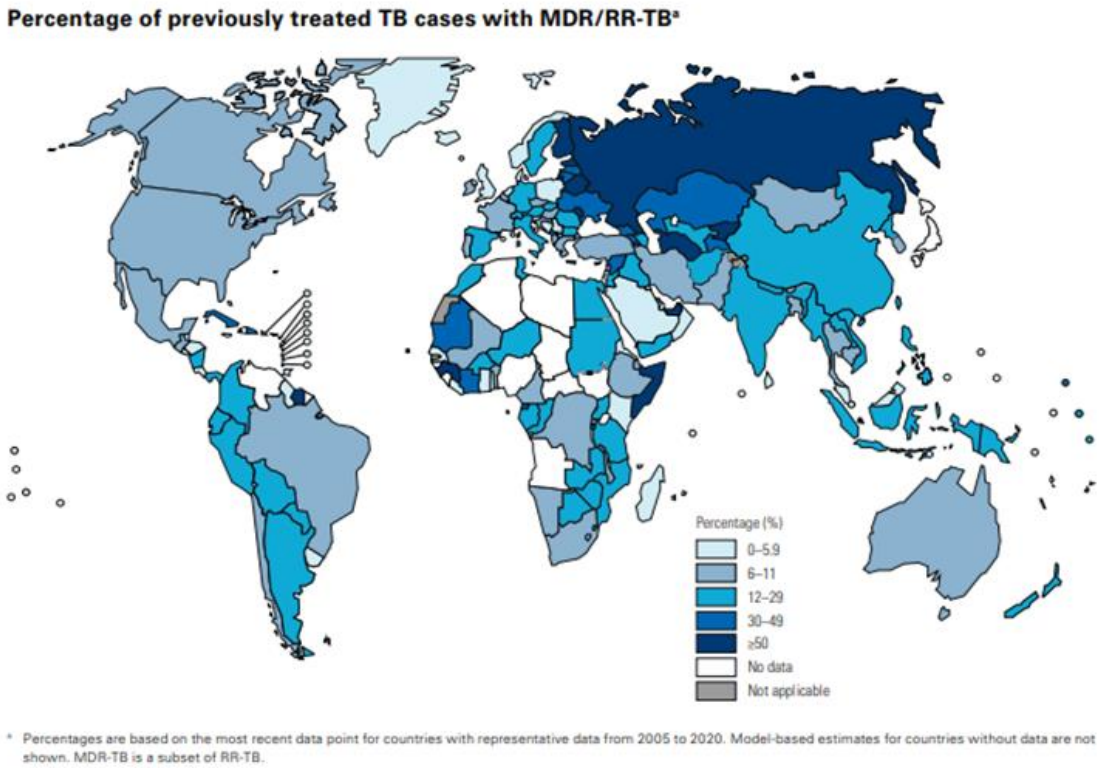

Figure 1.10: **Global Map showing the percentage incidence of Multi-Drug Resistant Tuberculosis (MDR-TB) arising in previously treated cases of Tuberculosis**. Previously Treated infections are defined as those infections which were treated and declared sputum negative only to reemerge at a later point (WHO, 2020).

1.2 Latent Tuberculosis and Non-Replicating Persistence

1.2.1 Epidemiology and Aetiology of Latent Tuberculosis

As previously discussed in **section 1.1.5**, when *M. tuberculosis* are packaged into a granuloma by the immune system, they enter a hostile environment that is restricted in both oxygen and nutrients and are bombarded by a nitric oxide assault (Ehlers & Schaible, 2012; Gibson et al., 2018; Guirado & Schlesinger, 2013). This stimulates *M. tuberculosis* to enter into a protective state known as Non-Replicating Persistence (NRP) (Wayne & Sohaskey, 2001). This NRP state allows the *M. tuberculosis* to persist asymptomatically in tissues for decades in a clinical condition called Latent Tuberculosis Infection (LTBI) (Lin & Flynn, 2010). This condition can persist until the host becomes immunocompromised or can no longer maintain the sanctity of the granuloma, this LTBI can reactivate can cause secondary active disease (Knechel, 2009).

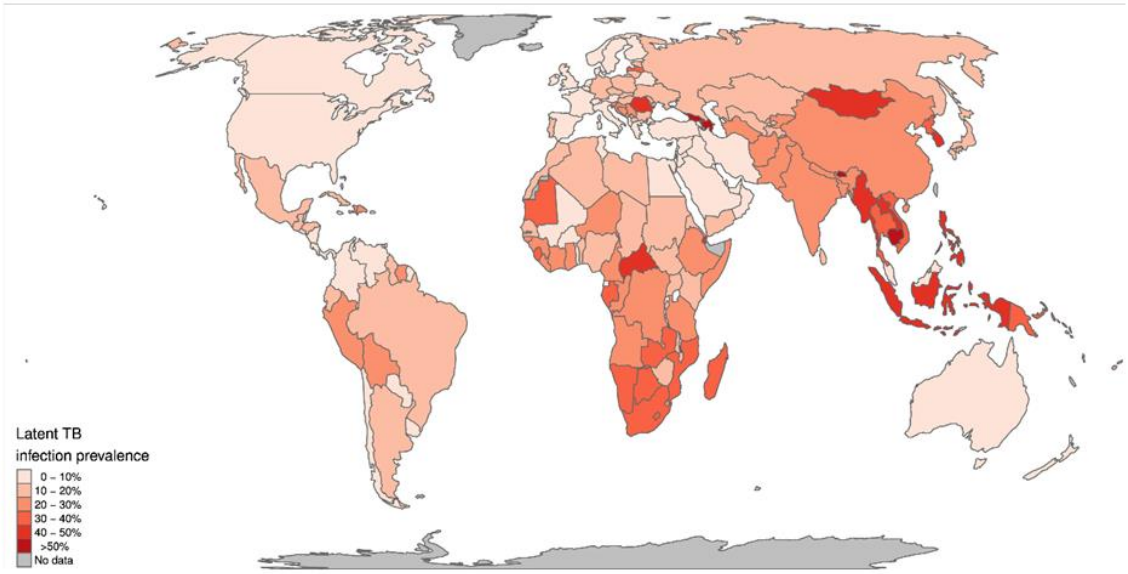

Figure 1.11: **Global Map of mathematically estimated LTBI incidence** (Houben and Dodd, 2016)

LTBI is complex to diagnose and this has led to ambiguity on the true burden of global disease. The most recent mathematical estimate places this at roughly 1.7 billion of the population latently infected with *M. tuberculosis* (Houben & Dodd, 2016). A global map was made that demonstrates the mathematically modelled hotspots of latent disease (Figure 1.11). A ballpark figure of 56 million of these latent cases are conceivably likely to reactivate, however, global conditions over time could dramatically change this (Houben & Dodd, 2016). Factors such as global pandemics or international war could influence a higher proportion of latent cases to reactivate (Marimuthu et al., 2020). If a larger proportion of these LTBIs were to reactivate than expected, this inveterate disease would have wide reaching ramifications (Figure 1.11).

A concerning relationship has appeared between LTBI and MDR-TB. As previously discussed (see **section 1.1.8)**, there is a worrying correlation between multi drug resistance and "previously treated" cases of TB (WHO, 2020) (Figure 1.9, Figure 1.10). Whilst only 3% of newly arising infections are classified as MDR, nearly 20% of previously treated cases are MDR (WHO, 2020) (Figure 1.9, Figure 1.10). Previously treated infections are classified as infections that were smear positive, were successfully treated and culture negative. At a later period, they develop active infection again despite previous treatment (Munje et al., 2015; Zignol et al., 2007). With 20% of previously treated cases being classified as MDR, there seems to be a link between reoccurring infection and MDR resistance. Whilst speculative, many share the view that these "previously treated" infections are not caused by reinfection or a new exposure to *M. tuberculosis* but instead to by a reactivation event of a population of NRP *M. tuberculosis* (Dyrhol-Riise et al., 2010). It is concerning that there are cases remerging that have been previously considered cured, especially coupled with that these cases seem to be remerging with resistance to frontline antibiotics. Considering the above, the WHO's decision to declare that eradicating LTBI is paramount to success for the eradication of TB as a whole (WHO, 2020; World Health Organization, 2015).

Mycobacteria can persist inside human tissues for decades, unaffected by the immune system, whilst retaining the ability to return to pathogenic, logarithmic growth (Wayne & Sohaskey, 2001). This unique ability is one of the key factors to successful pathogenicity as has allowed to TB evade eradication (Figure 1.12).

As early as 1933, *M. tuberculosis* was observed to have survival capabilities unseen in other bacteria (Loebel et al., 1933a, 1933b). Loebel and his team showed that *M. tuberculosis* could survive seemingly indefinitely in a “non-nutrient” medium and could remain viable throughout (Loebel et al., 1933a). This was the first indication that *M. tuberculosis* could possess a different state of existence than the traditional logarithmic growth observed in other microorganisms.

It was not until the 1990s that this was further investigated. It was observed that the granuloma is hypoxic in its interior. It was previously thought that *M. tuberculosis* was an obligate aerobe, so persistence in an anaerobic environment indicated a change in physiology to facilitate survival under hypoxia. Further testing proved that if you introduce *M. tuberculosis* directly to an anaerobic environment, the culture will rapidly die; the reaction expected from an obligate aerobe microorganism (Wayne, 1994). Nevertheless, if the *M. tuberculosis* is allowed time to adapt to the slow decrease in oxygen saturation, the culture ceases replication but remains very much alive (Wayne & Hayes, 1996). This unique survival adaptation was coined Non-Replicating Persistence (NRP) (Wayne & Sohaskey, 2001).

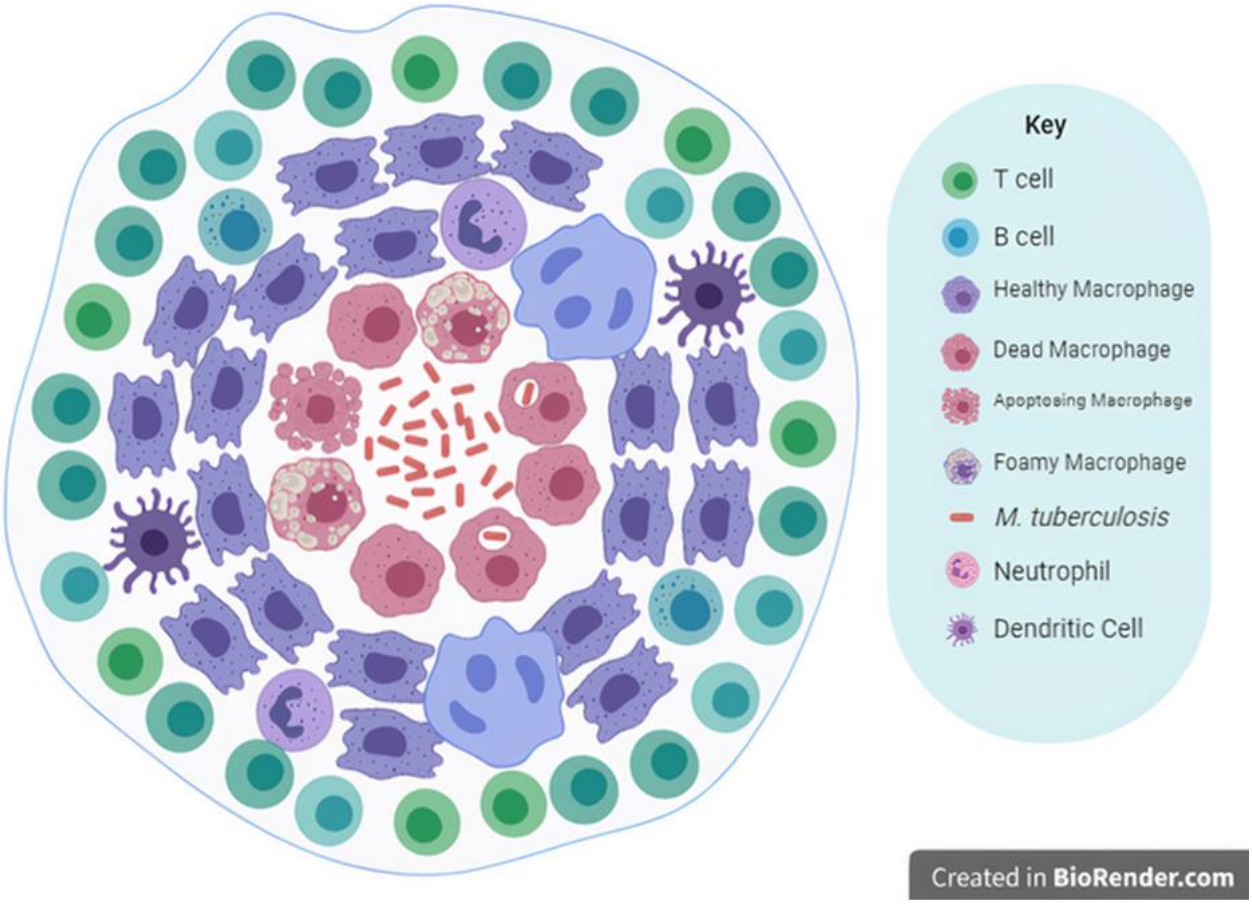

Figure 1.12: **Immunological Structure of the Granuloma as seen in human infection**

Since then, there has been a lot of research conducted into NRP. The main research question of what drives *M. tuberculosis* to enter into the NRP state has deep implications for this field of study. The NRP state is first and foremost a survival response to significant external pressure. The granuloma is a particularly hostile environment that has been designed to eradicate dangerous pathogens (Figure 1.12). Therefore, the immune system creates an environment as toxic and hostile as possible (Ehlers & Schaible, 2012; Martin et al., 2016). To do this, it utilises a combination of direct and indirect immune pressures; of which many of these pressures can induce *M tuberculosis* to enter the NRP state.

1.2.1.1 NRP-triggering factor: Hypoxia

One indirect pressure generated by the granuloma is hypoxia. Due to a lack of vascularisation, the interior of the granuloma undergoes a slow shiftdown in oxygen concentration into anaerobiosis (Wayne & Hayes, 1996). This shiftdown triggers the *M. tuberculosis* to prepare for full anaerobic conditions. One such preparation is to upregulate the hypoxic stress response protein, α-crystallin (Acr) (S. H. Cho et al., 2006; Mamo et al., 2014; Sherman et al., 2001). Acr was initially recognised as a potent antigen of *M. tuberculosis* that can often be detected is patient serum (B. Y. Lee et al., 1992; Yuan et al., 1998). Acr is coded for by *hspX* (also known as *acr* or *Rv2031*) has been showed to be dramatically induced upon lowered oxygen saturation (Sherman et al., 2001). This rapid induction upon hypoxia clearly shows the importance of Acr to *M. tuberculosis.* Indeed, Acr was demonstrated to not only be an antigen as previously thought, but a powerful regulator protein under hypoxic conditions. Knockout studies of *hspX* showed *M. tuberculosis* could not survive a hypoxic environment without its expression and regulation (Sherman et al., 2001; Yuan et al., 1998). This area of study was developed to investigate if other genes were rapidly upregulated and crucial to hypoxic survival. This successfully identified the DosR Regulon, a set of genes that were upregulated by hypoxic pressure and are required for persistence. The regulon encodes the activator protein *DosR* and *in vitro* knockout mutants have proved its essentiality for surviving hypoxia (Bartek et al., 2009; Mehra et al., 2015). This essentiality was further proven by a failure to show LTBI in a DosR regulon knockout in macaques (Mehra et al., 2015). Whilst activated by *dosR,* two oxygen-dependant proteins, *dosS* and *dosT* have been shown to activate *dosR* itself to then go on to activate the rest of the regulon (Honaker et al., 2009). These proteins are particularly interesting as they are activated by different levels of oxygen saturation: DosT seems to be activated in microaerophilic conditions and is responsible for activation of elements of the DosR regulon in the initial NRP stage I (Honaker et al., 2009). This flurry of activity from DosT drops off after entry to full anaerobic conditions and the activity of DosS begins to increase (Honaker et al., 2009). This oxygen-dependant activation of essential

survival regulatory proteins demonstrates the importance of adaptation to hypoxia is to *M. tuberculosis*; thus, demonstrating the high likelihood that hypoxic atmospheres are common in granulomas (Figure 1.12).

In the Wayne (hypoxia) model, there are no restrictions placed on nutritional bioavailability with the sole pressure being a hypoxic atmosphere. A particular area of the proteome that was noticeably upregulated was the fatty acid metabolism genes (S. H. Cho et al., 2006; Muttucumaru et al., 2004). In particular, it was found that isocitrate lyase – an enzyme involved in fatty acid catabolism - is highly upregulated under hypoxia-driven NRP (*aceA/*Rv0467 and *aceAa/b /*Rv1915/6) and are essential for infectivity and survival (Muñoz-Elías & McKinney, 2005; Muttucumaru et al., 2004).

These widespread genetic expression changes have such an effect on the bacilli that distinct physiological changes can be observed. Changes to the bacterial morphology have been well documented, with visible changes to the mycobacterial cell wall (Jakkala & Ajitkumar, 2019; Trutneva et al., 2020; Velayati et al., 2011). There is an observable thickening of the cell wall by approximately 5 nm coupled with bulging or budding over the perimeter of the cell wall (Velayati et al., 2011). These morphological changes under hypoxia progress to be more exaggerated until the traditional mycobacterial rod shape is replaced with an imperfect cocci shape (Jakkala & Ajitkumar, 2019). It is thought that this thickening and tightening of the cell wall make the cell more impermeable to antimicrobials such as Rifampicin (Jakkala & Ajitkumar, 2019).

1.2.1.2 NRP-Triggering Factor: Nutrient Starvation/Deprivation

Whilst the effects of hypoxia within the granuloma have been well studied, the effects of the other NRP-inducing factors have been somewhat neglected. The next most studied NRP-inducing factor is nutrient starvation and nutrient deprivation. There is a key distinction between these terms. Nutrient starvation indicates a lack in available nutrients to the bacteria in the granuloma (Figure 1.12). Nutrient deprivation infers that whilst nutrients are scarce and may not be optimal, there is some access to nutrients and the bacteria are not in a full starvation state (Pandey & Sassetti, 2008; Soto-Ramirez et al., 2017).

The granuloma prevents the bacteria accessing the rich range of nutrients present in the human host (Guirado & Schlesinger, 2013) (Figure 1.12). Resource denial is a key strategy employed by the immune system to eradicate incumbent infections (Ramakrishnan, 2012). However, mycobacteria can detect this deficiency of available nutrients and initiate the cell to enter the NRP state (Loebel et al., 1933a). Being in the NRP state facilitates *M. tuberculosis* to survive in Phosphate Buffered Saline (PBS); however, the genetic and metabolic adaptations are subtly different to when hypoxia is the NRP-inducing factor (Bacon et al., 2014; Betts et al., 2002; Loebel et al., 1933a).

An interesting point of disparity between Wayne-based (hypoxia) models and nutrient starvation models is respiration rates. Both Löebel and Betts showed that over the first 96 h after being placed into PBS, the respiratory rate rapidly declined but did not cease; additionally, methylene blue (an indicator of oxygen tension) present in the culture was not discoloured (Betts et al., 2002; Loebel et al., 1933a). However, Colony Forming Unit counts (CFU/mL) show that despite this lowered rate of respiration the culture remains the same. This is in contrast to the Wayne model where the bacilli stop replicating in response to a deficiency in oxygen (Wayne & Hayes, 1996).

The genetic profile of *M. tuberculosis* under nutrient starvation-driven NRP creates an interesting comparison to that of hypoxia-driven NRP. The key stress protein Acr1 that is so

heavily upregulated in hypoxia driven NRP is sless upregulated under starvation (Betts et al., 2002). From a whole-genome transcriptomic view, there is a widespread downregulation of genes once in the NRP phase; particularly downregulated are genes involved in amino acid biosynthesis, DNA replication and repair, lipid biosynthesis and virulence factors (Betts et al., 2002). Many enzymes involved in classical metabolism such as those in the Tricarboxylic Acid (TCA) cycle are downregulated (specifically: fumarase/*fum,* aconitase/*acn,* isocitrate dehydrogenase/*icd1*). Most genes involved with lipid biosynthesis (such as the FAS cycle) are downregulated under NRP conditions; some are highly downregulated (Betts et al., 2002)

There is an interesting subset of genes that are either switched on or become heavily upregulated during nutrient starvation NRP resulting in a change in metabolism (Betts et al., 2002). As seen in hypoxia-driven NRP, isocitrate lysase is highly upregulated under NRP conditions; further suggesting a change in metabolic focus (Betts et al., 2002; Muttucumaru et al., 2004).

It is particularly interesting that this proteomic and transcriptomic study showed that several genes of unknown functions are significantly upregulated under nutrient starvation driven NRP (Betts et al., 2002). One such gene *Rv2660c* has been found to be a powerful antigen; potentially due to the high upregulation during the NRP state, *Rv2660c* could be used as a method of diagnosing latent TB (Govender et al., 2010). These highly upregulated genes must have a purpose to the *M. tuberculosis* to be so highly upregulated during a time of stress. The mere fact that we do not know the function of these clearly essential genes depicts how much we still have left to discover about *M. tuberculosis.*

1.2.2 Cholesterol Catabolism

One of the main purposes of the granuloma is to contain, therefore, over time essential nutrients become scarce. This is a method for the immune system to eradicate an infection as many bacteria when starved of carbon sources do not remain viable. The accumulation of immune cells, especially foamy macrophages, provide a rich and largely solitary carbon source in the form of lipids, particularly cholesterol (Martin et al., 2016). Current research has shown that *M. tuberculosis* primarily metabolises fatty acids and particularly cholesterol when in the granuloma (Muñoz-Elías & McKinney, 2005). Whilst the presence of cholesterol inside the granuloma provides a crucial carbon source in an otherwise nutrient deprived environment, cholesterol catabolism is complex. Cholesterol is practically insoluble in water, which makes breaking the molecule down into easily metabolised small molecules extremely challenging (Tak, 1942). Many bacteria do not possess the proteomic machinery for this complex task. However, *Mycobacteria* have been shown to have the rare capability to metabolise cholesterol (van der Geize et al., 2007).

The unlikely relationship between cholesterol, *M. tuberculosis* and the immune system has also been highlighted as an area in urgent need of research. It would seem that the acquisition and subsequent metabolism of cholesterol effectively removes the threat of phagocytosis and mediates the survival of *Mycobacteria* within macrophages (Gatfield & Pieters, 2000; Nguyen & Pieters, 2005). In addition to this, it would appear that the metabolism of cholesterol is essential for survival in the granuloma, suggesting the transcriptional changes could be mediated by this process (Wilburn et al., 2018; Wipperman et al., 2014).

There is a lingering dogma about NRP *Mycobacteria* that they are “fat and lazy” and are considered metabolically dormant (Ehlers, 2009; Garton et al., 2008). However, advances in proteomics, lipidomics and transcriptomics studies show that this is not necessarily the truth (Muñoz-Elías et al., 2006; Muñoz-Elías & McKinney, 2005; Soto-Ramirez et al., 2017; Wipperman et al., 2014). Studies have shown that instead of being metabolically dormant, *Mycobacteria* in the NRP state undergo a shift in metabolic focus; a wide variety of genes

responsible for lipid metabolism have been found to be upregulated when in the NRP state (Griffin et al., 2012; Muñoz-Elías & McKinney, 2005; Nesbitt et al., 2010). This has prompted research into elucidating the cholesterol catabolism pathway in *Mycobacteria* as in the nutrient-deprived, single carbon source environment of the granuloma, this pathway could provide a crucial insight into the priorities of the bacterium when in the NRP state.

The leading research that established the groundwork for the cholesterol catabolism pathway in *M. tuberculosis* used a related soil bacterium *Rhodococcus* sp. to elucidate the pathway using a variety of transcriptomic methods (van der Geize et al., 2007). From that starting point, many other elements were studied in greater detail and proved to exist in *M. tuberculosis* (Wipperman et al., 2014). The ability of *M. tuberculosis* to metabolise cholesterol was confirmed by utilising 14C-radiolabeled cholesterol as a pulse-chase experiment, tracking the radiolabel through a variety of cholesterol catabolic products (Pandey & Sassetti, 2008). This research also confirmed that acquisition and breakdown of cholesterol is essential for NRP, perhaps confirming the intrinsic links between cholesterol catabolism and the NRP state (Pandey & Sassetti, 2008).

The proceeding sections are a summary of the current biochemical pathway of cholesterol catabolism in *M. tuberculosis* as far as it has been described at the time of writing. For a full picture of the pathway, the MetaCyc database has the pathway in full and it has been deeply useful in the writing of this section. It can be accessed using the link below or otherwise search for the "superpathway of cholesterol degradation II" (http://www.biocyc.org/META/NEW-IMAGE?type=PATHWAY&object=PWY-6947&detail-level=4&detail-level=3).

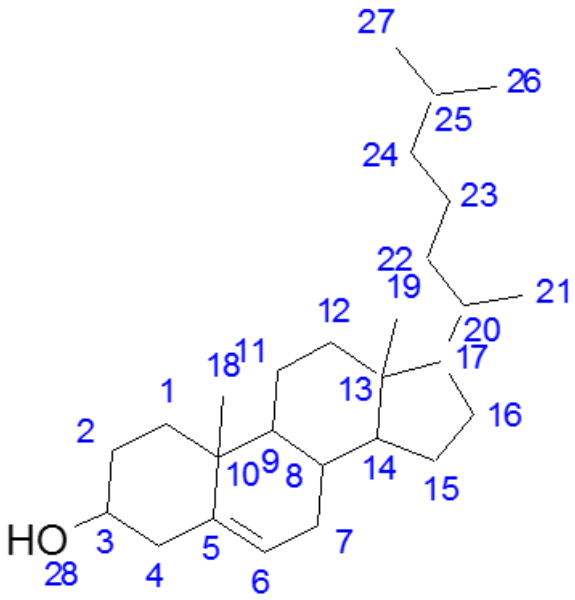

Figure 1.13**: Numbered Structure of Cholesterol**

1.2.2.1 Breakdown of the cholesterol side chain or β-oxidation

Cholesterol has a long side chain that requires breakdown before it can be fully metabolised. This breakdown is conducted by β-oxidation, a common method of metabolising long chain lipids. The overall yield of this is two molecules of propionyl-CoA and one molecule of acetyl-CoA (*see* **section 1.2.2.5)**. A diagrammatic summary of this process can be found in Figure 1.14. After the initial starting conversion of a cholesterol molecule to cholest-4-ene-3-one by 3β-hydroxysteroid dehydrogenase (3 β-Hsd), a hydroxylation process is initiated onto the side chain by one of two enzymes, Cyp125 or Cyp145. This hydroxylated side chain is then

carboxylated by FadD19 and activated by the addition of coenzyme-A (CoA). At this point the cholesterol breakdown product is now able to start the process of β-oxidation. The cholesterol side chain takes three rounds of β-oxidation to be completely broken down into the breakdown products. Each round of β-oxidation consists of four sequential enzymatic step and end with the release of either acetyl-CoA or propionyl-CoA (Figure 1.14). The first step is catalysed by an acyl-CoA dehydrogenase (FadE) and the second step in catalysed by an enoyl-CoA-hydratase (EchA). After this point, the third step of ß-oxidation is catalysed by a 3-hydroxy-acyl-CoA-dehydrogenase (FadB) and the fourth step is mediated by a 3-keto-acyl-CoA thiolase (FadA) (Figure 1.14). There is a lot of genetic diversity in *M. tuberculosis* especially concerning fatty acid metabolism (Wipperman et al., 2014). For example, *M. tuberculosis'* genome encodes 35 copies of FadE. It would be theorised that this genetic diversity allows a great deal of flexibility in an unstable environment and allowing adaptation of the pathway in spite of adverse conditions.

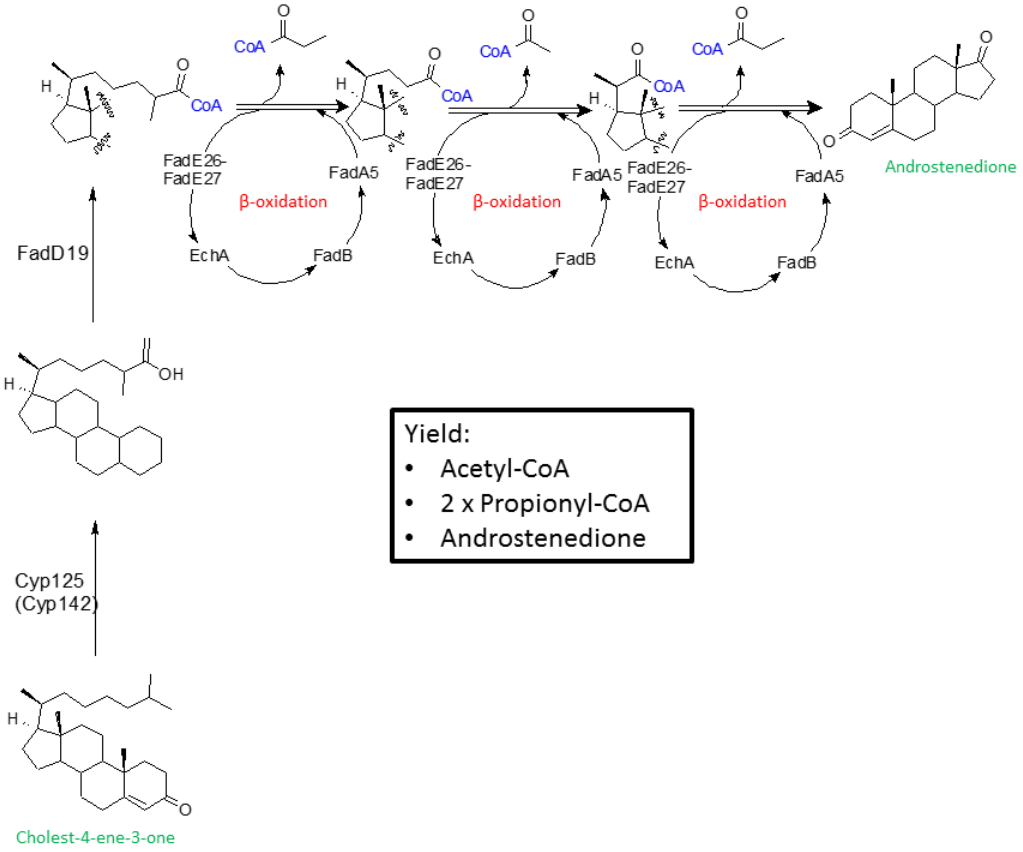

Figure 1.14: **β-oxidation subpathway of cholesterol catabolism**

1.2.2.2 Catabolism of the A/B Ring of Cholesterol

The first step to start the process of cholesterol metabolism is the conversion of cholesterol to cholest-4-ene-3-one by (3β-hydroxysteroid dehydrogenase) 3 β-Hsd as discussed above. For brevity's sake, this summary will pick up where the side chain oxidation left off with androstendione (AD), although in reality it is more likely that these two processes happen concurrently. The breakdown of the A and B rings of cholesterol start with the desaturation of the A ring by ketosteroid dehydrogenase (KstD) which gives the next breakdown product 1,4-androstendione (ADD) (Knol et al., 2008) (Figure 1.15). KstD is also essential *M. tuberculosis* growth in a minimal media supplemented cholesterol similar to the one used in this thesis (Griffin et al., 2011). The next step is catalysed by 3-ketosteroid 9α-hydroxylase (KshA/KshB) acting in complex as a monooxygenase/reductase pair (Capyk et al., 2009, 2011). This complex hydroxylates ADD to form an unstable intermediate, 9-hydroxy-androsta-1,4-diene-3,17-dione (9OHADD) (Figure 1.15). This instability in 9OHADD leads to the spontaneous cleavage of the B ring. Additionally, as a result of the above reactions the cholesterol A ring is aromatised. The activity of the KshA/KshB complex directly leads to the production of intermediate 3-hydroxy-9,10-seconandrost-1,3,5(10)-triene-9,17-dione (3-HSA), where the B ring has been completely opened (Figure 1.15).

The next step is the purview of two enzymes 3-hydroxy-9,10-seconandrost-1,3,5(10)-triene-9,17-dione 4-monooxygenase (HsaA/HsaB) acting as a flavin dependent monooxygenase with the oxidase being HsaA and the reductase HsaB (Dresen et al., 2010). The complex used activated riboflavin-5-phosphate or flavin mononucleotide (FMN/$FMNH_2$) and oxygen to hydroxylated 3-HSA to 3,4-DHSA. In the next step, the A ring of cholesterol is broken down. The step is catalysed by HsaC and linearises the A ring to produce 4,9-DHSA (van der Geize et al., 2007). HsaC is another protein in this pathway, which has been proven to be essential for growth on cholesterol media, however, when grown on glycerol (i.e as in ADC enriched 7H9 media) HsaC is not essential. At the point in the cholesterol breakdown pathway, the C

and D ring of cholesterol are as of yet untouched, but the A/B rings are completely linearised (Figure 1.15).

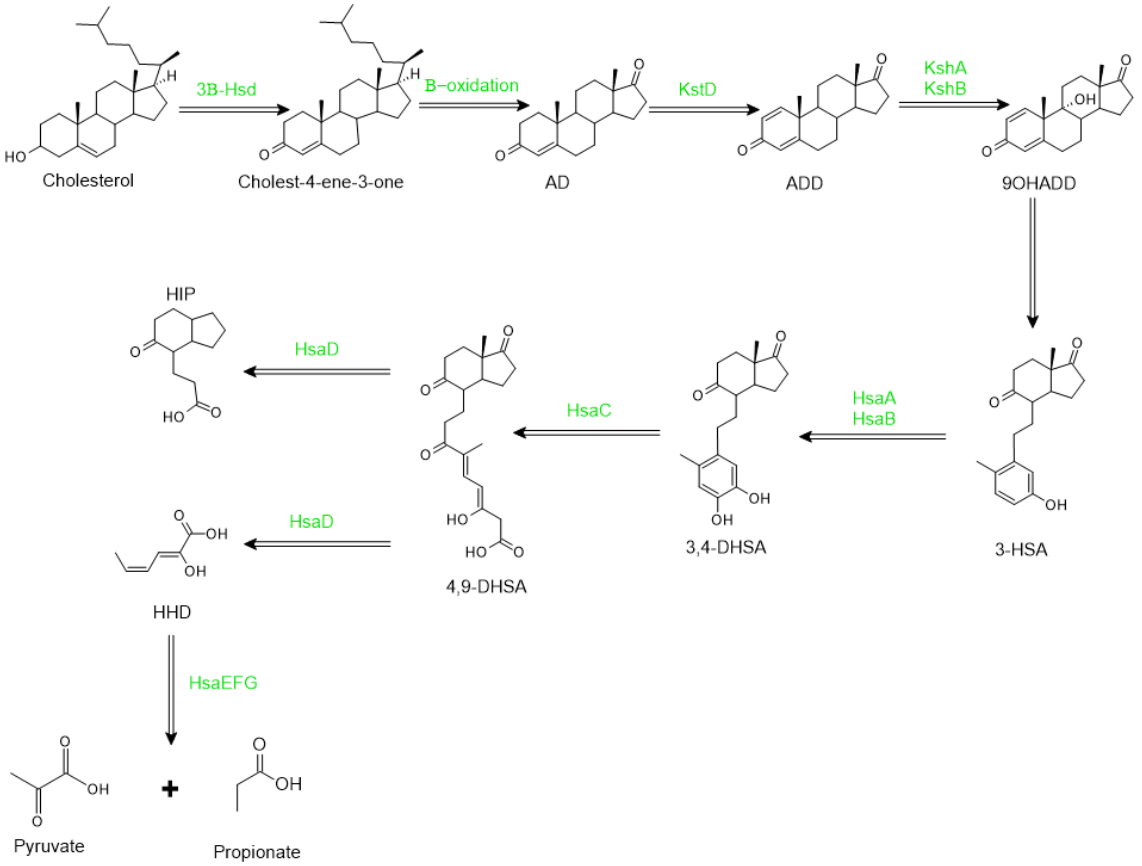

Figure 1.15: **Summary of the cholesterol catabolism pathway in *Mycobacterium tuberculosis*, specifically the A/B ring breakdown**

Acronyms are as follows: HSD: 3β-hydroxysteroid dehydrogenase; ChoE: cholesterol oxidase; KstD: ketosteroid dehydrogenase; KshA/B: 3-ketosteroid 9α-hydroxylase; HsaA/B: 3-hydroxy-9,10-seconandrost-1,3,5(10)-triene-9,17-dione 4-monooxygenase; HsaC: 3,4-dihydroxy-9,10-secoandrosta-1,3,5(10)-triene-9,17-dione 4,5-dioxygenase; HsaD: 4,5-9,10-diseco-3-hydroxy-5,9,17-trioxoandrosta-1(10),2-diene-4-oate hydrolase; HsaE: 2-hydroxyhexa-2,4-dienoate hydratase; HsaF: 4-hydroxy-2-oxohexanoate aldolase; HsaG: propanal dehydrogenase. Abbreviations of compound names: AD: 4-androstenedione; ADD: 1,4-androstenedione; 9OHADD: 9-hydroxy-androsta-1,4-diene-3,17-dione; 3-HSA: 3-hydroxy-9,10-seconandrost-1,3,5(10)-triene-9,17-dione; 3,4-DSHA: 3,4-dihydroxy-9,10-seconandrost-1,3,5(10)-triene-9,17-dione; 4,9-DSHA: 4,5–9,10-diseco-3-hydroxy-5,9,17-trioxoandrosta-1(10),2-diene-4-oic acid; HIP: 3aα-H-4α(3′-propanoyl-CoA)-7aβ-methylhexa-hydroindane-1,5-dione; HHD: 2-hydroxy-hexa-2,4-dienoic acid

The final intermediary in this section of the breakdown, 4,9-DHSA, is split into two different molecules by the hydrolase HsaD. 4,9-DHSA is broken down into HHD and HIP (Figure 1.15). HIP becomes the molecule taken forward into the C/D ring breakdown section of this pathway (*see* **section 1.2.2.3**). However, HHD is then split into the final breakdown products of this section of the pathway. The final elements of the of Hsa codon – HsaE, HsaF, HsaG – cleaves the HHD molecule and adds CoA to each part. This produces one molecule of pyruvate and one molecule of propionyl-CoA.

1.2.2.3 Catabolism of the C/D Ring of Cholesterol

The metabolism of the C/D rings of cholesterol are slightly more mysterious than the relatively well characterised metabolism of the A/B rings. The summary of the breakdown below consists of what the current theorised method is; several of these steps have not been proved. Additionally, the yield from the breakdown isn't particularly clear. This process will release a molecule of acetyl-CoA and possibly a molecule or either propionyl CoA or succinyl-CoA with the potential for additional molecules of acetyl-CoA.

The metabolism of the C/D ring of cholesterol is picked up when the acyl-CoA synthase (FadD3) ligates a CoA molecule onto HIP which was one of the final breakdown products of the A/B ring metabolism. From this point it becomes very novel, there are a few studies detailing some enzymes that could be involved in the degradation of HIP-CoA but we don't have the full picture. However, accumulation studies leads to the conclusion that the D ring is opened before the C ring.

1.2.2.5 Utilisation of the Breakdown products of Cholesterol Catabolism

The products of cholesterol catabolism are varied and fit into the metabolistic pathways in different ways. The major products from the above breakdown pathways are propionyl-CoA which unlike acetyl-CoA does not feed directly into the citric acid cycle (TCA cycle). Instead propionyl-CoA is incorporated into several separate breakdown cycles before the TCA cycle. These cycles are of critical importance to cholesterol catabolism for if propionyl-CoA is allowed to build up it becomes toxic to the bacterium. There are two different cycles that *M. tuberculosis* possesses for the anaplerotic metabolism of propionyl CoA into the central metabolism process. The methylcitrate cycle (MCC) which oxidises propionyl-CoA into pyruvate (Muñoz-Elías et al., 2006). Pyruvate, via the enzyme pyruvate carboxylase can be directly incorporated into the TCA cycle by conversion into oxaloacetate. The presence of the MCC in *M. tuberculosis* was discovered through a series of knockout studies which highlighted the essentiality of ICL1/ICL2 (Muñoz-Elías et al., 2006; Muñoz-Elías & McKinney, 2005). The second pathway used to metabolise propionyl CoA is called the methylmalonyl cycle (Savvi et al., 2008). The cycle exists separately to the previous MCC and functionally metabolises propionyl-CoA even if the other pathways have been compromised. The methylmalonyl also utilises a vitamin B-12 cofactor which perhaps is the indicator for a vitamin B-12 regulator for the cycle. A brief summary of the process of the methylmalonyl cycle is as follows. Propionyl-CoA is converted to methylmalonyl-CoA with the incorporation of CO_2 by methylmalonyl-CoA carboxylase. This is converted to succinyl-CoA by methylmalonyl-CoA mutase which is the enzyme that is vitamin B-12 dependant. Succinyl-CoA is incorporated into the TCA cycle as succinate and produces energy through this pathway. This is also the process for the possible molecule of succinyl-CoA produced by the C/D ring metabolism. The molecule of pyruvate that is produced from the metabolism of the A/B rings is typically incorporated into the TCA cycle as with the MCC cycle (Wilburn et al., 2018; Wipperman et al., 2014). The molecules of acetyl-CoA that are produced majorly from the β-oxidation of the side chain are directly entered into the TCA cycle to produce vital ATP.

1.3 Models of Latent Tuberculosis Infection and Non-Replicating Persistence

(Guirado & Schlesinger, 2013; Wayne & Sohaskey, 2001)Conditions found within the granuloma are key to the NRP state and accurately mimicking these conditions *in vitro* facilitates study and drug susceptibility testing of a fastidious bacterial state (Guirado & Schlesinger, 2013; Wayne & Sohaskey, 2001). The environment in the granuloma has a distinct profile that includes hypoxia, nutrient deprivation, limited carbon sources and a high concentration of Nitric Oxide (NO) (Parish, 2020). Most of the above environmental conditions have been shown to induce the NRP state in mycobacteria individually (Figure 1.16). Most *in vitro* models focus on one of the conditions in isolation - although there are a few that combine

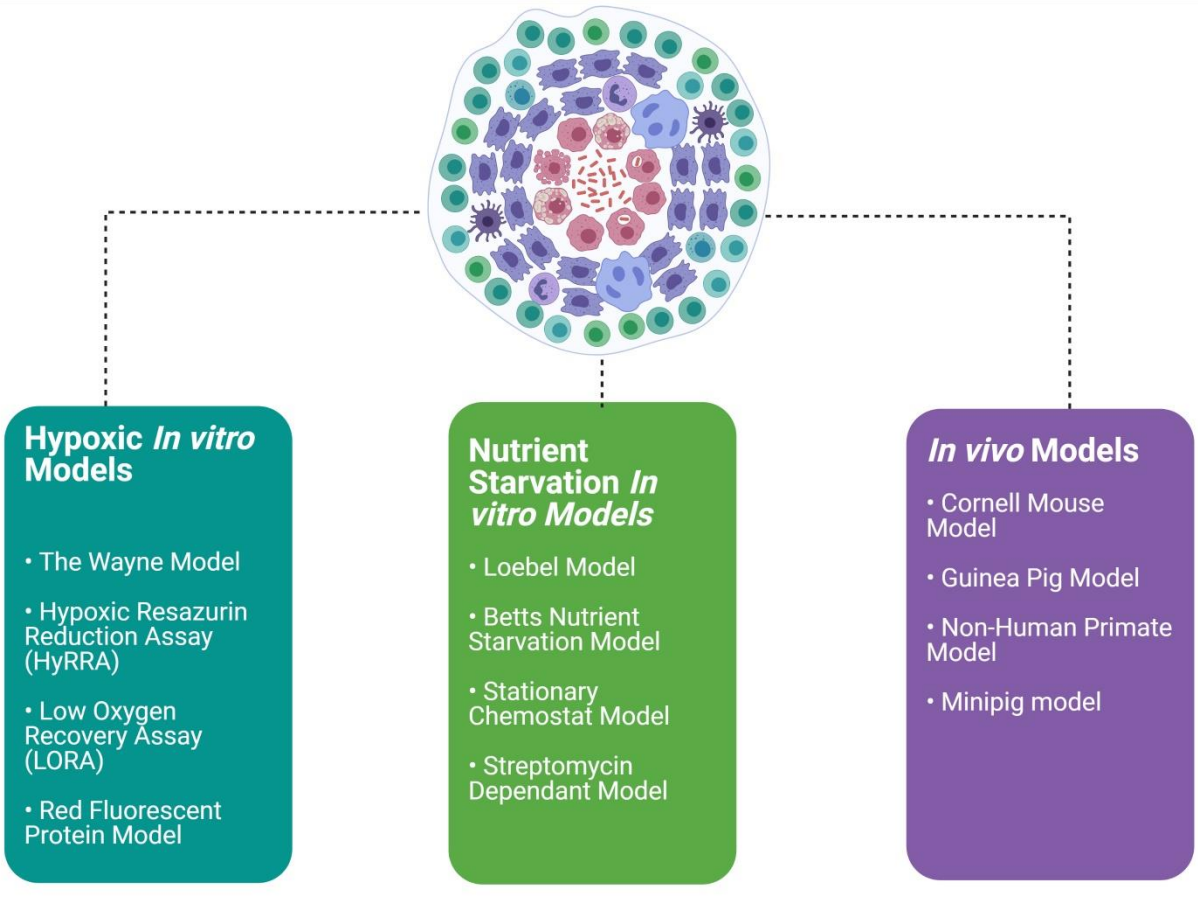

Figure 1.16: **Summary Figure of the *in vivo* Models of Latent Tuberculosis and the *in vitro* models of NRP *M. tuberculosis***

two conditions in their model.

Interestingly, despite using the same bacterium, a difference in NRP-inducing factor can completely alter the bacterial phenotype (Figure 1.16). There are differences in genetic expression, leading to differences in metabolism, physiology, and antimicrobial susceptibility.

Due to the differences in NRP when using different conditions of the granuloma, a lot of confusion has arisen about the true phenotype of NRP *M. tuberculosis.* This confliction is especially bewildering over drug susceptibilities. Certain *in vitro* models report antimicrobial resistances and susceptibility, but another *in vitro* model could report a different drug profile. This difference is due to only using a single NRP-inducing factor to trigger *M. tuberculosis,* whereas in a granuloma, these factors happen in synchronisation. A combination of NRP-inducing factors could then produce an additional phenotype; one that is potentially closer to that found clinically.

1.3.1 Hypoxia

the gradual depletion of oxygen until a hypoxic atmosphere is reached is a key element of the granuloma. Hypoxia was one of the first conditions of the granuloma identified and as such, it is the best characterised. The following models all focus on modelling the hypoxic element of the granuloma to trigger the NRP state, starting with the original and most famous NRP model, the Wayne Model (Figure 1.16).

1.3.1.1 The Wayne Model

In 1976, Lawrence Wayne made the observation that whilst an *M. tuberculosis* culture was aerated, growth would continue in a logarithmic fashion; if aeration was stopped, the culture settled and the concentration of dissolved O_2 (dO_2) decreases, growth would arrest seemingly indefinitely (Parish et al., 2003). The concentration of dO_2 was increased by shaking, which lead to the continuation of exponential growth after an extended period of time in an arrested state. He referred to this physiological state as non-replicating persistence (NRP) to reflect the differences (Boon et al., 2001; Wayne & Sohaskey, 2001). The aim of this model was to simulate the gradual depletion of oxygen in the granuloma. The organisms were grown in sealed containers with a controlled ratio of air to culture medium equalling 0.5. This ratio is called the Head Space Ratio (HSR). As the culture grows aerobically, it slowly uses up all the oxygen in the HSR: thus, creating the slow shift down into anaerobic conditions due to the reduction in dO_2. This model contains two distinct states of NRP. The first – or NRP stage I - occurs just as the oxygen saturation in the HSR reaches 1% (Boon et al., 2001; Desjardin et al., 2001; Wayne & Hayes, 1996). This stage is described as “microaerophilic”, where the bacilli are no longer replicating or conducting DNA synthesis but still have high levels of ATP production and some active mechanisms of DNA repair (Patel et al., 2011; Voskuil et al., 2004). This is followed by NRP stage II, characterised by fully anaerobic conditions defined as below 0.06% oxygen saturation (Gopinath et al., 2015; Jakkala & Ajitkumar, 2019). NRP stage II is the phenotype most often referred to when describing NRP *M. tuberculosis.* It is important to note that *M. tuberculosis* cannot survive if placed straight into NRP stage II conditions: the

process of steady decrease in oxygen saturation in NRP stage I is necessary to achieve NRP stage II (Wayne & Hayes, 1996). Hypoxia is confirmed by the decolourisation of methylene blue (concentration of 1.5 µg/mL) and by a stabilisation of the growth curve into a plateau, sometimes referred to as an early stationary phase (S. H. Cho et al., 2006; Wayne & Hayes, 1998). Under a hypoxia model, *M. tuberculosis* is indifferent to the presence of Isoniazid but the presence of Metronidazole (MET) has a bactericidal effect (Wayne & Sramek, 1994). This is directly opposed to the effect of these drugs in aerobic conditions where INH has a bactericidal effect on *M. tuberculosis* but MET has no inhibitory effect (Klinkenberg et al., 2008).

Nevertheless, this model is still frequently used in research and has provided significant contributions of knowledge and insight into NRP physiology. In addition, a large majority of recent models borrow heavily from the Wayne model. Therefore, this ground-breaking starting point has paved the way for a multitude of other models for NRP in *M. tuberculosis*.

1.3.1.2 Hypoxic Resazurin Reduction Assay (HyRRA)

The following model is an adaptation of the Wayne model to place the focus on high throughput screening (HTS). The HyRRA model is based on principles from the Wayne model and an aerobic HTS *M. tuberculosis* assay called Resazurin Microtitre Assay (REMA) (Collins & Franzblau, 1997; Sarker et al., 2007; Taneja & Tyagi, 2007). Colorimetric assays such as REMA or an Alamar blue assay have become as common as rapid, inexpensive methods of visual minimum inhibitory concentration (MIC) identification (Collins & Franzblau, 1997; Sarker et al., 2007).

The HyRRA was tested on *M. tuberculosis* H37Rv, *Mycobacterium smegmatis* and *Mycobacterium bovis* BCG (Taneja & Tyagi, 2007). This cell viability assay was then used to screen a large antibiotic panel using this model and compare the MICs of these compounds against previous models' findings and classic CFU/mL assay (Murugasu-Oei & Dick, 2000). The MICs identified by the colourimetric assay were found to be comparable to those found from CFU counts. They found activity against NRP *M. tuberculosis* from nitrofurans, such as

nitrofurantoin (Murugasu-Oei & Dick, 2000). As this is a hypoxia induced NRP assay, the bacteria tested show sensitivity to MET and tolerance to INH and RIF.

This model facilitates the scaling down of NRP *M. tuberculosis* drug testing to enable HTS, improving the discovery of new antimicrobials expeditiously. The HyRRA solely focuses on one stress condition that can induce the NRP state in mycobacteria (Taneja & Tyagi, 2007). This induction facilitates compound testing on mycobacteria in the NRP but without the other conditions, the compound testing does not accurately mimic the multiple stresses of the *in vivo* conditions and as such will produce many false positives. Additionally, many compounds could take longer than 96hrs to depict a sterilising action and so this method could exclude some potential slow actinng compounds.

1.3.1.3 Low Oxygen Recovery Assay (LORA)

Another example of a hypoxia driven NRP assay that's focus is HTS is the Low Oxygen Recovery Assay (LORA) (S. Cho et al., 2015; S. H. Cho et al., 2007). Large elements of this model are based on the Wayne model so perhaps could be characterised as an adaptation of the Wayne model instead of a standalone model (Parish et al., 2003; Wayne & Hayes, 1998). The LORA assay makes use of a luciferase reporter (*luxAB* gene) to depict the metabolic activity level of cells and the authors showed that, on entrance to the NRP state, luminescence decreased but remained present and constant as the experiment progressed (Chaiyen et al., 2001; S. Cho et al., 2015; S. H. Cho et al., 2007; Snewin et al., 1999). In short, the recombinant *M. tuberculosis* H37Rv was hypoxically triggered into NRP stage II via the Wayne model, albeit using a chemostat for higher regulation. After 22 days under these conditions with regular optical density readings (OD_{570nm}), CFU counts, and Relative Light Unit (RLU) readings taken, the cultures were spun down in PBS and frozen at -80 °C. These stocks were resuscitated and challenged with antimicrobial agents for 10 days under anaerobic conditions and then given a day's aerobic recovery. Again, luminescence and CFU counts were taken.

The authors tested 31 antimicrobial compounds using this model and compared this to a comparative aerobic counterpart and previously recorded results. As found in the Wayne

model, the hypoxic NRP *M. tuberculosis* is tolerant to the presence of INH. Other cell wall targeting drugs were also found to be inactive such as Ethambutol and Cycloserine (S. H. Cho et al., 2007). This speaks to the belief that without replication, production of cell wall building blocks is heavily slowed or stopped; rendering many cell wall targeting drug ineffective. Those drugs with intracellular targets such as Metronidazole and compounds, including Capreomycin that target the 30S ribosomal subunit, gain activity (Heifets et al., 2005).

An example of the LORA being used to identified novel compounds was shown by Bonnett *et al.* where they identify hydrazones as active against NRP *M. tuberculosis* (Bonnett et al., 2016, 2018). These hydrazones were previously identified as effective compounds against active TB. They drug target was found to be the enzyme LepB which is a crucial part of the general secretion pathway of *M. tuberculosis* (Bonnett et al., 2018).

The use of a luciferase reporter to monitor entry to the NRP state as well as drug activity is novel. This provides a wider range of information than what could be gleaned from previous models such as the HyRRA which uses a qualitative measure to determine the culture entry to NRP (Taneja & Tyagi, 2007).

This model is based on determining the MIC of novel compounds whose activity and target may not have been identified. The luciferase reporter enabled assessment of the metabolic activity observed in the NRP state. However, to transform the *M. tuberculosis,* a kanamycin selective marker was used (Snewin et al., 1999). This means that the recombinant *M. tuberculosis* H37Rv-*luxAB* is resistant to kanamycin (S. H. Cho et al., 2007). This has the potential to confer some level of resistance to other antimicrobials. This is especially relevant when conducting a HTS on novel compounds. This could lead to the elimination of some compounds that could have powerful sterilising activity.

Finally, this assay requires special instruments (Anoxomat system) and is expensive to run with a high cost of reagents and equipment. Generally, the optimal HTS should be as inexpensive as possible because of the potential low yield of active compounds (White, 2000)

1.3.1.4 Red Fluorescent Protein (RFP) Model (Paraffin Model)

This model is also a HTS of NRP *M. tuberculosis* that is based on the hypoxic element of the granuloma (Barry et al., 2009b; Sakamoto, 2012). The Red Fluorescent Protein (RFP) model aims to overcome this hurdle by combining molecular biology techniques and a different method of excluding oxygen (Yeware & Sarkar, 2018).

Red fluorescent protein can be utilised as a reporter for gene expression and so can be used to determine the difference between an actively growing culture, a stationary culture and a culture affected by a bactericidal drug (Carroll et al., 2010). RFP protein was transformed into *M. tuberculosis* H37Rv using the pCHERRY3 plasmid (Anand et al., 2015).

Cultures were grown aerobically in microtitre plates and then a layer of paraffin oil was added on top of the culture which oxygen cannot permeate (Hugh & Leifson, 1953). To test if the culture is hypoxic, methylene blue was added (1.5 µg/mL), which decolourises in the absence of oxygen (Wayne & Hayes, 1998). This was incubated for 13 days, at which point compounds were injected into the hypoxic cultures through the paraffin oil layer. This was then incubated for a further 20 days with daily fluorescence readings taken (Yeware & Sarkar, 2018).

A wide range of compounds were tested, each chosen for their differing modes of action (61). A notable feature of all the previous hypoxia models is sensitivity to MET (S. H. Cho et al., 2007; Iona et al., 2016; Taneja & Tyagi, 2007; Wayne & Sohaskey, 2001). Interestingly, the RFP model does not show any sensitivity to MET. The authors postulate that this discrepancy could be due to MET being a pro-drug and its activation is largely based on the state of the bacilli (Yeware & Sarkar, 2018). However, this sensitivity to MET is not seen in any *in vivo* test, therefore, this lack of sensitivity could indicate an improved physiological advantage to the Paraffin model (Hoff et al., 2008; Klinkenberg et al., 2008). This model also highlighted the extended period of time needed for some compounds to show activity such as the aminoglycosides. Many previous models did not expose the cultures to the compounds for this extended period. The drug tolerant nature of the bacilli can require a large lead time before the compounds take effect (Gopinath et al., 2015).

A large advantage of this model is that it maintains hypoxia throughout the experiment. Many of the previous models' test drug susceptibility through a regrowth assay; this has a danger that instead of drug testing on a hypoxic NRP mycobacteria culture, drug activity against resuscitating bacteria is being monitored.

Introduced in 2018, this model represents the most recent offering towards NRP research and addresses some of the issues with previous models. Nevertheless, there are disadvantages associated with this model. As with the LORA, this model utilises a transformed version of *M. tuberculosis* (S. H. Cho et al., 2007). This involved the transformation of *M. tuberculosis* H37Rv with RFP using the pCHERRY3 plasmid, which uses a hygromycin selective marker (Yeware & Sarkar, 2018). Using a culture that already has some resistance to antimicrobial is not ideal as it could lead to some level of cross-resistance to other antibiotics.

1.3.2 Nutrient Starvation and Selective Carbon Sources

Reports of *M. tuberculosis* survival date back to 1933 (Loebel et al., 1933a, 1933b) In recent years, this work has been further developed and has shown that granuloma-based bacteria that are not precisely nutrient starved, rather nutrient deprived (Loebel et al., 1933a, 1933b). Metabolism is restricted to odd chain fatty acids as the sole carbon source, and largely the fatty acid of choice is cholesterol (Muñoz-Elías et al., 2006; Soto-Ramirez et al., 2017). The effect of nutrient starvation has been less studied than hypoxia; however, the below models all demonstrably show that they can model NRP *M. tuberculosis* albeit with a different drug sensitivity profile to that observed in hypoxia-derived NRP *Mycobacteria* (Figure 1.16).

1.3.2.1The Nutrient Starvation Model

In 1933, *in vitro* TB research was still relatively new; Loebel and his team demonstrated that it is possible to transfer an *M. tuberculosis* culture out of rich media into PBS, which then can be left in solution for many years (Loebel et al., 1933a, 1933b). Respiration levels slowly decreased and the culture remained in early stationary phase; however, upon reintroduction to rich media, respiration levels increased and the bacterial cells resumed normal growth. Loebel concluded that it was possible for *M. tuberculosis* to survive for an extended period of time and that this virulence factor could be attributed to the bacteria's ability to "depress its oxygen consumption and to live off previously stored foodstuffs". This postulate was later proved to be correct by subsequent models (Betts et al., 2002).

M. tuberculosis from a granuloma has a different morphology to those grown *in vitro,* however, nutrient starved *M. tuberculosis* has a similar morphology to the *in vivo* phenotype (Bacon et al., 2014). This would suggest that nutrient deprivation is an essential environmental condition in the granuloma with an altered genetic profile that *in vivo* could work in conjunction with hypoxia-activated genes to produce the clinical phenotype (Betts et al., 2002; Gopinath et al., 2015; Soto-Ramirez et al., 2017). Betts and her research team developed a model based on Loebel's earlier work that would stop respiration and halt replication but kept the bacteria viable (Gengenbacher et al., 2010; Loebel et al., 1933a, 1933b).

In this model, bacteria are grown for 7 days in nutrient rich media at which point they are pelleted and resuspended in PBS and are incubated at 37 °C in sealed containers (Betts et al., 2002). Viability is determined by CFU counts at sequential points. Despite no growth at any point, the CFU counts remained consistent throughout, which indicated that the NRP state had been achieved. Interestingly, despite being cultured in a sealed container, similar to the Wayne model, there is no decolourisation of methylene blue which shows that oxygen is still present in the cultures (Betts et al., 2002).

The Wayne model was used as a control and as previously seen, after 10 days in sealed containers containing rich media, the culture decolourised methylene blue and entered hypoxia (Wayne & Hayes, 1996, 1998).

This led to the hypothesis that, instead of the oxygen being consumed, as in the Wayne model, the bacilli slowed down their respiration levels and thus entered the NRP state (Betts et al., 2002; Wayne & Sohaskey, 2001). In this model of NRP, bacteria gain resistance to INH and RIF, however, they do not gain susceptibility to MET (Betts et al., 2002). This is one of the primary differences between the Nutrient Deprivation model and the Wayne model.

Expression of *sigB* has been associated with the transition into stationary phase and has also been associated with stress conditions (Hu & Coates, 1999; Manganelli et al., 1999). An analysis of the whole transcriptome of *M. tuberculosis* in both models showed many similarities including an adaptation in metabolism. However, whilst the model shared 50 “top scoring” genes with the Wayne model, there were over 200 different upregulated genes (Betts et al., 2002).

This is also a widely accepted model of NRP, made interesting by its different drug susceptibility to the Wayne model. This difference could be attributed to its distinctly different transcriptome (Gengenbacher et al., 2010). Nevertheless, entry into the NRP state can be observed despite oxygen being abundant (Betts et al., 2002). All the above evidence seems

to imply that both nutrient starvation and hypoxia are essential conditions in the granuloma to provide the right environment for NRP.

1.3.2.2 Stationary Chemostat Model

Building on this work into investigating the effect of nutrient deprivation on *M. tuberculosis,* a new model was proposed which aimed to use a chemostat to tightly control conditions such as pH, temperature and dissolved oxygen (Betts et al., 2002; Hampshire et al., 2004; Loebel et al., 1933a, 1933b). This stationary chemostat model would allow the long-term maintenance of an NRP culture. Chemostats have been utilised by scientists attempting to culture many different bacterial species under challenging conditions as it allows greater control of the environment than traditional culture methods (Neijssel & Tempest, 1976; Tuomanen et al., 1986; van Andel et al., 1985).

This model cultured *M. tuberculosis* H37Rv in 750 mL of ADC enriched Middlebrook 7H9 broth with a defined dissolved oxygen concentration of 50%. This culture was then maintained until all the nutrients has been depleted; this slowing of growth was defined as stationary. The depletion of glucose and glycerol was monitored by biochemical assays over the duration of the experiment. Culture samples were extracted from the chemostat at intervals throughout the experiment and plated for CFU counts. To monitor the transcriptome of the culture, RNA was extracted at various time points throughout the experiment.

The authors have based this model on the theory that there is a proportion of bacteria that go into an extended stationary phase in response to an external pressure, similar to what is seen in *Escherichia coli* (Tuomanen et al., 1986). This could be generated *in vivo* by exposure to antibiotics to which a small proportion of the population would survive (persister population). They observed what they have defined as stationary phase up until day 80, which they attribute to nutrient deprivation, at which point the culture restarts growth. This revival is hypothesised to be the result of adaptation to the new growth environment.

The main advantage of this model is that it is conducted in a chemostat, which had not previously been explored as an option for NRP *M. tuberculosis.* Rigidly controlling the environment to simulate known conditions in the granuloma is a widely employed method of *in vitro* modelling.

An interesting facet of *M. tuberculosis* infection is the ability to survive extracellularly and intracellularly (J. D. Ernst, 2012). Hence, it is the intracellular bacterium that are mainly exposed to the conditions of the granuloma which are the driving force to the persistence of *M. tuberculosis* (Hernández-Pando et al., 2000; Wayne & Sohaskey, 2001). In addition, the culture showed a resuscitation at 80 days; as early as 1933, it was shown that *M. tuberculosis* can persist in sealed containers for 12 years (Corper & Cohn, 1951; Loebel et al., 1933a). This evidence in addition to patients reactivating after 20 years provides compelling evidence that this model does not achieve the persistent sate observed clinically (Gomez & McKinney, 2004).

Another hallmark of persistence of *M. tuberculosis* is the cessation of replication as observed by previous models (Betts et al., 2002; Corper & Cohn, 1951). The growth curves displayed in this model do not show a stable, persistent population but a population in a slow decline (Hampshire et al., 2004). This type of growth curve is more reminiscent of a culture in the decline phase of the growth curve: attributed to the depletion of glucose and glycogen. The original nutrient deprivation model utilised PBS, as have subsequent models, and have demonstrated long term persistence and viability (Betts et al., 2002; Loebel et al., 1933a).

This model has many promising features, such as the innovative use of a chemostat for NRP *M. tuberculosis* culture. However, to be utilised as a strict model of NRP, the media used in this study may need to be reviewed to reflect the long-term persistence seen in other models.

1.3.3 Streptomycin Dependant

A further example of an NRP model is the Streptomycin-dependant model which utilises 18b strain of *M. tuberculosis* which has mutated to only grow in the presence of Streptomycin (Hashimoto, 1955). When this antibiotic is removed, replication ceases (Sala et al., 2010). The

theory behind this model is that this cessation of replication due to the removal of Streptomycin could mimic the NRP state (Sala et al., 2010; Wayne & Sohaskey, 2001). Cultures were grown in Middlebrook 7H9 media in the presence of 50µg/ml of Streptomycin. The Streptomycin is removed, and the cultures are then starved for two weeks before being exposed to antimicrobial compounds. The protocol for drug testing is the REMA and it is the same method that the HyRRA is based on (*see* **section 1.3.1.2)** (Taneja & Tyagi, 2007).

This model reports an altered drug profile to those seen in more developed models (Sala et al., 2010). A full drug panel was screened against the model and showed no activity from INH but an increased susceptibility for front-line antibiotic Rifampicin (Sala et al., 2010). Also identified was the strong sterilising action of new TB compound of interest, PA-824 (Dawson et al., 2015; de Miranda Silva et al., 2019)

This model attempts to mimic entry into the NRP state by the removal of streptomycin. However, the NRP state is still not fully understood: the transcriptome and physiology can vary wildly between different models that exhibit different granuloma conditions (Betts et al., 2002; Wayne & Hayes, 1996). This model was presented as an easy, affordable and reliable way of conducting a HTS on NRP mycobacteria. The altered drug profile observed when using this model casts doubt on the ability to accurately screen *in vitro* for effective drugs *in vivo* (Klinkenberg et al., 2008). This is coupled with the model not mimicking any part of the granuloma, and as we do not yet know the implications of these environmental conditions, crucial elements of the NRP state could be missing from this model.

1.3.4 Low pH models

The core of the tuberculous granuloma is made up of the initial alveolar macrophages, which were first line of defence upon *M. tuberculosis* infection. Dependant on the activation state of the macrophages, the pH of the granuloma is lower than the external environment (Vandal et al., 2009). This added pressure is a by-product of macrophages activation and adds an extra layer of defence from the host macrophages (MacMicking et al., 2003; Schaible et al., 1998). Inside, the granuloma the *M. tuberculosis* reside in these activated macrophages and due to

this, they are exposed to this low pH environment of around 6.2 to 4.5 (Schaible et al., 1998; Vandal et al., 2009; Vla et al., 1998).

Interestingly, acidification is a known trigger in other pathogens to activate virulence factors and survival mechanisms in response to host defence. For example, *Listeria monocytogenes* recognises acidification as a sign to escape the phagosome (Beauregard et al., 1997; Conte et al., 1996). This gives a precedent for using the host defence mechanism of acidification as a transcription trigger.

As *M. tuberculosis* does not grow in a pH lower than 5.4, *Mycobacteria* were thought to be quite sensitive to acid; however, it was subsequently shown that whilst *Mycobacteria* no longer grew in a low pH environment, they remain alive (Parish, 2020; Vandal et al., 2009). This gives a precedent to suggest that low pH can be used as a trigger to drive the NRP state. Indeed, there is currently an *in vitro* model that is pre-publication that is investigating precisely whether low pH can be used as a sole NRP trigger *in vitro* and whether there is again, a different phenotype to be found (Parish, 2020).

1.3.5 Multi-Stress Models of NRP

As previously highlighted, the current models of NRP have provided a great deal of information about this elusive condition, however, contradictions from models using different NRP-inducing triggers has become bewildering. This has not gone unnoticed and scientists have attempted to find a more physiologically relevant alternative to the current single stress models with multi-stress models.

The first uses a combination of low oxygen, high CO2, nutrient deficiency and an acidic pH (5.0) to trigger *M. tuberculosis* H37Rv into the NRP state (Deb et al., 2009; Patel et al., 2011). Through a variety of methods including transcriptomic analysis via microarray an attempt was made to characterise the properties of the NRP bacteria. A change in morphology and loss of acid-fastness was also identified by this model (Deb et al., 2009)

1.3.6 *In vivo* models of NRP

LTBI has been acknowledged as a widespread problem for some time and many *in vivo* models have been developed to aid study into the infection and the bacterial adaptations (the NRP state) that occur (Guirado & Schlesinger, 2013; Houben & Dodd, 2016) (Figure 1.16).

Mice are typically the *in vivo* model organism of choice for many disease models such as cancer, auto immune and infectious disease. This is coupled with a relatively low cost and low maintenance levels. Indeed, mouse models are commonly used in active *M. tuberculosis* research to elucidate details on how the infection progresses (Orme, 2003). The common use of mice in medical research mean that the mouse is incredibly well characterised and can be utilised in a variety of ways. The most common mouse model for LTBI is the Cornell mouse model. In summary, the mice are infected with a high dosage of *M. tuberculosis* and then treated with high dosage antibiotics (Isoniazid and Pyrazinamide) to keep the infection quiescent (Gupta & Katoch, 2005; Hu & Coates, 2018; MCCUNE & TOMPSETT, 1956). Ostensibly, the antibiotic treatment is used to kill the actively replicating populations and preserve the NRP populations, however, there is a high rate of spontaneous reactivation to active disease after the antibiotic therapy (Miyazaki et al., 1999). Whilst this model is widely used in research, doubt has been cast on the reliability of it as a model of latent infection, the practice of keeping an infection quiescent using antimicrobial therapy is more in keeping with a chronic disease and may not be able to trigger the NRP state in the *M. tuberculosis* (Guirado & Schlesinger, 2013; Patel et al., 2011). Additionally, mice lack the lung immune system to form the complex granuloma structure seen in human disease (Rhoades, 1997). Therefore, the *M. tuberculosis* are never subjected to the harsh granuloma environment that triggers the NRP state. For these reasons, it could be argued that the Cornell mouse model cannot accurately model the NRP state seen in *in vitro* models and the phenotype observed is from antibiotic treatment persisters, hence why maintenance of this “latent” state rarely progresses past three months.

Another commonly used animal model is the guinea pig model. Guinea pigs are capable of forming a more human-like granuloma structure. The use of this model has allowed for a greater understanding of the granuloma structure as a whole (Kashino et al., 2008). However, guinea pigs are very susceptible to *M. tuberculosis* even at a low dosage and therefore cannot establish a long term LTBI (J. A. L. Flynn, 2006; Lin & Flynn, 2010). Nevertheless, the exposure of *M. tuberculosis* to a granuloma environment presents an interesting area of research into the initial phase of NRP.

As is so often the case, the best animal model for modelling human disease is the non-human primate. As the closest relative to humans, non-human primates have the complex lung immune structure required to truly model LTBI. The progression of *M. tuberculosis* infection is notably similar to the observations of human disease. Indeed, the presence of LTBI was first characterised in a macaque model (Capuano et al., 2003; J. L. Flynn et al., 2003). Whilst being undoubtably the best and closest *in vivo* models, there are obvious limitations with this model. To mention but a few difficulties, the huge ethical considerations of testing on non-human primates, the associated high cost, the necessity of trained staff to deal with the large primates (J. L. Flynn et al., 2003). Whilst this model is the closest, for the ethical reasons alone it should be reserved for the screening of new vaccines and pre-human clinical trials.

Another more representative *in vivo* model of LTBI is the minipig model. A relatively recent addition, it builds upon the remarkably similar lung structure shared between pigs and humans. Indeed, there have been several cases of pig lungs transplanted successfully into humans (Mariscal et al., 2018). The minipig, similar to the non-human primate, possesses the lung structure to effectively model the complex LTBI and can form a granuloma composed of multiple immune cells (Gil et al., 2010). This *in vivo* model provides an attractive alternative to the non-human primate with a lesser degree of ethical concerns (Guirado & Schlesinger, 2013).

1.4 *Mycobacterium abscessus*

Slow growing *Mycobacteria* are commonly thought of as the main group of “true pathogens” of the *Mycobacterium* genus. Examples of these include the aforementioned pathogens: *M. leprae, M. tuberculosis and M. bovis.* To this end, it has been commonly believed that only these complex pathogens have the capability to enter into the NRP state. In recent years, there has been a realisation of the pathogenicity of some of the fast-growing *Mycobacteria* commonly called Non-Tuberculous Mycobacteria (NTMs) (De Groote & Huitt, 2006; Nessar et al., 2012; Zweijpfenning et al., 2018).

One such group of NTM is *Mycobacterium abscessus* and subspecies; this ubiquitous environmental microorganism was first in in 1953 in a knee abscessus and was thought to cause self-limiting subcutaneous infections (Moore & Frerichs, 1953). In the last 20 years, *M. abscessus* has become a common cause of lung infections particularly in immunocompromised patients (Jarand et al., 2011). Individuals suffering for chronic illnesses such as Cystic Fibrosis (CF), Chronic Obstructive Pulmonary Disorder (COPD) or bronchiectasis are particularly at risk from *M. abscessus* infection (Esther et al., 2010; Koh et al., 2011; Schuurbiers et al., 2020).

A major part of why *M. abscessus* infections can be so devastating is an almost unprecedented level of antimicrobial tolerance (Griffith, 2019; Nessar et al., 2012). This has led to the use of a broad range of antimicrobials in combination therapies for extended periods of treatment (M. R. Lee et al., 2015; Novosad et al., 2016). Commonly selected antimicrobials are Amikacin (AMI), Cefoxitin and Clarithromycin to form the baseline of an antimicrobial combination therapy (Koh et al., 2011; Shen et al., 2010). Additional drugs are then added for example, tigecycline, moxifloxacin, imipenem, minocycline and clofazimine (Griffith, 2019; Novosad et al., 2016). Due to the complicated nature of *M. abscessus* infection, these therapies are normally designed on a case-by-case basis directed by sensitivity testing as resistance to all of the above frontline antimicrobials is not uncommon (Griffith, 2019). In addition, the antimicrobials used are aggressive and lead to a high rate of side effects. Studies have found

that commonly used combination therapies for *M. abscessus* infection have anywhere between a 51% to a 71% side effect rate. For example, some of the side effects of the fluroquinolone Moxifloxacin are liver failure, seizures and peripheral neuropathy (Dawson et al., 2015).

The treatment for *M. abscessus* infection is normally carried out for at least 1 month for the full range of antibiotics and can continue for up to a year in a “continuation phase” that involves less antimicrobials to lessen the burden on the patient (Novosad et al., 2016). Despite frequent testing and case by case designed therapies to combat the infection, it is frequently observed that even though the *M. abscessus* has shown *in vitro* susceptibility in testing this fails to translate over to the *in vivo* treatment of the patient (Griffith, 2019; Huang et al., 2010).

All the above factors taken together creates a perfect storm; a patient who is already immunocompromised from chronic disease battling an infection which requires a huge number of harsh antimicrobials to treat over a greatly extended period of time which may not even clear the infection. It is clearly of great importance to find more reliable treatments and to try and discover more about what makes this opportunistic pathogen so hard to treat.

1.5 Aims and Objectives of this Thesis

The Non-Replicating Persistent state of *M. tuberculosis* has been contentious since its discovery. The disparate results and phenotypes revealed by using different *in vitro* models have cast doubt upon the current research as it appears inherently contradictory. This doubt is then amplified by conflicting results between *in vitro* research and *in vivo* research.

The Non-Replicating Persistent state of *M. tuberculosis* exists in a highly specific and complex environment. Previous literature has used one facet of this environment to model the NRP state *in vitro* (see section). The hypothesis of this thesis is that if multiple factors of the granuloma environment could be combined into a single *in vitro* model the resulting phenotype could prove more physiologically relevant than from previous models. This combined, “multi-stress” phenotype could bridge the gap in knowledge and settle the contradictions in NRP state research.

The first aim of this thesis, therefore, is to create and validate a multi-stress model of the NRP state. This *in vitro* model should aim to faithfully reflect the clinical condition of Latent Tuberculosis. To ensure this, the stresses chosen should represent the major environmental factors within the granuloma and should be guided by the current literature. The stresses chosen should consist of those that have been shown to produce different phenotype with the aim that a combination should result in a middle ground phenotype.

Once the *in vitro* model is validated, the next aim of this thesis is to utilise it to study the NRP state of *M. tuberculosis* with a focus on the antibiotic susceptibilities. To conduct this a broad range of antimicrobials will be tested against *M. bovis* BCG in the novel multi-stress model and in a control model (the Hypoxic model) which is

based on Wayne's seminal model. To gain a good picture of any changes to the antibiotic susceptibility profile both known antimicrobials that are currently in the clinical trial pipeline and novel compounds should be tested. A shift in antibiotic susceptibility profile could also provide an indication of phenotypic shift.

Any positive drug hits should be further investigated to detect the mode of action of the antimicrobial against NRP *M. tuberculosis*. This investigation is an important objective due to the stark differences between actively growing *M. tuberculosis* and latent, NRP *M. tuberculosis.* It has already been observed that the NRP state is "antibiotic indifferent". This indifference could be attributed to a lack of transcription of drug targets, drug targets rendered vestigial by the NRP state or a blockade of sorts preventing access to the drug targets in question. It is the aim of this thesis to illuminate the differences in profile between these two states and suggests where this indifference originates from.

The newly-emerging yet concerning pathogen *M. abscessus* is also addressed in this thesis as, whilst it is not a close relative of *M. tuberculosis,* there is a noted problem in the literature with chronic reoccurring infection. Thus, one of the aims of this PhD was to establish whether *M. abscessus* has the capability to enter the NRP state and the greater impact of this state would have on the infection as a whole.

The overall objective of this thesis is to shed more light on a crucial area of pathogenesis for the world's most prevalent infectious disease. This investigation hopes to identify novel and exploitable targets that can be utilised to control the spread and impact of this disease.

Chapter 2:

Development of a multi-stress, physiologically relevant *in vitro* model of Non-Replicating Persistent *Mycobacterium tuberculosis*

Chapter 2 Development of a multi-stress, physiologically relevant *in vitro* model of Non-Replicating Persistent *Mycobacterium tuberculosis*

2.1 Introduction

2.1.1 Impact of multiple NRP-driving factors on the bacterial phenotype

Since the discovery of the NRP state by Wayne in the 90s, the focus of NRP research has been on stimulating *Mycobacteria* to enter the NRP state by using a sole pressure from the granuloma environment (Gopinath et al., 2015; Iona et al., 2016; Jakkala & Ajitkumar, 2019; Wayne & Hayes, 1996). As previously mentioned (*see* **section 1.2**), the granuloma environment pressures generally used to initiate *in vitro* entry into the NRP state are: hypoxia, nutrient starvation/nutrient deprivation, low pH or high nitric oxide concentration (Bacon et al., 2014; Betts et al., 2002; Gibson et al., 2018; Y. J. Li et al., 2002; Wayne & Hayes, 1996). Most of these stresses have been shown to initiate *Mycobacteria* to enter the NRP state in isolation. The crucial facet is that each individual granuloma pressure produces a subtly different phenotype of NRP *Mycobacteria*. These different phenotypes have distinct proteomes and antibiotic susceptibility profiles, indicating a shift in priority dependant on the environment. The majority of previous research has used a single pressure model to conduct wide ranging research on the NRP state, however, research using different models is often contradictory, causing to widespread confusion. As a result, comparatively little is known about the NRP state as many discoveries can be contradicted using a different model. For an *in vitro* model to accurately represent the clinical state of infection, the model needs to contain a microcosm of the environment the bacteria find in that clinical state. Providing one element of this environment, even an important one, does not yield a faithful representation of the clinical phenotype and thus, discoveries from this may not be directly relatable. To get a true reflection of the NRP state and to produce accurate research *Mycobacteria* need to be induced into the NRP state via a conglomerate of stresses.

This has proved challenging in the past as the precise stresses present in a granuloma are not consistent as they depend on the state of the host immune system and the confluence of bacteria among other factors (Guirado & Schlesinger, 2013). In addition, subjecting *Mycobacteria* to multiple environmental challenges is a complicated procedure as, if the stress becomes too much the cells will not survive. This delicate balancing act between survivability and physiological relevance is key to producing a reliable multi-stress model.

2.1.2 NRP-driving factors chosen to create the Multi-Stress, Cholesterol model

The project was set out to create a more physiological relevant, multi-stress *in vitro* model of NRP *M. tuberculosis.* The importance of hypoxia to the granuloma environment has been thoroughly described (S. H. Cho et al., 2006; Honaker et al., 2009; Iona et al., 2016; Muttucumaru et al., 2004; Wayne & Sohaskey, 2001). The immune system limits bacterial access to oxygen as a method of controlling bacterial growth and the generalised strategy of hypoxia induced bacterial cell death (Ehlers & Schaible, 2012). In Wayne's seminal work that first drew interest to (and coined) the NRP state, hypoxia is the pressure used to trigger entry into the NRP state (Wayne & Hayes, 1996). As previously discussed, the bulk of NRP *M. tuberculosis* research is conducted in hypoxia-based models and the importance of a slow shiftdown into hypoxia has been highlighted many times as a key factor in the NRP state (Wayne, 1994; Wayne & Hayes, 1998).

Nevertheless, there another major NRP-inducing factor to take into account, however, this pressure is slightly more muddied on the importance – and relevance – to the NRP state as a whole. Previous studies has shown that nutrient starvation (in most cases, "culturing" in PBS) is an effective trigger of the NRP in *Mycobacteria* (Bacon et al., 2014; Betts et al., 2002). This method has been used to great effect for transcriptome/proteome analysis and has provided a scientific foil to the narrative of hypoxia-based NRP research.

The major limitation of the Nutrient Starvation method is that the interior of the granuloma is not a nutrient starved environment (Marques et al., 2015; Soto-Ramirez et al., 2017). Due partially to the high concentration of foamy macrophages present in the granuloma, the hypoxic core contains a great deal of cholesterol for *M. tuberculosis* to scavenge from the dead macrophages (Russell et al., 2009b). In addition, the interior of a granuloma contains some other metabolisable carbon sources, namely fatty acids (J. Daniel et al., 2011; Ghazaei, 2018; Guirado & Schlesinger, 2013; Sakamoto, 2012; Santucci et al., 2016). Cholesterol, in particular, has been proven to be present inside the granuloma and previous research has highlighted its importance to the NRP state (Gatfield & Pieters, 2000; Marques et al., 2015;

Soto-Ramirez et al., 2017; Wilburn et al., 2018). Cultures in the nutrient starvation model cease replication when placed in the “culture medium” which is typically PBS (Betts et al., 2002; Gengenbacher et al., 2010; Loebel et al., 1933a).There has been a great deal of research detailing the existence and importance of cholesterol and fatty acid metabolism to *M. tuberculosis* within the granuloma (Marques et al., 2015; Pandey & Sassetti, 2008; Soto-Ramirez et al., 2017; van der Geize et al., 2007; Wilburn et al., 2018). Thus, in the clinical condition NRP *Mycobacteria* cannot truly be called nutrient starved; a more accurate reflection would be nutrient deprived. Indeed, the consensus is that cholesterol is the sole carbon source within the granuloma.

One of the main aims of this thesis was to create a physiologically relevant multi-stress *in vitro* model of the NRP state. Thus, when designing a multi-stress, physiologically relevant model, it needed to have a slow shiftdown into full hypoxia and be nutrient deprived with Cholesterol as the sole carbon source.

2.1.3 Chapter 2 Aims and Objectives

Crucial to the success of investigating the NRP state of *M. tuberculosis* is the ability to model the bacterial state correctly *in vitro.* As discussed, the current *in vitro* models struggle to portray a physiologically accurate reflection of the NRP state. Thus, the aim of this chapter is to develop and validate an *in vitro* model containing multiple stresses representative of the granuloma environment so that the bacteria are exposed to a similar environment *in vitro*. If this objective is met, the bacterium cultured within this *in vitro* model should enter the NRP state. The secondary aim of this chapter is to test that the model can provide successful entry into the NRP state by searching for a cessation of growth along with other indicators of the NRP state. If identified, validation of the different elements of the NRP state in this novel model as opposed to current models will be examined with an aim to detect all similarities and differences.

2.2 Results and Discussion

2.2.1 Development of a novel Multi-Stress, Cholesterol model

One of the chosen NRP-inducing triggers for the novel model was cholesterol catabolism, specifically, to limit metabolise to solely cholesterol. Most media used to culture *M. tuberculosis* is rich in carbon sources. Therefore, a minimal cholesterol medium needed to be developed. Firstly, a base for the media was chosen. This was decided to be Middlebrook 7H9 media, although the similar Dubos medium was also considered (Middlebrook & Cohn, 1958; Wayne & Hayes, 1996). Middlebrook 7H9 media requires its carbon sources (glycerol and dextrose) to be added separately in an additive, commonly called ADC (Bovine Serum Albumin, Dextrose, Catalase). Without ADC, the base broth provides a good foundation of necessary minerals and nitrogen sources needed for stability of bacteria (Table 2.1). Middlebrook 7H9 media also requires the addition of surfactant Tween80, however it has recently been identified that *M. tuberculosis* can metabolise Tween80 which in a minimal media would not be acceptable (Pietersen et al., 2020). Attempts to grow *M. bovis* BCG (which is being used as a model organism for *M. tuberculosis*) in a medium that did not contain a surfactant were not met with success due to a high levels of “clumping”. An alternative surfactant was identified, Tyloxapol (Regev & Zana, 1999). Tyloxapol is a branched surfactant that *Mycobacteria* cannot metabolise due to the branching. Tyloxapol is included in the media not only as a surfactant but also as a solvent for the cholesterol additive (Table 2.2).

Cholesterol is a particularly challenging molecule to metabolise due to its near insolubility in water (Tak, 1942). Successful breakdown of this complex molecule can prove rewarding for the bacterium but requires a complicated pathway with many enzymes to catalyses the process (Wilburn et al., 2018; Wipperman et al., 2014). The addition of a high concentration of cholesterol to the minimal medium proved problematic. Solvents, such as ethanol, were required to dissolve the cholesterol but had to be in a low enough concentration so as not to impede bacterial growth. Building on previous research, many ways of dissolving cholesterol aliquots were tested (Griffin et al., 2012; Q. Li et al., 2016). It was found that the best method

for dissolving cholesterol was to dissolve approximately 100mg of cholesterol in a 1mL of solvent solution. This solvent solution is a 1:1 ratio composed of 100% ethanol:tyloxapol. When added to 1L of broth base is results in the desired 0.1 mg/mL (Table 2.2). The 1:1 ethanol:tyloxapol ratio was found to be superior to the 2:1 ethanol:tyloxapol ratio as it had small enough concentration of ethanol to not have a negative effect on microorganism growth while still dissolving the high concentration of cholesterol required.

Table 2.2: **Constituent Parts of Middlebrook 7H9 Broth Base**. When the MS, Cholesterol model was designed several broth bases were considered (i.e Dubos broth base). The Middlebrook 7H9 broth base was chosen for its wide nutritional base.

Components	Concentration	Application
Ammonium sulphate	0.5 g	Provides a nitrogen source
Disodium phosphate	2.5 g	
Monopotassium phosphate	1.0 g	
Sodium citrate	0.1 g	Can be converted to citric acid. Citric acid holds inorganic cations in solution
Magnesium sulphate	0.05 g	
Calcium chloride	0.5 mg	
Zinc sulphate	1.0 mg	Inorganic zinc acts as a growth stimulator
Copper sulphate	1.0 mg	Inorganic copper acts as a growth stimulator
Ferric ammonium citrate	0.04 g	
L-Glutamic acid	0.5 g	
Pyridoxine	1.0 mg	Precursor of enzymatic activity
Biotin	0.5 mg	Essential cofactor (i.e fatty acid biosynthesis)

Table 2.1: **Dissolved Cholesterol Supplement**

Minimal Cholesterol Media uses a cholesterol supplement with cholesterol dissolved in a hot tyloxapol:ethanol mixture

Components	Concentration (In 1 mL aliquot)	Concentration (In 1 L of media)	Application
Cholesterol	100 mg	0.1 mg	Carbon Source
Tyloxapol	500 µL	0.5 µL	Surfactant
Ethanol	500 µL	0.5 µL	Solvent

2.2.1.1 Initial Development of two models of NRP using a High Volume, Glass Culture Tube Method

With the minimal cholesterol media method established, it was identified that a control model that reflected results found in the literature should be developed. The Wayne model was chosen to be the comparison model, as it is the most commonly used model of NRP. The Wayne method was initially created using *M. tuberculosis* grown, in ADC enriched Middlebrook 7H9 media (7H9-ADC) in glass culture tubes that were placed on a slow moving (approximately 50-100 rpm) shaking platform to create the oxygen gradient characteristic of his model (Parish et al., 2003; Wayne & Hayes, 1996; Wayne & Sramek, 1994). However, this method took a long time to established hypoxia within the culture. Experiments were conducted using an anaerobic chamber to flush culture tubes and establish hypoxia in a shorter period of time without causing cell death. These initial experiments were conducted in glass culture tubes. The reasoning behind this is that *Mycobacteria* have a high likelihood of survival when in a larger culture volume (for example, 3-10mL). Using an anaerobic cabinet to increase the speed of the slow shiftdown of oxygen, *M. bovis* BCG cultures at approximately 0.3OD_{600nm} were set up in two distinct ways. For the Hypoxic model (the control model based on the Wayne model), *M. bovis* BCG were set up in 7H9-ADC broth with 0.05% Tween80 as a surfactant (*see* **section 7.3.1**). For the MS, Cholesterol model (the novel model), the cultures were in the minimal cholesterol media (*see* **section 7.3.2**). To provide a visual aid for saturated oxygen concentration, sterile methylene blue was added into each culture to a final concentration of 1.5 µg/mL. Methylene blue is a vivid blue in an aerobic atmosphere; however it begins to decolourise in microaerophilic conditions and in full anaerobiosis becomes completely transparent (Sumitani et al., 2004; Wayne & Hayes, 1996). Full decolourisation can act as a rudimentary marker of entry into NRP stage I. In both models, the cultures were placed in the anaerobic cabinet with the lids on but loose – this allows for a slow gas exchange (Figure 2.1).

Initially, the method was developed with the removal of the lids upon entry to the anaerobic cabinet. This led to a quick gas exchange and, particularly in the Hypoxic model, resulted in bacterial cell death. If the oxygen gradient and exchange is too severe, the *Mycobacteria* cannot perform the necessary metabolic and transcriptomic shifts to adapt to the higher pressure environment. Whereas, in a real granuloma, once the bacteria are walled into the central granuloma environment oxygen decreases when it is utilised for respiration and is not replaced which results in a slow shiftdown of oxygen saturation . This protocol was therefore adapted to leaving the lids on but loose to facilitate a slower gas exchange. The finalised procedure for both models of NRP can be found in Figure 2.1.

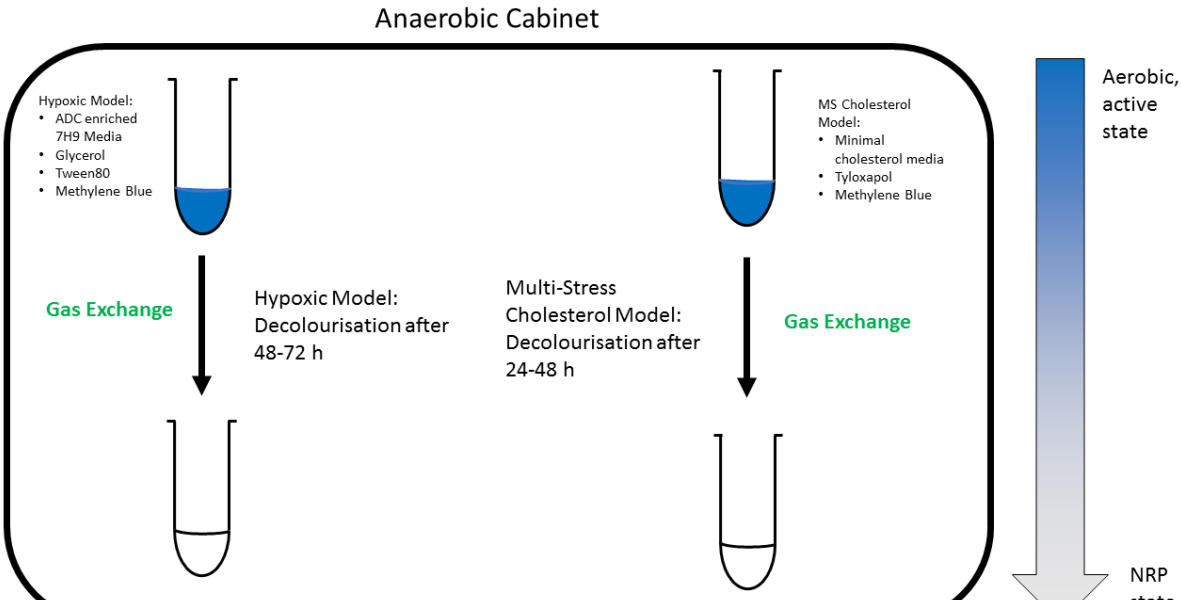

Figure 2.1: **The procedures of the two NRP models and their salient differences**. On the lefthand side is the Hypoxic model, which utilises 7H9-ADC media and requires a gas exchange period of 48-72 h in the anaerobic chamber. On the righthand side is the Multi-Stress, Cholesterol model (MS, Cholesterol model), which uses minimal cholesterol media and requires a shorter gas exchange period of 24-48 h before decolourisation occurs.

2.2.1.2 Identification of a stable, hypoxic sealant for glass culture tubes

Once the tubes were fully degassed in the anaerobic cabinet (characterised by the decolourisation of methylene blue), the tubes were sealed to preserve the anaerobic atmosphere and removed from the anaerobic cabinet to be incubated on a shaking platform (*see* **section 7.3**). Finding a sealant to reliably maintain an airtight seal was a challenging part of the development of this assay. Stereotypically, most bacterial assays do not progress past two weeks of incubation (~200 h) and are always incubated with seals that permit gas exchange. As in the NRP state, *M. tuberculosis* will remain stationary, if conditions remain the same, the assays for NRP *M. bovis* BCG needed to be designed for longevity.

Table 2.3: **Hypoxic Sealant Trials**

The creation of the MS, Cholesterol model involved the identification of a sealant that could maintain a hypoxic atmosphere over a 20,000 h incubation period, without allowing oxygen leaks. Paraffin Wax was identified as the only hypoxic sealant that could maintain hypoxia over this time period. The only other sealant to come close to this was a combination of parafilm and electrical tape with 312-384 h of hypoxic atmosphere before recolourisation of methylene blue. All sealant test were conducted in n=5.

Sealant Method	Hypoxic Atmosphere Maintained (h)	Issues Identified
Parafilm	216-288	Splits in Parafilm after extended incubation
Parafilm (Resealed)	96-192	Increased Splits
Superglue	72-144	Complicated to seal
Silicone Sealant	N/A	Acetic Acid Production
Electrical Tape	312-408	Glue Malfunction after extended incubation
Electrical Tape (Resealed)	288-384	Glue Malfunction after extended incubation
Silicon Grease	N/A	Grease acted as a lubricant
Silicon Grease/Parafilm	N/A	Grease acted as a lubricant
PTFE Tape	240-288	-
Parafilm/Electrical Tape	312-384	Splits in Parafilm and Glue Malfunction after extended incubation
Paraffin Wax	Indefinite	

Over ten sealants and combinations were tested for their ability to reliably maintain hypoxia (and thus keep *M. bovis* BCG in the NRP state) over an extended assay. The sealants tested and their results can be found in Table 2.3.

The first sealant tested was parafilm as it was initially thought to be the best method (Table 2.3). However, at around 200 h of incubation time, the parafilm seals began to leak oxygen and the methylene blue in the cultures recolourised in the following 48 h with the addition of oxygen. If cultures were left incubating after reoxygenating, the bacteria would return to logarithmic growth. The parafilm seal was kept at 37 C for an extended period of time, in addition, whilst being kept at this higher temperature it was constantly in motion and making contact with the rack the culture tubes were stored in. It is possible that this combination was responsible for rips and breaks appearing in the parafilm after a while of incubation. As the issue of breakages in the parafilm seemed to be mainly occurring after 200 h of incubation, the parafilm was topped up after 100 h and after 200 h (Table 2.3: parafilm resealing). This method did not fix the previous issue but negatively affected the maintained hypoxic atmosphere. Of the 5 culture tubes tested, 4 of the seals failed between 100 h and 200 h (Table 2.4). Thus, after the point where extra parafilm was added to bolster the original, the seal was more likely to fail than without any parafilm added.

Another sealant tested was superglue to tube lid (Table 2.3). This was surprisingly difficult to execute as completely sealing the lid to the culture tube was not easy. In consequence, this seal maintained hypoxia for 72 h to 144 h. All 5 cultures tubes sealed with this method failed at or before 144 h of incubation.

Silicone-based bathroom sealant (Unibond) was used to hypoxically seal as even if an imperfect seal was originally made with the bathroom sealant, it should expand to fill all the available space (Table 2.3). This method failed almost immediately for numerous reasons. While the bathroom sealant did expand while setting, it created air pockets that allowed limited but present oxygen transfer into the culture tube oxygenating the culture. In addition, the bathroom sealant expanded quite far under the culture tube lid. This led to the unforeseen

difficulty that when incubated at 37^{o}C, the constant elevated temperature caused the bathroom sealant to emit acetic acid. Due to the sealant's expansion up the culture tube, the acetic acid was emitted into the culture. This sudden addition of acetic acid produced a moderate bactericidal effect on the *M. bovis* BCG culture. Due to the above reasons, this sealant was discounted after 72 h incubation.

The culture tubes were sealed with electrical tape by tightening the culture tube lid, then tightly wrapping with electrical tape across the whole join (Table 2.3). The method proved, to an extent, effective at maintaining hypoxia. Cultures remained transparent with no return to replication for 312 h. Past this timepoint, the methylene blue started to slowly recolourise and OD_{600nm} started to increase at approximately 432 h. This method was repeated with the addition of more tape after 200 h incubation, however no improvement was observed. A possible explanation for this breakdown is that the glue on the electrical tape starts to wear out after a long period of incubation at a temperature higher than room temperature.

Silicon grease is a waterproof lubricant and sealant commonly used in chemistry laboratories (Table 2.3). It is thought to be a chemically inert sealant. The culture tubes were sealed by covering the thread of the culture tube lids with silicon grease and then tightening onto the culture tube. This method of sealant was discounted for health and safety reasons as handling. There was an attempt to seal the grease into the thread of the culture tube lid using parafilm. However, the grease rendering the parafilm unable to grip the glass of the culture tube and resulted in the parafilm sliding off (Table 2.3).

The next experimental sealant tested was polytetrafluoroethylene (PTFE) tape (Table 2.3). PTFE tape is commonly called thread seal tape and is mainly used in plumbing as a watertight seal for pipes. The PTFE tape bound well to the culture tube and the culture tube lid similarly to the electrical tape. This seal maintained the hypoxic atmosphere of the culture tube for approximately 250 h. After this point, the PTFE tapes seal on the culture seal started to loosen and became slack; this led to methylene blue slowly starting to recolourise and to the gradual resuscitation of *M. bovis* BCG.

Moreover, a combination of electrical tape and parafilm was tested to see if they could combine to overcome their individual shortcomings (Table 2.3). The method of sealant remained hypoxic for around 300 h, at which point the previously observed process of resuscitation occurred. This incubation time was an improvement on using solely parafilm. After approximately 300 h of incubation at 37^{o}C, the glue of the electrical tape began to breakdown and the grip on the culture tube began to weaken. This led to the tape slipping down on the culture tube. This created more pressure on the underlying parafilm which caused splits to appear. This combined method of sealing (electrical tape/parafilm) did improve on the seal quality of parafilm alone. As a sealant method, it was comparable in reliability to electrical tape in isolation; mainly due to the electrical tape being the limiting factor.

One more method of hypoxic sealing was tested, paraffin oil. This sealant method involves a layer of paraffin oil that sits on top of the bacterial culture in the culture tube. This layer of oil is impervious to oxygen can allows for antimicrobial to be injected into the cultures via a syringe. This method, whilst being an excellent method of sealant – was discounted as our model design incubated the cultures on a shaking platform. This would mix the oil into the cultures and could affect the viability of the microorganisms.

Another experimental sealant used was molten paraffin wax (Table 2.3). This sealant method involves using high grade paraffin wax (melting point: <70^{o}C) and melting the wax until liquid. In this state, it is poured in and around the join between the culture tube and the culture tube lid and allowed to set. Using this method, all five tubes sealed remained hypoxic for the full length of the experiment (1000 h). In two of the culture tubes, the paraffin wax broke down slightly over time but by topping up the wax seal the hypoxic atmosphere was maintained. This method of sealant maintained the hypoxic atmosphere far beyond the other sealant methods tested. The reliability of this method, especially in the light of the other methods tried, provided the main reason for using the paraffin wax method of sealing in all future experiments (*see* **section 7.3.1.2, section 7.3.2.2)**.

The paraffin wax was chosen as the sealant methods for both models of NRP when using the glass tube method. The elucidation of this meant that the protocol was successfully developed for both models (*see* **section 2.2.1.1)**

2.2.2 Assaying the Longevity of the NRP state in the Multi-Stress, Cholesterol model and the Hypoxic model

Wayne demonstrated that when *M. tuberculosis* is induced into the NRP state, it loses susceptibility to most frontline antibiotics, most notably Isoniazid (INH) and Rifampicin (RIF) (*see* **section 1.3.1)** (Wayne & Sohaskey, 2001). In this hypoxia based model, the mycobacteria also gained sensitivity to an anaerobic Metronidazole (MET) (Wayne & Sramek, 1994). To test if the new cholesterol, multi-stress model could achieve entry into the NRP state, *M. bovis* BCG was tested in both models in tandem using the glass tube method (*see* **section 7.3.2, section 7.3.1**).

These cultures remained at a stationary OD without recolourisation or change for over 10,000 h (Figure 2.2). The endpoint of this longevity experiment was chosen due to time pressures. As can be seen from the stationary nature of the absorbance curve, the cultures from both the Hypoxic model and the MS, Cholesterol model stayed at a constant OD_{600nm} for 10,000 h and showed no indications of change or stress (Figure 2.2). This suggests that at the end of this experiment, the cultures were viable and could have remained stationary in this state indefinitely (Figure 2.3).

Throughout 10,000 h of incubation, there was no significant change in OD_{600nm} in either model (Figure 2.2). The cultures were maintained at 37^{o}C at 100RPM to provide a slow agitation of the bacteria.

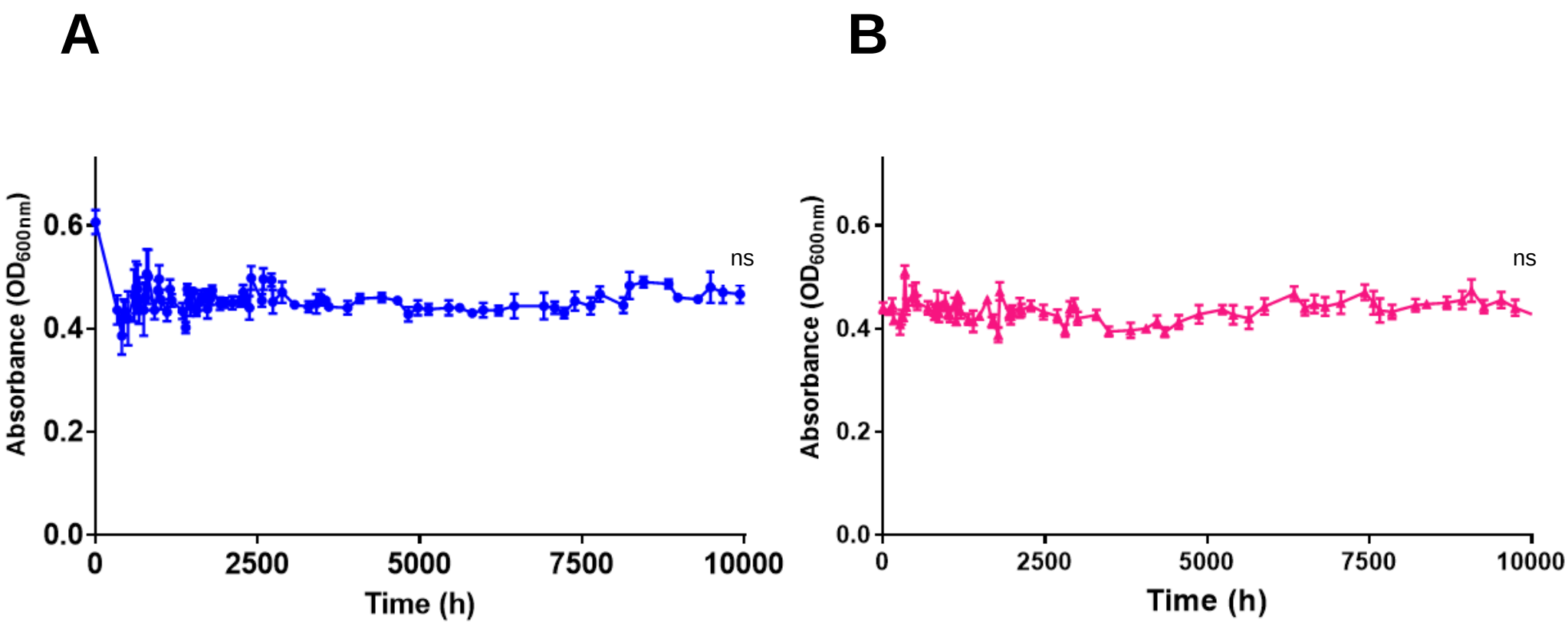

Figure 2.2 **Longevity NRP Curves of the Hypoxic Model (A) and the Multi-Stress, Cholesterol Model (B)**

Absorbance curve of *M. bovis* BCG in the Hypoxic Model over 20000 h of incubation. The assay was completed with 5 replicates and an overall ANOVA and an endpoint ANOVA was conducted, both resulting in non-significant p values. (B) Absorbance curve of *M. bovis* BCG in the Multi-Stress, Cholesterol model over 10,000 h of incubation. The assay was completed with 5 replicates and an overall ANOVA and an endpoint ANOVA was conducted, both resulting in non-significant p values

Both models showed a decolourisation of methylene blue and a cessation of growth, after which an unending stationary absorbance curve can be observed (n=5) (Figure 2.2). In both the deviations and fluctuations are shown to be not statistically significant (Hypoxic model p=0.4201; MS, Cholesterol model p= 0.8534). The cultures remained viable throughout a 10,000 h incubation period despite the challenging environment (Figure 2.2). This suggests that both models achieved entry into the NRP or a decline in OD would have been observed. In addition, if the *Mycobacteria* fail to enter the NRP state whilst in a hypoxic situation, the culture is observably affected. For example, in an early attempt at the Hypoxic model, the culture tube lids were removed for fast oxygen removal. This caused a fast degassing of the culture which did not allow time for entry into the NRP state. The *M. bovis* BCG culture used in this experiment noticeably changed and was accompanied by a sharp decline in OD_{600nm} . The clearest change was that the bacterial cells in the tube turned blue while the culture medium remained transparent. In assays that did not show a sudden decline in OD, the bacterial cells remain white. This was inferred to be a sign of a breakdown in the cell wall from bacterial cell death allowing them to be stained by the methylene blue.

In the Hypoxic model, at the start of the experiment for approximately the first 500 h, there were some fluctuations in OD_{600nm} and a slight negative correlation (Figure 2.2.A). After this time period, the OD_{600nm} stabilised and remained stable across the next 9,500 h (Figure 2.2.A). This would seem to indicate a stressful transition into the NRP state when using the Hypoxic model. In contrast, the absorbance curves for the cholesterol multi-stress model does not have this initial “settling” period of OD fluctuation. Throughout the entire growth curve, there is little change in absorbance over an extended time of incubation. These absorbance curves in both models show great stability over time, albeit the cholesterol, multi-stress model shows a greater level of stability than in the classic model (Figure 2.2). At 10,000 h, CFU/mL counts were measured (Figure 2.3). This resuscitation process is also discussed in more detail in section 2.2.8.

.

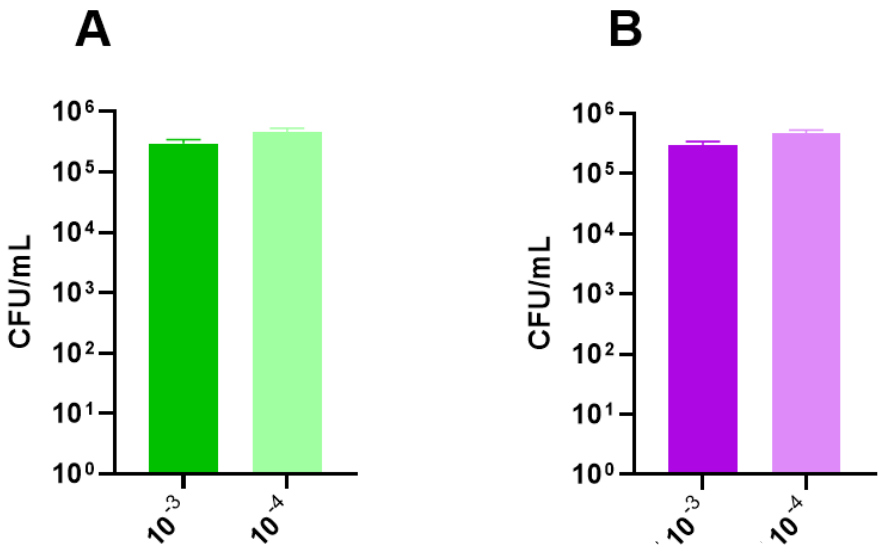

Figure 2.3: **Endpoint CFU/mL counts for the Longevity Assay** (Figure 2.2) in the Hypoxic model (A) and the Multi-Stress, Cholesterol model (B). CFU/mL counts taken from stationary NRP growth curves after 20,000 h of incubation. Clear growth of microorganisms to approximately $1x10^5$ CFU/mL for all organisms suggests the cultures were viable. The CFU/mL counts are from both the 10^{-3} and 10^{-4} dilutions. These results represent the men CFU/mL values of three replicates.

The NRP state is characterised by a cessation of replication, this is typically shown by a stationary absorbance curve showing an unchanging absorbance over a long period of time (Wayne & Hayes, 1996). Generally, this time period will extend past were an actively replicating culture would have passed into the death phase (Trutneva et al., 2020). Therefore, the stationary absorbance curves seen in Figure 2.2 suggest that the NRP state has been achieved and maintained over an extended time period. Additionally, the endpoint CFU/mL counts show that despite the experiment time, the cultures have remained viable. Therefore, the developed models of NRP, including the novel MS, Cholesterol model are capable of triggering *M. bovis* BCG to enter the NRP state.

The Hypoxic model undergoes some fluctuation upon entry to the NRP state. Previous research has shown that the shiftdown into hypoxia is a stressful process for *M. tuberculosis* or *M. bovis* BCG that commonly causes the *Mycobacteria* culture to lose some biomass upon

entry (Sohaskey, 2008; Wayne & Sohaskey, 2001). Presumably, this means that not all of the *Mycobacteria* successfully make the swap from active state to the NRP state. Therefore, the fluctuation shown at the beginning of this longevity assay was expected from a NRP state assay (Figure 2.2.A). More interesting is the lack of a “settling” period for the cultures under the cholesterol multi-stress model (Figure 2.2.B). These cultures remained extremely stable despite entry to the NRP state, something not previously shown in either our hypoxic model or in any previous hypoxic model. This leads to the inference that it is perhaps the presence of cholesterol or the process of cholesterol metabolism that allows for a less stressful entry into the NRP state. Previous literature has identified a group of proteins produced by *Mycobacteria* called resuscitation promoting factor (RPF) proteins (Biketov et al., 2007; Hu & Coates, 2018). These proteins act to facilitate and mediate a safe resuscitation process for the *Mycobacteria* when conditions become favourable (Kana et al., 2008). It is possible that something to do with the interaction between *Mycobacteria* and cholesterol may produce proteins which assist with entry into the NRP state, thus a portion of the colony population would not be lost to the stress of entry. Another possible hypothesis is that when *Mycobacteria* find themselves restricted to the sole metabolism of cholesterol, this acts as a stress indicator and prepares the bacteria to enter the NRP state. In contrast, solely hypoxia-based models do not have any mediation or preparation to enter the NRP state and thus find it a very stressful process as can be clearly seen in first 250 h of Figure 2.2.A.

Potential future work would be to investigate for the presence and identity of these “entry” RPF factors. Then, a coupled analysis with resuscitation assays could allow the identification of how these RPF factors are used and how they aid resuscitation.

2.2.3 Establishment of Growth in Both Culture Media

The two NRP models developed in this thesis are distinguished by the difference in culture medium (*see* **section 2.2.1**). The hypoxic model uses 7H9-ADC media which is commonly used for the growth of *Mycobacterium* microorganisms (Middlebrook & Cohn, 1958). It is an incredibly rich medium with many different carbon sources as *Mycobacteria* are fastidious microorganisms (Table 2.1).

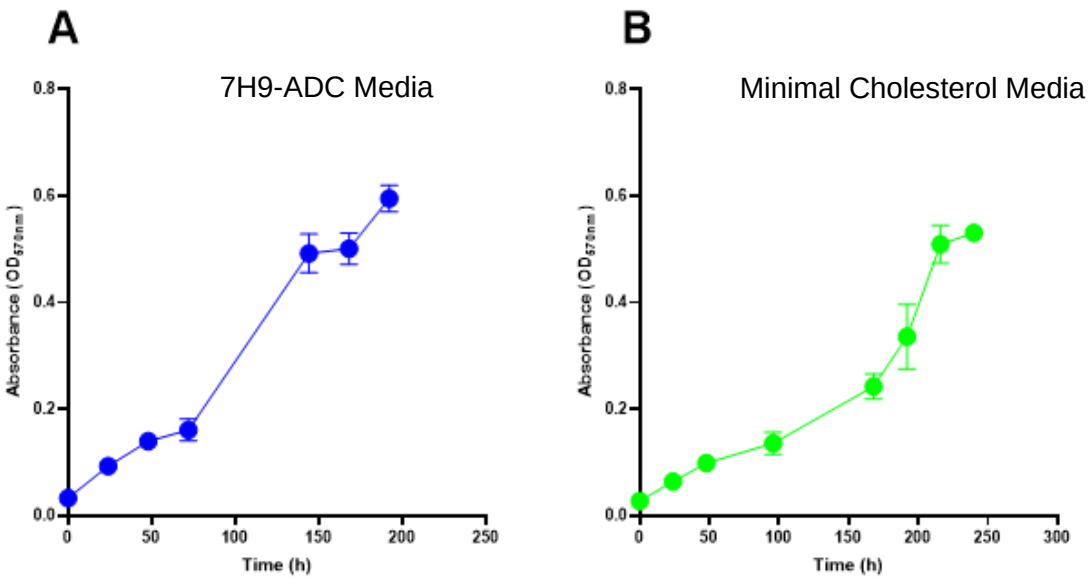

Figure 2.4: **Aerobic Growth Curves of *M. bovis* BCG in ADC enriched 7H9 Media (A) and Minimal Cholesterol Media (B).** Both growth curves were conducted with 5 replicates and the error bars associated are calculated from the standard error of the mean.

Whereas the minimal cholesterol media has no other components that can be metabolised other than the cholesterol, thus depriving the bacterium of nutrition but not starving it. Therefore, it became pertinent to establish whether culturing *M. bovis* BCG in the minimal cholesterol medium could trigger the NRP state without the added pressure of hypoxia. Figure 2.4.A shows a growth curve of *M. bovis* BCG when it has been grown in 7H9-ADC media

This depicts a traditional growth phase with a lag phase into a log (exponential) phase reaching an approximate 2.00 OD_{600nm} at the endpoint of the experiment (Figure 2.4). Interestingly, the growth curve for *M. bovis* BCG in minimal, cholesterol media appeared slightly different. *M. bovis* BCG does grow aerobically in minimal, cholesterol media (Figure 2.4.B). However, when compared with growth in complete 7H9 media, this growth is not as strong (Figure 2.4). The lag phase of growth in minimal, cholesterol media lasts perhaps 24 h more than that of *M. bovis* BCG growth in complete 7H9 media. The log phase for both media last for approximately 96 h and are comparable. The main difference between the two growth curves are the absorbance values reached after 200 h of incubation. *M. bovis* BCG grown in complete 7H9 media reached an OD_{600nm} of 2.00 at the end of the experiment (Figure 2.4.A). However, in minimal cholesterol media, *M. bovis* BCG only grew to an endpoint of 1.3 OD_{600nm} (Figure 2.4.B). Despite this, growth was observed throughout the experiment with a lag phase into a log phase that did tail off into a stationary phase. The inference that can be drawn from these results is that the minimal, cholesterol media does support the growth of *M. bovis* BCG, instead of triggering the NRP state as per PBS. However, the minimal nature of the media does appear to limit the growth of the bacteria, but it does allow for active replication and growth of *M. bovis* BCG.

The NRP state is characterised by a cessation of active replication, which can be seen in a stationary growth curve (Wayne & Sohaskey, 2001). Therefore, to initiate an NRP state using the minimal cholesterol media, a culture grown in this media also needs the added pressure of hypoxia to trigger *M. bovis* BCG into a NRP state.

2.2.4 Change in bacterial morphology between aerobic growth and the Non-Replicating Persistent state

It has been acknowledged that *Mycobacteria* when in the NRP state go through major physiological changes (*see* **section 1.2.1)**. Previous research has shown microscopy of the bacteria swelling and losing their rod-shaped physiology for a more spherical, bloated shape (Bacon et al., 2014). Interestingly, this major change in physiology has only been observed in NRP models based upon nutrient starvation, not hypoxia.

To see if an observable change in physiology could be detected, firstly between aerobic and NRP *M. bovis* BCG and secondly between NRP models, some microscopy was carried out. Figure 2.5 shows some very preliminary light microscopy of aerobic *M. bovis* BCG, hypoxic model *M. bovis* BCG and multi-stress, cholesterol model *M. bovis* BCG.

The microscopy does not show a major change in physiology between the aerobic bacteria and the hypoxic model bacteria (Figure 2.5). Throughout both images, the unequal rod of *M. tuberculosis/M. bovis BCG* is visible. The bacteria in the hypoxic model appear to be thinner than that of the hypoxic model, but there is no big shift in microscopy as previously described. However, in the cholesterol model, there is a potential shift of physiology from rods to cocci (Figure 2.5). The bacteria appear almost spherical in nature and do not appear structurally similar to either of the other conditions. The staining technique used was the *Mycobacterial* stain, Ziehl and Neelson (Z/N) staining (*see* **section 7.16**). This shows all mycobacterial bacilli as pink, whereas most other bacteria should appear green. Therefore, the pink colour of the bacteria in the multi-stress, cholesterol model shows that despite the spherical shape, they are *Mycobacteria.* The microscopy images are a very preliminary glimpse into an investigated element of TB pathogenesis (Figure 2.5). A major structural change in physiology and particularly in the cell wall is quite rare and could indicate a major change in pathogenesis. It is widely known that the unusual mycobacterial cell wall is responsible for a vast array of virulence factors from protective (arabinogalactan) to aggressive (mycolic acids) (Jankute et al., 2015) (*see* **section 1.1.3**). If perhaps this change from rod shaped to spherical is caused

by a change from 5-5 linkages in the peptidoglycan to 3-5 linkage, this could explain some of the widespread antibiotic resistance of the NRP state. It would be of great importance both clinical and for general knowledge to investigate thoroughly these apparent changes to physiology within the NRP state and how the cell wall is changed in the NRP state. If a full change in physiology was proven, this could guide future antimicrobial research to properly target the NRP Mycobacterial Cell Wall.

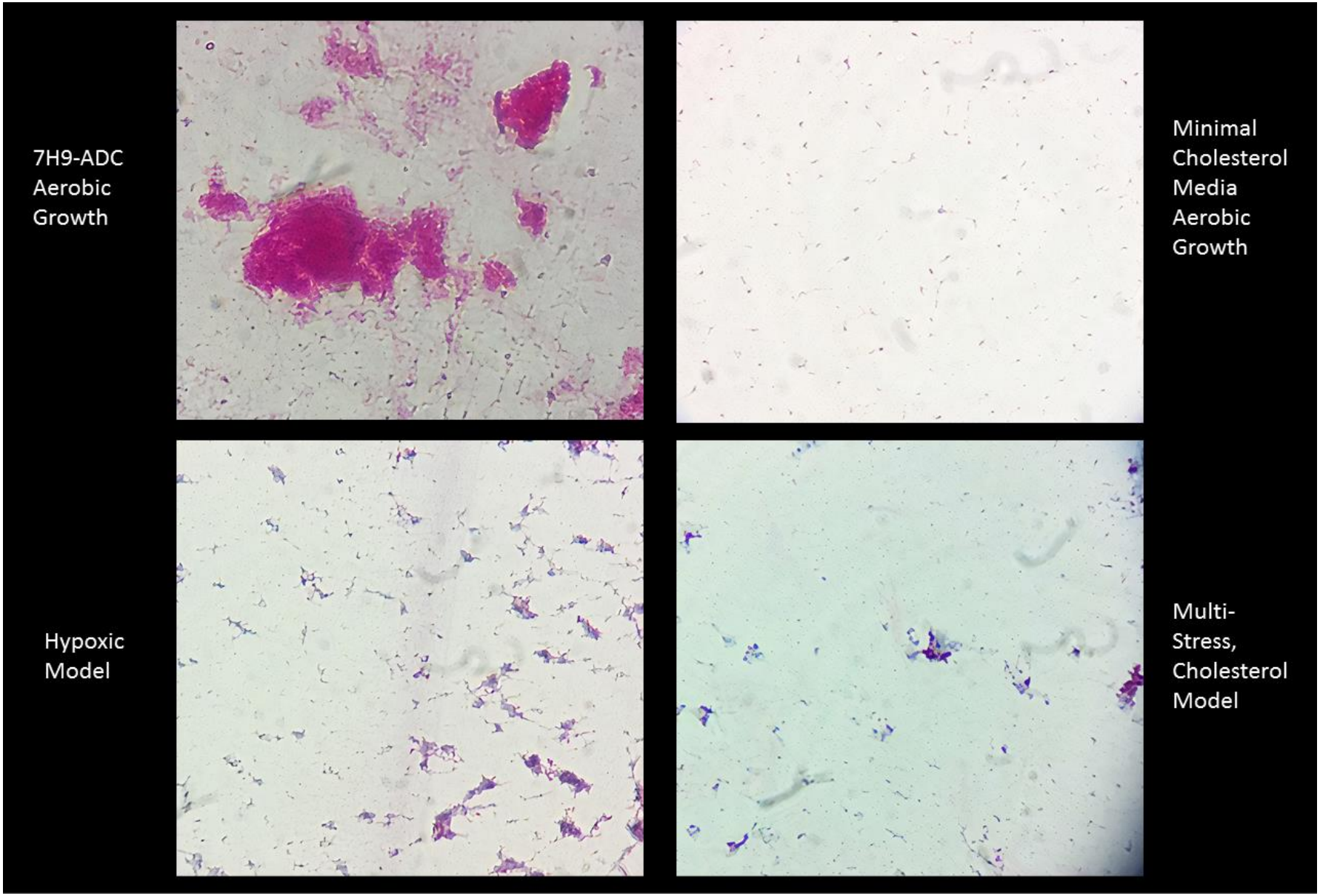

Figure 2.5: **Microscopy Photos of *M. bovis* BCG in all four conditions** Light Microscopy of *M. bovis* BCG actively growing in both media displays the expected rod shape previously described in literature. The rod shape can also be seen in the microscopy of the Hypoxic Model. In the Multi-Stress, Cholesterol Model, the bacteria show a distinct cocci morphology.

2.2.5 Comparison of Optical Density to Colony Forming Units of *Mycobacterium bovis* BCG

As the MS, Cholesterol model was developed, it became clear that to keep the culture in a completely hypoxic atmosphere the culture would have to be sealed. This was only raised in importance when paraffin wax was found to be the only sealant that could reliably maintain hypoxia over the extended assay *(see* **section 2.2.2**). Thus, it was not possible to unseal the cultures to remove aliquots of culture to measure CFU/mL throughout the experiment. As previous research as shown and it can be observed that *Mycobacteria* when going into the NRP state change morphology (Bacon et al., 2014). This is partly due to major structural changes happening in the cell wall. However, the direct effect of this is that the first 100-200 h of an NRP experiment can show quite a wide range of fluctuation in OD. This fluctuation has caused doubt to be raised as to the legitimacy of using OD as a method of measurement for such experiments as opposed to method that are potentially more reliable such as CFU/mL. To attempt to eliminate this doubt, an experiment to detail a “standard curve” comparing OD to CFU/mL experiments over a 1000 h NRP assay in both models was carried out (Figure 2.6). To circumvent the above difficulties about unsealing culture tubes, each replicate of this experiment was individually replicated to allow for the culture to be opened at the correct timepoint without compromising the experiment.

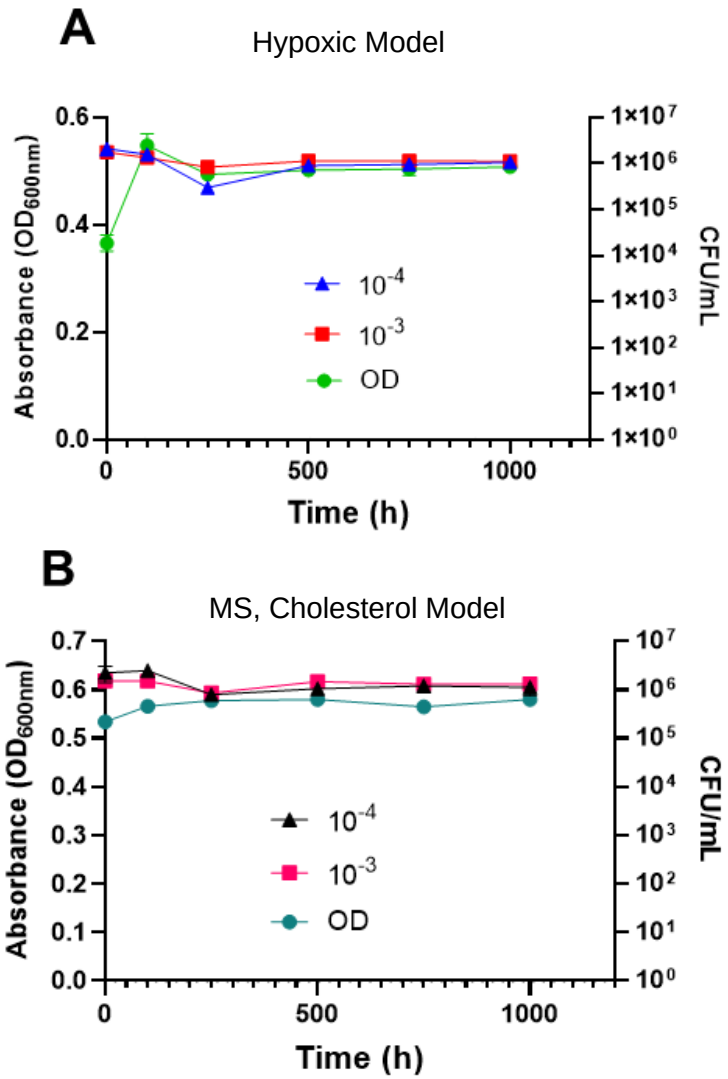

Figure 2.6 **Comparison of the CFU/mL and OD in the Hypoxic Model (A) and in the Multi-Stress, Cholesterol Model (B) over 1000 h of incubation.** The left axis represents absorbance (OD_{600nm}) and the right axis represents CFU/mL. For CFU/mL analysis both the 10^{-4} and 10^{-3} dilution were included. All line graphs depict a stationary curve, with no observable change in OD_{600nm} or CFU/mL respectively. All experiments were conducted in n=5 (five replicates) per data point.

The Hypoxic model – where *M. bovis* BCG was grown in ADC enriched 7H9 media before being exposed to hypoxia – was incubated and measured as per the typical NRP assay. However, at 0, 100, 250, 500 750 and 1000 h the concurrently running cultures were unsealed and aliquots were taken for CFU/mL. This produced the dual growth curve below with OD on the left-hand x axis and CFU/mL on the right hand x axis with time on the y axis (Figure 2.6.A). The growth curve clearly depicts the initial period of fluctuation in OD_{600nm} and an overall increase of approximately 0.075. The CFU/mL interestingly shows a similar period of oscillation albeit in the opposite direction. Within the first 250 h, the CFU/mL takes a slight decline and then, similarly to the OD_{600nm} settles into a stationary curve (Figure 2.6.A). This could indicate

that for *Mycobacteria* in enriched 7H9 media, being placed into a hypoxic atmosphere is incredibly stressful and causes some to lose viability. Nevertheless, after this initial period of stress, the remaining bacteria are in the NRP state and appear to have adapted to the hostile environment. After this, the curve for CFU/mL and the curve for OD_{600nm} are remarkably similar to each other (Figure 2.6.A).

The experiment for the MS, Cholesterol model repeated the same principle as the above one for the hypoxic model and kept the time points for all measurements the same (Figure 2.6.B). The growth curve for OD rose in OD by 0.05 but did not show the same fluctuation as seen in the curve for the hypoxic model (Figure 2.6). Additionally, the curve for CFU/mL remained almost completely stationary throughout the whole experiment with remarkably little change in OD (Figure 2.6.B). This would suggest that, especially in comparison to standard curve for the hypoxic model, if *Mycobacteria* are grown in minimal, cholesterol media it may promote preparatory proteins to ease entry into the NRP stress. Thus, we see the increase in OD due to the increased cell wall, but with no fluctuations or change in CFU/mL it seems this is a far less stressful process than in the hypoxic model.

Nevertheless, these “standard curves” both lead to the same conclusion, that a stationary absorbance curve produced from stationary OD readings directly correlate to a constant and consistent CFU/mL reading (Figure 2.6). Therefore, the initial period of fluctuation in OD appears to be due to bacterial cell size increase rather than replication or cell death. This standard curve also shows that with OD and CFU/mL being directly correlated in this assay, any decline in OD seen in the anaerobic microtitre plate assay or in the glass tube NRP assay indicates a decline in CFU/mL and thus a decline in live bacteria overall (Figure 2.6).

2.2.6 Frontline Antibiotic Assay

The longevity assays performed above show that despite a hostile environment, the *M. bovis* BCG remain viable over an extended assay by being in the NRP state (Figure 2.2, Figure 2.3). To find additional proof of both models reaching the NRP state, an MIC test was conducted in both models with INH and MET to test for sensitivity. In theory, NRP *M. bovis* BCG should be completely resistant to INH, whilst gaining susceptibility to MET (Wayne & Hayes, 1996). In addition to these drugs, the fluoroquinolone, moxifloxacin (MOXI) was also tested against both models (Dawson et al., 2015; de Miranda Silva et al., 2019; Gumbo et al., 2004). MOXI is being used in the majority of MDR-TB therapies and is currently undergoing clinical trials in a number of combination therapies touted to replace the current INH, RIF, ETH, PYZ combination therapy (Burki, 2019; Conradie, 2017). MOXI has been explicitly added to these combinations for its strong active TB activity but also for purported strong latent TB activity.

The Hypoxic model was designed to be as similar to the Wayne model as possible, whilst still providing a control for the cholesterol multi-stress model. Thus, the hypothesis was to see the same antibiotic profile as Wayne (Iona et al., 2016; Wayne & Hayes, 1996; Wayne & Sramek, 1994). However, the antibiotic susceptibility profile for the MS, Cholesterol model was unknown as there is difference between the profiles of hypoxic-based models and nutrient starvation-based model (Betts et al., 2002; Parish et al., 2003; Wayne & Hayes, 1996)

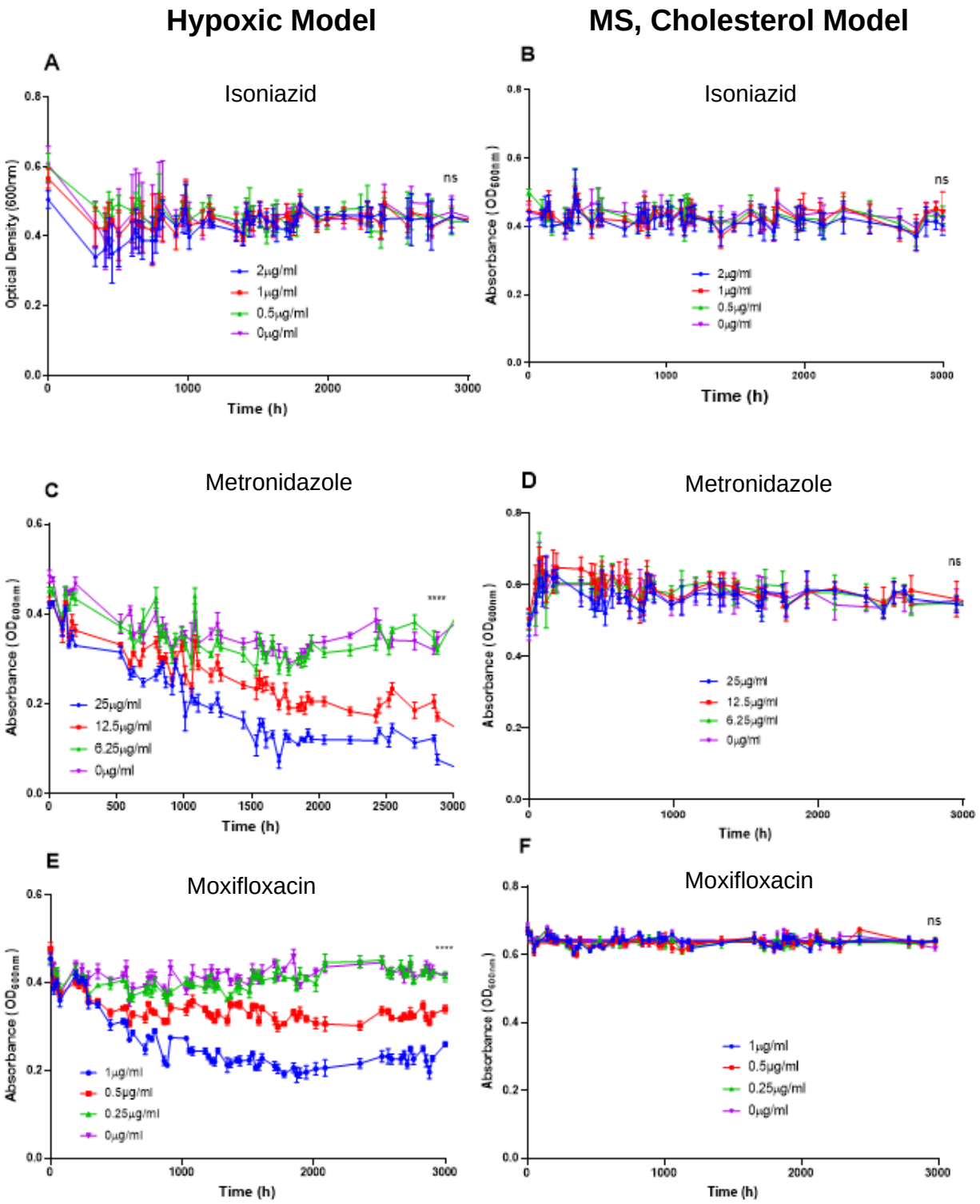

Figure 2.7**: Absorbance Curves showing the antibiotic inhibition of Isoniazid, Metronidazole and Moxifloxacin in the Hypoxic Model (A,C,E) and in the Multi-Stress, Cholesterol Model (B,D,F**) respectively.All of the above absorbance curve assays were conducted using the glass tube method across 3000 h of anaerobic incubation. All experiments were conducted in 5 replicates (n=5). All statistical ANOVA analysis was conducted using Graphpad Prism and was endpoint ANOVA analysis. (A) ANOVA analysis showed no significant difference of Isoniazid against the Hypoxic Model returning a p value=0.7161. (B) Isoniazid against the MS, Cholesterol model was not significant with p=0.8027. (C) Metronidazole against Hypoxic model showed a statistically significant response after 3000 h with a p value of <0.0001. (D) ANOVA analysis of Metronidazole against the MS, Cholesterol model was not significant after 3000 h. (p = 0.6909) (E) Moxifloxacin against the Hypoxic model was shown by ANOVA analysis to be statistically significant with a p value of <0.0001. (F) There is no significant change in OD with a p = 0.7165.

Figure 2.7.A shows an absorbance curve of NRP *M. bovis* BCG in the Hypoxic model challenged against frontline TB drug, INH. Similarly, to Wayne's finding, across 3,000 h there was no detectable change in OD for any dosed culture compared with the no drug control (Figure 2.7.A). All concentrations of INH were found to be non-significant when compared with the no drug control (p value = 0.7161). This would suggest that INH had no effect on NRP *M. bovis* BCG when under the Hypoxic model.

After an extended 20,000 h of incubation with varying concentrations of INH, the cultures shown in Figure 2.7.A were resuscitated on OADC enriched 7H11 agar. CFU/mL counts were obtained for all cultures (Figure 2.8.A). All cultures resuscitated on agar despite the presence of INH; this gives credence to the INH having no effect on NRP *Mycobacteria* despite its strong active TB activity.

Figure 2.7.C shows a clear dose dependant response to common anaerobic antibiotic MET in the Hypoxic NRP model is visible. The highest concentration of MET tested is 25µg/mL and this is the concentration depicting the strongest response. The decline in OD starts more rapidly than any other concentration at around 400 h where is 25 µg/mL absorbance curve starts to pull away from the no drug control (0 µg/mL). This decline in OD continues constantly until it reaches a low constant point of between 0.1-0.2 OD. This is a significantly lower OD than the no drug control which remains stationary at approximately 0.35 OD (Figure 2.7.C). This suggests that the antimicrobial is effective against NRP *M. bovis* BCG in the Hypoxic model.

Additionally, the second highest concentration of MET (12.5 µg/mL) shows a decline in OD when compared with the no drug control albeit neither as quickly nor as steeply (Figure 2.7.C). Nevertheless, there remains a clear reduction in OD over time when compared with a no drug control suggesting that despite the lower concentration, MET remains effective against NRP *M. bovis* BCG in the Hypoxic model. The lowest concentration of MET tested in this assay was 6.25 µg/mL (Figure 2.7.C). In direct contrast to the previous two concentrations of MET there is no discernible decrease in OD when compared with the no drug control. This dose

dependent response was shown to be statistically significant following ANOVA analysis (p=<0.0001).

The no drug control (0 µg/mL) used the same volume of DMSO without MET to determine that any change shown was not due to the DMSO. The absorbance curve in this case remained totally stationary across the experiment as expected. There was no decrease in OD, so the DMSO was not exerting any negative effect on the Mycobacteria.

At the end of 20,000 h of incubation with MET, the various cultures were spread out onto OADC enriched 7H11 agar and resuscitated to perform a CFU/mL count (*see* **section 7.1.5, section 7.4.1**). The results of this can be seen in Figure 2.8.C. The cultures with 25 µg/mL of MET did not resuscitate and grow back; neither did the cultures incubated with 12.5 µg/mL of MET (Figure 2.8.C). Conversely, both the cultures with 6.25 µg/mL of MET and the no drug control resuscitated on 7H11 implying that 6.25 µg/mL of MET was not of a high enough concentration to affect the NRP *Mycobacterium.* In addition, this shows that the decline in OD shown by the cultures at 25 µg/mL and 12.5 µg/mL was due to the bactericidal effect of MET (Figure 2.8.C).

Figure 2.7.E shows the activity of MOXI against NRP *M. bovis* BCG under the Hypoxic model. The highest concentration of MOXI tested against NRP *M. bovis* BCG was 1 µg/mL. The absorbance curve stays relative to curve of the no drug control for the first 300 h of incubation (Figure 2.7.E). After this time point, it breaks away and begins to rapidly decrease in OD despite the no drug control curve remaining steady (Figure 2.7.E). This steady decline of OD continues until approximately 900 h at whichpoint it begins to plateau. The difference in OD between the MOXI 1 µg/mL culture and the no drug control (0 µg/mL) is distinct by the endpoint of the assay (Figure 2.7.E). Likewise, the culture with 0.5 µg/mL of MOXI also shows a decline in OD from the control also starting at 300 h incubation (Figure 2.7.E). However, unlike the previous concentration, this decline in OD is not so steep. Whilst there remains a visible difference in OD from the no drug control, the MOXI at 0.5 µg/mL does not appear to have as great an effect on the bacteria as 1 µg/mL. When the concentration of MOXI is lowered again to 0.25 µg/mL, the drug activity seen in the previous two higher concentrations is no longer

happening. This absorbance absolutely mimics the curve of the no drug control, remaining at a consistent OD over the full length of the experiment (Figure 2.7.E). Statistical analysis shows that the dose dependent response attributed to MOXI activity was statistically significant with a p value of <0.0001 for the highest concentration of MOXI, 1 µg/mL.

Endpoint CFU/mL counts were taken for MOXI in the hypoxic model to confirm the results of the absorbance curve (Figure 2.9.E). *M. bovis* BCG treated with 1 µg/mL and 0.5 µg/mL MOXI showed no regrowth on OADC enriched 7H11 agar. This shows that the MIC seen in the absorbance curve is correct and the MOXI has antimicrobial activity against Hypoxic model *M. bovis* BCG (Figure 2.7.E, Figure 2.8.E).

The results found here also corroborate with Wayne and all other research that INH becomes inactive against *Mycobacteria* in the NRP state (Figure 2.7.A). It has also been generally accepted that as the *Mycobacteria* are not dividing under the NRP state, INH inhibiting InhA does not affect the bacterium in same negative way as when it is actively dividing (Timmins & Deretic, 2006). One of the key details and erstwhile controls of the hypoxia based NRP state is MET susceptibility. The results above show a clear dose dependant response to MET; this shows that the classic hypoxia model is a good representation of Wayne's model (Figure 2.7.C). As previously stated, the Wayne model – initiating the NRP state by using hypoxia only – is the main model used for drug discovery and latent TB research (Wayne & Hayes, 1996). The strong activity shown by MOXI (Figure 2.7.E) makes sense as this is the primary reason for its inclusion in the new proposed combination therapy for both active and latent TB (de Miranda Silva et al., 2019). This also shows that generating hypoxia via an anaerobic cabinet and largely adapting and expediating the Wayne model does still induce *M. bovis* BCG to enter a recognisable NRP state (i.e a long-lived stationary culture which is largely indifferent to antibiotics). Thus, this model seemed to be appropriate to be analysed as if not control, a comparator for the cholesterol multi-stress model.

The main point of contention for the Wayne model and all subsequent hypoxic models in the change in activity of MET. As previous discussed, in a solely hypoxia-based model, MET is

bactericidal to *M. tuberculosis*, however, when MET is tested against *in vivo* models this activity is no longer seen. In addition, in other models of NRP using a different NRP inducing stress (such as nutrient starvation) does not show MET susceptibility (Betts et al., 2002; Gengenbacher et al., 2010).

The above long-term antibiotic susceptibility assays were repeated but against *M. bovis* BCG sent into the NRP state under the multi-stress, cholesterol model (Figure 2.7.B, Figure 2.7.D, Figure 2.7.F).

Figure 2.7.B shows the absorbance curves for INH challenging MS, Cholesterol model NRP BCG. Again, this assay was conducted for approximately 20,000 h, however, for ease the first 1500 h are presented in these absorbance curves. All concentrations of INH tested (20 µg/mL, 2 µg/mL and 0.2 µg/mL) produced stationary absorbance curves throughout the assay (Figure 2.7.B). There was no significant deviation away from the no drug control (0 µg/mL) at any point during the assay. Indeed, there was comparatively little fluctuation throughout this assay indicating that the corresponding cultures were under very little stress (Figure 2.7.B). Statistical ANOVA analysis for these cultures show that when compared to the variance of the no drug control, no concentration of INH was able to produce statistically significant deviation (p value = 0.8027). Even by the extended end of the assay, a decline in OD had not been observed. The endpoint CFU/mL results can be found in Figure 2.8.B. These show clearly that all concentrations of INH grew back – despite the extended incubation and in spite of the presence of INH (Figure 2.8.B). Therefore, similar to the results in the hypoxic model, INH has no activity against NRP *M. bovis* BCG in this model

Three concentrations of MET were incubated with NRP *M. bovis* BCG over 20,000 h; Figure 2.7.D shows an absorbance curve of these cultures up to 3000 h. The absorbance curves are only shown to 30000 h as there was little change in OD past 900 h, perhaps showing that measurement past 1000 h is unnecessary as any further antimicrobial activity would show a corresponding noticeable change in OD.

For every concentration of MET tested (25 µg/mL, 12.5 µg/mL and 6.25 µg/mL), there is no deviation from the no drug control (0 µg/mL). This stability of absorbance curves throughout the whole time period, despite the presence of MET (Figure 2.7.D). Indeed, the difference in absorbance between the culture with 25 µg/mL of MET and the culture with 0 µg/mL of MET is statistically non-significant ($p = 0.6909$). Again, 12.5 µg/mL of MET showed inhibition in the Hypoxic model, but as can be clearly seen, no such decline in OD was observed in the cholesterol multi-stress model. These results are in direct contrast to the results seen in Figure 2.7.C. In the Hypoxic model, cultures dosed with 25 µg/mL of MET started to show a decline in OD after around 650 h of incubation. In the MS, cholesterol model, there is no decline in OD throughout the entire time. Likewise, to the previous absorbance curves, after approximately 20, 000 h of assay, the culture tubes were unsealed and plated out onto OADC enriched 7H11 agar to obtain endpoint CFU/mL data (Figure 2.8.D). The stationary absorbance curve denoting a lack of inhibition is corroborated by the CFU/mL results for MET (Figure 2.7.D, Figure 2.8.D). All cultures treated with varying concentrations of MET grew back to $1x10^5$ CFU/mL at the lowest to $8.3\ x10^5$ at the highest. Therefore, from the accumulation of these results, it can be concluded that MET does not have activity against MS, cholesterol model NRP BCG.

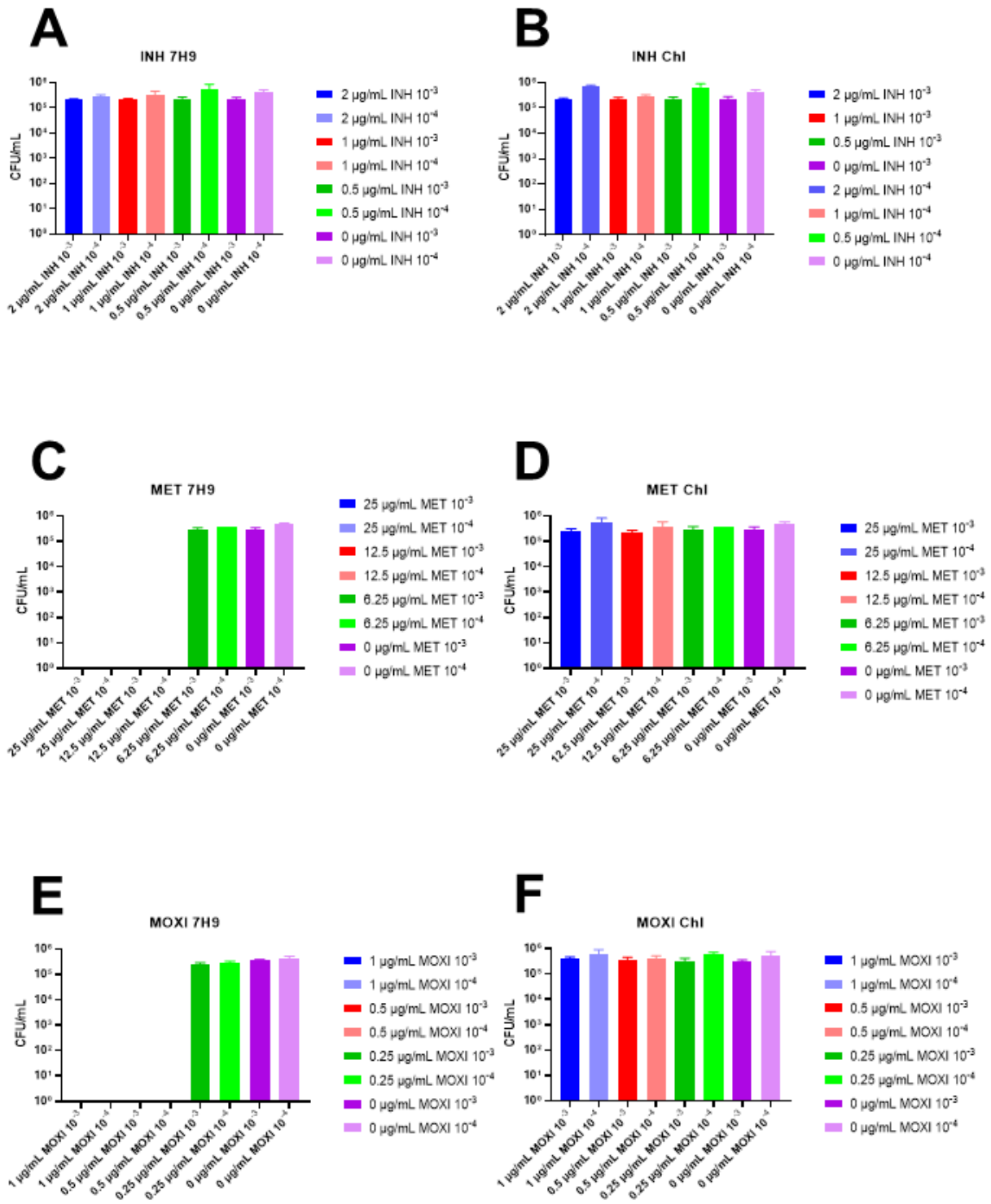

Figure 2.8: **Endpoint CFU/mL counts for all the Frontline Antibiotic Activity Assays.** The above bar charts show the mean endpoint CFU/mL counts for the absorbance assays shown in Figure 2.7. Individual CFU/mL counts represent the mean of 4 replicates. Error bars are calculated from the standard error of the mean. (A) shows the Endpoint CFU/mL counts for INH against the Hypoxic model. All cultures grew back despite different concentrations of INH. (B) shows the Endpoint CFU/mL counts for INH against the MS, Cholesterol model. All cultures grew back despite different concentrations of INH. (C) shows the Endpoint CFU/mL counts for MET against the Hypoxic model. All NRP *M. bovis* BCG cultures treated with 6.25 µg/mL MET showed regrowth to $1x10^5$ and above, whereas any higher concentration showed 0 CFU/mL (D) shows the Endpoint CFU/mL counts for MET against the MS, Cholesterol model. All cultures grew back to a similar CFU/mL. (E) shows the Endpoint CFU/mL counts for MOXI against the Hypoxic model. All NRP *M. bovis* BCG treated with 0.5 µg/mL MOXI or higher did not resuscitate and regrow at the end of the assay. Cultures treated with 0.25 µg/mL MOXI show regrowth to $1x10^5$ and above. (F) shows the Endpoint CFU/mL counts for MOXI against the MS, Cholesterol model. All cultures grew back despite different concentrations of INH.

MOXI is one of the great new hopes for LTBI treatment as it's NRP activity has been widely described. Therefore, the results of MOXI activity against the multi-stress, cholesterol model were greatly anticipated.

The absorbance curves for MOXI against the MS, Cholesterol model depict a stationary trend throughout the assay, with no obvious declines in OD away from the control (Figure 2.7.F). The absorbance curves for MOXI are remarkable for the stationary trend; there is little to no fluctuation away from the control with all of the concentrations of MOXI appearing almost on top of each other in the graph. The statistical analysis also shows that there is no statistical variance in OD with the highest concentration of MOXI having a p value of 0.7165. The consistency in OD regardless of MOXI concentration is consistent throughout the extended assay. Additionally, the CFU/mL counts show that at the endpoint, all cultures regrew despite the presence of MOXI (Figure 2.8.F). All of this data suggests that MOXI does not have activity against multi-stress, cholesterol model NRP *M. bovis* BCG. This lack of activity is in spite of the strong activity displayed by MOXI against the hypoxic model.

Antibiotic susceptibility is commonly used as an indicator of the NRP state; thus it has been widely studied. Most hypoxia-based models agree that NRP *M. tuberculosis* is resistant to INH but is susceptible to MET and MOXI (S. H. Cho et al., 2007; de Miranda Silva et al., 2019). These results have now been used to inform clinical trials. However, the MS, Cholesterol model (which still uses hypoxia as a stress) shows a different antibiotic susceptibility profile where NRP *M. tuberculosis* was resistant to all three drugs. This is an indication that the NRP phenotype has shifted to one with a heightened level of antibiotic indifference. This is perhaps, evidence that the MS, Cholesterol model is more phenotypically relevant, as particularly for MET, this susceptibility is not seen *in vivo* (Hoff et al., 2008; Klinkenberg et al., 2008)

2.2.7 Mass Spectrometry of NRP upregulated protein alpha-crystallin (acr)

Alpha crystallin (*acr/hspX/*Rv2031) is a chaperone protein that has been identified as a key protein in the NRP state, particularly when hypoxia is the triggering factor (Desjardin et al., 2001; Muttucumaru et al., 2004). Acr has also been identified as one of the proteins under the regulation of key NRP transcription factor, DosR (Park et al., 2003; Voskuil et al., 2004). Several studies investigating expression levels of Acr have found that it is dramatically upregulated by *M. tuberculosis* in NRP stage I and maintains this high level of expression through to NRP stage II (Desjardin et al., 2001; Muttucumaru et al., 2004).

Recent research has identified Acr as a key antigen for LTBI and has investigated using it as a disease marker for ELISPOT diagnostic testing as opposed to the common but problematic antigen, IFN-γ (Mamo et al., 2014).

In early NRP studies, MET susceptibility/INH resistance was seen as the main indicator of *Mycobacteria* reaching the NRP state (Wayne & Hayes, 1996; Wayne & Sohaskey, 2001). However, as research has expanded in this area, it was found that if the NRP state is triggered by an environmental factor other than hypoxia (for example, nutrient starvation), there is no gained susceptibility to MET. Therefore, upregulation of Acr has begun to be identified as a marker of *M. tuberculosis* achieving the NRP state.

To see if Acr was upregulated in either the hypoxic model or the multi-stress, cholesterol model compared with the aerobic phenotype, liquid chromatography-mass spectrometry (LC-MS) analysis was used to evaluate the presence and quantity of Acr in each sample. The samples tested are as follows aerobic, ADC enriched 7H9 media *M. bovis* BCG (7A), hypoxic model NRP *M. bovis* BCG (7AN), aerobic minimal cholesterol media *M. bovis* BCG (CA) and multi-stress, cholesterol model NRP *M. bovis* BCG (CAN). Bacteria were lysed and ran on SDS-PAGE gels to separate out the proteins (*see* **section 7.11**). Bands were cut out of the SDS-PAGE gel at approximately 16kDa -Acr has a molecular weight of 16kDa. Peptides were extracted from the bands by performing a trypsin digest. The extracted peptides were separated by liquid chromatography and ionised and measured by mass spectrometry.

MASCOT was used to interpret which peptides were present in each sample. The “hit” indicates how confident MASCOT is of the peptide being in the sample with 1 being the most confident. The “score” indicates how much of that peptide MASCOT believes is in the sample. The MASCOT analysed LC-MS results can be found in Table 2.5.

Table 2.4: **MASCOT Analysis of Mass Spectrometry of Acr-1**

	7H9 Media Aerobic	7H9 Media Anaerobic	Cholesterol Media Aerobic	Cholesterol Media Anaerobic
Hit	1	1	12	6
Score	746	1264	485	511
Normalised Score	17.74	28.31	5.39	6.88

For *M. bovis* BCG growing in the rich 7H9 media, Acr was the top peptide found in the 16 kDa band with a Hit of 1 (Table 2.5). Likewise, NRP *M. bovis* BCG in the hypoxic model Acr was also the number 1 hit (Table 2.5). However, MASCOT detects that there is almost double the quantity of Acr in the NRP culture as opposed to the aerobic control. 7A has a score of 746 whereas, 7AN has a higher score of 1264 (Table 2.5). This is indicative of an upregulation in the translation of Acr when in the NRP state as opposed to the active state.

For the CA sample, where bacteria are actively growing in minimal cholesterol media, MASCOT gives Acr a hit of 12. This means that there are 11 other proteins either present in the sample or that the peptide is more likely to be a part of. Simply put, MASCOT is unsure of the presence of Acr in this sample. Nevertheless, if it is present, it is given a score of 485 (Table 2.5).

CAN represents the multi-stress, cholesterol model. As shown in FIG, MASCOT is more confident of Acr’s presence in this sample with a score of 6 (Table 2.5). Despite this, it is not

as present as seen for 7H9 media. This higher hit is coupled with a higher score of 511. This could be interpreted that there has been a slight upregulation of Acr between CA and CAN on the basis of scores. However, if the hit values are taken into account, it seems likely that there has been an upregulation of Acr between active and NRP states.

2.2.8 Resuscitation

Resuscitation is arguably the most clinically important element of latent infection and NRP state M. tuberculosis (Biketov et al., 2007; Veatch & Kaushal, 2018). This is the crux event that treatment, diagnostics and prevention plans are attempting to avoid. Mycobacteria, when in the NRP state, are protecting themselves from the hostile environment of the granuloma, which in turn is a method utilised by the immune system as a way to eradicate infection (Ehlers & Schaible, 2012). As the granuloma (as a complex immune structure) is unable to exert any more pressure on the bacterial colony, a change in this stalemate hinges on the immune system being unable to keep up the pressure, in this case maintenance of the granuloma (Martin et al., 2016; Veatch & Kaushal, 2018). This can happen for a variety of reasons (for example, HIV infection, diabetes, a competing pulmonary infection) however, when this happens the encased Mycobacteria have an opening (Kana et al., 2008). Previous research has identified the presence of an excreted family of proteins called resuscitation promoting factors (RPF) which initiate and mediate the extended process of resuscitation (Biketov et al., 2007). By and large, the process of resuscitation is believed to be the exact opposite of entering the NRP state, with changes to the transcriptome, metabolism and phenotype as the bacterium becomes active again (Ehlers, 2009; Rustad et al., 2017; Veatch & Kaushal, 2018).

When the models were first developed, several cultures were set up in each model and monitored over a period of 20,000 h (Figure 2.2). These cultures were sealed and the measurements taking were OD (absorbance) readings, therefore at 10,000 h some of the replicates were unsealed. To assess whether the *M. bovis* BCG remained viable after 10,000 h, the bacteria were resuscitated after 10,000 h by being placed into ACD enriched 7H9 media under aerobic conditions. The culture was also spread out onto OADC enriched 7H11 media and incubated aerobically in a CO_2 static incubator to promote regrowth. The absorbance growth curves from the liquid media resuscitation can be found in Figure 2.9. These results are noticeably distinct from a regular growth curve with actively growing bacteria (Figure 2.5).

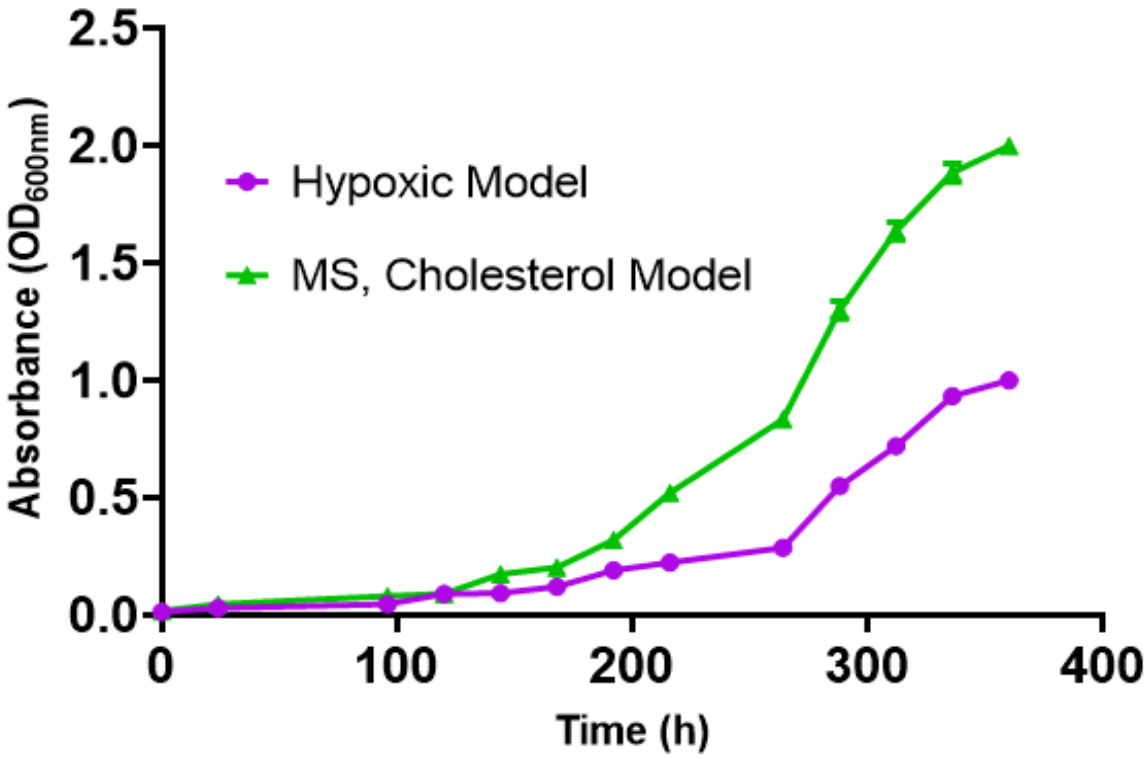

Figure 2.9: **Resuscitation of NRP Cultures in the Hypoxic Model and the Multi-Stress, Cholesterol Model (MS, Cholesterol Model)** After 10,000 h of anaerobic incubation, the regrowth of *M. bovis* BCG from both NRP models was investigated. This assay was completed in n=4 and the values presented represent the mean of these replicates. The associated error bars are the calculated standard error of the mean. The regrowth assays in both models were conducted concurrently and using the glass tube method (aerobically).

The particular difference between regular growth and resuscitated growth is the extended lag phase in the resuscitated growth curves (Figure 2.9). The lag phase in the hypoxic model lasts for 264 h after this, the culture does enter a log phase before tailing off into the stationary phase at approximately 350 h (Figure 2.9). Despite displaying all the features of a typical growth curve, the culture only reaches a maximum absorbance of 1.00 OD_{600nm} which is far below the maximum absorbance shown in normal active growth (Figure 2.10). This is different to active growth in 7H9-ADC media where completion of the full growth curve takes approximately 200 h (Figure 2.5). It is definitely interesting to highlight that resuscitating *M. bovis* BCG has extended lag phase before entering logarithmic growth (Figure 2.9). This delay could be held accountable as to why secondary infection is thought of as more resistant and more serious than the primary. The delay into active replication also perhaps indicates at the wide variety of changes being made by the bacterium as it resuscitates.

Figure 2.9 also shows the resuscitation of *M. bovis* BCG after 10,000 h of NRP under the multi-stress, cholesterol model. These absorbance curves again show an extended lag phase lasting approximately 175 h before entering a log phase that extends until just over 300 h (Figure 2.9). The growth curve does reach a stationary phase at the very end of the time period at a 2.00 OD_{600nm}.

The comparison of resuscitated growth curve for NRP *M. bovis* BCG in the hypoxic model and NRP *M. bovis* BCG in the multi-stress, cholesterol model reveals some intriguing and unexpected differences, particularly in the lag phase and in the final OD value (Figure 2.9). The hypoxic model seems to struggle to resuscitated with a longer lag phase and (if OD readings are taken as an indicator of biomass) achieves a far lower stationary phase OD than its comparator. In contrast, the multi-stress, cholesterol model resuscitates quickly with the initial lag phase lasting approximately 100 h less than in the hypoxic model. Additionally, once in the log phase the bacteria reach an OD of 2.00, almost doubling that achieved in the hypoxic model (Figure 2.9). This could be because the hypoxic model bacteria needed more time but the data shows that it reaches stationary phase. Therefore, it could be concluded that the *M.*

bovis BCG under the multi-stress, cholesterol model could resuscitate quicker and maintain more biomass than that of the hypoxic model (Figure 2.9).

This disparity of the multi-stress, cholesterol model facilitating resuscitation far beyond that of the hypoxic model could be attributed to adaptations made before the NRP state. The minimal, cholesterol media does not fully support *M. bovis* BCG growth in the same manner of the 7H9-ADC media. It could be that the change in metabolism away from sugars (dextrose) and glycerol to fatty acids (mainly cholesterol) could act as a transcriptional regulator to trigger the *M. bovis* BCG into producing NRP associated proteins, such as RPFs (Griffin et al., 2011; Marques et al., 2015). If this is the case, it would provide an explanation as to why entry and - as shown above – resuscitation is an easier and less stressful process in the Multi-Stress, Cholesterol model.

2.3 Conclusion

The true phenotype of NRP clinically has proved difficult to elucidate with each NRP-inducing trigger producing a slightly different phenotype (Bacon et al., 2014; Betts et al., 2002; Gengenbacher et al., 2010; Gopinath et al., 2015; Iona et al., 2016; Jakkala & Ajitkumar, 2019; Wayne, 1994). This study used a combination of hypoxia and a restriction on carbon sources to cholesterol to provide targeted nutrient deprivation to create a novel multi-stress model of NRP. From the distinct change in phenotype shown throughout this chapter, it is possible that this model is more phenotypically relevant than previous models (Figure 2.10).

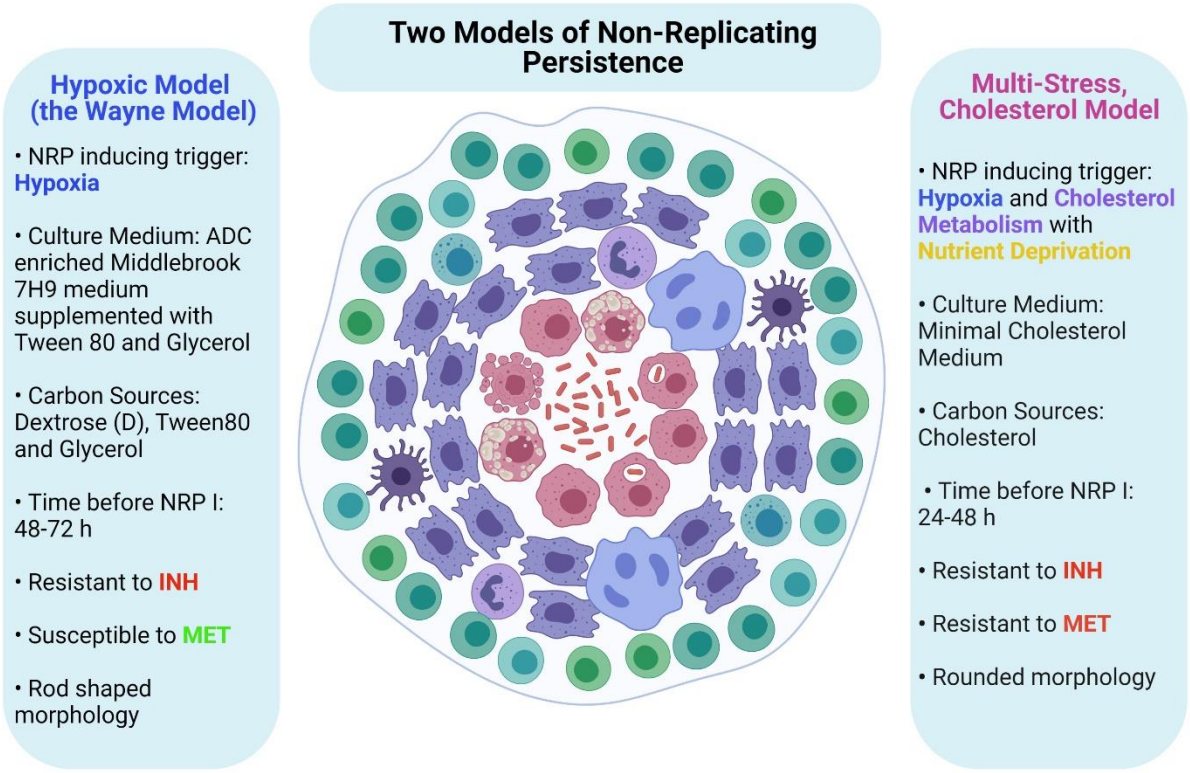

Figure 2.10: **Summary of two model of NRP developed in Chapter 2.** This summary contains the main points of each model and highlights the salient differences between the two.

The clearest difference between the two NRP models is the antibiotic susceptibility profiles (*see* **section 2.2.6)**. The antibiotic susceptibility profile of the multi-stress, cholesterol model is reminiscent not of the Wayne model results but of nutrient starvation model of NRP (Betts et

al., 2002; Gengenbacher et al., 2010). There has always been interest as to why the antibiotic profile for *M. tuberculosis* has changed between hypoxic NRP models and nutrient starved NRP models. The arguments for and against each model type can be found in the introduction (*see* **section 1.3**). Nevertheless, the multi-stress, cholesterol model is not a nutrient starved model of NRP. The nutrients inside the granuloma are indeed scarce and not diverse but they have been proved to be present (Ehlers, 2009; Soto-Ramirez et al., 2017; Wilburn et al., 2018). Thus, the minimal, cholesterol as the sole carbon source media was developed for this purpose. This is in the hope that the combination of a restricted medium, the cholesterol catabolism and the differences to transcription and hypoxia produce a phenotype more physiologically relevant. It is this that makes the loss of sensitivity to MET interesting (Figure 2.7). Technically, the only thing that has been changed between the models is the culture medium. By restricting the metabolism to cholesterol, thus making cholesterol metabolism the only viable method of energy metabolism, it appears that the entire phenotype has changed. This could mean that the metabolism of cholesterol acts as a transcription signal to start to change the phenotype into the protective NRP state. Of particular interest is that total resistance to MET has been identified before, albeit in nutrient starvation models (Betts et al., 2002). Indeed, MET sensitivity became a flashpoint between the two models and the first indication that the different NRP triggering stresses could give rise to distinct phenotypes. As previously discussed, the minimal cholesterol media does support the active growth of *M. bovis* BCG and certainly in isolation does not trigger the NRP state. Indeed, the NRP state is only achieved in the multi-stress, cholesterol model with the addition of hypoxia. As MET sensitivity is the hallmark of hypoxia based NRP models (firstly identified by Wayne) it would stand to reason that the results would echo that seen in the hypoxic model (Figure 2.7) (Wayne & Sramek, 1994). Instead, the results show total MET resistance, the hallmark of nutrient starvation NRP, nut not in a nutrient starvation model. This shows that a potential new phenotype has been created using this model. Perhaps, as MET activity has been shown to not work in many *in vivo* models including non-human primates, this lack of activity in a part hypoxia model shows that this phenotype is physiologically relevant.

Whether this novel multi stress model is an accurate representation of the NRP state as a whole was investigated thoroughly over the course of this chapter. The longevity curves showcase the remarkable level of stability and endurance of the NRP state (Figure 2.2). It provides an impenetrable sanctuary for *Mycobacteria* against environmental and antimicrobial stresses alike. The bacteria were in culture without nutrients or oxygen for two years and were able to fully resuscitate, seemingly without issue. LTBI has been identified as almost a chronic issue, as it is generally accepted that latent TB could resuscitate 30 years after the initial infection. This doggedly stable culture maintaining viability for two years is possibly the best proof of concept as the hallmark of the NRP state is its long-lived quality.

These longevity curves coupled with the display of antibiotic indifference provides yet more proof, albeit not as traditional, of the successful entry and maintenance of the NRP state (Figure 2.2, Figure 2.7, Figure 2.8). In addition, the change in morphology briefly glimpsed and the upregulation of acr-1 provides yet more proof of the NRP state in the multi-stress, cholesterol model (Table 2.5). There are also glimmers of an enhanced stability within the NRP state; with faster entry times and less initial fluctuation (bacterial cell death) observed when compared with the hypoxic model. These adaptations suggest that not only is the MS, cholesterol model capable of triggering and maintaining *Mycobacteria* in the NRP state, it forms a more physiologically relevant model of the NRP state than its counterpart.

Chapter 3:

Elucidating the Antibiotic Susceptibility Profile Utilising Both Models of Non-Replicating Persistence

Chapter 3 Elucidating the Antibiotic Susceptibility Profile Utilising Both Models of Non-Replicating Persistence,

3.1 Introduction

3.1.1 Chapter 3 Introduction

A key challenge of drug discovery is to find one active compound you first have to screen a thousand others (Hertzberg & Pope, 2000; Mayr & Bojanic, 2009). The Wayne model was originally developed in 3mL aliquots in culture tube, whereas most HTS are based in 96-well microtitre plate (Wayne & Hayes, 1996) (*see* **section 2.2)**. This low volume format allows a variety of large screens to be conducted without using too many resources. After Wayne developed and presented his model of NRP, many scientists then published their adaptation typically into a scaled down 96-well plate format (S. Cho et al., 2015; S. H. Cho et al., 2007; Taneja & Tyagi, 2007; Yeware & Sarkar, 2018). A main aim of this thesis was to conduct a wide range of antimicrobial screens on the novel model of NRP in tandem to a purely, hypoxia-driven model of NRP. However, it was impractical to test a large array of compounds using culture tubes. Therefore, to facilitate a wide range of antimicrobial testing, the NRP models needed to be scaled up.

The Multi-Stress, Cholesterol model (MS, Cholesterol model) and the Hypoxic model of NRP were validated as capable of triggering the NRP state in *M. bovis* BCG and therefore fit for purpose (Figure 2.2). Once it was established that both models were capable of triggering and maintaining *Mycobacteria* in the NRP state, experimentation turned to how the experimental volume could be scaled down. Other examples of downscaled NRP assay are the LORA and the HyRRA (*see* **section 1.3**) (S. Cho et al., 2015; Taneja & Tyagi, 2007). Both of these examples have been used to conduct HTS against NRP *M. tuberculosis*, however, both have advantages and disadvantages. The main disadvantage to these models is that, albeit using vastly different methodology, results are recorded by subjecting *M. tuberculosis* to the

antimicrobials and measuring regrowth to determine an MIC. In addition, both methods only use cultures that have been in the NRP state a short time period: (LORA, 10 days; HyRRA 96 h). Resuscitation and newly resuscitated *Mycobacteria* have a different phenotype to the NRP state and therefore basing a drug testing assay of NRP *M. tuberculosis* on MICs found by the resuscitation process is no assessment of activity against NRP *M. tuberculosis*. Other low volume Wayne-model based assays use genetic manipulation to transform cells with reported fluorescent genes (Yeware & Sarkar, 2018). However, this involves including resistance genes which can have a cross-antibiotic effect and therefore is not ideal for drug testing. Similarly with other models, this model only exposes *Mycobacteria* to antimicrobials for 14 days which is better than the LORA or HyRRA but possibly still misses the scope of NRP (Yeware & Sarkar, 2018)

It was important that the antimicrobial screening assays took place over an extended time period to gain the full scope of NRP as a chronic infection. Additionally, MICs were determined in real time – not via resuscitation – by the analysis of absorbance curves. As part of the validation conducted previously, it was shown that the OD of a stationary culture can be directly correlated to a stationary CFU/mL curve (*see* **section 2.2.5**). These modifications to existing assays will allow the results of this chapter to represent the profile of the NRP state in two models accurately.

3.1.2 Chapter 3 Aims and Objectives

Key to the aims of this thesis was to conduct a deep dive investigation into any differences in phenotype detected over the range of testing. This is particularly important to fully investigate the differences in antibiotic susceptibility profile as the previous chapter highlighted the resistance level of *M. bovis* BCG in the MS, Cholesterol model. Many of the compounds assayed in this chapter compromise part of the TB antibiotic pipeline; of which many are in the final stages of clinical trials. It is also important to note that some of these compounds are directly included into clinical trials for the treatment of LTBI. A key aim of this chapter is to establish if the strong anti-LTBI activity observed by these compounds in the Wayne model (Hypoxic model) was echoed in the MS, Cholesterol model. A major focus of modern drug discovery is the high throughput screening of compound libraries; this chapter aims to utilise the strength of the downscaling of the two NRP assays into HTS screens. Another clear aim of drug discovery is the repurposement of old antibiotics. This chapter aims to assay several established antimicrobials to assess whether any activity to against NRP *M. tuberculosis* can be established.

3.2 Results and Discussion

3.2.1 Scaling down the Glass Tube assay into a low-volume microtitre plate NRP assay

The biggest challenge to downscaling the models to produce an NRP assay was identifying a suitable anaerobic sealant. Most microtitre plate seals are designed to support aerobic exchange and thus are not oxygen impermeable as would be required to maintain hypoxia. Whilst the microtitre plates in question were largely incubated in an anaerobic cabinet, they had to be removed to measure culture absorbance. Therefore, any seal used had to be oxygen impermeable and transparent to support the primary method of measurement. A few seals were designed specifically for the purpose of Xray crystallography, and so were not designed to be permeable to the air. All of the plate seals tested and the results of this can be found in Table 3.1.

Table 3.1: Table detailing the different plate seals tested to identify one capable of maintaining a hypoxic atmosphere through the 1000 h of incubation.

Sealant Method:	Hypoxic Atmosphere Maintained (h):	Issues Identified:
Titer Top	0 (never sealed successfully)	Due to humidity in the anaerobic cabinet, the Titer Top seals struggled to bond to the microtitre plate and fell off after 24 h
EasySeal	1000 h +	These seals started as transparent seals however, after bonding to the microtitre plate, the plastic warped and became completely opaque. The hypoxic atmosphere was possibly maintained but measurements became impossible
Crystal Clear Tape	300 h	This seal was initially successful and did not warp but after around 300 h, the glue started to break down
ClearVue	1000 h +	The seal bonded well to the microtitre plate and did not warp. The hypoxic atmosphere was maintained using these seals for over 1000 h and the seal remained transparent

After establishing that the ClearVue seals maintain transparency throughout the experiment, whilst keeping the cultures anaerobic, the design of the NRP microtitre assay was completed (Table 3.1). After antibiotic testing, it became apparent that 1000 h of assay was long enough to see any drug activity (*see* **section 2.2.6)**. Additionally, after approximately 1000 h of incubation, issues with the cultures started to become common. These issues varied between evaporation, clumping or a generalised decline in absorbance. This is perhaps due to needing a large culture volume to be able to maintain the NRP state after 1000 h as in 3 mL the NRP cultures are stable for over 20,000 h. This effect was seen far more in Hypoxic model assays but as the Hypoxic model is acting as the comparator for the MS, Cholesterol model one it made sense to limit the assay to 1000 h (Table 3.1).

There are many ways of setting up the NRP microtitre assay for different types of antimicrobial screening. A summary of the setup used in this thesis can be found in Figure 3.1. These consists of a few drugs tested in a serial dilution (Figure 3.1.A); a HTS where each well is the maximum concentration of an individual compound (Figure 3.1.B); or a checkerboard which tests individual and synergistic activity of two compounds (Figure 3.1.C). All of these setups are used in both NRP models to test for a variety of antimicrobial activity.

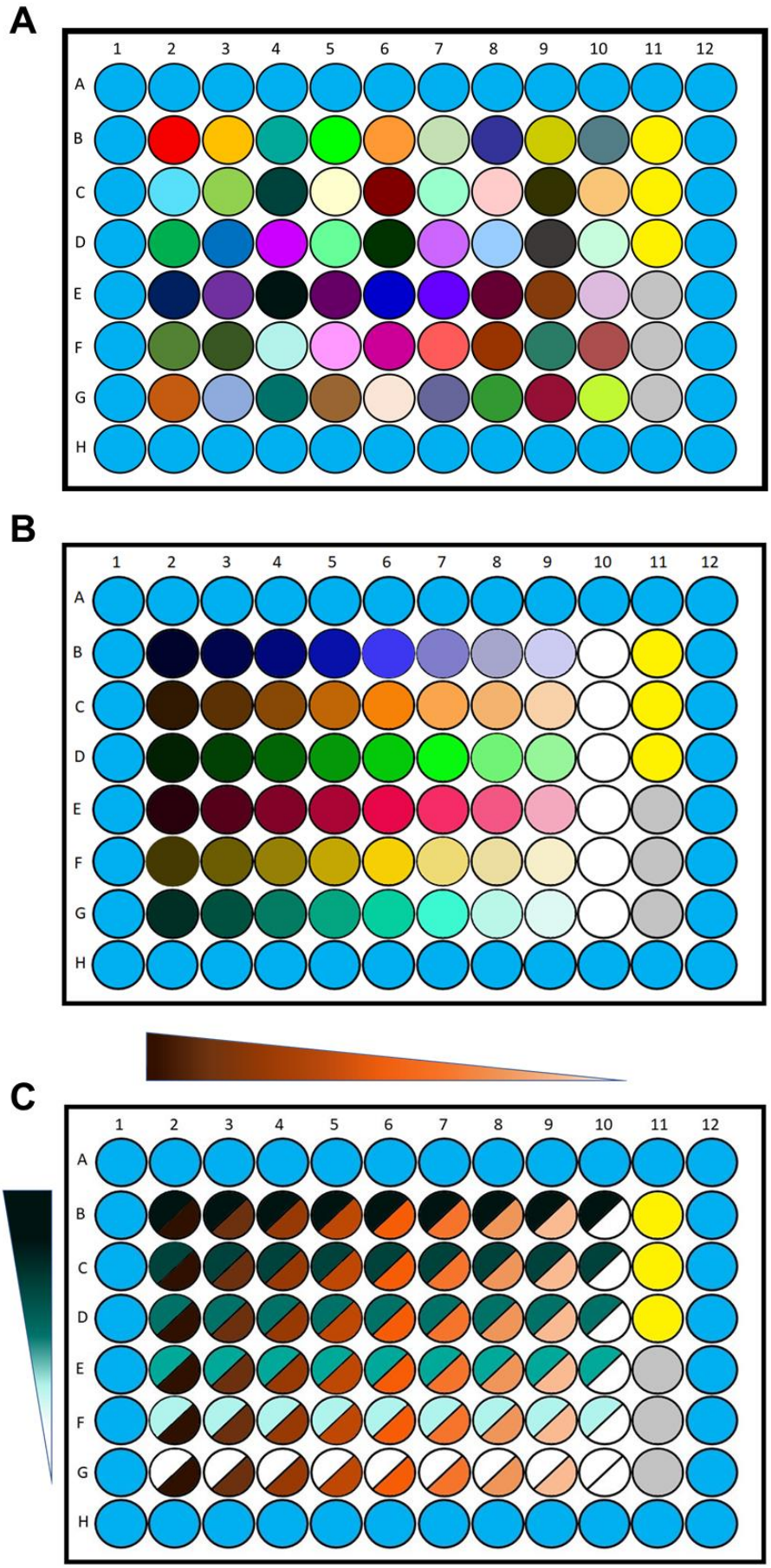

Figure 3.1: **Plate Maps of NRP Microtitre Assays** (A) shows an example of a high-throughput screen (HTS) where each well contains one compound. (B) shows a serial dilution of a few compounds where each row signifies one compound. (C) checkerboard assay of two compounds testing the individual and synergistic activity of the compounds.

3.2.2 Frontline or Proposed Tuberculosis Antibiotic Screens against Non-Replicating Persistent *M. bovis* BCG

3.2.2.1 IRMX Drug Screen

IRMX screen (Isoniazid, Rifampicin, Metronidazole and Moxifloxacin) was set up to validate the multi-stress, cholesterol model as a scaled down, microtitre-based screen. Isoniazid (INH) and Rifampicin (RIF) were chosen as they constitute two of the four frontline drugs for TB chemotherapy and are also used routinely in mainstay latent tuberculosis prophylaxis (Fraser et al., 2006; S. H. Lee, 2016; WHO, 2020). Due to over 50 years of effective TB treatment with these drugs; their effect on susceptible *M. tuberculosis* in active aerobic conditions is proven (Esmail et al., 2014; Maggi et al., 1966; Timmins & Deretic, 2006; WHO, 2020; World Health Organization, 2019). As previously discussed, this activity is lost in the NRP state (Gibson et al., 2018; Wayne & Sohaskey, 2001). Therefore, the loss of susceptibility to INH/RIF has become an excellent indicator of a culture in the NRP state (Heifets et al., 2005). Moxifloxacin (MOXI) was included because it is a drug that has recently been discovered to have activity against active and NRP *M. tuberculosis*, but only *in vitro* (de Miranda Silva et al., 2019; Gumbo et al., 2004). Clinical trials are currently ongoing to test this *in vivo* (Spigelman & Gillespie, 2006). Metronidazole (MET) does not affect aerobically growing bacteria; and *M. tuberculosis in vivo* it has no effect, however, in the Wayne model, sensitivity to MET is shown (Hoff et al., 2008; Klinkenberg et al., 2008; Wayne & Hayes, 1996). MET is commonly used as an antimicrobial against anaerobic bacteria (Freeman et al., 1997; Ursing & Kamme, 1975). Metronidazole therapy is used against *Clostridium difficile* and bacterial complications of Crohns disease (Sutherland et al., 1991; Teasley et al., 1983). It was theorised that triggering NRP by hypoxia is what causes sensitivity to MET (Wayne & Sohaskey, 2001).

To provide a point of comparison, the IRMX screen was also tested against aerobically growing *M. bovis* BCG in both media - 7H9-ADC media and minimal cholesterol media. The below aerobic tests were conducted using an aerobic drug testing microtitre plate assay where the chosen antimicrobial was serially diluted across a microtitre plate (*see* **section 7.2**).

Table 3.2: **Aerobic Minimum Inhibitory Concentrations (MICs) of the IRMX screen in ADC enriched 7H9 media and in minimal cholesterol media**

Antimicrobial	7H9-ADC Media	Minimal Cholesterol Media
Isoniazid	2 µg/mL	2 µg/mL
Rifampicin	0.01 µg/mL	0.01 µg/mL
Metronidazole	>50 µg/mL	>50 µg/mL
Moxifloxacin	0.05 µg/mL	5 µg/mL

As expected, *M. bovis* BCG was found to be susceptible to INH in both media. INH demonstrates an effective dose dependant response against *M. bovis* BCG to find an MIC of 2 µg/mL in both media (Table 3.2). Likewise, companion frontline antimicrobial RIF was found to be exceptionally effective against actively growing BCG despite the difference in media. The MIC of RIF was found to be the same in both media, 0.01 µg/mL. Common anaerobic drug and key NRP indicator, MET was found to have no activity at any concentration tested (max. concentration: 50 µg/mL) against *M. bovis* BCG in either media (Table 3.2). MOXI has always been reported to exhibit strong antimicrobial activity against *M. tuberculosis* and these aerobic susceptibility tests are no different (Table 3.2). In both media, MOXI was bactericidal against *M. bovis* BCG down to a concentration of 0.05 µg/mL in 7H9-ADC media and to 5 µg/mL in minimal cholesterol media. Overall, in the IRMX drug screen, no distinguishable difference was found in antibiotic susceptibility from *M. bovis* BCG grown in 7H9-ADC media or minimal cholesterol media (Table 3.2).

This drug screen was then tested against NRP *Mycobacteria* using the microtitre plate NRP assay as described in section 7.4. Briefly, NRP cultures in either the Hypoxic or the Multi-Stress, Cholesterol model were exposed to a serial dilution of the IRMX drugs over an incubation period of 1000 h. The experiments were measured by regular absorbance (OD_{570nm}) readings (Figure 3.2).

The hypoxic model of NRP aimed to be as close to the Wayne model as possible with a rich culture media and utilising hypoxia as the NRP driving factor. Over 1000 h of incubation with INH, the cultures remained comparable to the no drug control throughout regardless of the concentration of INH (Figure 3.2.A). The no drug control (0 µg/mL) maintained a relatively constant OD throughout despite the initial period of fluctuation. Statistical ANOVA analysis comparing the drugged cultures to the control confirm the visible results that INH even up to a maximum concentration of 50 µg/mL does not exert any effect on the bacteria (p value = 0.1052). The p values generated from ANOVA analysis comparing each dosed absorbance curve to the no drug control were all non-significant as well. This absorbance curve shows a clear loss in sensitivity to INH compared to the aerobic drug test (Figure 3.2.A, Table 3.2) The inference from this shift in MIC is that the NRP state gives *M. bovis* BCG resistance to INH. These results in this downscaled NRP assay are concordant to the results found in the initial validation antibiotic susceptibility testing of the hypoxic model which also reported a loss in susceptibility to INH.

The second drug in the IRMX screen was RIF, which in the aerobic drug tests gave an MIC of 0.05 µg/mL (Table 3.2). Throughout the assay, all concentrations of RIF mimicked the absorbance curve of the no drug control or 0 µg/mL (Figure 3.2.B). Throughout the 1000 h, even the highest concentration of RIF presents a stationary growth curve with no ostensible negative trajectory indictive of antimicrobial inhibition. Therefore, due to all cultures returning consistently stationary absorbance curves, no MIC can be found for RIF against hypoxic model NRP *M. bovis* BCG. This is augmented by statistical ANOVA analysis for each dosed absorbance curve compared with the no drug control, 0 µg/mL. All concentrations were found to be non-significant with the highest concentration of RIF, 10 µg/mL, returning a p value of 0.1261.

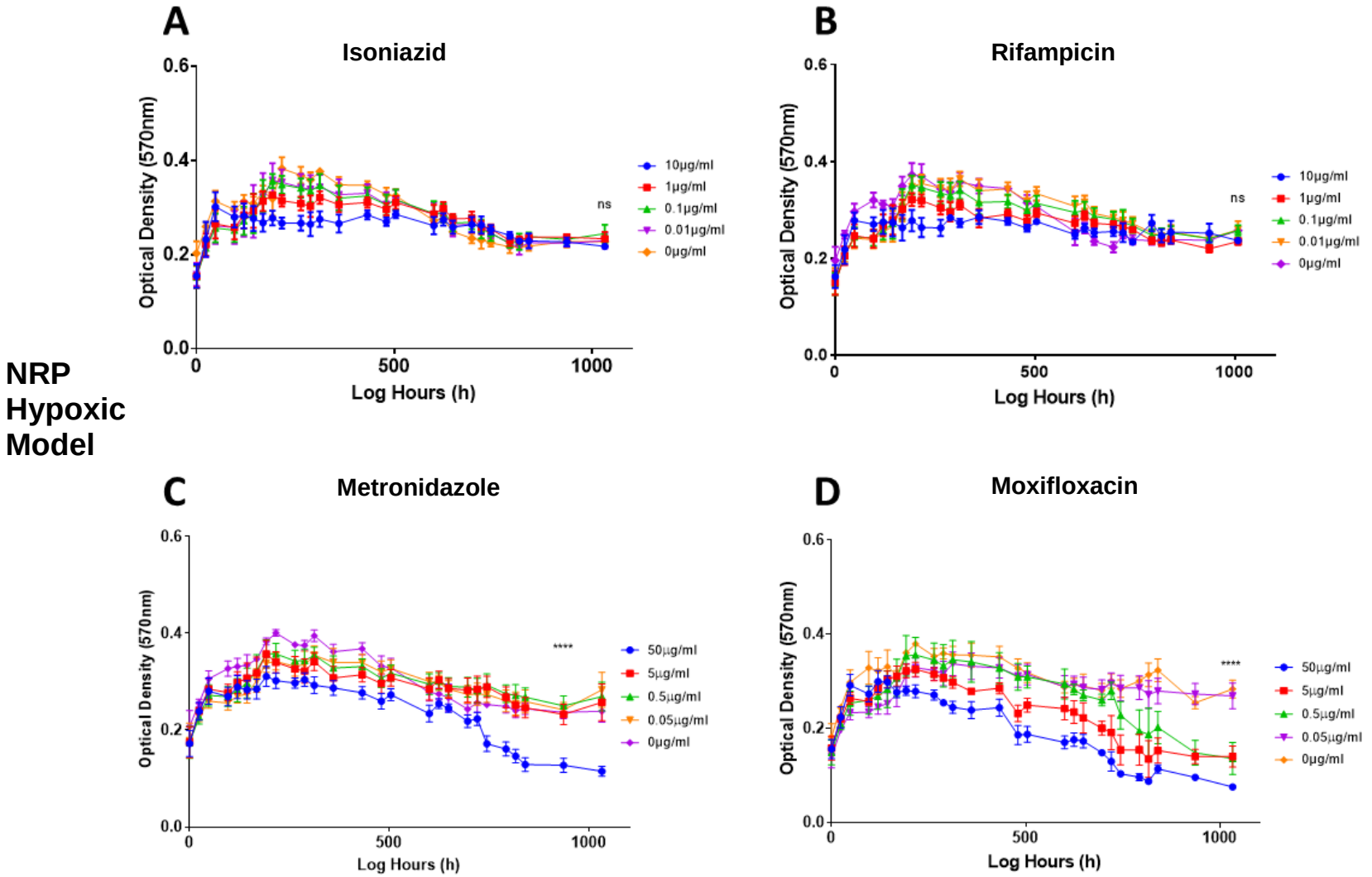

Figure 3.2: **Absorbance Curves of the IRMX screen tested against NRP Hypoxic Model. The IRMX screen consists of Isoniazid (A), Rifampicin (B), Metronidazole (C) and Moxifloxacin (D).** IRMX absorbance curves were conducted using the anaerobic microtitre plate method, thus all experimental volumes were 100 µL. The data points plotted here represent the mean of four replicates (n=4). All error bars represent SEM from the associated mean. The statistical analysis conducted for these experiments was endpoint ANOVA analysis in Graphpad Prism. The assay was measured for 1000 h. **(**A) At the endpoint of the assay, the p value for 10 µg/mL INH is 0.1052. (B) Endpoint ANOVA analysis shows that the p value for RIF is 0.1261 against the Hypoxic model. (C) Metronidazole against the Hypoxic model returned an endpoint ANOVA p value of <0.0001. (D) Moxifloxacin against the Hypoxic model returned an endpoint ANOVA with a p value of <0.0001.

Early testing of RIF identified a crucial error in the initial iteration of this assay. When this assay was first designed, the drugs and actively replicating bacteria were added into the microtitre plate at the same point and incubated in the anaerobic cabinet to add the pressure of hypoxia to trigger NRP. RIF inhibits RNA-synthesis and thus, its antimicrobial activity is very rapid – far more so than INH (Maggi et al., 1966; McClure & Cech, 1978). It takes approximately 72 h for *M. bovis* BCG to enter the NRP state after exposure to hypoxia. Crucially, for these 72 h, the bacteria are still replicating and are considered active. This resulted in RIF showing bactericidal activity early in the assay. As the IRMX is largely a validation exercise where the results – particularly in the hypoxic model – have already been proven, this result instead allowed the adaptation of the NRP microtitre assay. Currently, and all subsequent experiments, the cultures are subjected to hypoxia and reaches NRP stage I before any antimicrobials are added to ensure that any activity seen is against NRP *Mycobacteria.*

MET activity, originally seen as proof of the NRP state, has come into contention in recent years. In Table 3.2, it was shown that MET has no MIC against active *M. bovis* BCG which concurs with the common research findings. The absorbance curve shows a clear dose dependant inhibitory response for MET against Hypoxic NRP *M. bovis* BCG (Figure 3.2.C). Activity is shown at 50 µg/mL of MET and is demonstrated by a gradual decline in OD away from the curve of the no drug control (0 µg/mL). The activity, whilst clear, occurs quite late in the assay with the decline in OD stating at approximately 700 h of incubation (Figure 3.2.C). ANOVA analysis showed that the activity shown by 50 µg/mL (p value = <0.0001) is statistically significant. However, the next concentration in the dilution series (5 µg/mL) does not exhibit a decline in OD away from the control and also does not report a significant p value (0.6577). The activity of MET in the hypoxic model was investigated additionally in the initial validation using the glass tube assays (*see* **section 2.2.6**). The results of this scaled down microtitre plate NRP assay completely reflect the original results found in the glass tube assays with a dose dependant response to MET in the Hypoxic model (Figure 3.2.C).

Whilst not being a part of the main frontline therapy for TB, MOXI is commonly used as part of the MDR-TB treatment plan and has also been included into several clinical trials for new combination therapies, many of which are at stage three (Dawson et al., 2015; de Miranda Silva et al., 2019). Part of the draw to MOXI is the reported dual activity on both active TB infection and LTBI (de Miranda Silva et al., 2019). MOXI was previously tested in this thesis as part of Chapter 2 (*see* **section 2.2.6)**. There is an observable dose dependant response to MOXI being displayed in this growth curve (Figure 3.2.D). After an initial period of fluctuation, the no drug control (0 µg/mL) maintains a constant OD throughout the experiment commonly between 0.32 and 0.28 (Figure 3.2.D). The highest concentration of MOXI starts to affect the *M. bovis* BCG early on in the growth curve with the culture beginning to show a decline in OD from the control at 192 h (Figure 3.2.D). This culture (50 µg/mL) steadily declines in OD to an endpoint of 0.092 at the end of the experiment. It takes the second highest concentration of MOXI (5 µg/mL) slightly longer to depict a strong effect on the NRP *Mycobacteria,* however a noticeable difference in OD becomes apparent at 360 h (Figure 3.2.D). Again, there is not a sudden drop in OD but rather a steady decline through to the endpoint of the assay. The next concentration of MOXI (0.5 µg/mL) is the last effective concentration and it also takes effect the slowest. Indeed, the decline in OD is almost at the end of the assay; it starts to properly deviate from the control at 744 h. Like the other effected cultures, this starts a slow decline away from the control, but as the experiment has an endpoint of 1000 h it did not decline as far as the other two cultures (Figure 3.2.D). Statistical ANOVA analysis showed the deviation of the 50 µg/mL culture and the 5 µg/mL culture to be very significant with both p values being <0.0001. However, 0.5 µg/mL has slighter decline away from the control, due to the lower concentration of MOXI; therefore, its p value whilst still being significant is higher than the other two (p value =0.0303).

The results shown here and the results of the glass tube assay could act as a validation of the NRP microtitre plate assay (Figure 3.2) (*see* **section 2.2.6**).

The MS, cholesterol model showed some divergent results for antibiotic susceptibility from what was shown in the Hypoxic model or for what has been previously reported in the literature. A crucial element of validating this new scaled down experiment was to ensure that the new phenotype created by the multi-stress, cholesterol model was maintained despite the lower volume and different vessel type. The simplest way to test for the novel phenotype was to run the IRMX screen with the expectation that the NRP *M. bovis* BCG would lose sensitivity to INH and RIF, but unlike in the hypoxic model, there would also be no sensitivity to MET or MOXI as this would match the profile listed above in the glass tube assay (*see* **section 2.2.6**).

The growth curve for the IRMX screen in the MS, cholesterol model can be found in Figure 3.3. These assays were conducted using the same experimental procedure as the previous results from the hypoxic model (Figure 3.3).

The absorbance curve for INH in the multi, stress cholesterol model shows an overall constant OD over 1000 h of assay (Figure 3.3.A). This consistency is found over throughout the absorbance curve, regardless of concentration of INH. These curves show less initial variability than the corresponding INH assay in the Hypoxic model and do not include the initial period of fluctuation (Figure 3.3). Instead, the bacteria display stationary curves that do not deviate away from the no drug control (0 µg/mL) even within the first 100 h of assay (Figure 3.3.A). Statistical analysis confirmed the visual conclusion with none of the absorbance curves displaying any significant deviation away from the control. The highest concentration of INH, 10 µg/mL, had a p value of 0.5901. This suggests that INH has no activity against NRP *M. bovis* BCG under the MS, Cholesterol model.

RIF was one of two frontline drugs that *M. bovis* BCG gained resistance to as a perk of the NRP state (Figure 3.3.B). The growth curves in the novel, physiologically relevant MS, Cholesterol model are visually very similar to the previous absorbance curve (Figure 3.3). Over the 1000 h assay, no concentration of RIF exerts a negative effect on any the NRP cultures; all of which maintain a consistent, stationary absorbance curve. Again, similar to the absorbance curve for INH, there is no initial period of fluctuation in this experiment either

(Figure 3.3.B). ANOVA analysis ascertains the graphical conclusion, that no concentration of RIF tested in this experiment effects the bacteria (p value = 0.9832). This gained resistance is, again, particularly noteworthy as RIF is arguably the most important drug used to treat TB as it is valued for its speed in infection clearance.

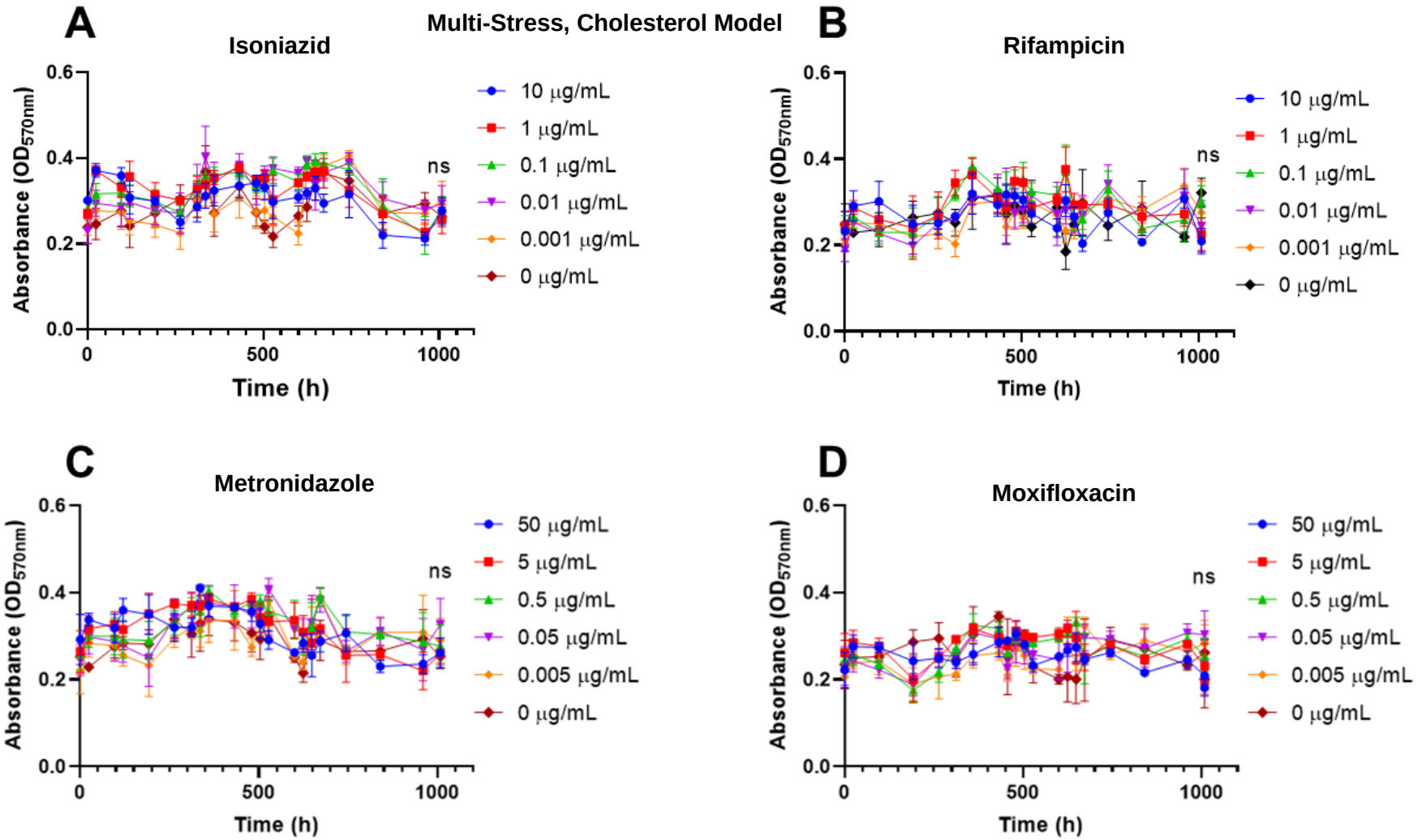

Figure 3.3: **Absorbance Curves of the IRMX screen tested against the MS, Cholesterol Model. The IRMX screen consists of Isoniazid (A), Rifampicin (B), Metronidazole (C) and Moxifloxacin (D)**. IRMX absorbance curves were conducted using the anaerobic microtitre plate method, thus all experimental volumes were 100 µL. The data points plotted here represent the mean of four replicates (n=4). All error bars represent SEM from the associated mean. The statistical analysis conducted for these experiments was endpoint ANOVA analysis in Graphpad Prism. (A) shows INH challenging the MS, Cholesterol model. The ANOVA analysis of this assays shows a non-significant p value of INH is 0.5901. (B) There is no significant response for RIF against the MS, Cholesterol model with a p value of 0.5901. (C) Endpoint ANOVA analysis resulted in a non-significant p value (0.3335) for MET against the MS, Cholesterol model. (D) Endpoint ANOVA analysis resulted in a non-significant p value (0.4351) for MET against the MS, Cholesterol model.

One of the most interesting findings from the initial antibiotic susceptibility testing in glass tubes (*see* s**ection 2.2.6**) was that the NRP *M. bovis* BCG did not show any response to the presence of MET, even at high concentrations. This conflicts with the results from the hypoxic model where MET showed the expected dose-dependant response (Figure 3.2). However, this susceptibility to MET is not found in other models of NRP nor is it observed *in vivo*. Therefore, this lack of susceptibility to MET, despite the use of hypoxia as an NRP driving factor, is indicative of the novel model showing a physiologically relevant phenotype (*see* **section 2.2.6)**. The absorbance curves show that throughout the 1000 h of the experiment, no concentration of MET deviated in absorbance from the control curve (Figure 3.3). The statistical analysis of the experiment results in none of the curves returning a significant p value, 50 µg/mL p value = 0.3335. This stationary growth curve with non-significant deviation for all concentrations of MET suggests that MET does not have antimicrobial activity against BCG when in the NRP state in MS, cholesterol model.

MOXI showed efficacy against hypoxic model NRP *M. bovis* BCG and the associated growth curve showed a dose-dependant response (Figure 3.3.D). The glass tube assays also showed a dose dependant response to MOXI in the hypoxic model. However, when tested MOXI in the glass tube assays in the multi-stress, cholesterol model, this susceptibility was lost. Throughout the experiment, all absorbance curves stay at a steady OD despite a serial dilution of MOXI. Statistical analysis found that no concentration of MOXI was significantly effective on NRP *M. bovis* BCG.

3.2.2.2 LNSP Antibiotic Screen

The LNSP screen consists of Linezolid (LIN), Nitazoxanide (NTZ), Streptomycin and Pretomanid (PA824). All of above antibiotics were chosen for strong anti-tubercular activity and inclusion into current clinical trials for novel combination therapies such as the BPaL and NIX-TB (Burki, 2019; Conradie, 2017). This screen was tested against NRP *M. bovis* BCG in both the hypoxic model and the MS, cholesterol model with the hypoxic model acting as the control model of NRP. That said, the absorbance curve results for the LNSP screen against the Hypoxic model NRP can be found in Figure 3.4.

LIN is a part of the oxazolidinones antibiotic class and briefly the mechanism of action is protein synthesis inhibition (García-Tapia et al., 2004). LIN binds to the 23s RNA of the 50s ribosomal subunit and thus stops the formation of the ribosome and preventing translation (Livermore, 2003). LIN is a relatively novel antibiotics and is the first in class to be approved; it is typically used in drug-resistant, Gram-positive infections (Livermore, 2003). However, it is associated with a heavy patient burden due to severe side effects cause by LIN treatment. Despite this, due to the severity of drug resistant TB infections it is commonly prescribed. It is also included in two prospective combination therapies that are currently in clinical trials (Gupte et al., 2021). Previous research has indicated that LIN is effective against *M. tuberculosis* when in the NRP state (García-Tapia et al., 2004).

Hypoxic Model

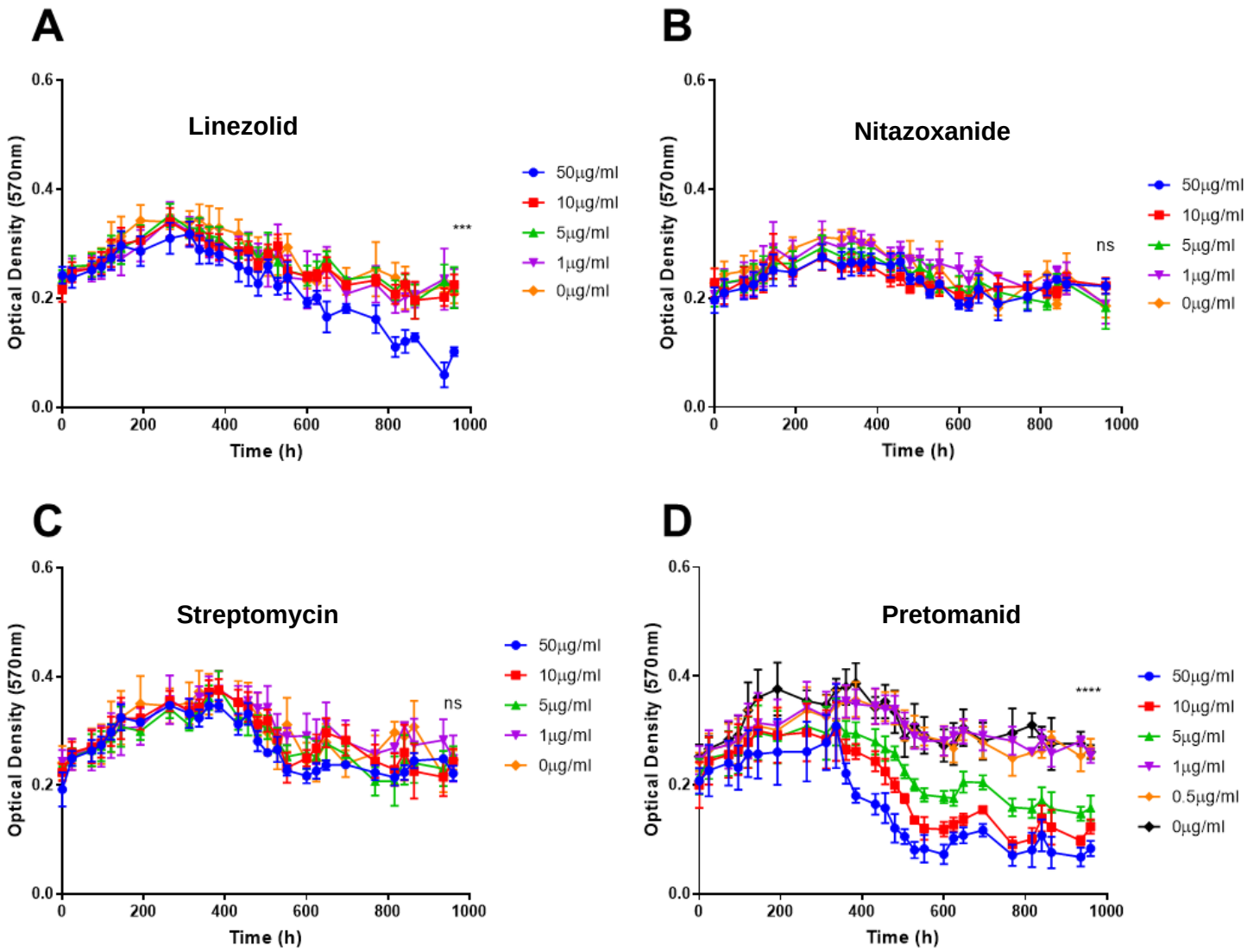

Figure 3.4: **Absorbance Curve Results of the LNSP Screen against NRP *M. bovis* BCG under the Hypoxic Model.** The LNSP screen consists of Linezolid (A), Nitazoxanide (B), Streptomycin (C) and Pretomanid/PA-824 (D). LNSP screen absorbance curves were conducted using the anaerobic microtitre plate method; thus, all experimental volumes were 100 µL. The data points plotted here represent the mean of four replicates (n=4). All error bars represent SEM from the associated mean. The statistical analysis conducted for these experiments was endpoint ANOVA analysis in Graphpad Prism. The results of endpoint ANOVA analysis for the LNSP screen are: 0.0003, 0.2496, 0.9082 and <0.0001 respectively. This shows Pretomanid as the only compound with a statistically significant response.

This experiment exposed hypoxic model NRP *M. bovis* BCG to a serial dilution of LIN and measured the absorbance (OD_{570nm}) throughout (Figure 3.4.A). The absorbance curves generated from this data show some efficacy for LIN. The highest concentration of LIN deviates away from the control by 600 h of incubation (Figure 3.4.A). From this point, there is an observable steady decline in absorbance across the rest of the time period. No other concentration of LIN displayed the same decline away from the control absorbance curve. Statistical ANOVA analysis of all the concentrations reported a significant p value for 50 µg/mL at 0.0003. However, all other concentrations after analysis gave non-significant p values ranging between 0.7297-0.9996. Therefore, the data appears to show that LIN against the Hypoxic model NRP *M. bovis* BCG is effective but at a very high concentration which given the high rate of side effects is not an ideal result (Schecter et al., 2010) (Figure 3.4.A).

Nitazoxanide is a relatively novel antimicrobial which also displays a wide range of antiviral and antiparasitic activity (De Carvalho et al., 2009; Shigyo et al., 2013). NTZ has also been recently identified as reducing the viral load of COVID-19 patients (Mahmoud et al., 2020; Martins-Filho et al., 2020). This impressive range of activity extends into tuberculosis where it purportedly is active against both active and NRP *M. tuberculosis* (De Carvalho et al., 2009; Shigyo et al., 2013). However, despite this wide-ranging activity and relatively few side effects, the mechanism of action of NTZ has not yet been elucidated. Nevertheless, NTZ is viewed as a promising drug candidate and is being proposed as part of new combination therapies (J Libardo et al., 2018). To investigate NTZ activity against hypoxic model NRP *M. bovis* BCG, the microtitre plate assay was carried out (Figure 3.4.B). Throughout the 1000 h assay, all concentrations of NTZ maintained a stationary curve that correlated with the absorbance curve of the control (0 µg/mL), with no significant deviation in absorbance from the absorbance of the control, demonstrating NTZ is not effective against Hypoxic model NRP *M. bovis* BCG despite strong active anti-tubercular activity (Figure 3.4.B). Statistical ANOVA analysis does confirm this visible trend and reports non-significant p values for all concentrations of NTZ.

Streptomycin (STR) was one of the first antimicrobials discovered in 1944 and the first antimicrobial identified as effective in TB infection (Schatz et al., 1944; Schatz & Waksman, 1944). Streptomycin is an aminoglycoside that inhibits the 30S ribosomal subunit and inhibiting protein synthesis (Spotts & Stanier, 1961). It is occasionally included in TB therapies but unfortunately because of quickly arising resistance and route of administration in the 1950s it fell out of favour (Crofton & Mitchison, 1948). However, due to its mechanism of action (protein synthesis inhibition), it could possibly retain activity against NRP bacteria. So, the results of the experiment of STR against NRP *M. bovis* BCG can be found in Figure 3.4.C. The absorbance curve appears similar to NTZ as all the concentrations of STR remain at a consistent OD throughout the experiment including 0 µg/mL. There is a lack of change in absorbance even for the highest concentration of STR all through the experiment (Figure 3.4.C). This insinuates that STR has no efficacy against Hypoxic model NRP *M. bovis* BCG at any concentration tested.

Finally, the last antibiotic included in the LNSP screen for the Hypoxic model NRP microtitre assay was Pretomanid (PA-824). PA-824 is an exceptionally novel antibiotic which was approved in the US in 2019 and the EU in 2020 (Conradie, 2017). PA-824 was hailed as one of the new antibiotics along with Bedaquiline after a 20-year lack of new, approved antitubercular compounds (Dawson et al., 2015; de Miranda Silva et al., 2019). It has a particularly complex MOA with what could be described as dual activity. Against aerobic, active *M. tuberculosis* it acts as a mycolic acid biosynthesis inhibitor; against anaerobic bacteria, it acts as a respiratory poison by NO assault (Baptista et al., 2018). As can be inferred, PA-824 is reported as highly effective against NRP *M. tuberculosis* (de Miranda Silva et al., 2019). Indeed, this activity is a major part of the interest in this drug as it would seem that PA-824 can act as a magic bullet for *M. tuberculosis* infection, handily providing compound with comprehensive anti-tubercular activity that neatly removes the issue of LTBI. However, all the examination into PA-824's anaerobic activity has been conducted using some adaption of the Wayne model, therefore hypoxia (de Miranda Silva et al., 2019). The activity of PA-824 in NRP

models using other or multiple triggers has not been examined. So, in Figure 3.4.D the absorbance curves of hypoxic model of NRP *M. bovis* BCG challenged against a serial dilution of PA-824. As expected from the above analysis, PA-824 does show activity against hypoxic model NRP *M. bovis* BCG (Figure 3.4.D). Indeed, the three highest concentrations of PA-824 (50 µg/mL. 10 µg/mL and 5 µg/mL) shows strong activity against hypoxic model NRP *M. bovis* BCG. These three absorbance curves show a clear dose-dependant response to PA-824 over the course of the assay (Figure 3.4.D). The absorbance curve for 50 µg/mL is the first culture to deviate from the control but does so in a uniquely slow manner. The curve starts to show a difference after about 200 h incubation; however, this drop is kept somewhat stationary for another 100 h of incubation at which point it starts to decline steeply away from the control curve over a period of 200 h and then remains unchanged until the end of the experiment (Figure 3.4.D). The second highest concentration of PA-824, 10 µg/mL presents a reasonably similar pattern to 50 µg/mL. It takes slightly longer before any significant change in OD can be observed (decline starts at 300 h approximately). After this, the absorbance curve dramatically drops in OD albeit not quite as steeply as for its more concentrated counterpart. Nevertheless, this fall in OD drops to the same low point as seen in 50 µg/mL and maintains this throughout the remaining assay (Figure 3.4.D). The absorbance curve for 5 µg/mL also deviates from the control absorbance curve indicating inhibition at approximately 400 h into the experiment. The curve for 5 µg/mL shows a shallower decline than 50 µg/mL or 10 µg/mL. This does indicate inhibition of the bacteria but to a lesser extent than at higher concentrations. The absorbance curve for 1 µg/mL PA-824 in remains stationary and correlated to the control. This experiment shows an MIC for PA-824 of 5 µg/mL against Hypoxic model NRP *M. tuberculosis* (Figure 3.4.D).

The absorbance curves for PA-824 are uniquely different than any other presented in this thesis. All of the other active drugs tested show a steady and slow decline in absorbance that progresses over the course of the assay. Whereas PA-824 shows a dramatic and steep decline that take around 200 h from the start of the decline to the low point. This unique difference

between PA-824 and other successful drugs can possibly be attributed to the drugs mechanism of action (MOA). Most, if not all, successful antibiotics tested against NRP *M. tuberculosis* inhibit protein synthesis in one way or another. This produces a slow increase of synthetic lethality which eventually kills the cell. Thus, other absorbance curves from active drugs for example MOXI, we see a slow and steady decline in bacteria attributed to tsynthetic lethality (Figure 3.2.D). However, the anaerobic MOA of PA-824 is to almost act as cyanide with a burst of NO release that disrupts the bacteria through respiratory poisoning (Dawson et al., 2015; Manjunatha et al., 2009). It is possible that this steep decline in absorbance observed in Figure 3.4 is a reflection of a dramatic MOA of poisoning instead of a lack of protein synthesis.

The LNSP screen in the multi-stress, cholesterol model was viewed as deeply important as LIN and PA-824 are specifically included in current clinical trials to treat NRP *M. tuberculosis* or LTBI (Conradie, 2017; J Libardo et al., 2018; WHO, 2020). The absorbance curves for the LNSP screen against multi-stress, cholesterol model NRP *M. bovis* BCG are in Figure 3.5.

All cultures dosed with differing concentrations of LIN show a stationary absorbance curve which remains closely correlate to the control (0 µg/mL) throughout the 1000 h of experiment (Figure 3.5.A). Any change or fluctuation seen is non-significant with no concentration returning a significant p value. There is a lack of initial fluctuation in OD, just a smooth increase in OD through NRP 1 before settling into the stationary curve. This data shows that in the MS, Cholesterol model, LIN has no MIC against NRP *M. bovis* BCG. Therefore, with the change of NRP model, susceptibility to LIN is lost. It could be argued that at a concentration higher than tested here such as 100 µg/mL, LIN susceptibility could be observed. However, at that high a concentration it would no longer be clinically relevant as it would be above the toxic dose.

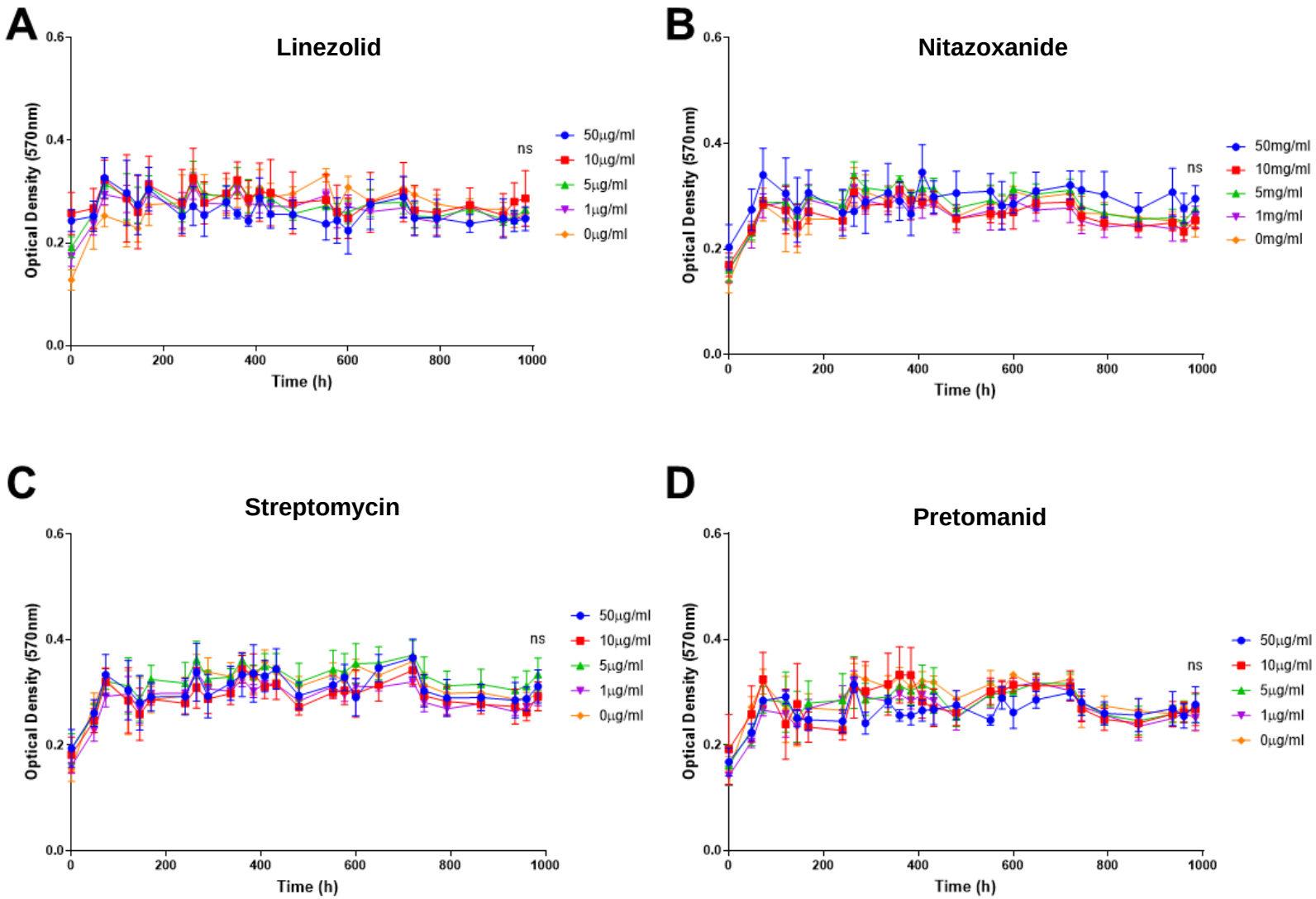

Figure 3.5 **Absorbance Curve Results of the LNSP Screen against NRP *M. bovis* BCG under the Multi-Stress, Cholesterol Model.** The LNSP screen consists of Linezolid (A), Nitazoxanide (B), Streptomycin (C) and Pretomanid/PA-824 (D). LNSP screen absorbance curves were conducted using the anaerobic microtitre plate method; thus, all experimental volumes were 100 µL. The data points plotted here represent the mean of four replicates (n=4). All error bars represent SEM from the associated mean. The statistical analysis conducted for these experiments was endpoint ANOVA analysis in Graphpad Prism. The results of endpoint ANOVA analysis for the LNSP screen are: 0.9431, 0.4416, 0.3498 and 0.7643 respectively. Thus, all compounds in this screen were not statistically significant.

NTZ did not show any activity against hypoxic model NRP *M. bovis* BCG (Figure 3.5.B). The resistance is matched in the multi-stress, cholesterol model with no concentration tested showing a significant change in absorbance to the control. Nevertheless, throughout the experiment all cultures remained constant and stationary and does not display an initial period of fluctuations. In fact, the highest concentration of NTZ ended the experiment at a very slightly higher OD than the other curves (Figure 3.5.B). Due to the above results, NTZ does not have an MIC in the multi-stress, cholesterol model.

The third drug in the LNSP screen, STR, did not have an observable MIC against hypoxic model NRP (Figure 3.5.C). In the MS, Cholesterol model, this resistance was also observed. The bacteria are completely unaffected by the presence of STR, even at the highest concentrations. Statistical ANOVA analysis confirmed this with all cultures being non-significant. This would infer that in the NRP state, *Mycobacteria* are completely resistant to the inhibitory effects of STR (Figure 3.5.C).

The fourth drug in the screen was PA-824. Throughout the 1000 h of assay, all concentrations of PA-824 remain completely stationary. Even the highest concentration of PA-824 (50 µg/mL) - which is 10 fold higher than the hypoxic model MIC – shows a stationary growth curve that mimics the absorbance curve of the control from start to finish. Indeed, by the endpoint of this assay, the absorbance data are all remarkably grouped and comparable despite the differing concentrations of PA-824 (Figure 3.5.D). Statistical ANOVA analysis confirms this lack of activity with all concentrations showing non-significant p values. Unlike in the hypoxic model, there is no sudden and dramatic drop in OD associated with the NO release MOA. Therefore, the conclusion from this data is that PA-824 is not effective against multi-stress, cholesterol NRP *M. bovis* BCG

PA-824 was the most effective antibiotic in the LNSP screen against the Hypoxic model. PA-824 comprehensively showed strong activity against NRP *M. bovis* BCG despite it being in the hypoxic model NRP state. The MIC found was 5 µg/mL (Figure 3.5.D). This result was somewhat unsurprising due to the great interest in its anaerobic activity shown in the literature.

It would not be unfair to say the PA-824 is the antibiotic regarded by most scientists as the predominate novel drug specially for LTBI (Parveen et al., 2020). This highlights the results shown in Figure 3.5.D in a highly interesting light. The loss in susceptibility to PA-824 in the MS, Cholesterol model has wide reaching implications for LTBI treatment. The data suggests that cholesterol catabolism triggers *M. tuberculosis* to a heightened level of protection that results in the bacilli being unaffected by NO assault. As cholesterol is the main carbon source in the granuloma, this suggests that the lack of activity shown in Figure 3.5.D is also observed in human infection.

3.2.2.3 BATP Antibiotic Screen

Like the previous two antibiotic screens, the BATP screen consists of four antimicrobials: Bedaquiline (BDQ), Amikacin (AMI), Tigecycline (TIG) and para-aminosalicyclic acid (PAS). The discovery of BDQ was hailed as major development as it was the first anti-tubercular antibiotic to be identified in 20 years (Hards et al., 2015; Mahajan, 2013; Pontali et al., 2019). It was found to be highly effective against *M. tuberculosis* and is specifically used for multi-drug resistant tuberculosis (MDR-TB). The MOA is the inhibition of mycobacterial ATP-synthase preventing ATP production and killing the cell (Hards et al., 2015). Whilst it is highly effective, BDQ treatment is also associated with a high rate of severe side effects which has meant that prescription of BDQ is typically reserved for MDR-TB (Conradie et al., 2020; Pontali et al., 2019). AMI is common aminoglycide antibiotic that inhibits protein synthesis and is sometimes prescribed for MDR-TB (Modongo et al., 2014). TIG is a broad-spectrum antibiotic that also inhibits protein synthesis that is sometimes used for MDR-TB (Deshpande et al., 2019). PAS was discovered just after STR and was commonly used to treat TB until INH/RIF therapy became common (Minato et al., 2015a; WHO, 2017). The MOA was discovered a long time after it was commonly prescribed. It was found to be a pro-drug that inhibits the folic acid biosynthesis pathway. It is activated by DHPS, an enzyme within the folic acid biosynthesis pathway, and is proceeds down the pathway to inhibit DHFR (Chakraborty et al., 2013; Minato et al., 2015a).

BDQ is a highly effective part of TB chemotherapy, it is incredibly effective but very toxic. Nevertheless, it is a part of many combination therapies that are currently being tested in clinical trials, such as BPaL (Burki, 2019; Conradie et al., 2020). The absorbance curves where NRP *M. bovis* BCG was tested against a serial dilution of BDQ in both models can be found in Figure 3.6.C and Figure 3.6.D.

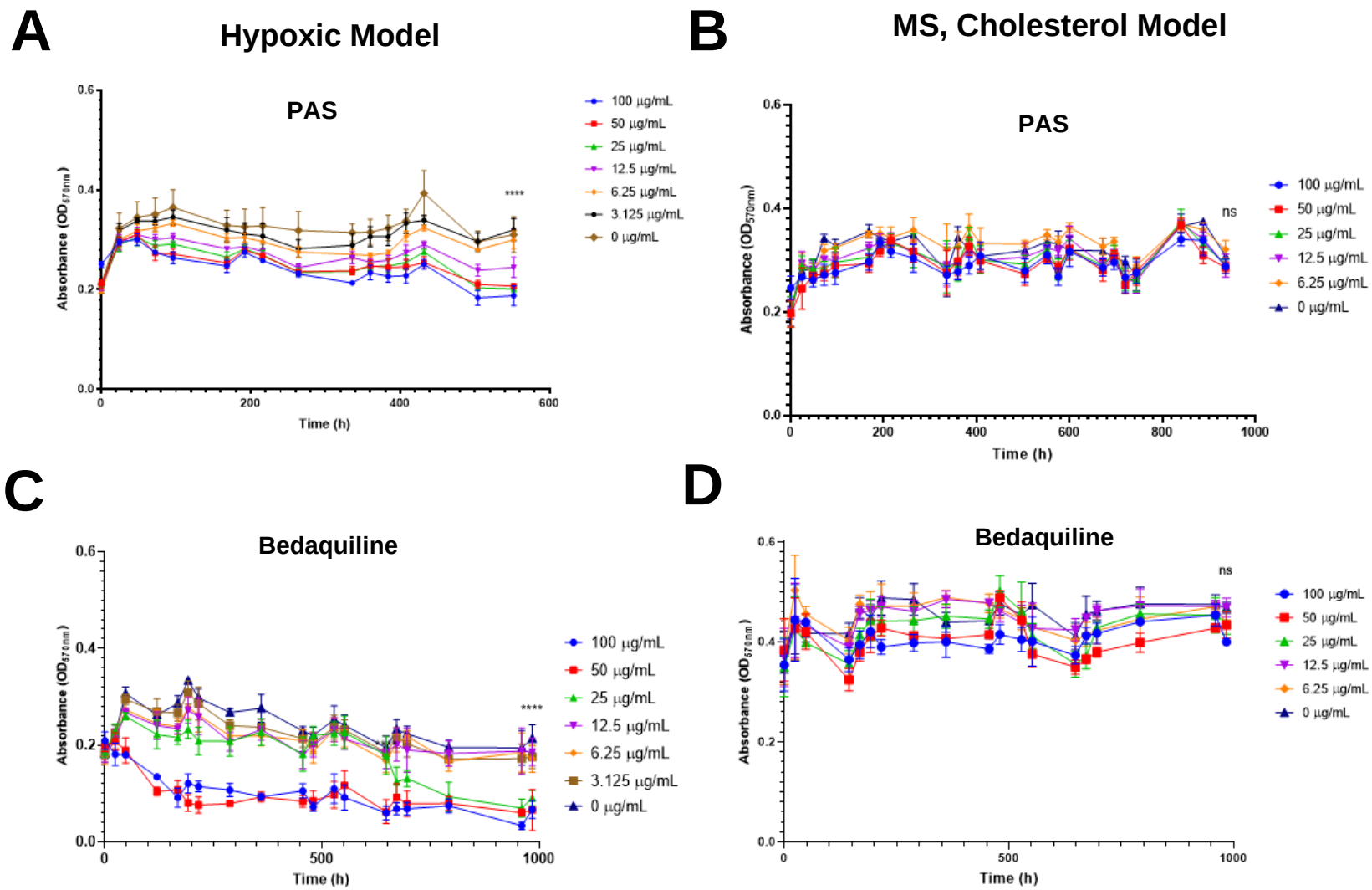

Figure 3.6: **Absorbance Curves showing Bedaquiline (BDQ) against the Hypoxic Model (C) and the Multi-Stress, Cholesterol Model (D) and PAS against the Hypoxic Model (A) and the Multi-Stress, Cholesterol Model (B)**. These absorbance curve assays were conducted using the anaerobic plate method with four replicates (n=4). The data points plotted represent the mean of these replicates. Endpoint ANOVA analysis was conducted for all assays. (A) shows a dose dependent inhibitory response to PAS which endpoint ANOVA analysis found statistically significant (p=<0.0001). (B) This absorbance curve shows the MS, Cholesterol model challenged with PAS; the statistical analysis found there to be no significant effect (p = 0.7643). (C) BDQ showed a statistically significant response against the Hypoxic model (p=<0.0367). (D) MS, Cholesterol model challenged with a serial dilution of BDQ. Endpoint ANOVA analysis after 1000 h showed a non-significant p value of 0.9290.

In the hypoxic model (Figure 3.6.C), a very dose dependant curve is displayed. Indeed, the top two concentrations of BDQ (100 µg/mL and 50 µg/mL respectively) show a sharp drop in absorbance at the very beginning of the experiment at approximately 100 h. After this initial sharp drop, the absorbance is maintained at this low level throughout the rest of the experiment. Interestingly, the next concentration (25 µg/mL BDQ) displays a more expected antibiotic activity absorbance curve (Figure 3.6.C). In this case, the absorbance curve mirrors the control curve until 648 h at whichpoint a smooth decline in OD is observed until the endpoint of the assay. The next concentration (12.5 µg/mL) mimics the control curve throughout the experiment and does not show any significant change away (Figure 3.6.C). Indeed, the ANOVA analysis highlights the stark difference between concentrations with 100 µg/mL ($p=0.0129$), 50 µg/mL ($p=0.0123$) and 25 µg/mL (0.0367) all returning significant p values. However, the p value for 12.5 µg/mL is not significant ($p=0.9290$) which allows the conclusion that BDQ has an MIC of 25 µg/mL in hypoxic model NRP *M. bovis* BCG. These p values are not as significant as they potentially could be as during the assay, the anaerobic cabinet had some humidity issues which especially at the end of the experiment meant that there were some problematic absorbance readings which caused many data points at the end of the absorbance curve to be excluded. Whilst it has been previously shown that OD does correlate to CFU/mL in the case of these stationary NRP absorbance curves, some additional testing was conducted specifically for the BDQ activity assay to confirm the results of the absorbance curve (*see* **section 2.2.8**). Figure 3.7 shows these results. The cultures treated with 100, 50 and 25 µg/mL of BDQ did not resuscitate and regrow, however, all other concentrations including the no drug control did (Figure 3.7.A). This additional data confirms the above MIC of 25 µg/mL whilst acknowledging difficulties with the end of the experiment.

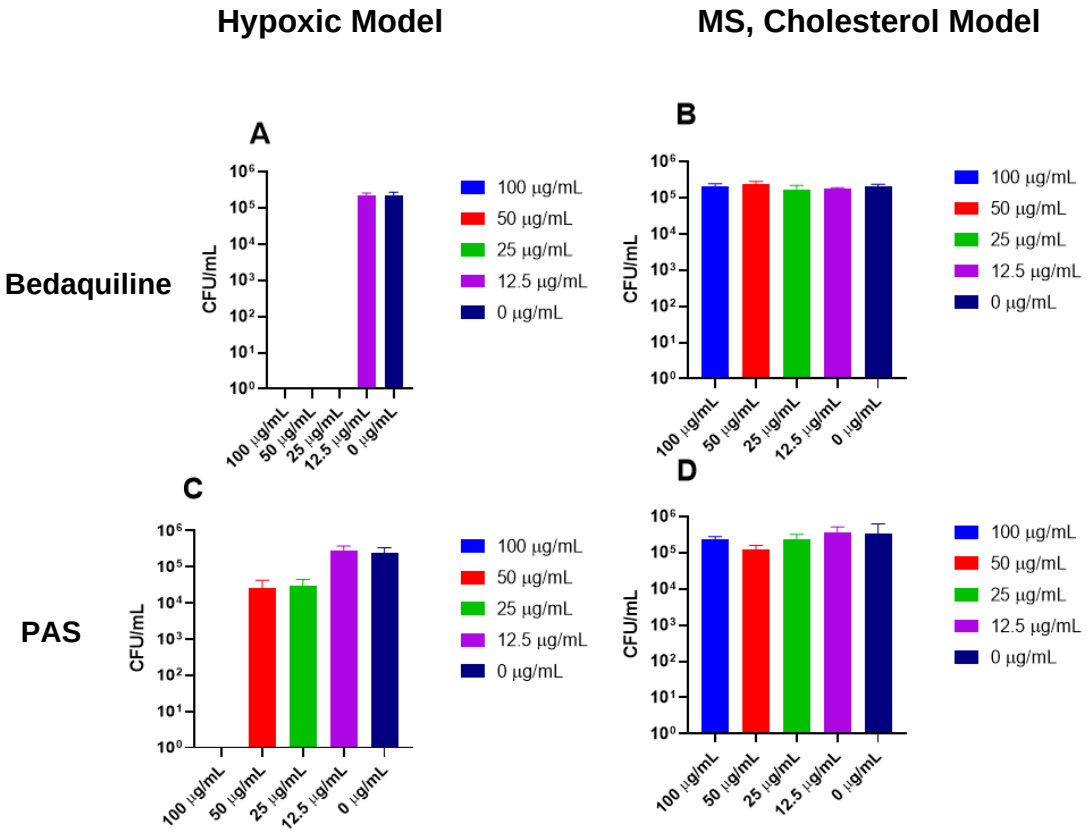

Figure 3.7: **Endpoint MBCs for Bedaquiline against the Hypoxic model (A) and the Multi-Stress, Cholesterol model (B) and for PAS against the Hypoxic model (C) and the Multi-Stress, Cholesterol model (D).** The above CFU/mL counts represent the mean resuscitated growth from the absorbance assays found in Figure 3.6. The experiment was conducted in triplicate (n=3).

The MS, cholesterol model has been notable for even, compared with traditional models of NRP, a heightened level of antibiotic resistance. Nevertheless, BDQ is arguably the most potent anti-tubercular drug currently in our arsenal. Therefore, ascertaining the susceptibility of NRP *M. bovis* BCG to BDQ in this novel model was highly important and interesting. The absorbance curve for MS, Cholesterol model NRP *M. bovis* BCG challenged with a serial dilution of BDQ can be found in Figure 3.6.D. The highlight is that no concentration of BDQ is showing activity against NRP *M. bovis* BCG in this model despite the activity seen in the hypoxic model. Indeed, all concentrations of BDQ closely mimic the 0 µg/mL control curve over a period of 1000 h (Figure 3.6.D). There is a slight deviation in OD for 100 µg/mL at approximately 300 h but this deviation returns to the stationary curve around 75 h later. By the endpoint of the assay, all concentration of BDQ were closely correlated to the 0 µg/mL (Figure 3.6.D). As discussed in the BDQ results for the Hypoxic model, this antibiotic activity assay

was completed during humidity fluctuations in the anaerobic cabinet. Again, to provide some more evidence for these MICs, endpoint MBC analysis was undertaken (Figure 3.7). All cultures tested resuscitated upon rich agar and oxygenated environment, independant of the concentration of BDQ (Figure 3.7.B). This data shows that BDQ has no effect on *M. bovis* BCG if it is specially in MS, Cholesterol model NRP.

Throughout this drug screening process, it has become clear that the NRP state does indeed confer “antibiotic indifference”, however, the true scale of this has been underestimated (Wayne & Sohaskey, 2001). The heightened level of antibiotic resistance in the multi-stress, cholesterol model has been fascinating to discover and holds real world implications. It is a commonly held belief that BDQ treatment acts as a last resort silver bullet, that will probably kill the *M. tuberculosis* infection but may have severe side effects that could be debilitating to the patient (Mahajan, 2013; Pontali et al., 2019). It was thought to be effective on *M. tuberculosis* at all times no matter the physiological environment, as ATP-synthase in theory should be an enzyme that is constantly active. This is reflected in the activity shown against the Wayne model based hypoxic model of NRP. The juxtaposition between the two models, this heightening of resistance, could not be more clearly shown than in Figure 3.6.

The MIC testing for PAS was done separately to the above assays and was later grouped with BDQ, AMI and TIG to form the BATP screen. Unfortunately, the antibiotic testing for PAS was conducted as the outbreak of COVID-19 hit in March 2020 whereas the rest of the screen was conducted earlier in 2019. Therefore, due to staggering of experiment set up, the testing of PAS against the multi-stress model was mostly completed (936 h instead of 1000 h) just before the outbreak; whereas the experiment for PAS in the hypoxic model only reached 554 h of assay before the laboratory was closed (Figure 3.6). The absorbance curves have been included as the hypoxic model was already displaying clear antibiotic susceptibility and the multi-stress, cholesterol curve had essentially reached the endpoint. With that said, the lack of carrying out the experiment to the endpoint may result in this MIC being conservative and lower concentrations could have shown susceptibility

It demonstrated a strong effect towards NRP *M. bovis* BCG in hypoxic model resulting in an MIC of 12.5 µg/mL. This dose dependant response to PAS can be seen in Figure 3.6.A. There is a clear dose dependant reaction from the highest concentration of 100 µg/mL down through to 12.5 µg/mL but 6.25 µg/mL does not show any decrease in OD (Figure 3.6.A). It would be expected that if this assay had been taken to completion at 1000 h, the inhibitory trend for 100 µg/mL - 25 µg/mL would have continued and then settled back to stationary in a similar way to all other MIC tests carried out in this model (Figure 3.6.A).

Yet again, when tested in the MS, cholesterol model, this efficacy is completely lost. There is no change in absorbance value for any culture throughout the assay which at 936 h is practically at completion, particularly as PAS showed activity against the hypoxic model by 400 h of assay (Figure 3.6.B). The control curve remains stationary and unmoved throughout and all other cultures mirrors this pattern. There is no change despite varying levels of PAS. Therefore, there is no activity for PAS against NRP *M. bovis* BCG in the multi-stress, cholesterol model (Figure 3.6.B)

Table 3.3: **Table showing the activity of Tigecycline and Amikacin against NRP *M. bovis* BCG in two models of NRP: the Hypoxic model and the Multi-Stress, Cholesterol model.**

Antimicrobial	Hypoxic Model	MS, Cholesterol Model
Tigecycline	> 100 µg/mL?	> 100 µg/mL?
Amikacin	> 100 µg/mL	> 100 µg/mL

AMI is an aminoglycoside occasionally used in MDR-TB treatments and was hence included in this screen to test against NRP *M. bovis* BCG (Modongo et al., 2014). In both models of NRP, the absorbance curves stay representative to the control curves regardless of concentration of AMI (Table 3.3). Despite high levels of AMI present in the cultures there is no significant change in absorbance away from 0 µg/mL. There was also no difference in AMI susceptibility between NRP models tested (Table 3.3).

The testing for TIG was carried out as a part of this screen, however, at the higher concentrations the strong colour of TIG obscured the absorbance reading. This meant that the highest concentrations tested 100 µg/mL, 50 µg/mL and 25 µg/mL of TIG the data has been discounted. As can be seen at these concentrations of TIG there is no difference between absorbance curves despite differing concentrations of TIG (Table 3.3). This lack of susceptibility is consistent across both models. Therefore, there is no MIC for TIG against NRP *M. bovis* BCG (Table 3.3).

3.2.3 Testing the Novel Compound (DR10) series against NRP *M. bovis* BCG

All the previously discussed antimicrobial testing was against established antibiotics and are being either repurposed into TB therapy or are in late-stage clinical trials, however, most have a proven efficacy against active TB. The following results involve the testing of a novel compound series created by Dr. Dan Rathbone of Aston University who identified compound V4 as the lead compound. Dr. Rathbone designed these compounds to have an MOA that acted against the mycobacterial cell wall; however. To establish the activity profile the DR10 series has against *M. bovis* BCG in all forms, aerobic MIC testing was conducted followed by the NRP microtitre plate assay using both models.

All of the DR10 molecules were tested against activity growing *M. bovis* BCG using the aerobic MIC test assay (see **section 7.2**). In short, a growth curve was formed after 200 h of aerobic incubation. Analysis of the trends in growth curves compared with the control allowed the identification of hits. A summary table of the results can be found in Table 3.4

Table 3.4: **Summary Table of the Aerobic activity of DR10 compounds in the Hypoxic Model (7H9-ADC Media) and Multi-Stress, Cholesterol Model (minimal cholesterol media).** Susceptible MIC values indicated in Green, Resistance indicated by Red.

DR10 Compound	Hypoxic Model	Cholesterol Model
V4	100 µg/mL	100 µg/mL
V6	>100 µg/mL	>100 µg/mL
A	1 µg/mL	>100 µg/mL
B	100 µg/mL	100 µg/mL
D	>100 µg/mL	>100 µg/mL
F	>100 µg/mL	>100 µg/mL
G	10 µg/mL	100 µg/mL
J	>100 µg/mL	100 µg/mL

Of the 8 novels compounds, there was some success in the aerobic assay (Table 3.4). The lead compound V4 showed activity against *M. bovis* BCG growing in 7H9 media and against *M. bovis* BCG growing in cholesterol media at the highest concentration tested, 100 µg/mL. There did not appear to be any differences in antimicrobial susceptibility between the two media for V4. (Table 3.4). The second compound, V6, did not show any efficacy against *M. bovis* BCG in either media. A was the third compound and showed activity against *M. bovis* BCG but only in 7H9 media. However, it displayed the strongest MIC of the compound series at1 µg/mL despite this activity only being shown in one medium (Table 3.4). In cholesterol media, no MIC was found as no change in absorbance was observed. The fourth compound, B, met with slightly more success and gave an MIC of 100 µg/mL in both conditions, displaying a similarity not seen in A (Table 3.4). No MIC was found for either D or F in either condition with no statistically significant deviation found in any of the associated growth curves. The penultimate compound, G, resulted in an interesting set of MICs with 7H9 media (10 µg/mL) and cholesterol media (100 µg/mL). The MIC values for G show a fascinating MIC shift between the media not seen in any other DR10 compound (Table 3.4). The last compound in

the series tested was J, who similar to G, gave some unexpected results. With everything tested previously, the pattern appeared to be that if activity was going to be shown, it would appear in 7H9 media and if it was particularly effective then there would also be efficacy in cholesterol media. The activity of J is the antithesis of this. J has an MIC against *M. bovis* BCG growing in cholesterol media of 100 µg/mL but has no MIC found against *M. bovis* BCG in 7H9 media (Table 3.4).

The aerobic results of the DR10 series contribute a fascinating insight into the state of the bacteria when they are logarithmically growing (Table 3.4). It was previously identified that there was some attenuation of growth in the cholesterol media however, this was mainly attributed to the minimal nature of the medium. However, the disparity in MICs between the two media lead to the inference that there is a possible subtle change in phenotype for *Mycobacteria* between the two media. Perhaps, this is indicative of the cholesterol media having a slightly more protective phenotype as it prepares for the possibility of entry into the NRP state.

Following the aerobic screening of the DR10 novel compound series, the compound screen was progressed into the NRP microtitre plate using both models. The progression into the NRP assay was augmented by the proof of anti-tubercular activity across many of the novel compounds not just the lead compound, V4.

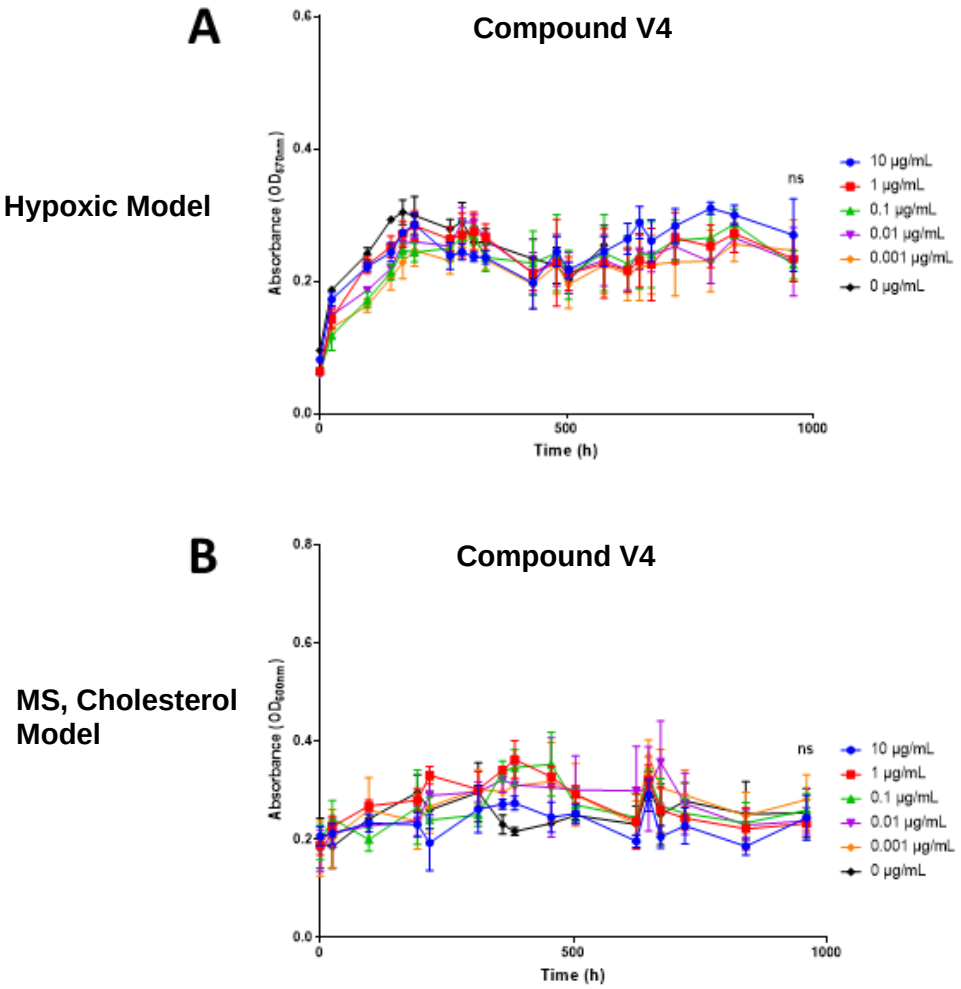

Figure 3.8: **Absorbance Curves of NRP *M. bovis* BCG challenged with DR10 compound V4 in the Hypoxic model (A) and the Multi-Stress, Cholesterol model (B).** These assays were conducted in the anaerobic microtitre methodology and measured for 1000 h. The data is the plotted means of four replicates for each concentration. Statistical analysis was completed for each assay by endpoint ANOVA analysis. In both models, Compound V4 was found to be non-significant with p values of 0.4387 and 0.3128 respectively.

Therefore, the compounds were tested as a serial dilution against both models of NRP in the microtitre plate assay (Figure 3.8, Table 3.5). The compound series was based around the lead compound V4 which was thought by the chemists responsible for the creation of the screen to have the best efficacy. Therefore, the absorbance curves for the V4 assay against NRP *M. bovis* BCG against both models are presented in Figure 3.8. No MIC for V4 was found against *M. bovis* BCG in either model at any concentration tested. There are some fluctuations in this experiment, however the same trend in fluctuation can also be observed in the no drug control (Figure 3.8). Indeed, statistical analysis of these growth curves show that any change

in absorbance away from the mean was down to chance and not attributable to drug activity (hypoxic p value = 0.9307, cholesterol p value = 0.7033). The full results of the DR10 screen in both models can be found in Table 3.5.

Table 3.5: **Summary Table of the activity of the DR10 compound series**

DR10 Compound	Hypoxic Model MIC	Cholesterol Model MIC
V4	>100 µg/mL	>100 µg/mL
V6	>100 µg/mL	>100 µg/mL
A	>100 µg/mL	>100 µg/mL
B	>100 µg/mL	>100 µg/mL
D	>100 µg/mL	>100 µg/mL
F	>100 µg/mL	>100 µg/mL
G	>100 µg/mL	>100 µg/mL
J	>100 µg/mL	>100 µg/mL

As a caveat, compound D was tested but after approximately 200 h of incubation, the two highest concentrations of D precipitated out of solution therefore the results of this assay were inconclusive. Table 3.5 shows that no compound in the DR10 screen had a significant inhibitory effect on NRP *M. bovis* BCG at any concentration tested. There was no significant decline in absorbance away from the control curve for any culture treated with a DR10 compound. Therefore, no MIC can be reported for any of the DR10 compound series (Table 3.5).

Unfortunately, this lack of an ostensible effect from any DR10 compound on *M. bovis* BCG in either model shows that this compound series is unlikely to be a contender for any future LTBI treatment (Figure 3.8, Table 3.5). This lack of activity is potentially due to the proposed mechanism of action of the compound series, cell wall inhibition. As demonstrated by INH,

most cell wall inhibitors lack activity against NRP TB. As in the NRP state, the bacterium is not replicating, inhibition of the varied enzymatic processes that go into the synthesis of the mycobacterial cell wall are inconsequential to the bacterium. A lack of replication results in many common cell wall drug targets becoming non essential meaning that inhibition of these targets does not negatively affect the bacterium (Wayne & Sohaskey, 2001). If this compound series is indeed inhibiting cell wall synthesis, it would explain why this series is greatly effective against replicating aerobic *Mycobacteria* but loses all activity when the bacteria are in the NRP state. It is for these same reasons that INH loses its activity in NRP.

However, this compound series did show a broad activity on actively growing *M. bovis* BCG so even if these compounds are not suitable drugs for LTBI, they remain a compound series of interest for active TB treatment (Table 3.4).

3.2.4 Antimicrobial Testing of the University of Hertfordshire Novel Compound series (HERTS)

This antimicrobial screen was conducted as part of a collaborative project with the University of Hertfordshire to screen their novel compound series against NRP *M. bovis* BCG. Previous research had established anti-tubercular activity for this compound, particularly for lead compound 1B. These compounds are based on INH are derivatives of INH. The request from the collaborators was to test this compound series in the hypoxic model only as this research was to form part of a larger set of research about the development of the novel compound. This testing was completed under the understanding that if any efficacy was shown, experiments would continue into the multi-stress, cholesterol model to ascertain if this efficacy would be maintained.

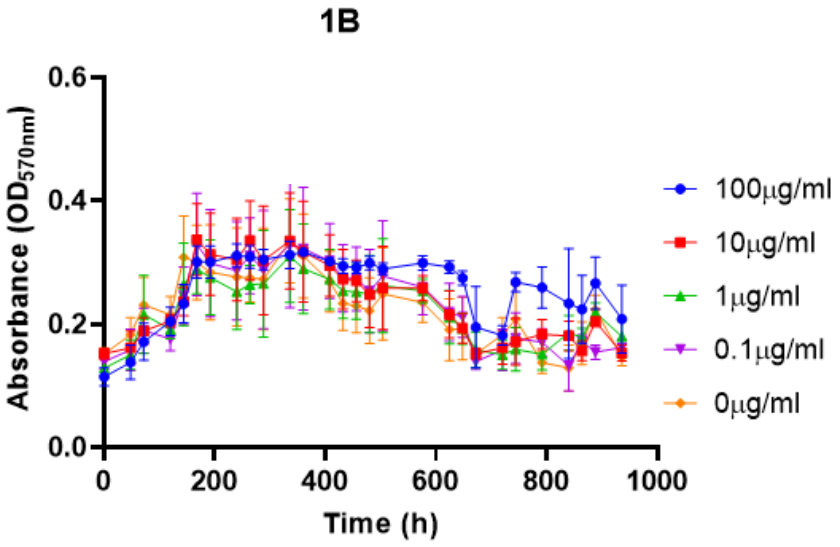

Figure 3.9: **Absorbance Curve of lead HERTS compound 1B against the Hypoxic model**

The above assay was conducted in the anaerobic microtitre methodology and measured for 1000 h. The data shows the plotted means of four replicates for each concentration. Statistical analysis was completed for each assay by endpoint ANOVA analysis. HERTS compound 1b was found to be non-significant with p values of 0.9792

The lead compound, 1B, was tested in the NRP microtitre assay as a serial dilution and these absorbance curves can be found in Figure 3.9. Throughout the assay, no concentration of 1B is showing a significant decline in absorbance. This is consistent throughout the experiment

that all curves stay similar to the control absorbance curve (0 µg/mL) (Figure 3.9). This lack of any change in absorbance away from the control indicates that 1B is not effective against hypoxic model NRP *M. bovis* BCG. The statistical ANOVA analysis conducted showed that no concentration of 1B was significant (p value = 0.9792) which adds credence to the conclusion that 1B has no activity in the Hypoxic model of NRP.

All of the other HERTS compound results can be found in Table 3.6 which summarises the MICs found. This table includes the results for INH which are less of a result in this case and are acting as a control and as the parent compound (Table 3.6). The serial dilution was carried up to 100 µg/mL however, compound G and compound J were strongly coloured so for these compounds the concentration of 100 µg/mL was excluded. Table 3.6 reports that no MIC was found for the HERTS compounds against hypoxic model NRP *M. bovis* BCG. However, a summary of these curves is that no concentration of any HERTS compound inflicted a decline in the absorbance of *M. bovis* BCG. These absorbance curves do show a great deal of fluctuation; however, all of these fluctuations are matched by the no drug control, indicating that these fluctuations are not due to drug activity but more probably to plate reader error. Statistical ANOVA analysis was conducted on each HERTS compound's absorbance curves and these p values greatly range however. all are over 0.05 and are thus deemed non-significant.

Table 3.6: **Summary Table of the activity of HERTS compounds in the NRP state using the Hypoxic Model**

HERTS Compound	Hypoxic Model MIC
1B	>100 µg/mL
1E	>100 µg/mL
1G	>100 µg/mL
1H	>100 µg/mL
1J	>100 µg/mL
1N	>100 µg/mL
INH	>100 µg/mL

All of the above data comes together to show that the HERTS compound series does not show any activity against NRP *M. bovis* BCG (Figure 3.9, Table 3.6). This result is not totally unexpected as this compound series is derived from INH, which due to its MOA has no activity against NRP *Mycobacteria.* The collaborators hoped that due to the modifications and novel nature of these compounds that efficacy would be acquired against LTBI. However, as far as can be seen with these compounds, the MOA is still involved in cell wall synthesis. As the bacterium is not dividing in the Non-Replicating Persistent state, inhibition of this process does not have the expected negative effect on the culture. Indeed, the hallmark of the NRP state is said to be “drug indifference”, however, it is possible that we are just targeting the wrong things. The one thing is about the mycobacterial NRP state is that the priorities and processes of the bacterium have utterly changed from that of an active state. Whilst the HERTS compound series has fantastic anti-tubercular activity against active TB, there was unfortunately no antimicrobial activity against LTBI.

3.2.5 High Throughput Screen consisting of Antibiotic and Natural Products (ASNP)

The ASNP screen was created by Dr. Jonathan Cox as a HTS to be investigated against *Mycobacteria* sp in as many ways as possible. Therefore, these are the results for the screen against both the Hypoxic NRP model and the MS, cholesterol model of NRP *M. bovis* BCG. The ASNP screen consists of a mixture repurposed antibiotics, antimicrobials and natural products. The full list of what the ASNP screen consists can be found in Appendix A. For ease, codes for each compound were made are referred to as such. As this was a HTS, there was not a dilution of compounds, just a straight shot of the highest concentration of each compound. The results of this are presented in Figure 3.10, where Figure 3.10.A shows the plate map, Figure 3.10.B is a heat map of the Hypoxic model results and Figure 3.10.C is a heat map of the MS, Cholesterol model results. This was completed to show a snap shot of the results that was easy to read, the full absorbance curves are found in Appendix B. As there are so many "experiments" in a HTS, they are grouped by row of the plate (Figure 3.10.A).

In a typical HTS, it is common practice to have a positive and a negative drug, or one drug that clearly shows activity and one that will show no activity. In the hypoxic model HTS assay, this is relatively simple with MET as the positive drug and INH as the negative. However, as previously discussed, MET has no activity in the multi-stress, cholesterol model which means that in the novel model MET is not capable of being the positive control (*see* **section 2.2.6**). This resulted in there not being a positive control for the HTS in the MS, Cholesterol model. Therefore, the result from MET in the Hypoxic model was used as the positive control.

A

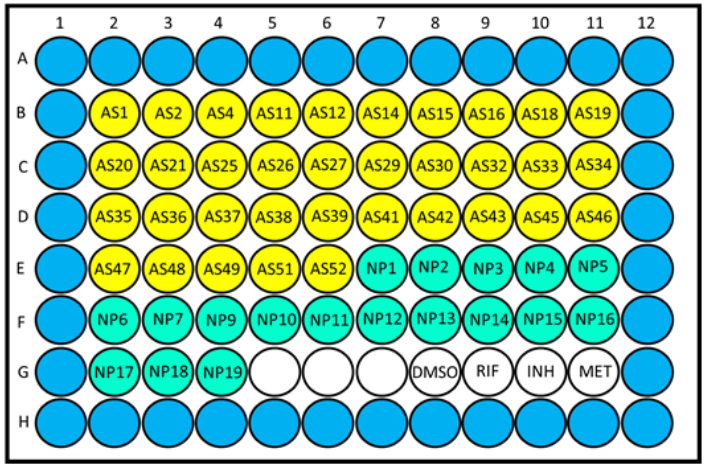

B

	1	2	3	4	5	6	7	8	9	10	11	12
A												
B		0.14167	0.151	0.11933	0.13133	0.131	0.13033	0.20725	0.154	0.213	0.13325	
C		0.196	0.14667	0.19033	0.18167	0.15267	0.16233	0.15633	0.163	0.17567	0.206	
D		0.14875	0.13133	0.231	0.24367	0.148	0.155	0.15433	0.15667	0.14267	0.15367	
E		0.13	0.14833	0.133	0.15567	0.14633	0.16	0.182	0.2	0.1825	0.184	
F		0.1995	0.2285	0.20125	0.228	0.208	0.4345	0.2595	0.30925	0.21575	0.20933	
G		0.17993	0.25767	0.2395				0.19133	0.184	0.18833	0.0515	
H												

C

	1	2	3	4	5	6	7	8	9	10	11	12
A												
B		0.2705	0.24275	0.2975	0.27467	0.23925	0.2585	0.30575	0.296	0.31933	0.2965	
C		0.3235	0.23375	0.23475	0.27575	0.26775	0.25725	0.3035	0.2595	0.2515	0.30425	
D		0.29	0.2995	0.29175	0.29525	0.2875	0.3065	0.32725	0.271	0.31275	0.293	
E		0.26975	0.28	0.25833	0.24925	0.2785	0.33525	0.2625	0.31175	0.30875	0.276	
F		0.292	0.3115	0.30075	0.30375	0.301	0.61525	0.37975	0.3875	0.357	0.377	
G		0.3155	0.33067	0.28575		0.0515		0.29075	0.2845	0.29125	0.2945	
H												

Figure 3.10: **(A) Identifying Plate Map of the ASNP screen:** AS (yellow) stands for Antibiotic Screen and NP (blue) stands for Natural Product. The controls (white) were DMSO, Rifampicin (RIF), Isoniazid (INH) and Metronidazole (MET). **(B) Heat Map Results of ASNP screen tested against the Hypoxic Model, (C) Heat Map Results of ASNP screen tested against the Multi-Stress, Cholesterol Model.** The values represented in both heat maps depict the mean endpoint OD readings of these assays. All assays were completed in n=4. The heat map for the MS, Cholesterol model in well G6 shows the result of MET from the Hypoxic model as at the time of measurement, no positive control had been identified for the MS, Cholesterol model.

The results for the Hypoxic model HTS overall demonstrated the “drug indifference” referred to when talking about the NRP state (Figure 3.10.B). Of all the compounds tested, there are perhaps only two that show activity AS4 and AS19 (cetylpyridium chloride and cetylpyridium chloride S). Regarding their growth curve, there is a distinct negative trend seen at the beginning of the assay that remain consistent throughout and it ends the experiment on a lower OD than the other compounds. Otherwise, the majority of other compound tested remain relatively consistent with the associated no drug control (designated as positive in this experiment). It could also be argued that D9 shows slight activity for an initial decrease in OD but this does not stay consistent and recovers.

The most apparent drug activity in the whole HTS is clearly the positive control MET with the lowest reduction away from the control and this can be clearly seen in the Row G growth curve (Figure 3.10.B). Likewise, the curve for INH acts as expected by remaining close to the no drug control.

This HTS, perhaps shows glimmers of hits but particularly in comparison to the positive control (MET) the drugs tested in this screen are not effective against NRP *M. bovis* BCG.

This HTS was also conducted in the multi-stress, cholesterol model which aims to be more physiologically relevant than the hypoxic model and somewhat in proof of this, it has shown a heightened drug indifference to its comparator. One of the strengths of the HTS in the hypoxic model was being able to contrast the results with positive control which conducting a HTS in this model it does not have. However, there was no drug activity to even potentially investigate by comparison to a positive control (Figure 3.10.C). Indeed, all of the compounds in the ASNP screen tested against the multi-stress, cholesterol model show no activity throughout the assay with all absorbances remaining close to absorbance of INH (Figure 3.10.C). The heat maps of activity do not highlight any of the drugs tested as having even slight activity against NRP *M. bovis* BCG. It appears that in this model there is a heightening of resistance that can be clearly observed in this HTS (Figure 3.10). The hypoxic model displays a broad range of resistance, but it is not as clean cut. Several compounds appear to exert a moderate antimicrobial effect

against hypoxic model NRP *M. bovis* BCG (Figure 3.10.B). When the NRP model is changed to the multi-stress, cholesterol model, there is no distinct decline in OD comparable to the decline seen by MET in the hypoxic model.

Whilst this HTS did not result in the identification of any hits against our novel model, it has served to highlight the huge drug resistance displayed by the multi-stress, cholesterol model. If this novel model is a closer representation of the physiological LTBI, this drug resistance seen *in vitro* could change the ways latency is viewed in regard to TB.

3.2.6 Leprosy Drugs, Dapsone and Clofazimine, Checkerboard Assay

Clofazimine and Dapsone (DAP), along with Rifampicin (RIF), form the combination therapy used to treat *Mycobacterium leprae* – the causative agent of Leprosy (Cambau & Williams, 2019; World Health Organization, 2012). First discovered by Hansen in 1873, *M. leprae* is a notoriously fastidious bacterium that is view as the most essential *Mycobacteria* (Gillis & Williams, 2000; Macdonald, 1914). Another facet of *M. leprae* is the essentiality of cholesterol catabolism and an interaction with foamy macrophages to gain access to lipid droplets (Marques et al., 2015).

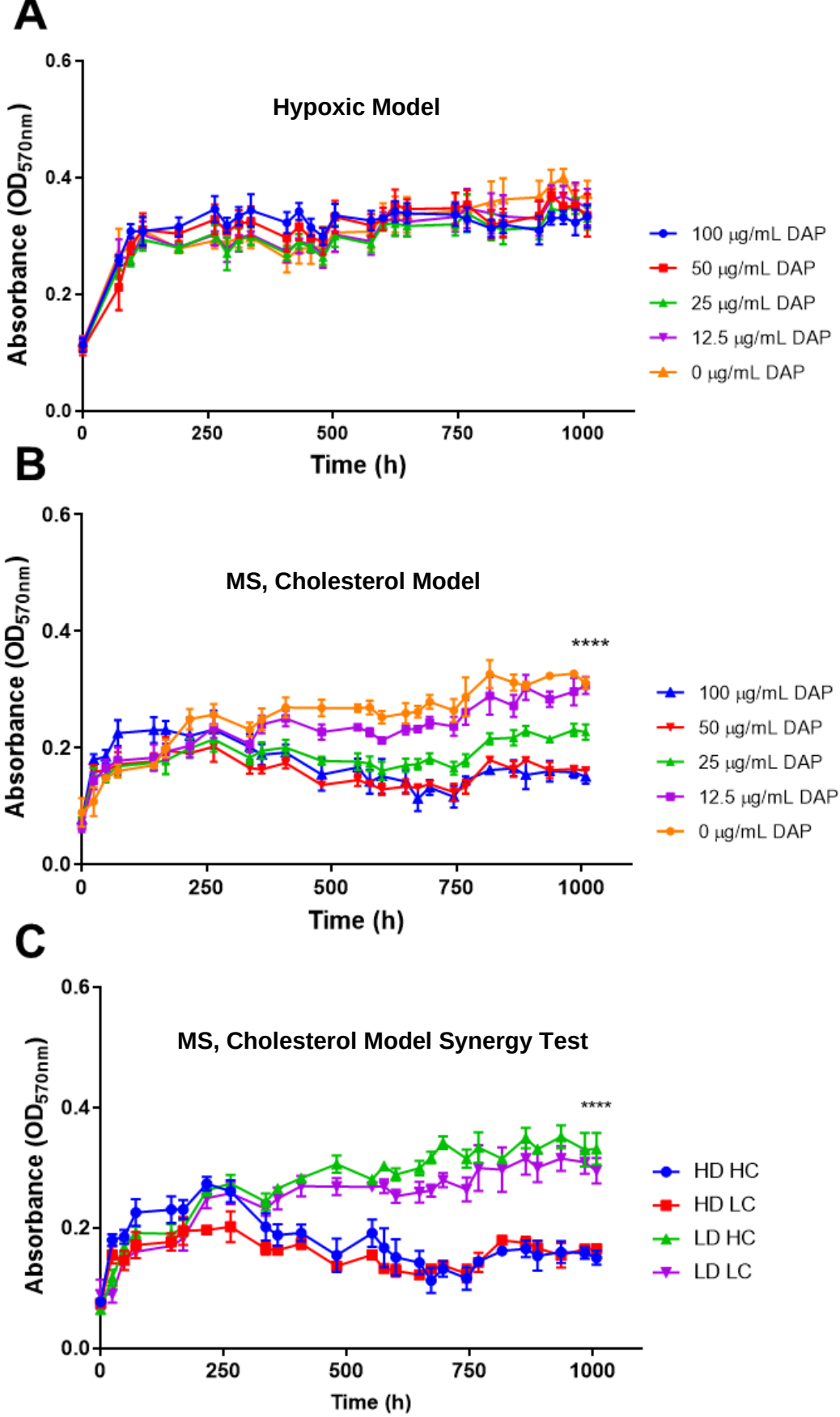

Figure 3.11: **Checkerboard Assay of Dapsone and Clofazimine.** The results of Dapsone with no added Clofazimine are shown in (A) for the Hypoxic model and (B) for the MS, Cholesterol model. The results of the synergy "checkerboard" assay are shown in (C). This experiment was conducted in the anaerobic microtitre plate method for 1000 h, in four replicates. The statistics shown are endpoint ANOVA analysis. (A) shows no statistical significance for DAP in the Hypoxic model, p value = 0.7592. (B) MS, Cholesterol model against Dapsone showed a statistically significant response with a p value of <0.0001 (C) Checkerboard Analysis of the top concentration of each drug in the Multi-Stress, Cholesterol Model. Thus, HD,HC indicates 100 µg/mL DAP, 12 µg/mL CLZ; HD, LC indicated 100 µg/mL DAP, 0 µg/mL CLZ; LD, HC indicates 0 µg/mL DAP, 12 µg/mL CLZ; finally, LD,LC indicates 0 µg/mL DAP, 0 µg/mL CLZ. LD,LC in this assay is acting as the no drug control.

M. leprae is considered the most essential *Mycobacteria* and has a minimal genome to reflect this (Lowe, 1950; Macdonald, 1914). It could be argued that the NRP state of *M. tuberculosis* is more reminiscent of *M. leprae* than active *M. tuberculosis*. Therefore, as RIF has already been extensively tested and used as the current therapy for TB; DAP and clofazimine were tested against NRP *M. bovis* BCG in both models as, in theory, if there is drug activity in the essential *M. leprae* perhaps this carries across into the NRP state.

Clofazimine (CLZ) was first identified in the 1950s as an anti-tubercular agent, however, despite widespread use from 1968, its MOA remained poorly defined (Arbiser & Moschella, 1995; Shen et al., 2010; Xu et al., 2012). Nevertheless, in 1981 the WHO highlighted CLZ for its strong antimicrobial and anti-inflammatory activity and recommended it for inclusion in a combination therapy for leprosy (Lowe, 1950; Smith et al., 2017). The MOA for CLZ is now suggested to be redox cycling production of radical oxygen species (ROS) (Cholo et al., 2017). CLZ is effective against *M. tuberculosis* and is sometimes included as part of the combination therapy for drug resistant TB (Xu et al., 2012).

Dapsone is part of the Sulphone family of chemicals which was first synthesised in 1908 by German chemists, Fromm and Whittman and was first tested *in vivo* in 1937 against a murine model of Streptococcal infections (Buttle et al., 1937; Fromm & Wittmann, 1908). Dapsone, and its derivative Promin, was found to be active against *Mycobacterium leprae* and was moved into treating patients by 1943 (Faget et al., 1966; Faget & Pogge, 1945). Dapsone is still used today as part of a combination therapy to treat *M. leprae* cases, along with Rifampicin and Clofazimine (World Health Organization, 2012). Due to its relatively weak activity against *M. tuberculosis,* it was discounted from drug regimens in favour of other more potent drugs with less severe side effects, for example, Streptomycin, Isoniazid, Rifampicin etc. Currently, Dapsone is included occasionally in cases of MDR- and XDR-TB (Wozel & Blasum, 2014).

This experiment investigated the activity of DAP and CLZ against NRP state *M. bovis* BCG as a checkerboard assay (Figure 3.11). Therefore, this data is present in three parts. One

absorbance curve shows the activity of DAP in isolation, the next shows the activity of CLZ in isolation and the third presents the combination of the two (Figure 3.11).

Figure 3.11.A shows DAP showing no chemotherapeutic effect on NRP *M.bovis* in the hypoxic model. Throughout 1000 h of incubation, there is no significant change in absorbance away from the control for any concentration of DAP (Figure 3.11.A). The initial 100 h which show a fluctuating increase in absorbance typical of NRP stage I. After this, all absorbance curves settle into a stationary curve which remains consistent for the duration of the assay (Figure 3.11.A). Statistical ANOVA analysis confirms the visual result, that there is no statistically significant deviation away from the control for any concentration of DAP. Endpoint MBCs from the culture exposed to 25 µg/mL of DAP were also taken. This resulted in resuscitated culture growth of $2.6x10^6$ CFU/mL (Table 3.7).

When tested against the MS, cholesterol model, Dapsone showed a perspicuous dose dependant response (Figure 3.13.B). A clear decline in absorbance for the three highest concentrations of DAP (100 µg/mL, 50 µg/mL and 25 µg/mL) can be observed from approximately 250 h of incubation (Figure 3.13.B). After this time point, the cultures with 100 µg/mL and 50 µg/mL DAP proceed with a steady decline in absorbance until 750 h at which point it becomes stationary again. The absorbance curve for 25 µg/mL also starts showing a decline in OD at 250 h but does not reach the same low point in absorbance as the other two concentrations (Figure 3.13.B). Instead, this curve declines slowly and become stationary again at around 650 h. At the endpoint of the assay, it forms a midpoint between the clearly inhibited cultures (100 µg/mL and 50 µg/mL) and the unaffected 12.5 µg/mL and the no drug control (0 µg/mL) with an OD of 0.221 (Figure 3.13.B). Statistical ANOVA analysis ($p = <0.0001$) demonstrated that the reduction in growth curve from the control is significant. This was further tested by an endpoint MBC test (Table 3.7) in which at 25µg/mL of DAP, no bacterial growth was observed. To test that this was not skewed by the added factor of resuscitation the endpoint MBCs for 12.5 µg/mL of DAP and the negative control were also measured. The aforementioned cultures regrew to $1.3x10^6$ CFU/mL and $2.4x10^6$ CFU/mL. Both

showed confluent growth despite the resuscitation process showing that the null growth from 25 µg/mL is a direct result of DAP chemotherapy (Table 3.7

Table 3.7: **MIC and MBC of DAP in the Hypoxic Model and in the MS, Cholesterol Model.** The Hypoxic model does not report an MIC for DAP >100 µg/mL. Likewise, all Hypoxic models treated with DAP regrew, thus no MBC was found (>100 µg/mL). In the MS, Cholesterol model, DAP was effective to a minimum concentration of 25 µg/mL, and showed no regrowth at the same DAP concentration.

Growth Conditions	MIC (µg/mL)	MBC (µg/mL)	CFU/mL at MBC
Hypoxic Model	>100	>100	$2.6x10^6$
MS, Cholesterol Model	25	25	0

Clofazimine (CLZ) showed no inhibitory activity against NRP *M. bovis* BCG in either model; producing two consistently stationary absorbance curves with no deviation found. However, due to the strong colouration of CLZ, it was only able to be assayed up to a maximum concentration of 12 µg/mL. The results for 12 µg/mL CLZ assayed against the MS, Cholesterol model without Dapsone can be found in Figure 3.13.C: LD,HC. This absorbance curve produces a stationary curve without any decline that closely follows the trend of the no drug control (Figure 3.13.C: LD,LC)

3.2.8 Resuscitation of *Mycobacterium bovis* BCG in the presence of frontline antimicrobials, Isoniazid and Rifampicin

The resuscitation of NRP state *Mycobacteria* back to an active state is a poorly defined, yet fascinating area of research (Rustad et al., 2017; Trutneva et al., 2020; Veatch & Kaushal, 2018). For clear reasons, studying the process of resuscitation *in vivo* has proven immensely challenging – not least for the fact that most of the *in vivo* latency models do not have an NRP state to resuscitate from. In the previous chapter, resuscitation growth curves were presented form both models that consisted of *M. bovis* BCG resuscitating after 10,000 h of incubation (*see* **section 2.2.6**). This highlighted a distinct difference in resuscitation between the two models. To investigate this further, NRP *M. bovis* BCG from both models was resuscitated in the presence of INH and RIF.

Figure 3.14 contain a set of growth curves from *M. bovis* BCG which had been in the NRP state for 20,000 h. These cultures were chosen instead of cultures at the end of 1000 h of NRP as instead of looking the antibiotic susceptibility, this experiment was aimed at discovering the antibiotic susceptibility profile of a culture which had been NRP for an extended time period as in chronic LTBI.

These cultures were unsealed and placed into fresh ADC enriched 7H9 media to resuscitate. However, some were also resuscitated in the presence of INH or RIF to see if they could inhibit the resuscitation of the bacteria (Figure 3.14).

This resuscitation period has a considerable lag phase lasting around 300 h of incubation (*see* **section 2.2.8**). Nevertheless, cultures from both models which were not drug treated successfully resuscitated despite being in the NRP state for 20,000 h (Figure 3.14). The culture that was in the MS, cholesterol model NRP state began to actively replicate and grow far faster than bacteria in the hypoxic model (Figure 3.14). Additionally, the multi-stress, cholesterol cultures resuscitated to far higher and OD than the hypoxic model

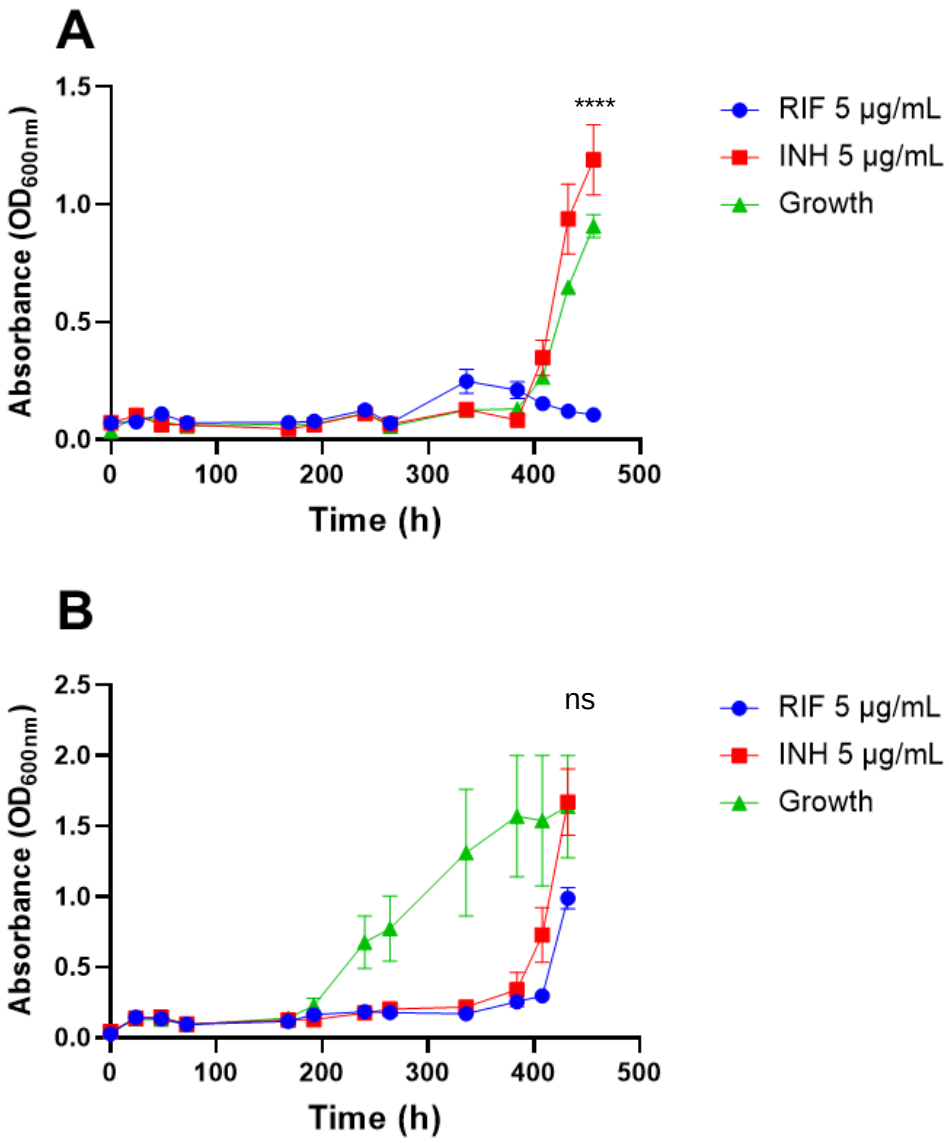

Figure 3.12: **Resuscitation in the presence of frontline antimicrobials** (A) Resuscitation of Hypoxic Model NRP *M. bovis* in the presence of high concentration frontline antimicrobials and by itself (Growth). The difference between the Growth curve and the RIF curve was found to be statistically significant by endpoint ANOVA analysis ($p = <0.0001$), however, between INH and Growth there was no statistical significance ($p = 0.0980$). (B) Resuscitation of Multi-Stress, Cholesterol NRP *M. bovis* in the presence of high concentration frontline antimicrobials and by itself (Growth). Endpoint ANOVA analysis found no statistical difference between Growth and INH and Growth and RIF; p values were 0.9940 and 0.1757. All experiments were conducted with five replicates (n=5).

The main focus point of these experiments however, is not if the cultures can resuscitate, it is if they can in the presence of frontline drugs, INH and RIF. In the NRP state, *M. bovis* BCG was totally drug resistant to the effects of both of these antimicrobials. Conversely, active *M. bovis* BCG is susceptible to both. These growth curves show that when *M. bovis* BCG from the hypoxic model is resuscitated in the presence of 5 µg/mL of RIF, the culture (n=4) fails to resuscitate (Figure 3.14.A). None of the replicates gained a higher OD than the initial starting value. Certainly, this culture did not show a period of exponential growth that the resuscitating culture that was not treated with RIF shows. Therefore, it can be assumed that the presence of RIF inhibits the resuscitation of hypoxic model *M. bovis* BCG and possibly exerts a bactericidal effect (Figure 3.14.A). This is in direct contrast to the growth curve from the resuscitated culture treated with INH (Figure 3.14.A). Likewise, to the RIF experiment, *M. bovis* BCG that had been in the hypoxic model NRP state for 20,000 h was attempted to resuscitate in the presence of 5 µg/mL of INH (Figure 3.14.A). In this a full growth curve was obtained despite the presence of INH. There is an extended lag phase but after approximately 350 h of incubation, a clear log phase can be observed (Figure 3.14.A). Indeed, this log phase reaches a higher OD than the untreated culture. This clearly demonstrates the ability of ex-NRP state *M. bovis* BCG to fully resuscitate despite frontline antibiotic INH.

This fantastic result is shown even more clearly in the multi-stress, cholesterol model (Figure 3.14.B). The untreated culture resuscitates in a similar way as described previously despite the additional 10,000 h of incubation (*see* **section 2.2.8**). Indeed, the similarity between the two growth curves speaks to the longevity of the NRP state. The cultures treated with 5 µg/mL RIF remain in the lag phase slightly longer than the untreated culture (Figure 3.14.B). However, a period of strong exponential growth is then shown for these cultures, in spite of the presence of 10xMIC RIF. This exponential phase shows the active replication of *Mycobacteria* to a high OD of 2.00, which matches the final OD of the untreated culture (Figure 3.14.B). The cultures treated with INH also show a delay in the lag phase when compared with the untreated culture and the RIF cultures, starting the log phase at approximately 450 h of incubation (Figure

3.14.B). However, after this a log phase is reached and similarly to RIF, once replication is started it continues strongly and exceeds the final OD shown by the hypoxic model but not quite as high as the untreated culture and the cultures treated with RIF (Figure 3.14.B).

This result is a pivotal point of this thesis and perhaps for this area of research as a whole. Scientists tend to view active TB and latent TB as very binary with a singular shift in phenotype followed by a reversal back to the original phenotype. These results completely stand against this paradigm. This has shown that even in the Wayne model (hypoxic model) *M. bovis* BCG can resuscitate in the presence of INH. The stakes are raised even higher when in the multi-stress, cholesterol model, *M. bovis* BCG resuscitated in the presence of both INH and RIF. Obviously, these two antibiotics are the current WHO LTBI therapy so if resuscitation was going to take place clinically, INH and RIF would be the drugs first encountered to try and stop the resuscitation. This temporary resistance to the frontline antibiotics could be the reason why secondary infections of TB are viewed as far more complicated and dangerous than primary TB.

3.3 Conclusion

M. tuberculosis is perhaps the world's best stealth agent. The most common fact heard in reference to LTBI is that a third of the world's population in latently infected with tuberculosis. The most recent attempt to is a number on the sheer breadth of this problem used a mathematical model to reach an estimate of 1.7 billion people (Houben & Dodd, 2016).

As previously mentioned, the current TB pipeline has several drugs that are purported to have efficacy against latent TB (J Libardo et al., 2018). By and large, using the hypoxic model, our findings agreed with previous literature (Wayne & Sohaskey, 2001). A broad range of drug indifference was found and particularly targeted at antimicrobials with a cell wall synthesis MOA. Nevertheless, several key antimicrobials tested in this chapter retained activity in the (hypoxic model) NRP state; for example, Linezolid, Moxifloxacin, Nitazoxanide and Pretomanid (Conradie, 2017). All of the above drugs have been identified for the treatment of LTBI to a greater or lesser extent, presumably for the clear inhibition shown in Wayne's model and seen here in the hypoxic model. However, when the same drugs were tested in the MS, Cholesterol, in which cholesterol is the sole carbon source, better representing the *in vivo* conditions of LTBI, all antibiotic efficacy was lost with the exception of dapsone.

The loss of PAS activity is intriguing due to its mechanism of action (Minato et al., 2015a). Presumably, despite the essential nature of the NRP state, the folic acid biosynthesis pathway is still active. Therefore, the prodrug activator DHPS must still be active. Likewise, it is unsurprising that ATP-synthase will still be active and again it clearly is in the hypoxic model (Hards et al., 2015). As BDQ can clearly inhibit the bacteria in the hypoxic model but cannot exert the same pressure in the MS, cholesterol model, there must have been some physiological change initiated by the change in model to render the bacterium more resistant to highly potent antimicrobials. This again shows the elevated level of protections granted in the multi-stress, cholesterol model as opposed to the hypoxic model. If accepting the hypothesis that DHPS is still produced and is active, there is ostensibly no reason as to why PAS is shouldn't be active. This hints at the possibility of an elevated and different form of

protection. Perhaps, the cell wall in this model becomes even more lipid dense and starts to become near impenetrable to antimicrobials which could be attributed to the change in morphology observed (*see* **section 2.2.4)** (Bacon et al., 2014). What can be concluded from this surprisingly widespread heightened level of resistance is that the change in models in conferring more resistance than previously thought. If, indeed, this multi-stress, cholesterol model is more physiologically relevant than its predecessors, this heightened resistance must be drawn attention to. Many of the antimicrobials tested above are the current MDR-TB therapy or the part of the upcoming novel combination therapies in clinical trials (Esmail et al., 2014; World Health Organization, 2019). The resistance detected in these experiments could not be more clinically relevant. If the drugs we are prescribing as last resort measures are not effective against LTBI because of the antibiotic indifference of the NRP, this leaves the patient still vulnerable. The correlation between "previously treated" *M. tuberculosis* infection and MDR. If these infections are allowed to retreat into the NRP state where none of our therapies are effective, this risks a far more dangerous infection if it resuscitates. The need for an effective drug that can target *M. tuberculosis* bacilli in the NRP state could not be clearer.

The development of this new *in vitro* model is robust in the light of the failings of current *in vivo* models to effectively produce a physiologically relevant NRP phenotype of a latent infection (Guirado & Schlesinger, 2013). Current *in vivo* models, such as the Cornell mouse model and the zebrafish embryo model, lack the lung structure and immune function to form and maintain a granuloma; thus, cannot produce a true latent infection. There are *in vivo* models which are capable of maintaining a true latent infection, such as the minipig model and the non-human primate model (Guirado & Schlesinger, 2013). These models, however, come hand in hand with ethical concerns, high costs and do no lend themselves well to high throughput drug and phenotypic screening. The lack of a physiologically relevant *in vivo* model combined with wide scale relapsing of previously treated cases define that perhaps current treatment series are not effective at sterilising LTBI.

DAP is currently used in a wide variety of medical conditions (Wozel & Blasum, 2014; Zhu & Stiller, 2001). It is almost one of the oldest antibiotics in existence and has been actively used for the last 100 years. It was primarily developed as an anti-leprosy antibiotic, but resistance became common and in the 1950s, the side effects caused by DAP treatment were seen as severe. However, it also gained attention when DAP was shown to have potent anti-inflammatory activity. So much so that DAP is now a common treatment for dermatitis. Of particular interest in DAP dermatological uses is it is used in the treatment of granuloma faciale and granuloma annulare (Kassardjian et al., 2015; Martín-Sáez et al., 2008; Wozel & Blasum, 2014). Both of the above are minor skin conditions that are caused by immune system forming a granuloma type structure typically to an allergen. DAP is used as an anti-inflammatory to break up the immune cells and disperse the problem. This potentially could be very interesting in the treatment of LTBI which is a condition defined by complex immune interactions.

The conclusion of this chapter is to highlight the all-encompassing antibiotic resistance of *M. bovis* BCG in response to cholesterol as a sole carbon source, which nears total drug indifference. This result is stunningly impactful as LTBI treatment is a crucial part of the eradication of tuberculosis (WHO, 2020; World Health Organization, 2015)

If the NRP state can provide situational antibiotic resistance, eradication of this pervasive pandemic will never be achieved. The NRP state requires focussed research to aid further understanding of how *M. tuberculosis* becomes drug indifferent and to identify compounds active against NRP *M. tuberculosis*.

Chapter 4:

Elucidating the target of the solitarily successful compound and the discovery of novel proteomic activity specific to the Non-Replicating Persistent state of *M. tuberculosis*

Chapter 4 Elucidating the target of the solitarily successful compound and the discovery of novel proteomic activity specific to the Non-Replicating Persistent state of *Mycobacterium tuberculosis*

4.1 Introduction

4.1.1 Chapter 4 Introduction

The results shown in Chapter 3 pertaining to the sulphone, Dapsone (DAP), as a potential new, physiologically relevant (*see* **section 3.2.6**). The Sulphone family of chemicals was first synthesised in 1908 by German chemists, Fromm and Whittman and was first tested *in vivo* in 1937 against a murine model of Streptococcal infections (Buttle et al., 1937; Fromm & Wittmann, 1908). Dapsone, and its derivative Promin, was found to be active against *Mycobacterium leprae* and was moved into treating patients by 1943 (Faget et al., 1966; Faget & Pogge, 1945). Dapsone is still used today as part of a combination therapy to treat *M. leprae* cases, along with Rifampicin and Clofazimine (Eichelmann et al., 2013; Smith et al., 2017).

In addition to the antimicrobial effects displayed by Dapsone, this peculiar drug has a purported wide range of other effects. Dapsone regularly is prescribed as an anti-inflammatory to treat a range of dermatological conditions (Wozel & Blasum, 2014). One of these dermatological conditions is called granuloma annulare, which is typically a benign granuloma of the dermis (skin) and has a potential variety of causes (Martín-Sáez et al., 2008). Dapsone is commonly used as a topical treatment for this skin-based granuloma and does so by an anti-inflammatory, immunosuppressive route (Kassardjian et al., 2015; Martín-Sáez et al., 2008). Another condition of interest where Dapsone treatment is deployed is granuloma faciale; again a largely benign granuloma skin problem (Van De Kerkhof, 1994). Intriguingly, it is commonly misdiagnosed as a mycobacterial skin infection (Van De Kerkhof, 1994). It is clear that from the above clinical applications, Dapsone has anti-inflammatory effects on granuloma structures.

Dapsone was later thoroughly tested against active *M. tuberculosis* but had remarkably poor effectiveness, especially when in comparison with *M. leprae* (Baca et al., 2000; Shen et al., 2010). Due to its relatively weak activity against *M. tuberculosis*, it was discounted from main drug regimens in favour of Streptomycin initially, and then the combination of Isoniazid and Rifampicin. Currently, Dapsone is included occasionally in cases of MDR-TB and XDR-TB (Pontali et al., 2019).

The target of DAP in *Mycobacteria* is 6-hydroxymethyl-7,8-dihydropteroate synthase (DHPS), which is a part of the folic acid biosynthesis pathway (Baca et al., 2000; Gillis & Williams, 2000; Nakata et al., 2011; Williams et al., 2000). DHPS (*folP1*) combines PABA with H_2PtPP to form the next intermediate in the pathway, H_2Pte. DAP competitively inhibits DHPS (*folP1)* to effectively block this pathway and halt folic acid biosynthesis (Baca et al., 2000; Gengenbacher et al., 2008). Unlike eukaryotes, prokaryotes cannot scavenge folic acid form the environment, so folic acid biosynthesis is an evolutionary necessity. Therefore, the enzymatic pathway is closely conserved between species. Both *M. leprae* and *M. tuberculosis* possess two DHPS: the functional FolP1 and a non-essential, putative ortholog, FolP1 (Gengenbacher et al., 2008; Liu et al., 2015; Nakata et al., 2011; Williams et al., 2000).

The literature on the functional DHPS, *folP1* and its role in the folic acid biosynthesis pathway is plentiful (Figure 4.1) and discusses whether it can be inhibited and how commonly resistance mutations can arise in bacterial populations (Gillis & Williams, 2000; Minato et al., 2015a; Williams et al., 2000). The DHPS enzyme (*folP1)* is also the activating enzyme of the common pro-drug antimicrobial PAS, which then proceeds to inhibit dihydrofolate reductase (DHFR) further downstream (Mugumbate et al., 2015).

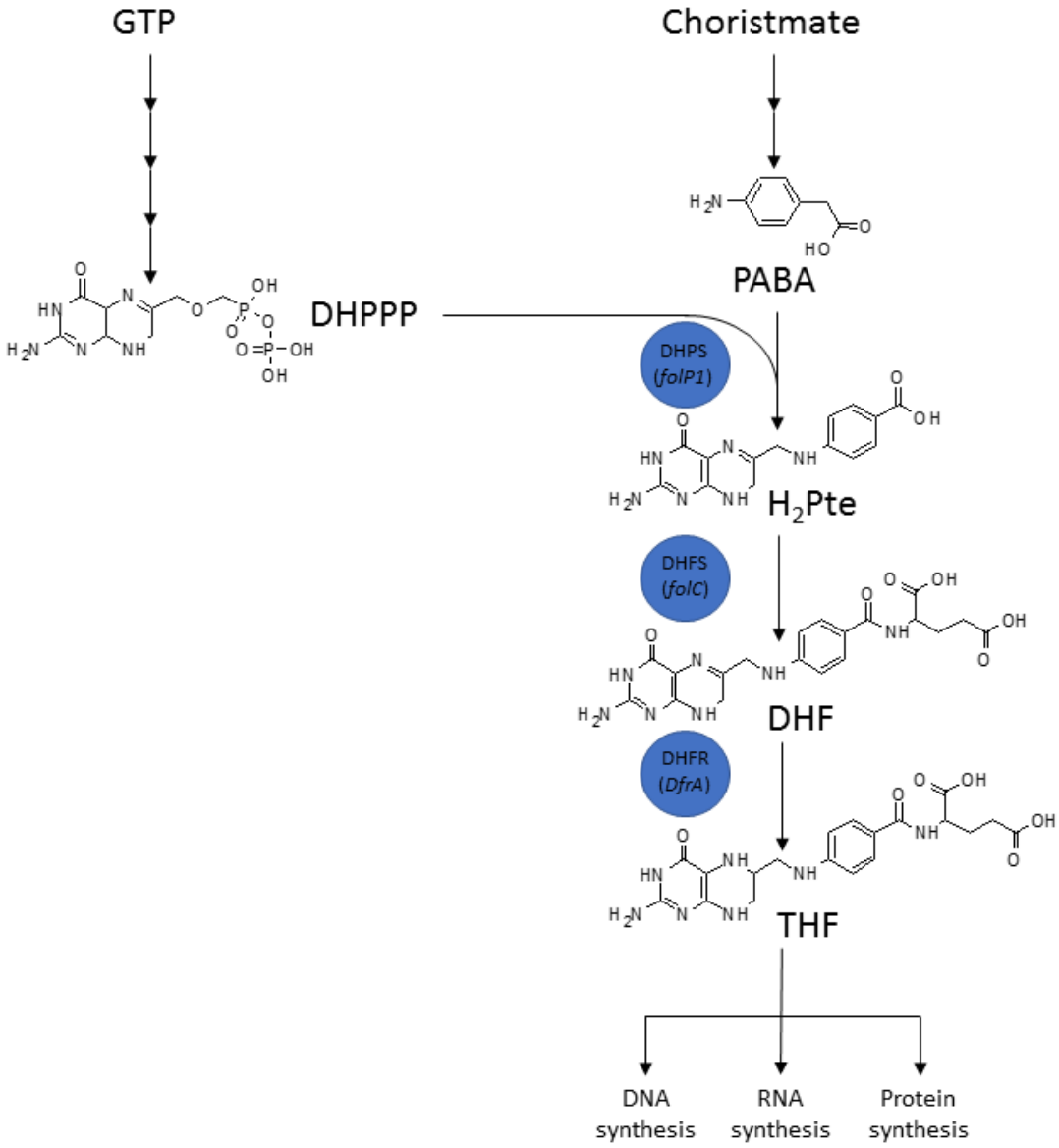

Figure 4.1: **Summary of the Folic Acid Biosynthesis Pathway**

There has been a previous investigation carried out on the non-functional homolog (*folP2)* to determine whether *folP2* could function as a biological "spare part" in case of *foP1* inhibition due to the high level of sequence homology (Gengenbacher et al., 2008). The findings were conclusive; despite a heavy level of conservation for *folP2* throughout most *Mycobacteria* species, it can only weakly bind the substrate H_2PtPP and it does not have the ability to form a functional DHPS (Gengenbacher et al., 2008).

The same investigation into Fol*P2* also quantified the expression of *folP1* and *folP2* in the NRP state by Western blot analysis. DHPS (*folP1)* was found to be expressed aerobically, under hypoxia-based NRP and under nutrient starved NRP. Despite conservation, *folP2* was not expressed aerobically nor under either NRP condition (Gengenbacher et al., 2008).

Previously in Chapter 3, DAP did not show activity against the Hypoxic NRP Model, but did show activity against the MS, Cholesterol NRP Model (*see* **section 3.2.6**). To investigate this disparity in DAP, it was attempted to find the drug target of DAP that appear to be expressed and active in the Multi-Stress, Cholesterol model but not in the Hypoxic Model.

4.1.2 Chapter 4 Aims and Objectives

Anti-Leprosy drug, Dapsone, proved to be sole compound with activity against NRP *M. bovis* BCG in the MS, Cholesterol model. This finding was unexpected, especially considering the calibre of compounds tested in the previous chapter which all failed to show any activity. With this context, elucidating the mechanism of action of Dapsone became the major aim of this chapter. As Dapsone was first created in 1908, its mechanism of action – a DHPS competitive inhibitor in the folic acid biosynthesis pathway – is widely described. This chapter seeks to find if Dapsone is using the established mechanism or providing inhibition in another manner.

4.2 Results and Discussion

4.2.1 Overexpression of *fol*P1 and *fol*P2 to elucidate the mechanism of action of Dapsone on Non-Replicating Persistent *Mycobacterium bovis* BCG

In chapter 3, DAP was shown to have antimicrobial activity against MS, Cholesterol model NRP *M. bovis* BCG but had no activity against Hypoxic model NRP *M. bovis* BCG (*see* **section 3.2.6**). PAS was shown to be active against Hypoxic model NRP *M. bovis* BCG but lost activity against MS, Cholesterol model NRP *M. bovis* BCG (*see* **section 3.2.2.3**). PAS is activated by the drug target of DAP, DHPS. This should mean that antimicrobial activities are similar due to similar MOAs.

This contradiction raised some doubts as to the target of DAP under NRP conditions; looking through the literature, DAP had never been tested before against NRP *M. tuberculosis* or *M. bovis* BCG presumably due to its poor active TB performance. To elucidate and confirm the drug target of DAP in *M. bovis* BCG under the NRP state, *fol*P1 and *fol*P2 were constitutively overexpressed (100% identity between *M. tuberculosis* H37Rv and *M. bovis* BCG for both genes) in *M. bovis* BCG (*see* **section 7.6.2, section 7.7**) using the mycobacterial specific plasmid, pVV16. This process of overexpression for both genes (*fol*P1 and *fol*P2) is detailed in Figure 4.2.

All of the following overexpressing assays were based on the same anaerobic microtitre plate assay as the original MIC testing (*see* **section 7.3**). The hypothesis being that if either *folP1* or *folP2* were the target of DAP, there would be a demonstrative MIC shift in the corresponding overexpressing strain in terms of an induced reduction in susceptibility to the drug. The antimicrobial screen was repeated using four strains of *M. bovis* BCG: the wild type *M. bovis* BCG, an empty vector control (pVV16-only), pVV16-*folP1* strain and *pVV16-folP2*

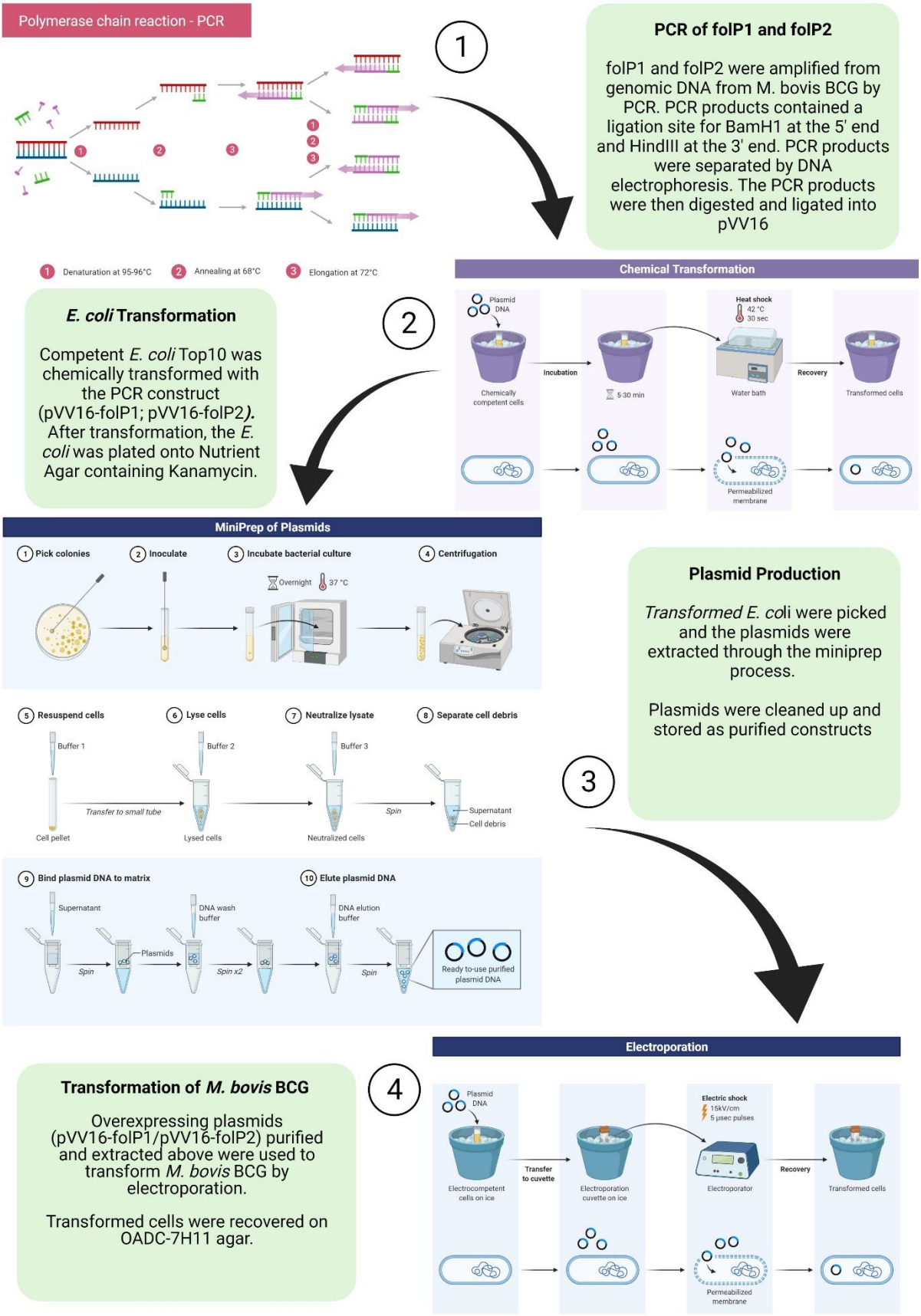

Figure 4.2: **Schematic of the production of overexpressing strains of *M. bovis* BCG. This process was completed for both *fol*P1 and *fol*P2.**

Created in Biorender.com

Overexpressing mutants were produced and grown in both 7H9-ADC media and minimal cholesterol media, with the intention of testing the activity of DAP against overexpressing mutants in both models. Unfortunately, all of the transformed strains, including the empty vector control, were not viable in the Hypoxic model. All cultures lost viability and it was impossible to complete the experiment using these strains. Cultures prepared in the MS-Cholesterol model seemed to be more stable than the Hypoxia model comparators. It could be inferred that the stress of hypoxia and the sudden necessity to enter the NRP state, coupled with the demand of a constitutive overexpressing plasmid (pVV16) proved to be too much stress. Another reason could be the physiological impact of overexpressing an essential enzyme, which would change the cell's metabolic flux. When faced with cholesterol media, it is possible the bacteria are better able to tolerate the change because the enzymes are now functional. By comparison, cultures under the MS, Cholesterol model remained viable giving credence to this model being closer to the human infection NRP state. Nevertheless, whilst the lack of overexpression data for the Hypoxic model is unfortunate; DAP did not seem to have any effect on the bacteria under this model, therefore, investigating an upwards moving MIC shift would be likely be impossible (*see* **section 3.2.6)**. NRP *M. bovis* BCG (wild type) showed a significant dose dependant reduction (p=>0.0001) to an MIC of 25 µg/mL DAP (Figure 4.2.B). Again, this bactericidal effect was clearly present in the anaerobic growth curves and was corroborated by endpoint MBC testing. This same MIC was maintained when the experiment was repeated with an empty vector control – pVV16 (Figure 4.4.A). The endpoint CFU/mL counts for the empty vector control showed an identical inhibitory response to the wild type and it was from now on included as a control (Figure 4.2.B, Figure 4.4.A). The identical result observed between empty vector and wild type shows that any MIC shift observed in the overexpressing mutants cannot be attributed to the resistance genes in the transformed plasmid.

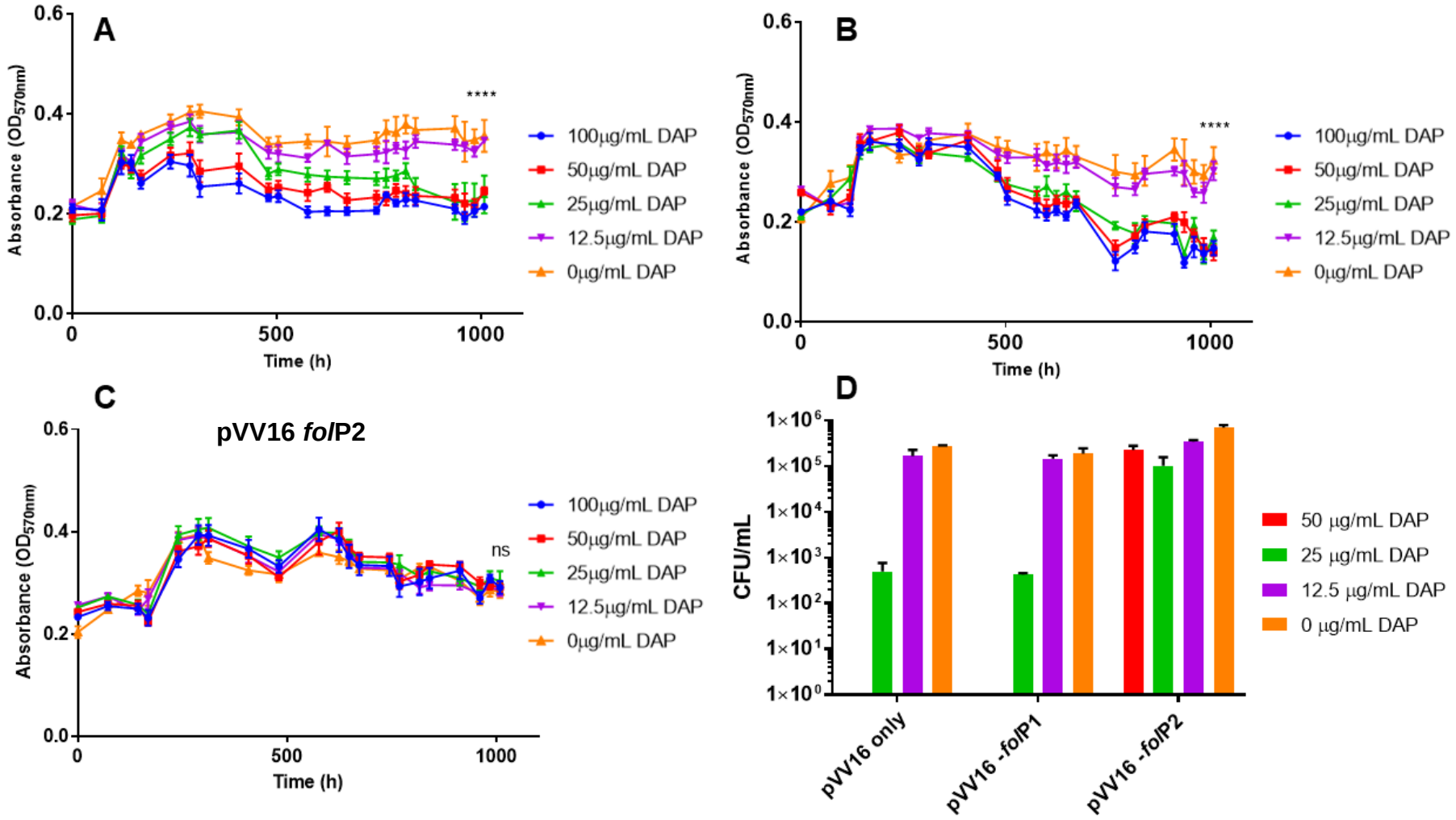

Figure 4.3: **Constitutive Overexpression of *fol*P1 (B) or *fol*P2 (C) compared with an empty vector (pVV16 only) control (A). Bar graph showing the endpoint CFU/mL values found for each absorbance curve (D)**. Both (A) and (B) show a dose-dependent inhibitory response to Dapsone, showing an MIC of 25 µg/mL in both cases. Both (A) and (B) show statistically significant deviation away from the control with both reporting a p value of <0.0001. (C) shows a serial dilution of DAP challenging MS, Cholesterol model *M. bovis* BCG overexpressing *fol*P2. All cultures remain stationary throughout the experiment and there was no significant change away from the control (p = 0.8225). All experiments were conducted with four replicates, including the CFU/mL assay.

The target of DAP in *M. leprae* and aerobic *M. tuberculosis (mt*DHPS) was overexpressed in *M. bovis* BCG and tested against dosage series of DAP (Figure 4.3.B). Upon overexpression of *fol*P1, the traditionally expected target of DAP, no shift in MIC was observed, with DAP still having a significant effect (p=>0.0001) against NRP *M. bovis* BCG at 25 µg/mL (Figure 4.3.B). The endpoints CFU/mL counts bolster the results shown in the growth curves. At the MIC for the pVV16 (plasmid)-only control, 25 µg/mL DAP, there is a clear three log reduction of CFU/mL down to 4.2 x10^2 CFU/mL, however at 12.5 µg/mL, the CFU/mL is not reduced (1.5 × 10^5 CFU/mL), indicating that this concentration is below the MBC (Figure 4.3.D). Along with the differences in OD from the growth curve, this data shows that the dose-dependent response of DAP has not differed from the wild type or empty vector control. Therefore, despite the overexpression of the supposed well-characterised target of DAP, there has been no change in MIC from wild type; so, whilst DAP is inhibiting the bacilli, it is not directly inhibiting the action of FolP1. In conjunction with the results from PAS, this suggests that it is not the folic acid biosynthesis pathway that is inhibited by DAP in the Multi-Stress, Cholesterol model.

The hypothesis that DAP does not inhibit the folic acid biosynthesis pathway was further supported by the results of the overexpression assay for *folP2 (*Figure 4.3.C). The *M. bovis* BCG mutant overexpressing *folP2* was subjected to the same microtitre dilution scale of DAP as *folP1* albeit, under the NRP state (Multi-Stress, Cholesterol model). No change in MIC was detected between the wild type and the empty vector control. The NRP culture showed no statistically significant difference in OD over 1000 h in spite of high concentration of DAP (p=0.8225) (Figure 4.3.C). Indeed, the highest concentration of DAP tested was 100 µg/mL, which is 4x the inhibitory concentration needed in both the WT and the empty vector control. This is corroborated by the CFU/mL counts showing resuscitation of bacteria across all concentrations of DAP to a minimum of 1 × 10^5 CFU/mL (Figure 4.3.D).

This shift in MIC observed in the *folP2* overexpressing mutant was quite informative; the overexpression of the *folP2* gene resulted in 100 µg/mL of DAP proving ineffective. This growth curve over 1000 h shows remarkably little increase or decrease in OD from the non-treated

control (0 µg/mL) and any change observed was found to be not statistically significant (Figure 4.3.C). This suggests that DAP is effective against NRP *M. tuberculosis*, even though under these conditions, it has a different target then it does against active tuberculosis infection. The protein FolP2 lacks the capability to function as a DHPS and does not act as a part of the folic acid biosynthesis pathway (Baca et al., 2000; Gengenbacher et al., 2008). So, its antimicrobial activity against NRP *M. tuberculosis* must be a result of successful inhibition of a different metabolic pathway (Gengenbacher et al., 2008).

There was no MIC shift when *fol*P1 was overexpressed, but there was a defined MIC shift when *fol*P2 was overexpressed. It was also previously shown in Chapter 3 that the antimicrobial activity of DAP is bactericidal, which infers that FolP2 as the drug target of DAP is essential in the Multi-Stress, Cholesterol model NRP state.

4.2.3 Conservation of FolP2 throughout the *Mycobacterium* Genus

Dapsone is an old, well characterised drug that has been identified to competitively inhibit FolP1 (DHPS). However, the overexpressor assays seen in Figure 4.4 identified FolP2 not FolP1 as the target of Dapsone in the Multi-Stress, Cholesterol model. One of the main features of FolP1 is high conservation throughout *Mycobacteria* sp., and high levels of conservation throughout a species can be a good indication of essentiality. A sequence alignment of FolP2 throughout many different *Mycobacteria* species to identify if FolP2 is highly conserved, similarly to FolP1. The *Mycobacteria* species chosen for the sequence alignment are as follows: *M. tuberculosis, M. bovis, M. leprae* and *Mycobacterium marinum* (Table 4.1)

Table 4.1: **Table showing the identity and size of *fol*P2 across five different Mycobacterial species**. Gene length was identified on Mycobrowser. Sequence identity was found using BLAST analysis using the *M. tuberculosis fol*P2 as a comparator.

Organism:	Gene Name/Identifier:	Length:	Sequence Identity:
M. tuberculosis	Rv1207	318 aa	-
M. bovis BCG	Mb1239	318 aa	100%
M. leprae	ML1063	291 aa	86.2%
M. marinum	MMAR_4231	292 aa	90.34%
M. smegmatis	MSMEG_5085	291 aa	80.28%

The sequence alignment shows a high level of conservation in the FolP2 protein throughout the species of *Mycobacteria*. Particularly *M. tuberculosis* and *M. bovis* share 100 % identity between the two genes (Table 4.1, Figure 4.4). Even in *M. leprae,* which whilst being part of the same genus, is typically considered very distinct to *M. tuberculosis* shares a high sequence identity of FolP2 with *M. tuberculosis*. This data suggests that FolP2 is highly conserved throughout the *Mycobacteria* genus, which subsequently suggests that FolP2 is an essential protein. This conserved and possible essential nature could provide a reason as to why inhibition of this protein by Dapsone is so effective. Perhaps, FolP2 is only essential under the environment of the Multi-Stress, Cholesterol model; namely a hypoxic environment with high

levels of cholesterol catabolism. If this hypothesis was correct, it would explain why no previous research has found FolP2 to be an essential protein, despite the high levels of conservation seen in Figure 4.4.

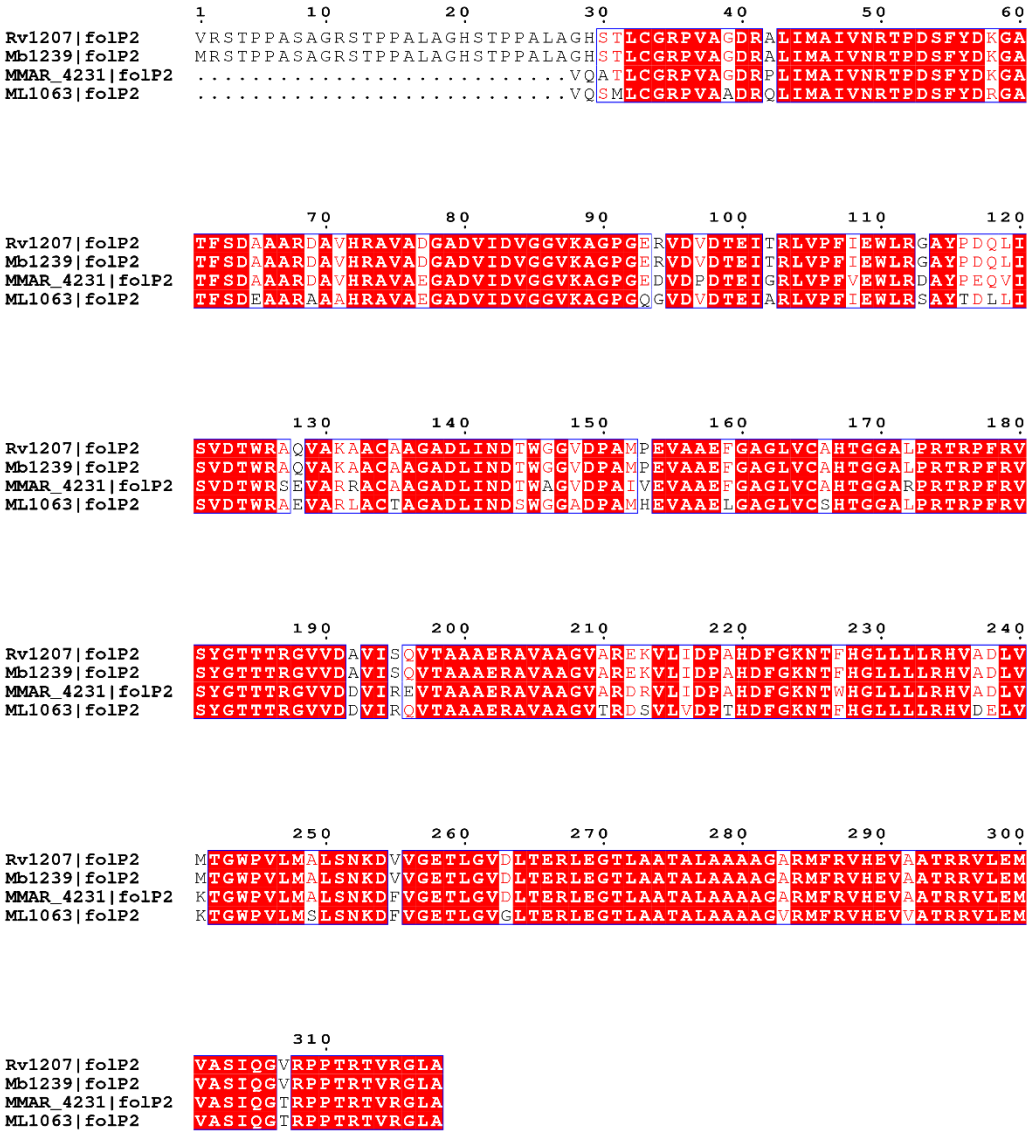

Figure 4.4: **Protein sequence alignment of FolP2 from different bacterial species**. *M. tuberculosis, M.bovis BCG*, *M. marinum* and *M. leprae* display a high level of homology between sequences, indicated by residues in red. Residues highlighted in red indicate identity across all species aligned, showing conserved residues. Secondary structure information is seen above all sequences.

4.2.4 Evaluation of FolP2 activity against aerobic *Mycobacterium bovis* BCG in minimal cholesterol media

The previous results indicate that FolP2 is not a part of the folic acid biosynthesis pathway as previously believed (Figure 4.1). Previous literature has shown that in hypoxic-based NRP conditions, folP*2* is not expressed (Gengenbacher et al., 2008). Therefore, why does *folP2* under the MS, Cholesterol model become so essential to the bacterium that inhibition of this enzyme leads to bacterial cell death? Perhaps this overlooked protein has an intrinsic role in the NRP state that as previously gone entirely unnoticed.

This protein seems to become essential when placed under hypoxic, nutrient-deprived, cholesterol-metabolising NRP conditions. However, it is not essential in hypoxic NRP conditions; neither is it essential in nutrient starved NRP conditions (bacteria sealed in PBS) (Gengenbacher et al., 2008). The glaring point of difference in this information is the presence of cholesterol metabolism. To ascertain if *folP2* is important to cholesterol metabolism, we assayed the activity of DAP aerobically against *M. bovis* BCG growing in cholesterol media.

The results of the aerobic microtitre assay (Figure 4.5) clearly depicted the same weak inhibitory effect, regardless of the media used. In particular, the MIC of DAP against active *M. bovis* BCG is 50 µg/mL in reduced cholesterol medium (*see* **section 7.1.3**) (Figure 4.5.B). When grown in complete 7H9 medium, where the bacterium has plentiful carbon sources to metabolise (*see* **section 7.1.1**), the MIC remains unchanged from that found against cholesterol metabolising BCG, 50 µg/mL (Figure 4.5.A). Both models show non-statistically significant reductions (7H9-ADC media p= 0.1833, minimal cholesterol media p = 0.2092) that suggest that the OD growth curve does not differ significantly from that of the control. There does seem to be a clear reduction in OD compared with the control but because the OD of the affected growth curves is still increasing but at a lower rate this returns non-significant p values.

These weak MICs depict a clear picture of a weak antimicrobial whose target is not affected by a change of carbon source. This aerobic inhibition could therefore be attributed to the weak DAP inhibition of *fol*P1. Therefore, for *folP2* to become active/expressed, it needs an anaerobic environment and an ongoing cholesterol catabolism process.

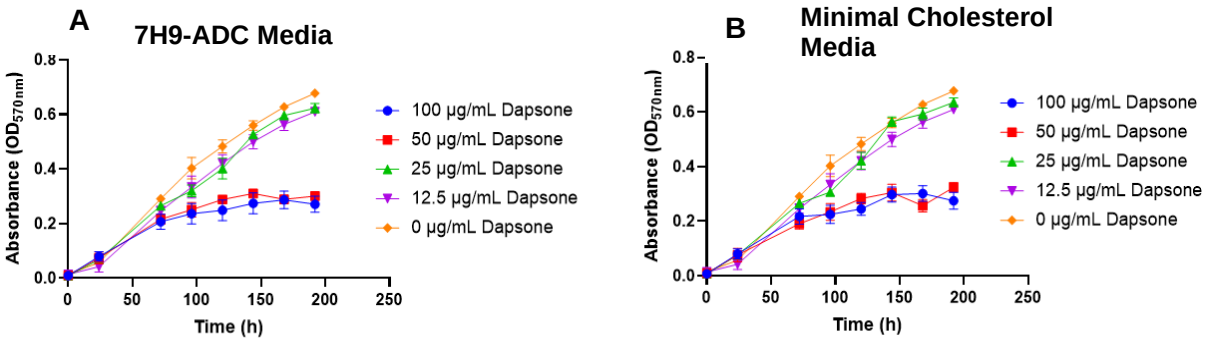

Figure 4.5: **Aerobic Growth Curves of Logarithmically Growing *M. bovis* BCG challenged against a serial dilution of Dapsone.** (A) shows logarithmic growth in 7H9-ADC media. After 100 h, it appears that 100 µg/mL DAP and 50 µg/mL DAP appear to inhibit growth weakly. Statistical ANOVA showed that this inhibition does not deviate enough from the 0 µg/mL control ($p = 0.1833$). (B) shows logarithmic growth of *M. bovis* BCG in minimal cholesterol media. Statistical ANOVA showed no statistical significance ($p = 0.2092$).

4.2.5 Investigating the *Mycobacterium tuberculosis* cholesterol catabolism pathway under anaerobic conditions

The cholesterol catabolism pathway of *M. tuberculosis* has been well defined and over recent years, the importance of cholesterol in infection has become increasingly clear (Griffin et al., 2012; Savvi et al., 2008; van der Geize et al., 2007; Wilburn et al., 2018; Wipperman et al., 2014) (*see* **section 1.2.2**). The process of highlighting the importance of the correlation between cholesterol catabolism, hypoxia and the activity of DAP presented an opportunity to re-examine the cholesterol catabolism with a focus on oxygen consumption.

Figure 4.6 shows the oxygen limiting steps of the cholesterol catabolism pathway. These steps directly require molecular oxygen as part of the reaction. Of the whole pathway, four steps required oxygen: Cyp125 (Cyp145), KshA/KshB, HsaA/HsaB and HsaC (Figure 4.6.C).

There has been a plethora of research showing the importance of cholesterol as the main and sometimes only carbon source of the granuloma (Garton et al., 2008; Soto-Ramirez et al., 2017). Nevertheless, there has also been countless research showing the hypoxic nature of the granuloma (Iona et al., 2016; Muttucumaru et al., 2004; Wayne & Sohaskey, 2001). If accepting both schools of thought as correct, the current process of cholesterol catabolism is not possible in these conditions due to the oxygen demand it requires (Figure 4.6).

This conclusion led to a hypothesis as to the function of FolP2; this protein could be acting as a bypass for one of the above steps that requires oxygen (Figure 4.6). This would allow the bacterium to still metabolise the only source of carbon present despite the anaerobic environment

A

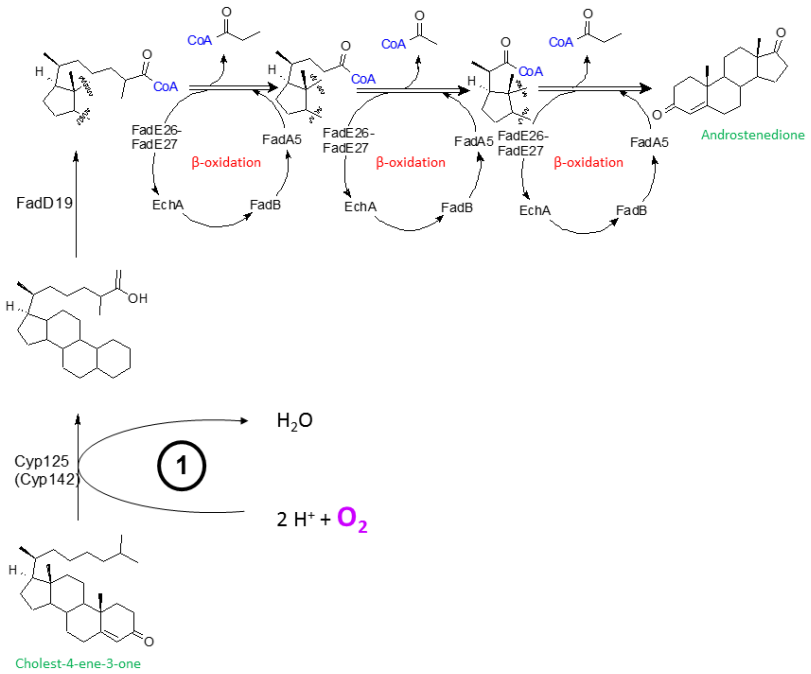

B

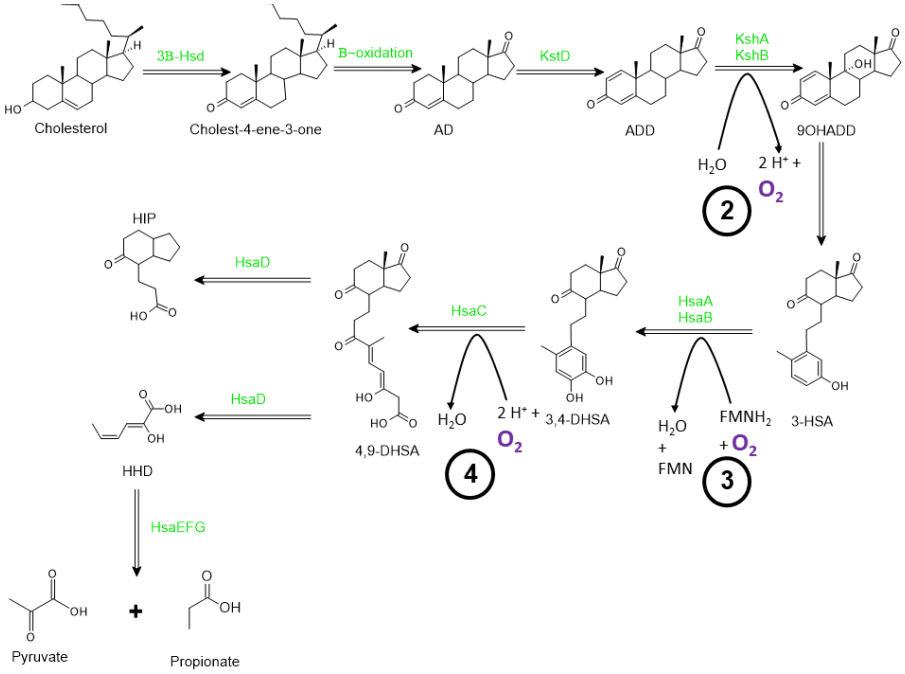

C

Oxygen Limiting Step	Enzyme	Process
1	Cyp125 (Cyp142)	Hydroxylation of cholesterol side chain
2	KshA/KshB	Hydroxylation of ADD
3	HsaA/HsaB	Hydroxylation of 3-HSA
4	HsaC	Cleavage of 3,4-DHSA

Figure 4.6: **Summary of Cholesterol Catabolism Pathway in *M. tuberculosis* with focus on the steps limited by oxygen consumption.** (A) the β-oxidation subpathway specifically the Cyp125 (Cyp145) step that consumes oxygen (B) The A/B ring catalysis subpathway which contains three oxygen consuming steps (C) Table detailing the four oxygen limiting steps in the elucidated part of the cholesterol catabolism pathway

The main source of confusion surrounding FolP2 comes from its similarity to FolP1, the *mt*DHPS. It has been established that these two proteins neither work together, nor do they perform the same process (Gengenbacher et al., 2008). However, presuming that protein structure leads to protein function; the structure, folding and active site of these two proteins are so similar that it has been erroneously presumed to form the same protein, DHPS. Therefore, it stands to reason that the ligands and substrates of FolP2 bear some resemblance to those of FolP1 (Gillis & Williams, 2000; Minato et al., 2015b; Williams et al., 2000). Out of all the reactions in Figure 4.6, there is only one reactions where the ligands involved bear a resemblance to that of *mt*DHPS; the hydroxylation of 3-HSA to 3,4-DHSA by HsaA/B (Dresen et al., 2010; van der Geize et al., 2007). This hydroxylation has been found to be mediated by a two component flavin monooxygenase, HsaA/B. HsaA/B use reduced riboflavin-5-phosphate ($FMNH_2$) and oxygen to hydroxylate the substrate, 3-HSA (Dresen et al., 2010). This hydroxylation process essentially turns a phenol (3-HSA) into a catechol (3,4-DHSA) (Figure 4.7).

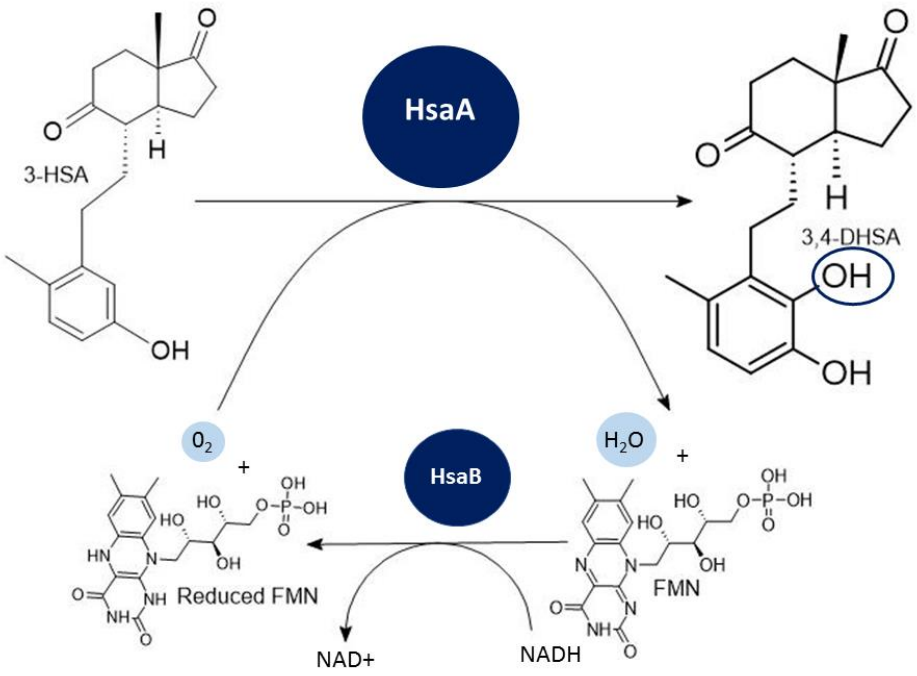

Figure 4.7: **Schematic showing the currently proposed mechanism of 3-HSA hydroxylation to 3,4-DHSA** as elucidated aerobically by Dresen *et al*. HsaA/HsaB acts in complex to form a two-component flavin monooxygenase with HsaA acting as the hydroxylase with HsaB acting as the reductase.

4.2.6 Investigating the activity of FolP2 as an anaerobic enzyme to recycle Flavin Mononucleotide (FMN)

4.2.6.1 Protein Purification of FolP2 for enzymatic activity assays

A His-tagged FolP2 expression vector (pet28a-*folP2*) was constructed (*see* **section 7.6.1**) and used to transformed *Escherichia coli* BL21. This overexpressing *E. coli* mutant was then aerobically grown in large volume shake flasks. The bacteria were lysed and the protein was purified from the lysate (Figure 4.8) (*see* **section 7.10**). This purification proved to be complicated and resulted in an unstable protein of a small yield.

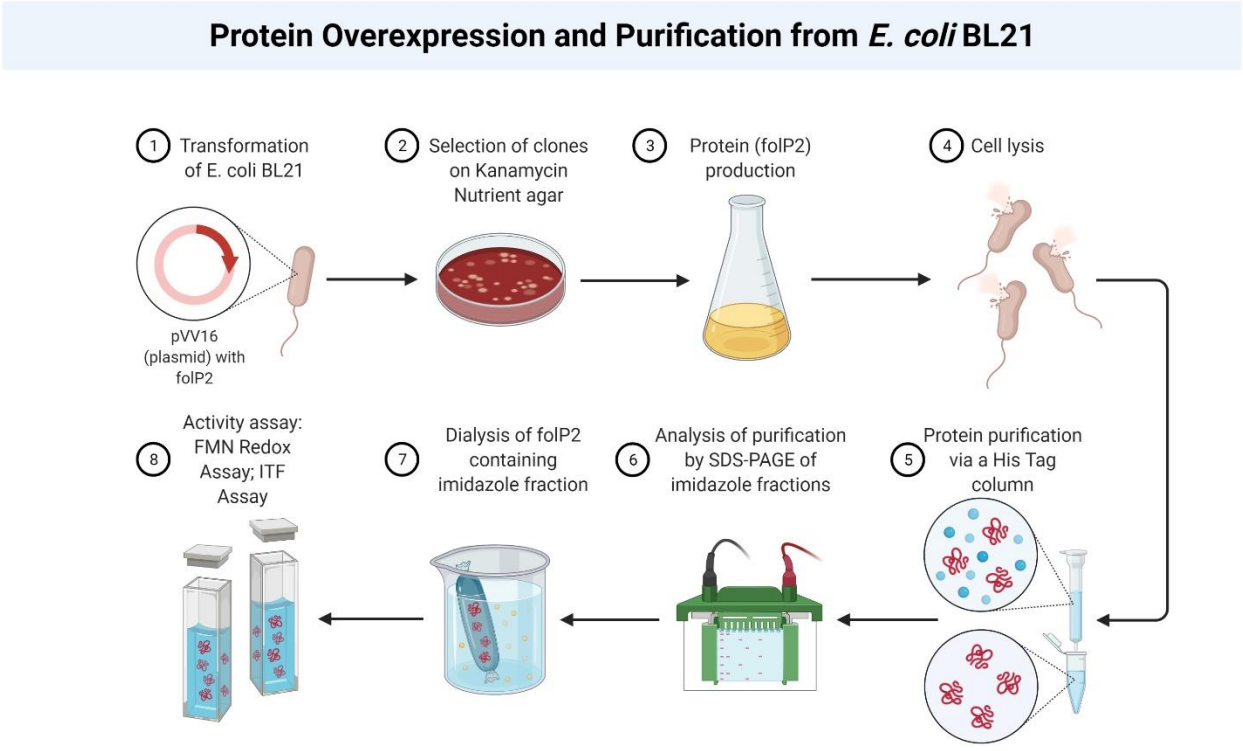

Figure 4.8: **Procedure of Protein Purification of *fol*P2.** The above figure summarises the process of transforming *Escherichia coli* BL21 using pet28a-*fol*P2. The transformed *E. coli* are stimulated to produce *fol*P2 from the addition of 1M IPTG. The protein is then extracted and purified using an imidazole gradient and dialysis in a Tris buffer (created in Biorender.com)

The SDS-PAGE gels for the protein purifications can be found in section 7.10. The His-tagged protein was separated using an imidazole gradient and eluted between 200-300 µM imidazole

and in the greatest quantity in the 250 μM fraction. These gels reflect the poor yield obtained through the relatively small bands at 33 kDa. Many steps were taken to optimise the purification of FolP2, such as changing the purification buffers from phosphate buffers (*see* **section 7.1.11**) to Tris-based buffers (*see* **section 7.1.13**) and strictly controlling the overnight expression temperature to 17℃. These steps managed to increase the yield by 20-fold from approximately 0.01mg/mL to 0.2 mg/mL. This modest increase in protein expression allowed for the conducting of the following biochemical assays. Protein yields were quantified using a ThermoFisher Nanodrop (*see* **section 7.10**). Yields of the three utilised protein purifications were as follows: 0.02mg/mL, 0.112 mg/mL and finally 0.2 mg/mL.

The protein purification in *E. coli* was very challenging. Even if protein was purified it was not stable enough and would crash out of solution within a matter of days. To improve the overall yield and the stability of the protein extracted, it would be more advantageous to express *folP2* in *M. smegmatis* instead of *E. coli.* This would allow access to specific mycobacterial chaperone proteins and would allow an easier purification; it would however be a harder transformation process due to the fastidious nature of *Mycobacteria*. Another option would be to anaerobically purify the protein. It has become apparent that FolP2 is active only under anaerobic conditions so purifying the protein under anaerobic conditions could improve the stability of the protein and facilitate a longer life span before it crashed out of solution.

4.2.6.2 Intrinsic Tryptophan Fluorescence of FolP2

In previous literature, FolP2 has never been shown to have any activity despite its similarity to FolP1. To investigate the hypothesis that it provides a hypoxic bypass for the bacterium during the oxygen demanding cholesterol catabolism pathway, an attempt was made to detect the intrinsic tryptophan fluorescence (ITF) of FolP2. ITF is a method commonly used to detect the activity of a protein *(see* **section 7.12)**. In brief summary, tryptophan fluoresces with an excitation wavelength of 28 nm and emits at a wavelength between 315 nm – 350 nm. If a protein has a tryptophan amino acid in the active site, an unbound protein will fluoresce but upon ligand binding, this signal will be “quenched”.

The fluorescence of FolP2 was tested within a black-bottomed microtitre plate, 100µL of FolP2 (yield: 0.112 mg/mL) provided a total RLU of 230,041. The protein was excited at a wavelength of 280nm and the emission was read at 320nm. This method provided a small peak of fluorescence, which could mean that the protein concentration was too low to detect the fluorescence properly.

To assess the hypothesised interaction of FolP2 with the hydroxylation of 3-HSA, the ITF of FolP2 was assayed in isolation and when exposed to a dilution series from 0 mM to 1mM of riboflavin-5-phosphate (FMN) and a fixed concentration of the ligand (3-HSA) substitute 3,4-dimethylphenol (3,4-dMP). This combination of protein and ligands resulted in a very low signal from the protein (Figure 4.9). In addition, the dilution series of FMN seemed to produce a similar curve when assayed with buffer and 3,4-dMP (excluding FolP2). This suggests that instead of detecting any protein activity, the 3,4-dMP could itself be fluorescing and masking the signal from the protein (Tomas Vert et al., 1987). It is possible that the phenol group could

be fluorescing at these wavelengths. Therefore, it was concluded that ITF was not a suitable assay due to these unreliable results (Figure 4.9).

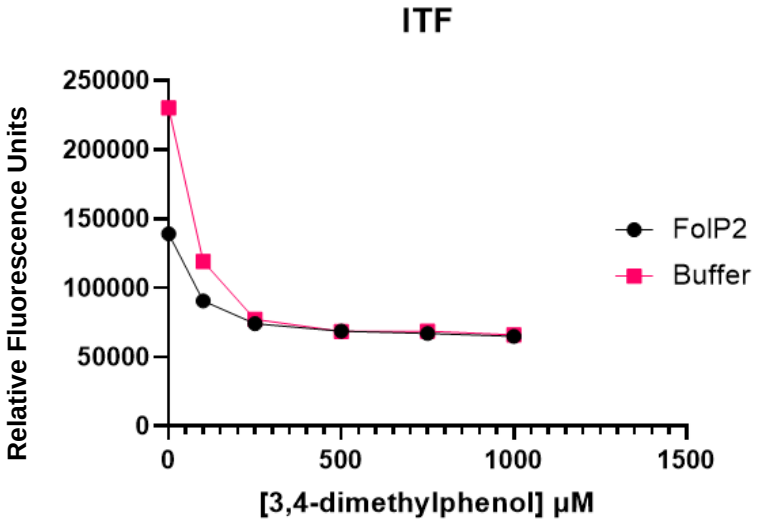

Figure 4.9: **Intrinsic Tryptophan Fluorescence (ITF) of FolP2 with a fixed concentration of 3,4-dimethylphenol at 100 µM with a dilution series of FMN.** Due to high levels of fluorescence from 3,4-dimethylphenol and the FMN, any change in FolP2 is exceeded by the fluorescence of the buffer.

4.2.5.3 Measuring the redox state of FMN to assess FolP2 activity

Due to the difficulties experienced using a fluorescent assay (see section 7.12) in combination with highly fluorescent and brightly coloured ligands, it was decided that a different approach was necessary. Instead of testing and measuring the effects that the varying potential ligands had on FolP2*;* the new approach was to measure the effect of FolP2 on the ligand. In particular, the new procedure was to measure the effect that FolP2 has on FMN (*see* **section 7.13**). The reaction is a particularly complex part of the mycobacterial cholesterol catabolism pathway (Dresen et al., 2010; Wilburn et al., 2018; Wipperman et al., 2014). This step is part of the A/B ring metabolism subpathway. In short, 3-HSA is hydroxylated to form 3,4-DSHA (Figure 4.8) utilising both reduced FMN ($FMNH_2$) andO_2 (Dresen et al., 2010). If we focus on the FMN, it is possible to see that during this reaction it goes from a reduced form to an oxidised form by HsaA and is then recycled back to its reduced form by HsaB for the next reaction (FIG 4.8) (Dresen et al., 2010). The different redox states of FMN have two distinctly different absorbances which can be detected by a spectrophotometer (Finn et al., 2003; Oprian & Coon, 1982; Walker & Nicholas, 1961). At 450nm, FMN should have a high absorbance reading whereas at the same wavelength, $FMNH_2$ should be much lower. Therefore, by measuring change in absorbance over time, if a positive correlation in regard to absorbance over time is detected or the inference could be made that $FMNH_2$ is being oxidised to FMN. However, if a negative correlation in regard to absorbance over time is found, the opposite inference can be made. The protein activity would be reducing FMN to $FMNH_2$, so hydroxylase activity would be represented by an increase in absorbance at 450nm and reductase activity would be represented by a decrease in absorbance at 450nm. Naturally, if no change in absorbance is detected, the addition of protein has no effect on the redox state of FMN.

To test if FolP2 could affect the redox state of FMN in isolation, the final concentration of 5 µM of protein was mixed with 100 µM of riboflavin (50 µL of protein:50 µL of FMN resulting in 100 µL final volume). Absorbance measurements at 450 nm were taken every 30 s for 10 mins (Figure 4.10). Simultaneously, the same experiment was conducted with the protein buffer replacing FolP2 in the experiment to act as a control (Figure 4.10). Over 10 mins, the absorbance of FMN treated with protein showed no significant difference to the FMN treated with buffer. As can be seen in Figure 4.10, the FMN remained at a consistent and steady OD throughout the experiment regardless of the presence of protein. Therefore, this suggests FolP2 neither reduces nor oxidises FMN as there is no change in absorbance similar to the lack of change in the corresponding buffer experiment.

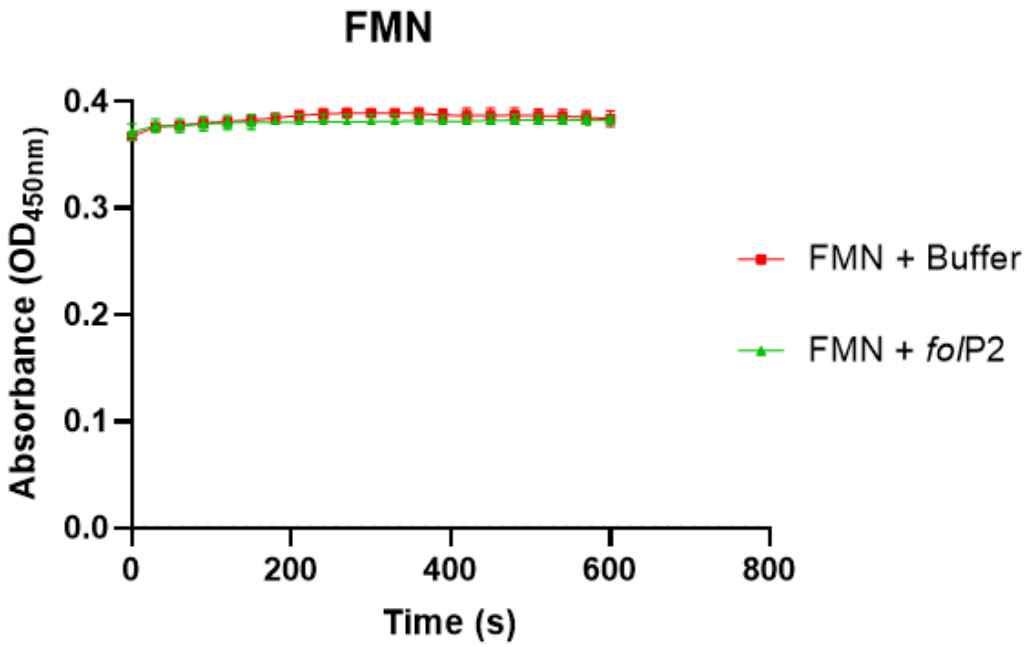

Figure 4.10: **Absorbance of FMN over 600s in combination with Tris buffer (Red) or FolP2 (Green**). Both assays with FMN show no change over the course of the assay (600 s). Assay was completed in n=3. No 3,4-dimethylphenol was included in this assay and the concentrations of FMN and FolP2 were fixed.

In short, to look at this reaction is that the substrate needs to be hydroxylated from a phenol to a catechol. We could not obtain the correct initial cholesterol breakdown product 3-HSA so in lieu of the correct substrate, 3,4-dimethylphenol (3,4-dMP) was used. Another potential

pseudo-substrate considered was 4-phenylphenol but unfortunately it was not water soluble. The already unstable nature of the protein meant that another solvent such as chloroform would have resulted in the precipitation of FolP2.

Consequently, a new experiment was designed to test if FolP2 is involved in the 3-HSA reaction and if it requires both FMN and a phenol based molecule to initiate the reaction (*see* **section 7.13**). The concentration of FolP2 and FMN were fixed at 5 µM and 100 µM, respectively. As previously explained, this experiment was repeated completely albeit with buffer replacing FolP2 in all cases, to ensure that any change in absorbance observed was directly caused by the activity of FolP2. As additional controls, the protein, buffer and the substrate were all assayed individually at OD_{450nm} to ascertain whether they could be distorting the assay. After 10 mins of readings, all three were comprehensively shown not to absorb at 450nm and therefore do not contribute to the absorbance detected in this experiment. For the actual experiment, absorbance readings were taken at 450nm at 0 mins, 5 mins and at 10 mins. This time course is shown in Figure 4.11.

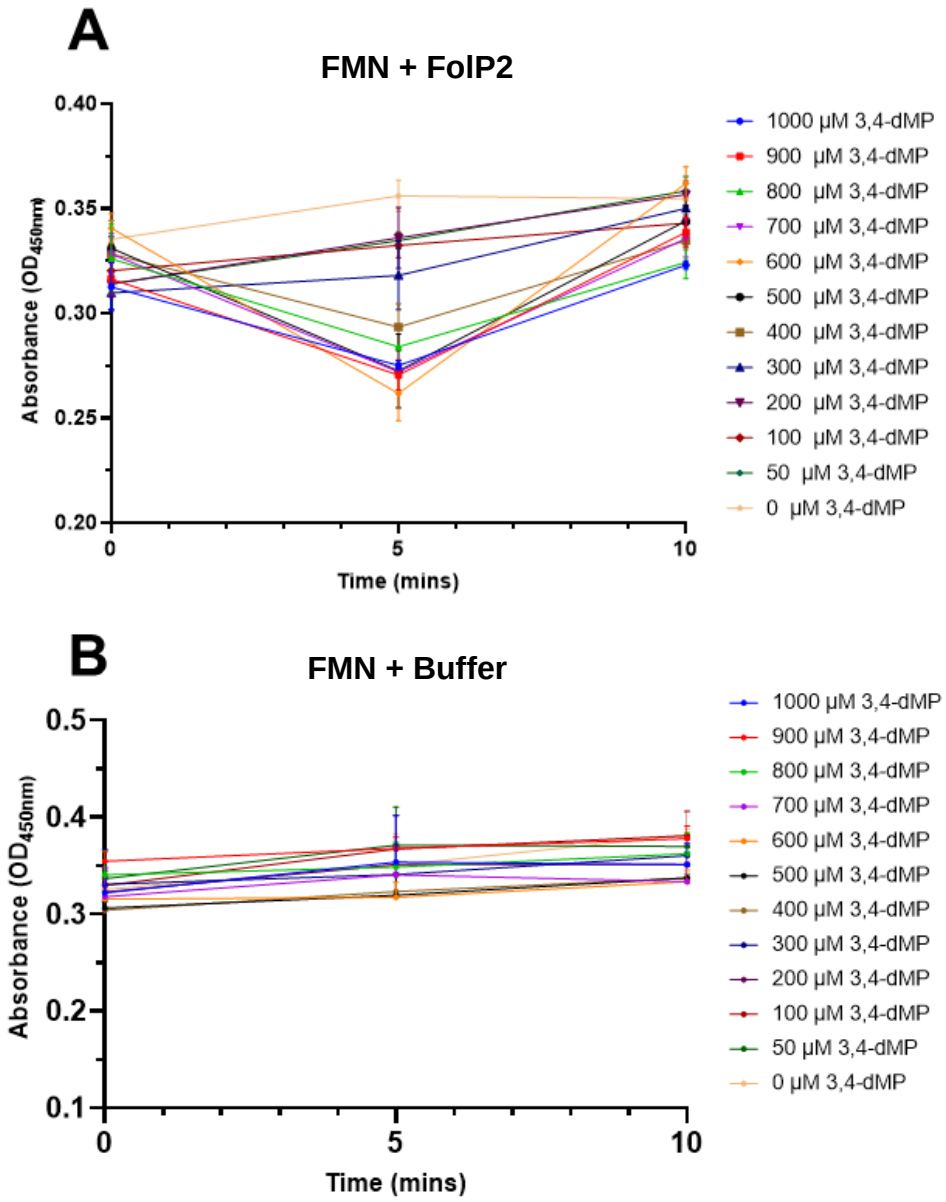

Figure 4.11: **Initial absorbance activity assay** of (A) fixed concentration of *fol*P2 at 5 µM in combination with fixed 100 µM FMN and a dilution series of 3,4-dimethylphenol and (B) activity of Tris storage buffer in combination with 100 µM FMN and 3,4-dimethylphenol

This time course shows a rudimentary activity for FolP2 in a dose-dependent response of 3,4-dMP. For the higher concentrations of 3,4-dMP (400 µM and above), there is a distinct decrease in absorbance from the starting point (Figure 4.11). Additionally, this decrease in absorbance seems to be lessened by a lower concentration of 3,4-dMP. However, even at the lowest concentration of 3,4-dMP (50 µM) there was still a slight decrease from the control (Figure 4.11). The results observed for the control (0 µM 3,4-dMP) showed no change in

absorbance over time. Likewise, the enzyme free control showed no change in absorbance over time either independently of the 3,4-dMP concentration (Figure 4.11.B). This would suggest that the decrease in absorbance observed in Figure 4.11.A could be attributed to the action of FolP2.

Intriguingly, the time course shows the absorbance to be decreasing, not increasing (Figure 4.11.A). This would suggest that FMN is being reduced to $FMNH_2$ over time instead of the hypothesised $FMNH_2$ oxidising to FMN. Even more interestingly, the decrease observed in absorbance seems to be reversed to the starting OD after 10 mins of the assay. It is possible that after being reduced the $FMNH_2$ returns to the oxidised state (FMN) naturally. In summary, even though Figure 4.11.A shows very preliminary data, it also shows that FolP2 might have an activity completely different to previously thought. It is possible that FolP2 is a NRP state specific protein/drug target which is exclusively active in the anoxic cholesterol catabolism pathway which would explain why it hasn't been found to be expressed in any other condition (Chiang et al., 2008; Gengenbacher et al., 2008). This corroborates with the lack of DAP activity in the Hypoxic model as there is no cholesterol catabolism taking place in that model.

To confirm the results seen in Figure 4.11, the experiment was somewhat repeated under greater controls and measured more closely. The experiment was conducted in tandem with the control experiment under the same parameters but using protein storage buffer instead of protein (FolP2). The concentration of FolP2 was fixed at the lower concentration of 0.5 μM due to issue during the protein purification which resulted in a low yield (0.02 mg/mL).

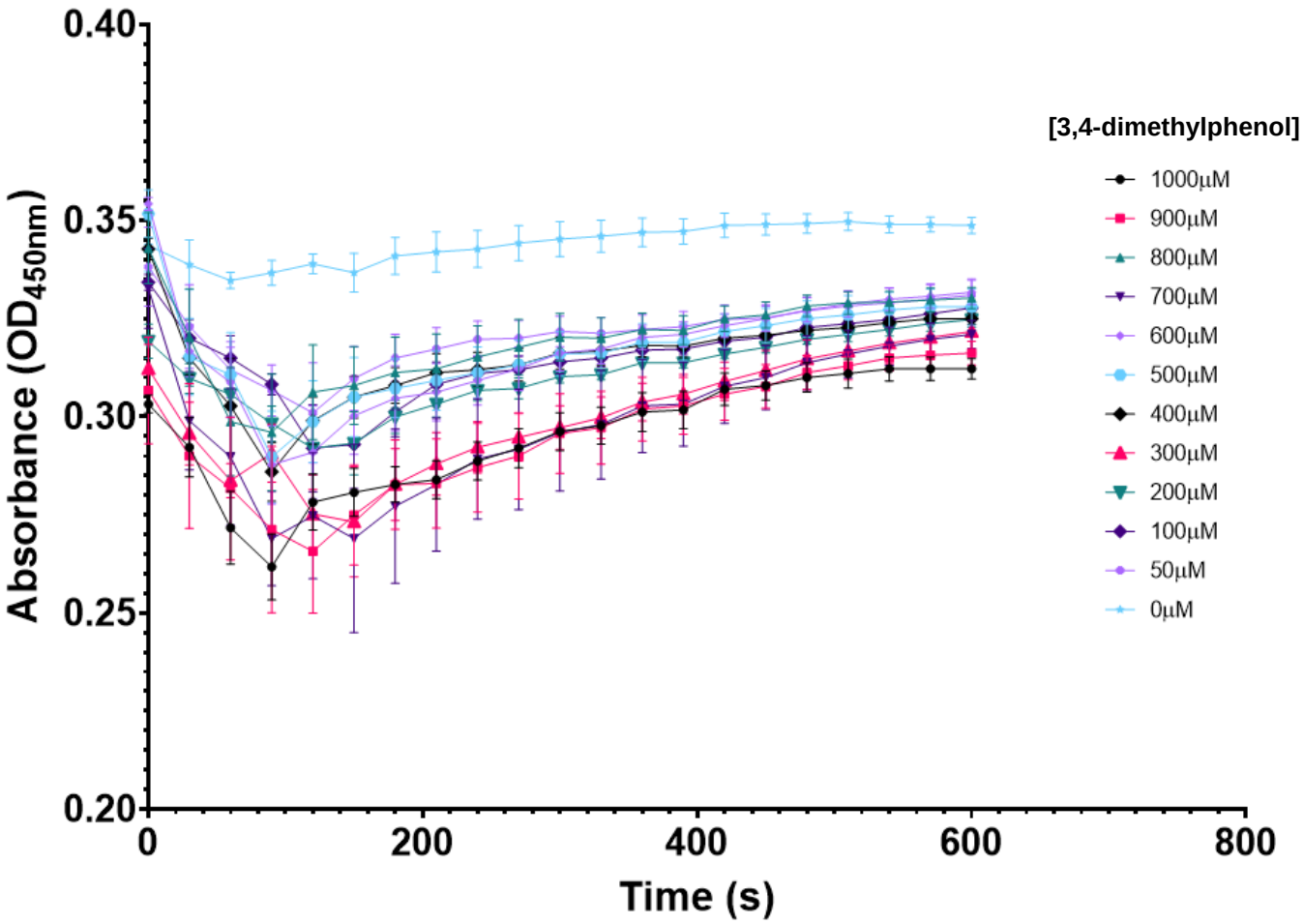

Figure 4.12: **Activity of FolP2 with FMN and 3,4-dimethylphenol across 10 m (600 s**). The control (0 µM) does not contain any 3,4-dMP and shows the interaction between FMN and FolP2 in isolation of 3,4-dMP. Both FMN and FolP2 concentration and was challenged with a serial dilution of 3,4-dimethylphenol.

The concentration of FMN was fixed in the well at 100 μM as in Figure 11. The experiment was initiated with the addition of protein as the combination of 3,4-dMP and FMN are non-reactive as shown previously. A dilution series of 3,4-dMP was assayed: this dilution series was identical to the one seen in Figure 4.12; however, this time each experimental well was measured every 30 s for 10 mins. The increased measurement intervals were used to gain a better understanding as to how fast FolP2 can reduce FMN in combination with differing concentrations of 3,4-dMP. The absorbance data over time can be seen in Figure 4.12. Figure 4.13 shows a clear, dose-dependent reduction in absorbance, with steeper curves found with higher concentration of 3,4-dMP. Indeed, there is no decline in absorbance seen for 0 μM of 3,4-dMP indicating that without the presence of the 3-HSA substitute, there is no change in redox state of FMN (Figure 4.12). This clear decrease in absorbance with a stationary control suggests that there is a change in redox state in FMN dependent on concentration of 3,4-dMP. The trend seems to be that a higher concentration of 3,4-dMP results in steeper decrease in $OD_{450nm.}$ The control reaction with buffer showed completely stationary absorbances despite the presence of both FMN and 3,4-dMP (Appendix C). This indicated that FolP2 might be responsible for the observed reduction in FMN in Figure 4.12. The reaction also appears to be quicker with higher concentrations of 3,4-dMP up to around 500 μM at which point this trend seems to tail off at 700 μM; from this point onwards experimental wells with higher concentration of 3,4-dMP produce trends with absorbance decreases not as severe as lower concentrations (Figure 4.12). The protein and ligand presumably react in a 1:1 ratio, it would seem that past 700 μM the reaction becomes oversaturated and the rate slows down. Therefore, this reaction is displaying typical Michaelis-Menten kinetics (Johnson & Goody, 2011)

Another interesting finding of this experiment was the speed of the reaction. Previously, readings were only taken at 0, 5 and 10 mins so it was known that there was a decrease and then an increase in absorbance however, the gradient of either direction was not known (Figure 4.11). In this later experiment, there is a steep decline from the starting absorbance to a low

point at approximately 100 s (Figure 4.12). From 100 s to the endpoint at 600 s, the absorbance slowly recovers to nearly reach the initial starting absorbance. The decline to the low point of this assay is particularly quick; in fact, so quick that it was a challenge to take the initial reading fast enough (Figure 4.12). The inference from the obvious speed at reducing FMN is that despite a structurally similar, but not exact substrate (3,4-dMP in place of 3-HSA) FolP2 is well adapted for reducing FMN.

As the component being measured in this experiment was FMN, the concentration had to be fixed for the experiment to remain reliable. A high concentration of FMN results in a particularly high absorbance reading and this can saturate the absorbance reader. This saturation can sometimes mask subtle changes in absorbance caused by the protein. It was found that 500 µM appeared to show the most reliable level of absorption reading at OD_{450nm} with the absorbance of 500 µM FMN being approximately 1-1.25 OD. This concentration of FMN produced a high enough absorption that a change was clearly detected but not so high as to oversaturate the reader. Therefore, in all future experiments, FMN was set at a final concentration of 500 µM.

Throughout these experiments, the protein reaction has been initiated with the addition of FolP2 following by an immediate absorbance reading (t=0).

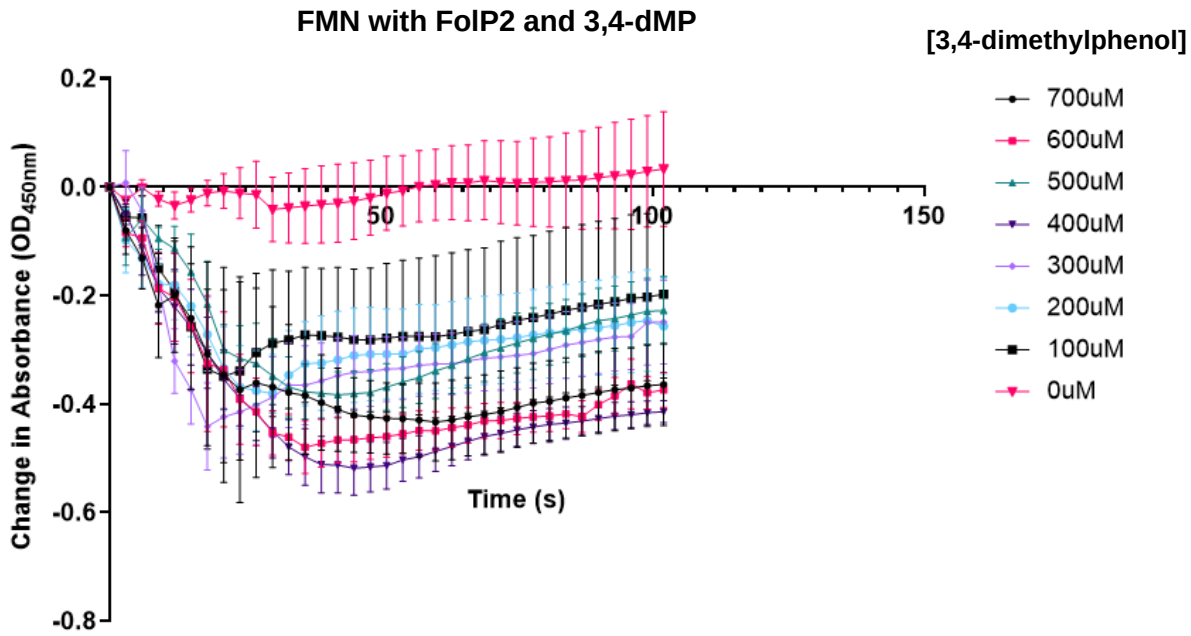

Figure 4.13: **Change in absorbance of FMN over 100 s with FolP2 and 3,4-dimethylphenol.** Both FMN and FolP2 concentrations were fixed and were challenged with a serial dilution of 3,4-dimethylphenol. The absorbance was then read every 5 s for 100 s. All experiments were conducted in n = 3

As the previous experiment showed, the reduction of FMN by FolP2 takes approximately 100 s. The next experiment was designed at capitalising on this first 100 s to fully investigate the activity of FolP2. The experiment below was conducted with FolP2 from a different protein purification so the concentration of protein used experimentally could be far higher. This purification yielded protein at a far higher concentration and far more stable than the two protein purification products used previously. The concentration of FolP2 was fixed at 5 μM in this experiment. The concentration of FMN was fixed at 500 μM as this was the concentration previously shown to depict the reduction process best without oversaturating the reaction. Finally, a dilution series of 3,4-dMP was tested in n=4 from 0μM to 700 μM (Figure 4.13). This experiment utilised a lower concentration of 3,4-dMP than in previous experiments because beyond 700 μM, higher concentrations of 3,4-dMP began to slow down the experiment. As shown in Figure 4.14, 700 μM of 3,4-dMP was enough to produce a consistent protein mediated reduction of FolP2. From the previous data, it was inferred that the reaction velocity

of FolP2 was hyperbolically dependant on the combination of FMN and 3,4-dMP. The first 30 s of this assay were used to calculate the initial velocity of the reaction for each substrate concentration. From this the enzyme kinetics of this experiment were investigated in a Michaelis-Menten kinetics graph (Figure 4.14). This allowed for the Michaelis constant or the K_m to be calculated using the equation $V = \frac{\text{Vmax x [Substrate]}}{\text{Km+[Substrate]}}$. This Michaelis Menten kinetics graph can be seen in Figure 4.14. This produces a reasonable K_m of 95.47 with an R^2 of 0.6143 (Figure 4.14). Whilst this shows a clear increase in rate with substrate concentration, it is imperative to bear in mind that these experiments were conducted using a structurally similar substrate for 3-HSA, not the exact substitute itself. It stands to reason that repeating experiment again using 3-HSA instead of 3,4-dMP would yield a lower K_m and a higher R^2. Nevertheless, this Michaelis-Menten curve does show that FolP2 does reduce FMN in the presence of a phenol (Figure 4.14)

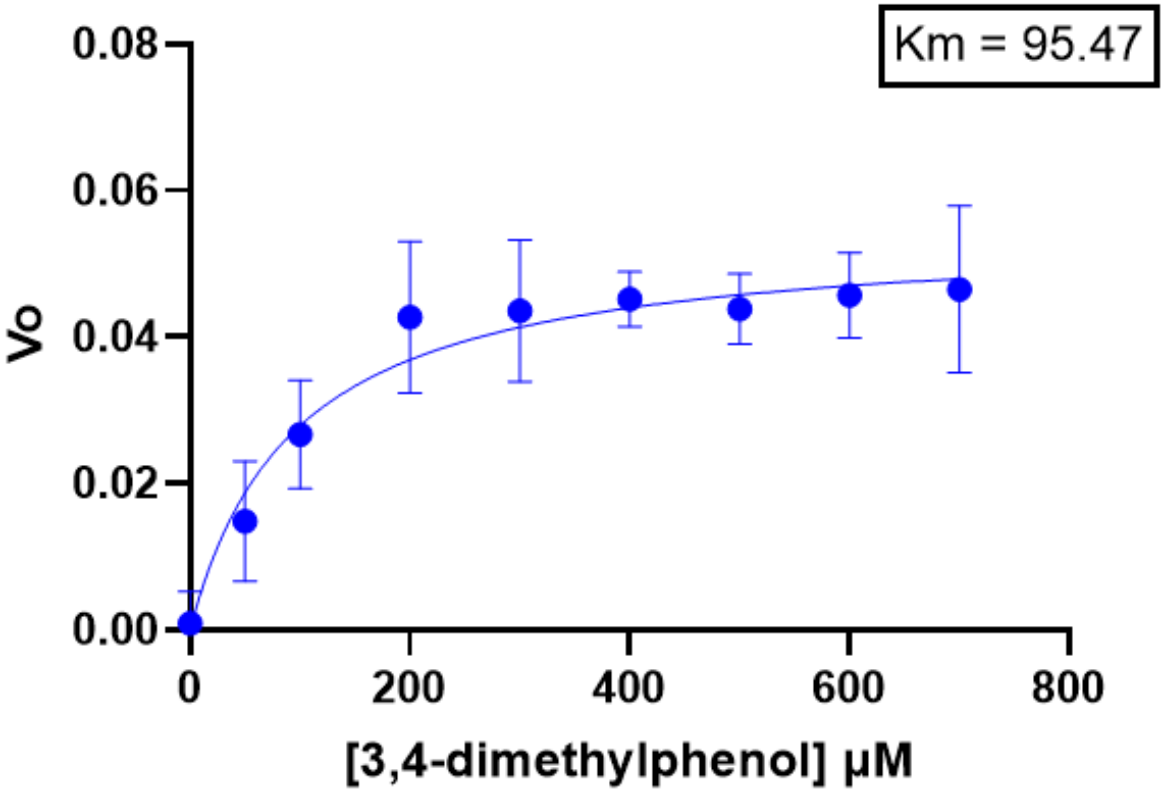

Figure 4.14: **Michaelis-Menten graph of FolP2 with FMN and a dilution series of 3,4-dimethylphenol.** The Km for this reaction was 95.47 and was found using Graphpad Prism. The R^2 was 0.6143.

This potentially proves our hypothesis; that FolP2 is acting as a hypoxic bypass so that this super pathway can continue albeit in an anoxic fashion using mainly the same proteins with different electron acceptors.

The discovery of the crucial role of cholesterol in the NRP state in relatively novel, thus the idea of oxic and anoxic pathways hasn't been particularly highlighted in the literature to date (Chiang et al., 2008). Nevertheless, the existence of such an anoxic pathway is a clear evolutionary advantage for *M. tuberculosis* survival. The cholesterol catabolism pathway was elucidated in large parts by comparison to related bacterial species *Rhodococcus* (van der Geize et al., 2007). The steps were largely proved to exist in *M. tuberculosis* through discovery of the homologs and their respective activities. In other facultative anaerobes, the oxic and anoxic pathways normal bare resemblance to each other; indeed it would be a waste of cellular energy to have an entirely distinct pathway (Chiang et al., 2008; Harder & Probian, 1997). However, in the oxic catabolism pathways, the electron donor is oxygen, whereas in typical anoxic pathways the electron donor is commonly either nitrate or nitrite (Chiang et al., 2008; Harder & Probian, 1997). The more energy-efficient route for facultative anaerobes is to have "hypoxic bypasses"; a work around for bacteria needing to complete the same processes albeit in differing conditions.

In all previous two-component flavin monooxygenase reactions, the FMN is reduced by the reductase component of the dimer utilising NADH as the electron doner (Dresen et al., 2010; Galán et al., 2000; van Berkel et al., 2006). When these experiments were originally designed it was with the hypothesis that FolP2 would replace the HsaA/B complex (FolP2 acting as a flavin monooxygenase). The data appears to show that FolP2 could potentially replace HsaB as the reductase and work in complex with HsaA (FolP2 as a one part of a two-component flavin monooxygenase (TC-FDM)).

All the redox assays show that FolP2 was utilising oxidised FMN and reducing to $FMNH_2$ (Figure 4.11, Figure 4.12, Figure 4.13, Figure 4.14). This could suggest that FolP2 would replace the activity of the reductase HsaB despite the lack of similarity between the two

proteins. This does somewhat make sense, as the research that discovered this complex in *M. tuberculosis* proved that HsaB had quite a substantial oxygen demand, independently of the oxygenase HsaA (Dresen et al., 2010). Previous research postulated that it was HsaA that bound the O_2 molecule which would then be activated by the reduced flavin to then to finally hydroxylate 3-HSA to 3,4-DHSA. The same research also points out that HsaA has been found to be essential for survival in macrophages, whereas its counterpart (HsaB) was not found to be essential (Griffin et al., 2011; Sassetti et al., 2003).

It would make sense that *M. tuberculosis* would replace this protein whilst in an anaerobic environment as due to the oxygen demand, HsaB could not function in an anaerobic environment. However, this would leave HsaA without a reductase; which is possibly the unknown function of FolP2.

However, the problem remains that in this experiment NADH was not included as it was not presumed to be required and despite this, a reduction process still occurred. This could be explained by the protein buffer in which the experiment was conducted (Tris-HCl) could be acting as an electron donor. Flavins have been identified as promiscuous towards electron donors and will utilise weak donors, such as Tris (S. Ernst et al., 2020; Gonçalves et al., 2019; Goncąlves et al., 2019). Nevertheless, even in the absence of NADH, FolP2 still clearly reduces the FMN in a substrate 3,4-dMP concentration dependent manner. One hypothesis as to why this occurs could be that FolP2, has a dimer pocket that is shared with HsaA and upon substrate binding to this dimer pocket, the protein structure shifts to reveal the FMN binding pocket. This hypothetical shift could allow the FMN and electron donor to bind and thus reduce the FMN to $FMNH_2$. This theory opens up yet more questions such as to which protein would bind the O_2 substrate (potentially NO_2-) or would this also be bound in the potential shared pocket?

The process of hydroxylation for an anaerobic bacterium is a complex one, especially for a facultative anaerobe. In an aerobe, O_2 is a readily available resource for these reactions. Most anaerobic bacterium have a work around for just such a quandary, for example, proteins that

used hydroxylases with a molybdenum cofactor (Dermer & Fuchs, 2012; Mendel, 2013; Szaleniec et al., 2018). In this case, something else must be used. There has been research showing that occasionally proteins convert nitrite to nitric oxide or nitrate to nitrate to hydroxylate varying substrates (Harder & Probian, 1997). Nitrite is highly present in the granuloma and it has been shown that *M. tuberculosis* survives much better in the NRP state in the present of nitrite (Sohaskey, 2008; Wayne & Hayes, 1998). Perhaps this is because it can be used in the place of O_2 in these oxygen-dependant assay as it has been previously shown that largely, the oxic and anoxic catabolism pathways will remain the same (Chiang et al., 2008; Dermer & Fuchs, 2012).

There have been proteins discovered that use a reduced flavin in an oxygen independent manner to act as a nitroreductase (Zenno et al., 1996). It is possible that nitrate (NO_3-) or nitrite (NO_2-) could be reduced to either nitrite or nitric oxide respectively to produce oxygen molecules for the hydroxylation process (Harder & Probian, 1997; Zedelius et al., 2011). If FolP2 is reducing NO_3- or NO_2- for the production of oxygen, this would effectively allow the difficult hydroxylation process to proceed and this activity would also potentially explain why nitrite is so crucial to the NRP state (Sohaskey, 2008). It is possible that FolP2 used reduced flavin to convert nitrite into nitric oxide and with the oxygen release formed an intermediate subspecies of flavin, called a hydroxyflavin (Ballou et al., 2005). This subspecies can then be used to hydroxylate molecules in the absence of oxygen.

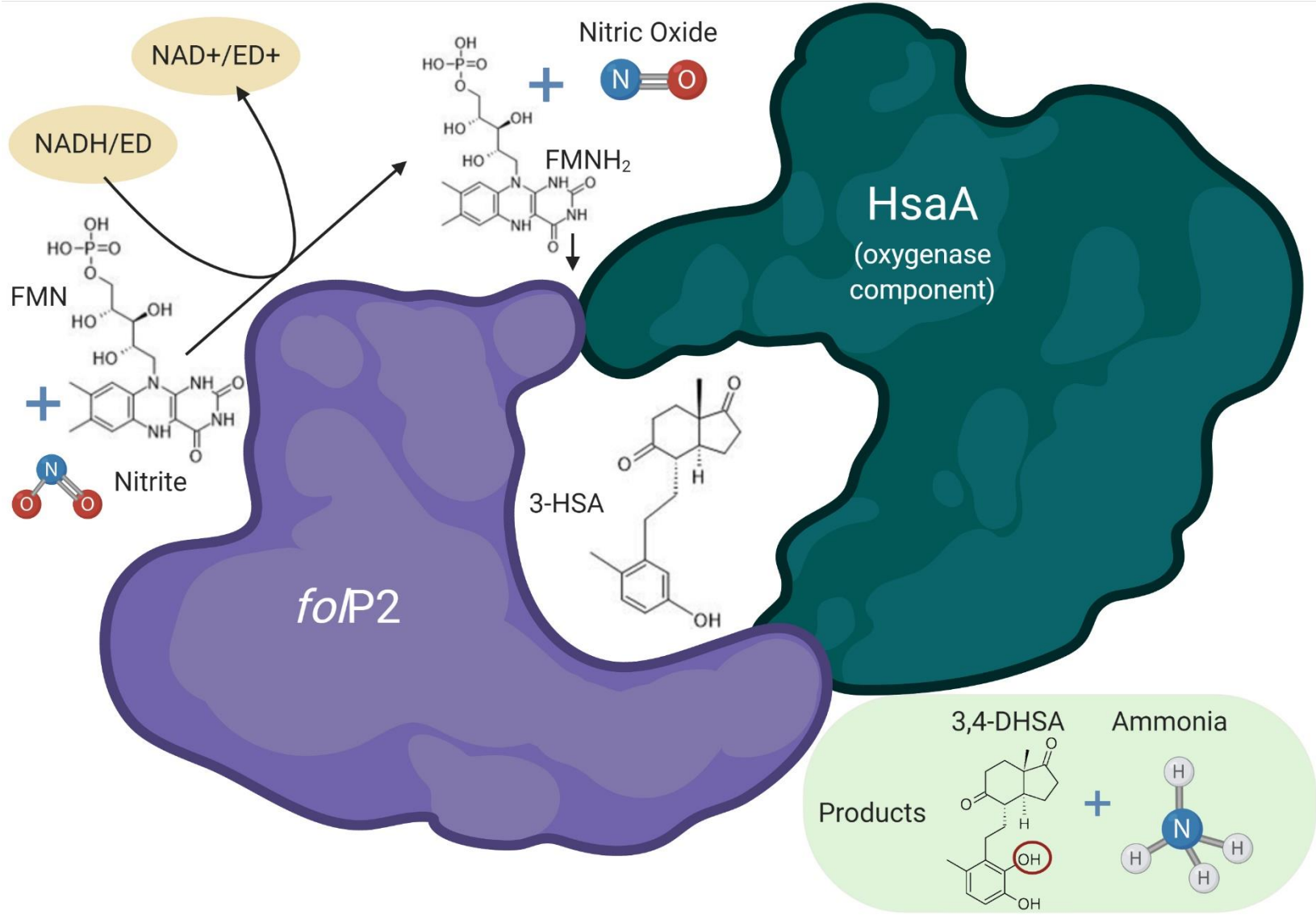

Figure 4.15: **Proposed Mechanism of FolP2 in complex with HsaA as a reducatase to form an anaerobic two component hydroxylase.** This is one proposed mechanism, alternatively nitrate could be oxidised to nitrite and then to nitric oxide. Created in biorender.com

The research shown above led to a potential deduction as to the activity of FolP2 (Figure 4.15). With the presumption that FolP2 and HsaA are working in complex and have a shared dimer binding site; HsaA would continue to catalyse the hydroxylation of 3-HSA, but perhaps FolP2 acts as a reductase, not only for FMN but also for nitrate. In theory, perhaps, FolP2 passes HsaA a reduced hydroxyflavin instead of simply a reduced flavin. This would circumvent the oxygen demand for HsaB and still allow for the hydroxylation process to occur with relatively little disruption. This proposed mechanism would also explain why inhibiting the activity of FolP2 has such a significant effect on the cell as without this process, the cholesterol molecules cannot be broken down. Figure 4.15 shows the potential theoretical mechanism of action for FolP2 in this system

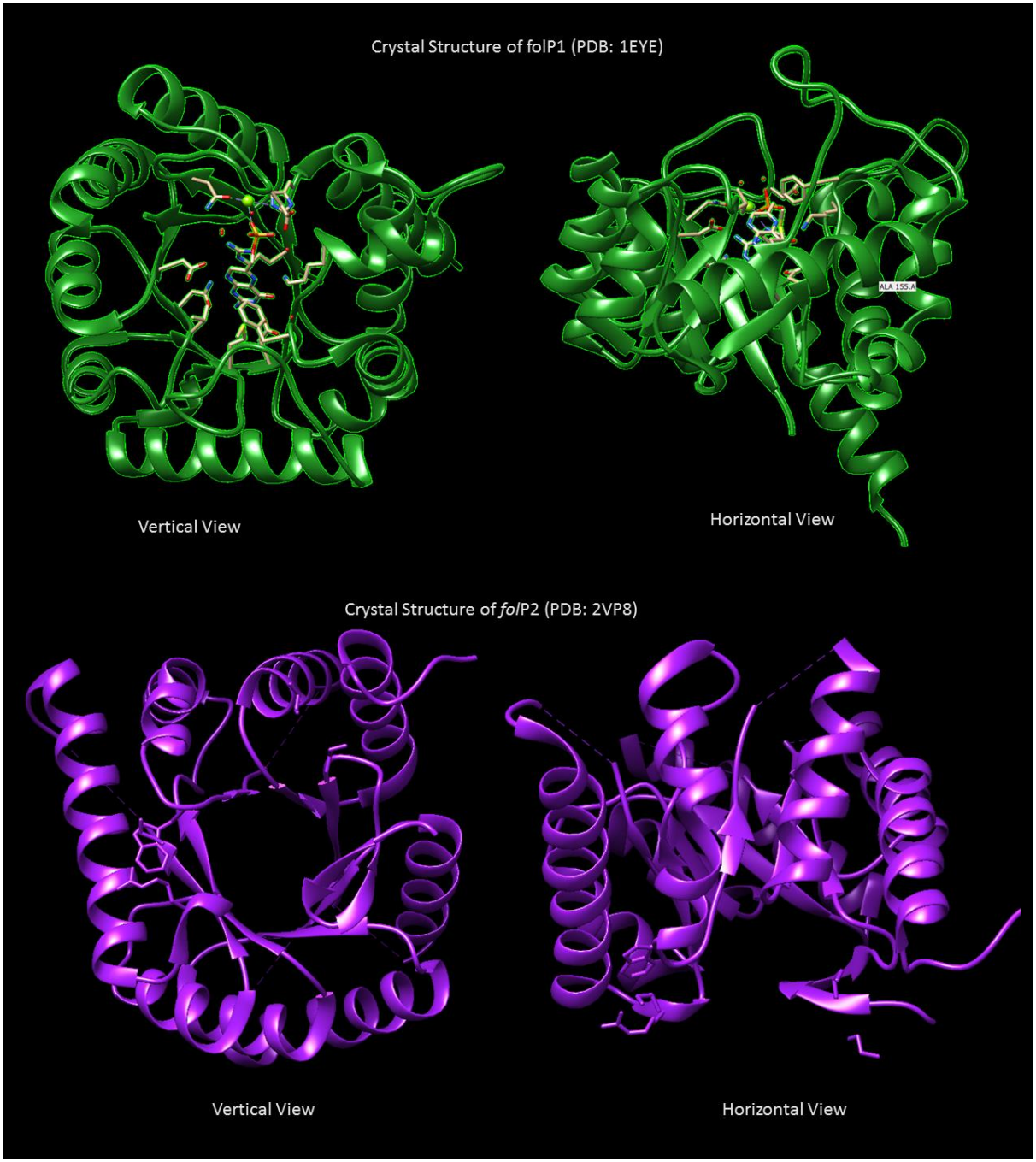

Figure 4.16: **Crystal Structure of FolP1 (1EYE) and FolP2 (2VP8).** Crystal structures were visualised using USCF Chimera.

The crystal structure of FolP2 (PDB: 2VP8) has been solved in a basic way by building off of the crystal structure of FolP1 (PDB: 1EYE) (Figure 4.16). However, it is not a complete structure and forms more of a guide to the structure than a definitive crystal structure. Due to these issues, it was not possible to perform any molecular docking assays using the crystal structure of FolP2.

There is a clear need for more research into this exciting and secretive protein, namely to establish whether the proposed mechanism above functions in the way proposed by this thesis or another way entirely (Figure 4.16). First and foremost, now that there is more information and a basic proof of the activity of FolP2, the above experiment should be repeated using a traditional electron donor such as NADH. It is encouraging that it was possible to attain a Michaelis-Menten curve and see defined protein activity without a traditional electron donor. However, it is expected that with NADH, the Km generated would be far lower and the protein activity would be far greater than what is shown above. Additionally, the inclusion of the correct substrate, 3-HSA, instead of the structurally similar 3,4-dMP could also improve the Km of FolP2 activity.

This leads into another issue with this assay is that it was completed with unstable protein. The protein used to gain the Michaelis-Menten curve was from the protein purification that gained the highest yield and also appeared to be far more stable in solution. However, the inherent instability of this protein may have affected the activity shown as the concentration of active FolP2 could not be known. It was postulated earlier when discussing the difficulties of purifying stable protein (*see* **section 4.2.6.1**), perhaps this concept extends into activity testing. It may be possible to vastly improve the activity of FolP2 by testing it anaerobically with a supply of nitrite for example in an anaerobic chamber or in a degassed cuvette.

To further this initial research, it would be interesting to purify HsaA and test the theory that FolP2 and HsaA work together. HsaA was proven to be essential to mycobacterial survival within macrophages and it did not have the same oxygen demand as HsaB so it is possible that it has an aerobic and an anaerobic activity dependant on which protein it is in complex

with (Dresen et al., 2010). It would also be interesting to detect whether FolP2 is present in a macrophage model of NRP *Mycobacteria* as it is not expressed in *M. tuberculosis* aerobically or in a nutrient starved NRP or hypoxia NRP model (Gengenbacher et al., 2008). This would lend evidence to FolP2 being an essential protein under the NRP state clinically.

4.2.7 Dapsone Inhibition of FolP2 activity

The initial result that led to this investigation into the novel activity of FolP2 was that DAP inhibits NRP *M. bovis* BCG under the Multi-Stress, Cholesterol model in a bactericidal manner. From overexpressing assays, it was determined that DAP was inhibiting FolP2 to exert bactericidal effect. Previous research into FolP2 activity as a DHPS used Dapsone as a surrogate for PABA (Gengenbacher et al., 2008). Whilst this research showed that FolP2 lacked the capacity to act as a DHPS, it also showed that Dapsone could bind to FolP2. Therefore, to completely connect the dots after discovering the potential activity of FolP2, the previous redox assay (*see* **section 7.12**) was repeated but with the addition of dilutions of DAP.

One issue encountered in this assay was that DAP in only soluble in DMSO and is completely insoluble in water at any concentration. Unfortunately, FolP2 was unable to tolerate any higher than 1% DMSO. In the assay, to ensure the function of the protein stayed intact, despite the addition of DMSO, a final concentration of 0.5%. A dilution scale of DMSO only was conducted and a control was added of only DMSO to guarantee that any effect seen in this assay was directly attributable to DAP. In this inhibitor assay, the concentration of FMN was fixed at 500 µM and the substrate, 3,4-dMP was fixed at 300 µM. These concentrations were chosen as, at these concentrations, the reaction does not proceed as fast as higher concentrations however, it still depicts a strong activity (Figure 4.14).

This assay showed comparable activities for FolP2 for 250 µM, 125 µM and 0 µM (Figure 4.17). The reactions with FolP2 treated with 250 µM and 125 µM showed a comparable rate of reaction to the 0 µM DAP control. This clearly depicts that at these concentrations of DAP, the activity of FolP2 is not inhibited (Figure 4.17). Nevertheless, at the highest concentration of DAP (500 µM); all activity of FolP2 is lost. Unlike in all the previous concentrations of DAP tested – including the DMSO only control – there is no reduction in absorbance from the initial value. This lack of reduction in absorbance shows that the oxidation state of FMN stays the same despite the presence of FolP2 and a sufficient concentration of substrate. Thus,

considering the DMSO only control and the no drug control, it would appear that the activity of FolP2 is completely inhibited with 500 μM of DAP (Figure 4.17). The MIC of DAP in NRP *M. bovis* BCG is 25 μg/mL or 100 μM. Despite a higher concentration of DAP needed to inhibit FolP2 in the redox assay than the antimicrobial testing, the inhibitory effect is still very clear. Therefore, it could be concluded that DAP can inhibit the reduction of FMN by FolP2, even at the protein level. It is important to note that the assay used to measure FolP2 requires optimising before it can reflect the true activity (i.e, 3-HSA instead of 3,4-dMP and addition of NADH) and this is possibly why it takes 5xMIC for DAP to inhibit FolP2 activity in this assay .In future experiments, it would be ideal to test a dilution series of DAP ranging between 500 μM and 250 μM so the activity of DAP can be seen to be decreasing with increasing DAP concentration.

Therefore, this inhibitory assay coupled with the overexpressor NRP assays suggest that FolP2 is an essential protein of *M. tuberculosis* when in the NRP state. All of the assays in this chapter have notable weak points but are bolstered by each other. The overexpressor assay identified FolP2 as the drug target of DAP; the redox assays showed that in combination with 3,4-dMP, FolP2 could alter the redox state of FMN but the addition of DAP to this assay knocked out this activity. These results reveal a compelling narrative about a novel drug target with a previously undefined mechanism of action. The most exciting part of this discovery is

that not only is this presumed inactive protein acting in a completely novel way; this novel and essential activity can be inhibited by an old, well-characterised drug

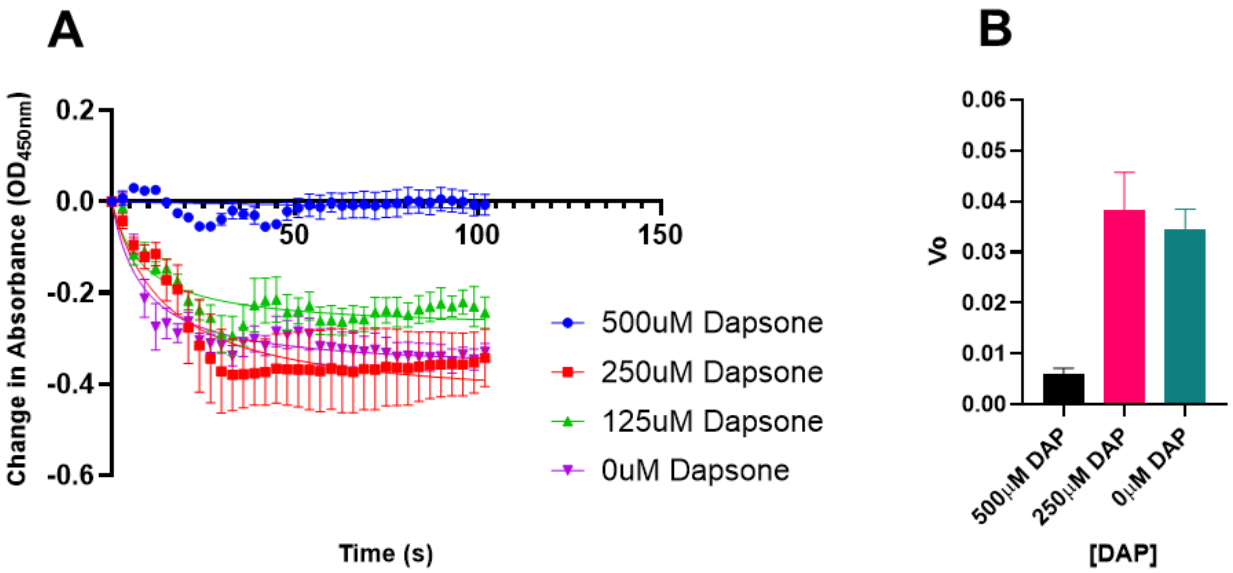

Figure 4.17: **Inhibition of FolP2 by Dapsone (DAP)**. (A) Change in absorbance graph of FolP2 with fixed FMN, fixed 3,4-dMP and several dilutions of DAP. Experiment was conducted in n = 4. (B) Bar graph depicting the calculated Vo of each concentration of DAP. The Vo was calculated from the gradient of the first 100 s of reaction in (A). A high Vo indicates activity of FolP2 in combination with FMN and 3,4-dMP. The low Vo seen in the culture for 500 µM indicates an inhibition of FolP2 activity.

As a limitation of this study, it is recognised that the inhibitory data is still very preliminary. These experiments were not set up to find enzyme kinetics such as finding the Ki; they were set up purely to answer whether DAP could block the potential protein activity found previously. It is very encouraging that this initial inhibitory data shows that DAP can inhibit the protein activity; this would be further accentuated by testing and obtaining full inhibitory kinetic data including the Ki. This testing would also confirm that DAP was competitively inhibiting FolP2. In addition, the inhibitory data only proves that DAP can inhibit, it does not really give any information as to why or how this inhibition is happening. It would be interesting to investigate the binding of DAP to FolP2, especially in regard to the anaerobic activity in complex with HsaA. Furthermore, testing more sulphonamides for inhibitory activity against FolP2 and more broadly against NRP *Mycobacteria* is an exciting, novel area of research that could have many real world implications.

4.3 Conclusion

Whilst the proposed mechanism in Figure 4.15 is a good possibility, it has to be highlighted that all the data this is based on is very preliminary and that there is simply not much research into anoxic cholesterol catabolism other than the identification that it happens (Chiang et al., 2008; Harder & Probian, 1997). Nevertheless, FolP2 is thought to be an inactive ortholog of DHPS and is a non-essential protein with no ostensible purpose (Gengenbacher et al., 2008; Williams et al., 2000). The identification of FolP2 being the drug target of DAP opened up a wide range of possibilities for activity. It was theorised that FolP2 could possibly have some activity in the cholesterol catabolism pathway and potentially that step could be the hydroxylation of 3-HSA (Dresen et al., 2010). This hypothesis seems to have been somewhat proved, as the combination of buffer, fixed FMN and a dilution series of 3,4-dMP produces no change in absorbance and thus no alteration of the redox state of FMN. The addition of FolP2 does alter the redox state of FMN, but only in the company of 3,4-dMP and in a dose dependent manner too. It seems that FolP2 has a role in the anoxic cholesterol catabolism pathway of *M. tuberculosis* and this activity can be inhibited by DAP at a cellular level and at a protein level.

Clearly, these results whilst being fascinating and entirely contrary to expectations, show that there is so much work still to be done to fully elucidate the activity of FolP2. The results shown above give an intriguing insight into a previously undiscovered pathway of TB, and even more excitingly, show that this pathway can be the Achilles' heel of TB whilst in the NRP state. Not in the least, repetition of the activity experiment but with the addition of NADH as the electron donor is crucial to proving the activity of this protein. Furthermore, purifying HsaA and attempting to assaying FolP2 and HsaA together to see if they can acts in complex to complete this crucial step of the cholesterol catabolism pathway is crucial. In addition, there are several other steps in this pathway that utilise molecular oxygen to complete their reactions. The findings of these chapters provide strong evidence that *M. tuberculosis* probably also has a work around for these oxygen dependant steps as well. It would be enlightening to rese arch the expression levels of these proteins under the multi-stress model.

Chapter 5:

Non-Replicating Persistent State of *Mycobacterium abscessus*

Chapter 5 Non-Replicating Persistent State of *Mycobacterium abscessus*

5.1 Introduction

5.1.1 Chapter 5 Introduction

Mycobacterium abscessus is a highly resistant, opportunistic pathogen which can cause serious and potentially fatal infections in immunocompromised patients (*see* **section 1.4)**. One of the main difficulties in treating *M. abscessus* infection is a seemingly disparate relationship between *in vitro* testing and *in vivo* treatment (Griffith, 2019; Huang et al., 2010). There has been a lot of discourse as showing that the lab can find susceptibility for if not many at least a few key antimicrobials against that specific strain. Nonetheless, when implemented, the *M. abscessus* does not seem to be affected. This brings us to the reasons for this chapter. Whilst *M. abscessus* is a fast-growing opportunistic pathogen, it is still a member of the *Mycobacteria* family. Throughout this thesis, it has been highlighted that when *M. tuberculosis* finds itself in a hostile environment, either through immune system action or antibiotic inhibition, it retreats into the NRP state as a method of survival. Once protected within the NRP state, the bacterium remains cognizant of its surroundings and when the environment becomes hospitable, the *Mycobacteria* resuscitate and begin to actively divide once more. One of the hallmarks of the NRP state is unexplained antibiotic tolerance and reoccurring infection. It is entirely possible that *M. abscessus* could have the capability to enter into the NRP state once challenged and use it as a survival mechanism to become completely tolerant to otherwise active antimicrobials. This hypothesis could also answer another issue of *M. abscessus* infection. It is generally thought to be exceptionally hard to clear the infection as there is a high rate of reinfection. Indeed, this is often the reason given for the extended treatment period. It is possible that what is being observed by clinicians as reinfection is actually recurrence of the original infection. If some of the bacteria became latent and awaited a change in environment, i.e cessation of antibiotic therapy, when conditions where favourable, the bacteria could resuscitate back to active disease (Lopeman et al., 2019). This could explain the issue of

“chronic” infection (Jarand et al., 2011). Nevertheless, if this hypothesis proved correct, the implications for this disease are huge. As previously stated in the case of TB, the hallmark of the NRP state and indeed latent disease as a whole is widespread drug indifference. If *M. abscessus* can enter the NRP state, an urgent review of all antibiotics would be required to identify an antimicrobial capable of targeting the microbe in this protective state.

5.1.2 Chapter 5 Aims and Objectives

The bulk of research conducted in the Mycobacteria genus is targeted towards the Tuberculosis complex. It is only recently that research has been focused onto the previously neglected Non-Tuberculous Mycobacteria (NTMs). A figurehead of this group of microorganisms is *Mycobacterium abscessus*. Particularly known for its complex and resistant infection, *M. abscessus* is becoming a pathogen of interest. The aim of this chapter, however, is to examine a crucial part of *M. abscessus* pathogenesis, chronic infection. It has long been known that *M. abscessus* can show susceptibility in biomedical testing to certain antibiotics but when this treatment is given to the patient, resistance is observed. It is possible that this changing antibiotic susceptibility profile could be attributed to the NRP state, as in M. tuberculosis.

With this hypothesis in mind, the aim of this chapter is to firstly establish whether *M. abscessus* can enter the NRP state in either model. If the NRP state is observed, an antibiotic susceptibility assay will be performed against all the frontline drugs commonly used in *M. abscessus* treatment. These aims will facilitate a greater understanding of the pathogenesis of *M. abscessus* as a whole

5.2 Results and Discussion

5.2.1 Genetic Framework of *Mycobacterium abscessus*

The first and most important element of this line of inquiry was to investigate whether *M. abscessus* could go into NRP state. There has been little to no research on *M. abscessus* surviving a hypoxic environment or how the bacterium reacts in a nutrient deprived or starved environment (Santucci et al., 2019). Nonetheless, it is apparent that *M abscessus* has considerable interactions with macrophages and can survive phagocytosis. This sets up the possibility of a granuloma formation and potentially yields the right conditions to induce *M. abscessus* into the NRP state.

Throughout all the research into the NRP in *M. tuberculosis,* there have been several genetic codons identify that are essential for mycobacterial survival in the NRP state. A notable example is the DosR regulon which has been heavily identified with hypoxia and adaptations for hypoxia (Bartek et al., 2009; Du et al., 2016; Park et al., 2003). Previous studies have shown that *M. abscessus* does have a DosR regulon (Gerasimova et al., 2011). The DosR proteins such as Dos S and DosR have *M. abscessus* orthologs. This can be seen in the sequence alignment shown below between *M. tuberculosis, M. bovis* and *M. abscessus.*

The sequence alignment found in Figure 5.1 shows an identical match between the protein sequence of *M. tuberculosis* and *M. bovis* for the DosS protein*. M. abscessus* also shows broad similarity of protein sequence albeit not fully. BLAST shows that between *M. tuberculosis* H37Rv and *M. abscessus* ATCC the DosS gene has a 51% identity but a 98% query cover. This would seem to show that *M. abscessus* has the genetic framework for the DosR regulon

as DosS is a key regulator. It stands to reason that if *M. abscessus* has coding for the regulators, it will have orthologs for the rest of the regulon

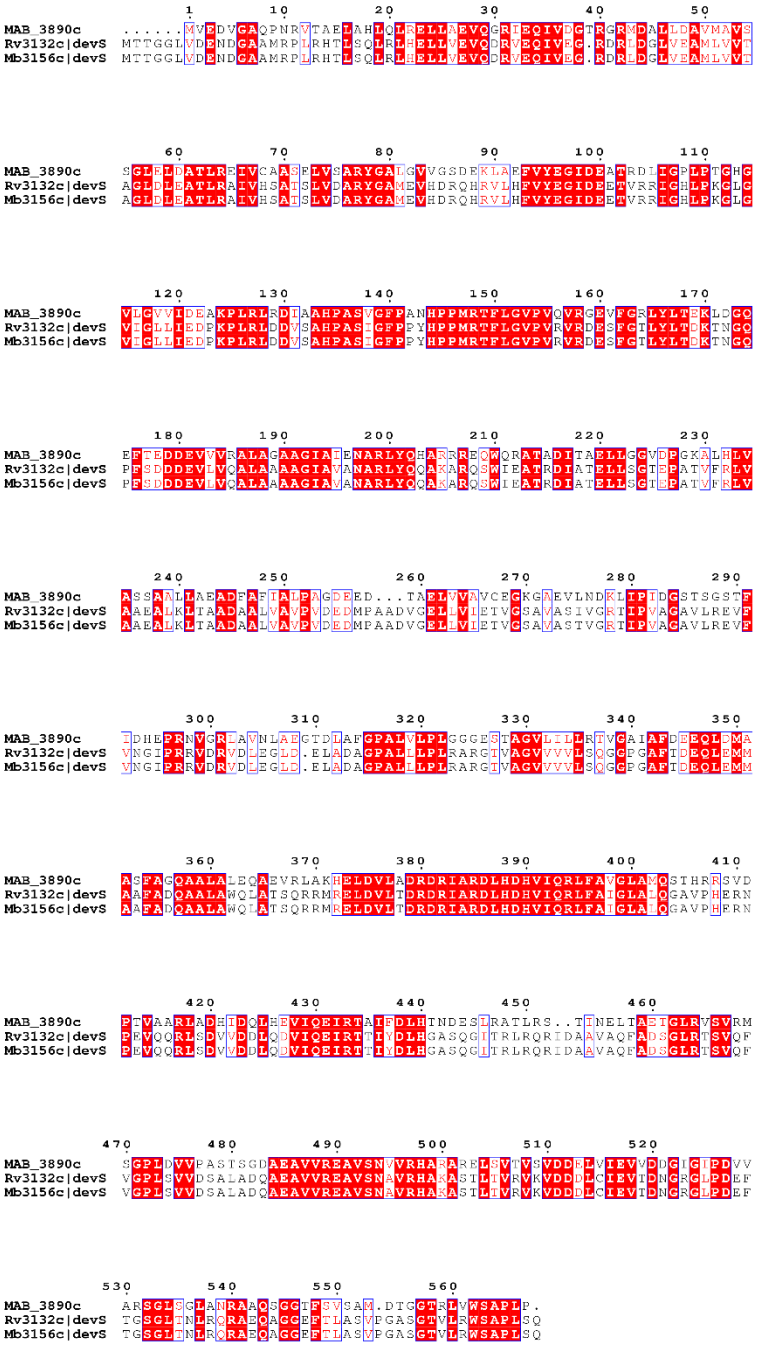

Figure 5.1: **Multiple protein sequence alignment of DosS from different mycobacterial species** Protein sequence alignment of DosS from different mycobacterial species display a high level of homology between sequences, indicated by residues in red. Mycobacterial species are *M. abscessus* MAB_3890c, *M. tuberculosis* Rv3132c and *M. bovis* Mb 3156c Residues highlighted in red indicate identity across all species aligned, showing conserved residues. Secondary structure information is seen above all sequences.

5.2.2 Validation of the ability of *Mycobacterium abscessus* to enter the Non-Replicating Persistent State

With the knowledge that *M. abscessus* at least has some of the genetic capability to enter the NRP state akin to *M. tuberculosis* it was placed in both of the NRP models developed in this thesis *(see* **section 2.2.1**). The key identifier of the NRP state is newly acquired drug tolerance. Therefore, similarly to the initial testing on *M. bovis* BCG to develop the model, the experiment was not only investigating for a halt in replication, it was also detecting drug indifference. There are many new and arising strains of *M. abscessus* with differing levels of antibiotic tolerance, however, for this line of experiments the NCTC 13031 strain was used (*see* **section 7.15**).

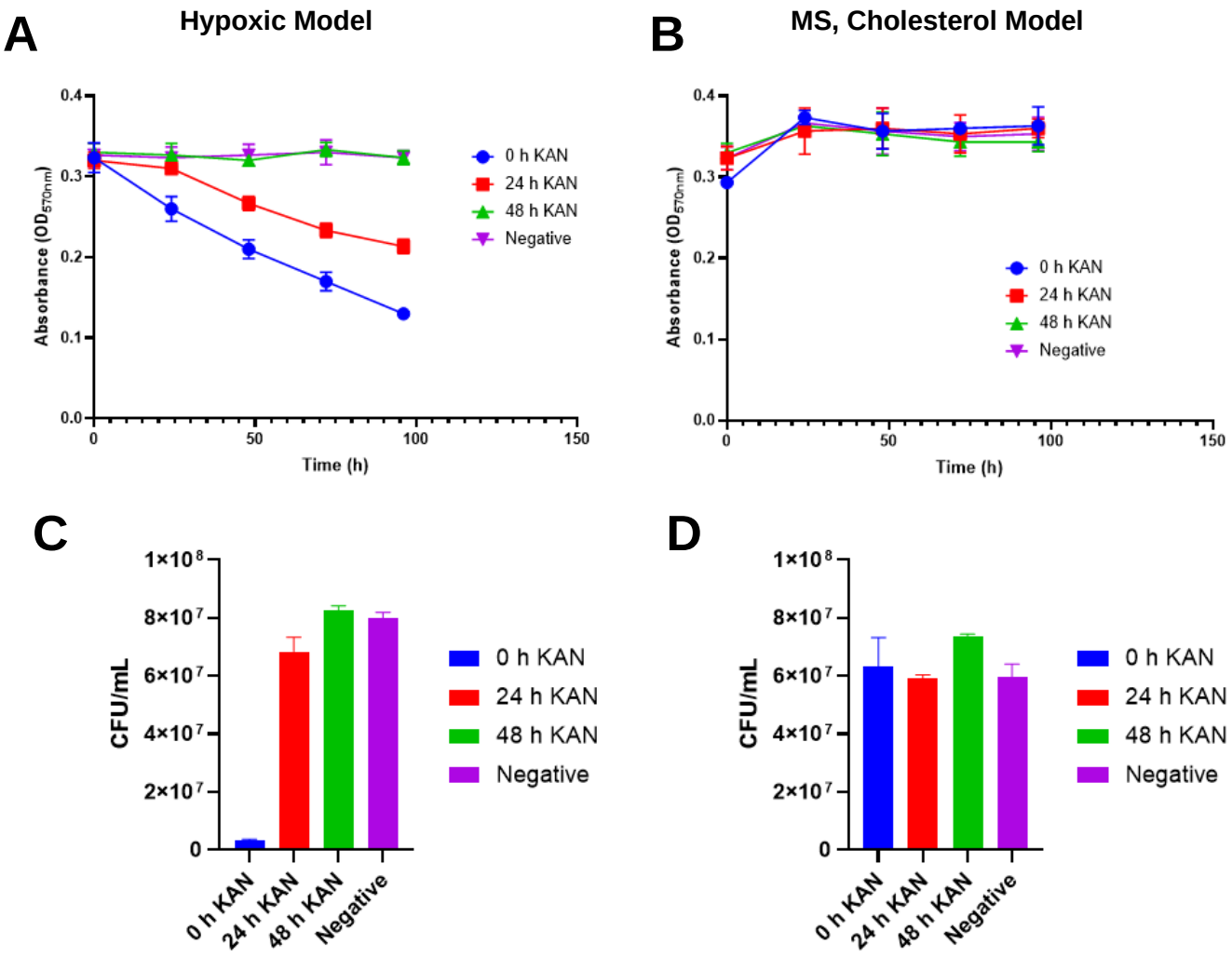

Figure 5.2: **Establishment of the NRP state in *M. abscessus*.** Cultures of *M. abscessus* were sent into the NRP state using the Hypoxic model (n=4) (A) and the Multi-Stress, Cholesterol model (B). Kanamycin was added to its respective experimental set at the correct time point (0h, 24h, 48h). The Negative cultures did not have any Kanamycin added. After 100 h of incubation, CFU/mL counts were taken for all cultures. (C) shows a bar graph of the Hypoxic model cultures. The 0 h culture did not resuscitate indicating that it was susceptible to Kan. All other concentrations resuscitated indicated a change in susceptibility to Kan. (D) shows a bar graph of the MS, Cholesterol model cultures. All concentrations of Kan resuscitated which indicated a change in susceptibility to Kan. All experiments were conducted in n = 4.

M. abscessus when tested under a NRP model appears to reach the NRP state similar to *M. tuberculosis*. Figure 2.5 shows arrested growth under both models followed by a stationary growth curve. No evidence of stress induced cell death was observed in either the absorbance readings or the resuscitated CFU/mL counts (Figure 2.5). Methylene blue within the cultures decolourised in the Hypoxic model around 24 h. However, in the multi-stress cholesterol model, decolourisation was observed as early as 4 h into anaerobic incubation. The cultures dosed with Kanamycin returned some interesting results. In the Hypoxic model, a decline in OD can be observed in the set of cultures dosed with Kanamycin at 0 h (Figure 2.5.A). This corresponds to no observable growth on the endpoint CFU/mL plates (Figure 2.5.C). As this

decline in OD is not observed in the no drug control, it is concluded that this effect can be attributed to the activity of kanamycin. Therefore, these results show that these cultures were still sensitive to kanamycin. The cultures dosed at 24 h and 48 h of incubation do not show any decline in OD_{600nm} and therefore seem to no longer be susceptible to kanamycin. The CFU/mL plates all corroborate the absorbance curves with all cultures apart from the 0 h resuscitating.

In contrast to the above results, the cultures under the cholesterol multi-stress model do not seem to show any susceptibility to kanamycin at any time point (Figure 2.5.B). The absorbance curves remain stationary across the experiment without any noticeable decline. In addition, every culture resuscitated at the endpoint of the assay despite the presence of kanamycin (Figure 2.5.D).

The results from the cholesterol model are really interesting. It seems that in this model, *M. abscessus* can not only enter the NRP state, the bacterium enters the protective NRP state faster than kanamycin activity. The fact that the culture where kanamycin was added upon entry to the anaerobic cabinet (0 h) survived unscathed adds weight to this theory. In addition, the visual conformation of hypoxia, by the decolourisation of the methylene blue was apparent after a 4 h of anaerobic incubation gives added weight that *M. abscessus* enters the NRP state quickly and efficiently. Whilst thinking about why this entry into the NRP state could be so much quicker than that of *M. tuberculosis,* it was proposed that that this was due to the far faster doubling time of *M. abscessus* when compared to the slow growing *M. tuberculosis* or *M. bovis.* On closer examination of the data, this does not seem to be the case. In the hypoxic model, until 24 h of incubation, *M. abscessus* is still susceptible to kanamycin. Inferring from this that until this point *M. abscessus* has not yet reached the NRP state. In *M. bovis* BCG, a difference in entry time can be observed, with the hypoxic model taking between 48-72 h to enter the NRP state and the cholesterol multi-stress model around 24-48 h (see section). This disparity in entry times seems to have carried over to *M. abscessus* with the cholesterol multi-stress model entering NRP far faster than the hypoxic model.

5.2.3 Aerobic Antibiotic Susceptibility of logarithmically growing *Mycobacterium abscessus*

After establishing that *M. abscessus* can enter into the NRP state under granuloma environmental stresses and shows antimicrobial tolerance, a range of antibiotic susceptibility testing was conducted. As previously mentioned, treatment of *M. abscessus* infection is increasingly difficult with a plethora of different classes of antimicrobials prescribed. Antimicrobial resistance in *M. abscessus* is increasingly common and becoming of great clinical significance to an already complicated infection. Therefore, clinicians try to use as wide a range of antimicrobials as possible to combat this (Novosad et al., 2016)

Therefore, when this experiment was designed, the panel of antimicrobials was chosen to reflect common prescribed antimicrobials and with a broad a range of mechanism of action as possible. The antimicrobials chosen, their class and the mechanism of action (if elucidated) is shown in Table 5.1.

Table 5.1**: Panel of Frontline Antibiotics commonly used to treat *M. abscessus* infection and their mechanisms of action.**

Antimicrobial	Class	Mechanism of Action
Amikacin	Aminoglycoside	Inhibits protein synthesis by irreversibly binding to 30S ribosome subunit
Clofazimine	Phenazine Dye	Prodrug which is reduced by NADH dehydrogenase to release active oxygen species
Clarithromycin	Macrolide	Inhibits protein synthesis by binding to 50S ribosome subunit
Linezolid	Oxazolidinone	Blocks the initiation of protein synthesis by preventing the binding of the 30S and 50S ribosome subunit
Moxifloxacin	Fluoroquinolone	Inhibits DNA gyrase
Tigecycline?	Gylcylcycine	Inhibits protein synthesis by irreversibly binding to 30S ribosome subunit
Dapsone	Sulphone	

In addition, to what is shown in Table 5.1, Tigecycline was also tested in all methods and is still included for the active MICs. Unfortunately, in anaerobic testing (in both models) the Tigecycline, especially at high concentrations, precipitated out of solution. This rendered further anaerobic testing impossible, but if work was continued on this project, perhaps the use of a different solvent or different concentrations would allow the investigation of Tigecycline anaerobic activity.

It should be noted that beta-lactam antimicrobials such as Imipenem and Cefoxitin are often prescribed for *M. abscessus* infection; commonly combined with a beta-lactamase for example clavulanic acid (Lavollay et al., 2014; Takei et al., 2020). Despite this, these antimicrobials were excluded due to an NRP incompatible MOA. In short, beta-lactams work by inhibiting cell wall synthesis which is highly effective when the bacteria are actively replicating. However, mycobacteria in the NRP state are no longer replicating, and thus are no longer producing cell wall in the same volume as when active. Imipenem, for example, inhibit penicillin binding proteins (PBPs) which are not active when the bacteria are not replicating (Takei et al., 2020).

Therefore, imipenem is incapable of exerting an antimicrobial effect against NRP *Mycobacteria* thus all antimicrobials with this MOA can be widely excluded.

Firstly, to provide a point of comparison, active *M. abscessus* MICs were found for all antimicrobials (*see* **section 7.17**). These were found to use as a comparator between active and latent disease to elucidate whether there is a distinct shift in antibiotic susceptibility towards a drug indifferent phenotype. The aerobic susceptibility testing was completed in ADC enriched 7H9 media and was completed by Rose Lopeman and James Harrison as a part of the Cox Laboratory and in collaboration for this project (Table 5.2).

Table 5.2: **Minimum Inhibitory Concentrations (MICs) against *M. abscessus* NCTC** for the panel of frontline antibiotics. These MICs were found through growth absorbance assays conducted by Rose Lopeman and James Harrison

Antimicrobial	Aerobic *M. abscessus* MIC (µg/mL)
Amikacin	16
Clofazimine	>4
Clarithromycin	1
Tigecycline	1
Linezolid	64
Moxifloxacin	8
Dapsone	50

As can clearly seen in Table 5.2, all antimicrobials chosen for this panel have an MIC against active *M. abscessus* to a greater or lesser extent. Particularly, Moxifloxacin with an aerobic MIC of 8 µg/mL and Clarithromycin with an aerobic MIC of 1 µg/mL. Clofazimine also showed an effective level of activity with an MIC of 4 µg/mL. Interestingly, Linezolid and Amikacin did not perform as effectively as the other frontline drugs with MICs of 64 µg/mL and 16 µg/mL, respectively.

As this panel of antimicrobials consists mainly of the frontline antibiotics against *M. abscessus* and the strain of *M. abscessus* being used is the relatively drug susceptible laboratory strain NCTC 13031; this high level of drug susceptibility is expected. In a clinical isolate of *M. abscessus,* a far greater level of antimicrobial resistance is expected.

5.2.4 Anaerobic frontline antibiotic susceptibility testing of Non-Replicating Persistent *Mycobacterium abscessus* under the classic hypoxia model

The next stage of testing was to conduct antibiotic susceptibility testing on the above drug panel against NRP *M. abscessus* under the hypoxia model. The MICs identified in this experiment can be found in Figure 5.3. Figure 5.3 shows a distinct shift away from the aerobic phenotype in regard to antibiotic susceptibility profile. Whilst under active, aerobic conditions *M. abscessus* was sensitive to all antimicrobials tested. In this experiment, we see the loss of this wide range of susceptibility.

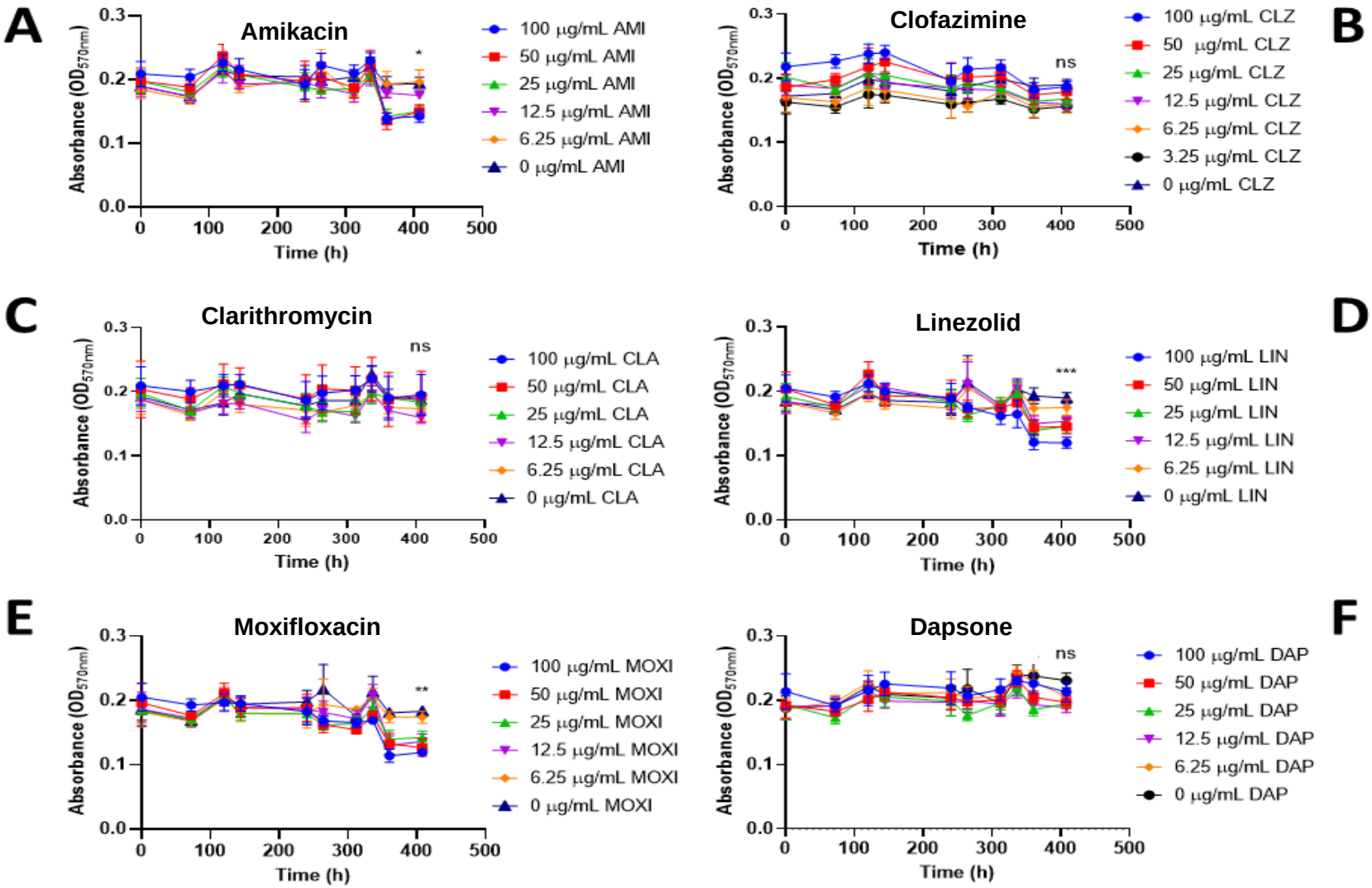

Figure 5.3: **Hypoxic NRP Model *M. abscessus* MIC testing against the antibiotic panel.** (A) shows a serial dilution of Amikacin (AMI) against NRP *M. abscessus*. statistically significant way (p = 0.0392). (B) shows a serial dilution of Clofazimine (CLZ) against NRP *M. abscessus*. Throughout the experiment, all cultures remained stationary and similar to the control in a non significant way (p = 0.9997). (C) shows a serial dilution of Clarithromycin (CLA) against NRP *M. abscessus*. a non significant way (p = 0.9190). (D) shows a serial dilution of Linezolid (LIN) against NRP *M. abscessus*. control in statistically significant way (p = 0.0002). (E) shows a serial dilution of Moxifloxacin (MOXI) against NRP *M. abscessus*. (p = 0.0002). All experiments were conducted in n = 4.

The results from frontline antibiotic, clarithromycin (CLA) are particularly interesting (Figure 5.3.C). CLA is one of the most commonly prescribed antibiotics against *M. abscessus* infection and the above aerobic MIC reflects this at 2 µg/mL (Table 5.2). However, the results show that under a hypoxic model of NRP, *M. abscessus* becomes completely indifferent to the presence of CLA even at the highest concentration of 100 µg/mL. This would infer that in the NRP state, *M. abscessus* is completely resistant to the effects of CLA despite strong active antimicrobial activity (Table 5.1; Figure 5.3). The daily OD readings produced a stationary absorbance curve were there was no statistically significant deviation away from the no drug control (0 µg/mL).

Clofazimine (CLZ), in a comparable fashion to the results of amikacin, showed no efficacy against hypoxic model NRP *M. abscessus* (Figure 5.3). Again, despite a high top concentration of 100 µg/mL, no significant decline in OD was observed across the length of the experiment (Figure 5.3.B). In fact, all concentrations of CLZ showed no statistically significant deviance away from the absorbance curve of the no drug control over 400 h of assay. This indicts that under hypoxia in the NRP state, *M. abscessus* is resistant to the effects of CLZ.

Whilst not having as strong an activity as it does against active *M. abscessus,* amikacin (AMI) showed an MIC against hypoxic model NRP *M. abscessus* (Figure 5.3.A). In the hypoxic model, clarithromycin gives an MIC of 25 µg/mL. The cultures with 100 µg/mL, 50 µg/mL and 25 µg/mL of AMI show a slight decline in OD from the control (Figure 5.3.A). Whilst this negative trend is present and shows a level of disparity away from the no drug control, it is slight. Indeed, this decline is only noticeable in the last 50 h of the assay. An endpoint one-way ANOVA was conducted to statistically analyse the data and found the only concentration to show significant deviation away from the control was 100 µg/mL AMI with a p value of 0.0392 (*). All other concentrations of AMI had p values ranging from 0.0936-0.9998 and thus classified as not significant. The inference from this weak change in OD is that whilst AMI is showing some inhibitory effect, it isn't particularly effective. Whilst *M. abscessus* has not become completely resistant to AMI, there has been a dramatic MIC shift between

logarithmically growing *M. abscessus* and NRP *M. abscessus.* This data demonstrates the mild inhibitory effect clarithromycin has on the hypoxia based NRP culture.

Linezolid also shows an observable but weak antimicrobial effect on the hypoxic model NRP cultures (Figure 5.3.D). At 100 µg/mL there is a clear decline in OD from the no drug control. However, at 50 µg/mL there is a possible decline in OD but it is still quite similar to the no drug control so the decline could be attributed to OD measurement error (Figure 5.3.D). Subsequent statistical analysis showed that only the culture treated with 100 µg/mL LIN showed a significant deviation from the control culture ($p=0.0002$). Therefore, the MIC for Linezolid against hypoxic model NRP *M. abscessus* is 100 µg/mL. The p value for the culture with 50 µg/mL LIN was 0.0747 and therefore not significant. The comparison between the aerobic MICs and the hypoxic MICs is pronounced; there is a clear and major MIC shift between the two experiments. Indeed, the MIC for Linezolid in the hypoxic model is so high, it may no longer be a viable option clinically. Thus, it may be treated as essentially resistant to Linezolid as it is no longer of therapeutic use.

Moxifloxacin provided some interesting results in this experiment. Moxifloxacin was previously tested against *M. bovis* BCG in both models as it is currently touted in clinical trials as a solution of latent infection (2019) (s*ee* **section** 2.2.6). When tested against hypoxic model NRP *M. abscessus*, it became the only antimicrobial tested to retain a similar MIC to the aerobic counterpart (Figure 5.3.E). The anaerobic MIC was 12.5 µg/mL, whereas the aerobic MIC is 16 µg/mL. This MIC is clearly demonstrated by the decline in OD of the 100 µg/mL, 50 µg/mL and 25 µg/mL cultures (Figure 5.3.E). The absorbance curve in which the decrease in OD is clearest in the 100 µg/mL culture. The four top concentrations of MOXI return a significant p value after ANOVA analysis with 100 µg/mL having the most significant p value at 0.001. All subsequent concentrations of MOXI returned a not significant p value.

5.2.5 Anaerobic frontline antibiotic susceptibility testing of Non-Replicating Persistent *Mycobacterium abscessus* under the multi-stress, cholesterol model

After the establishment of the ability of *M. abscessus* to enter the NRP state, furthered by the showcase of "gained" susceptibility using a hypoxia model of NRP (Wayne's); the outstanding hypothesis remained that if *M. bovis* BCG could achieved an enhanced level of resistance in the multi-stress, cholesterol model, could *M. abscessus*? The previous antimicrobial screen was repeated but using NRP *M. abscessus* under the multi-stress, cholesterol model.

From the initial experiments to check whether *M. abscessus* – as it is an NTM and not part of the TB complex – could enter the NRP state, there was a clear difference between the two models (see section 2.2). *M. abscessus* when triggered by the cholesterol model entered the NRP state far quicker and with less visible stress than when triggered by the hypoxic model. This would appear that the grand scale adaptations that are made upon entry to the NRP state are easier to complete when under an environment of hypoxia and cholesterol catabolism for both *M. abscessus* and *M. bovis* BCG.

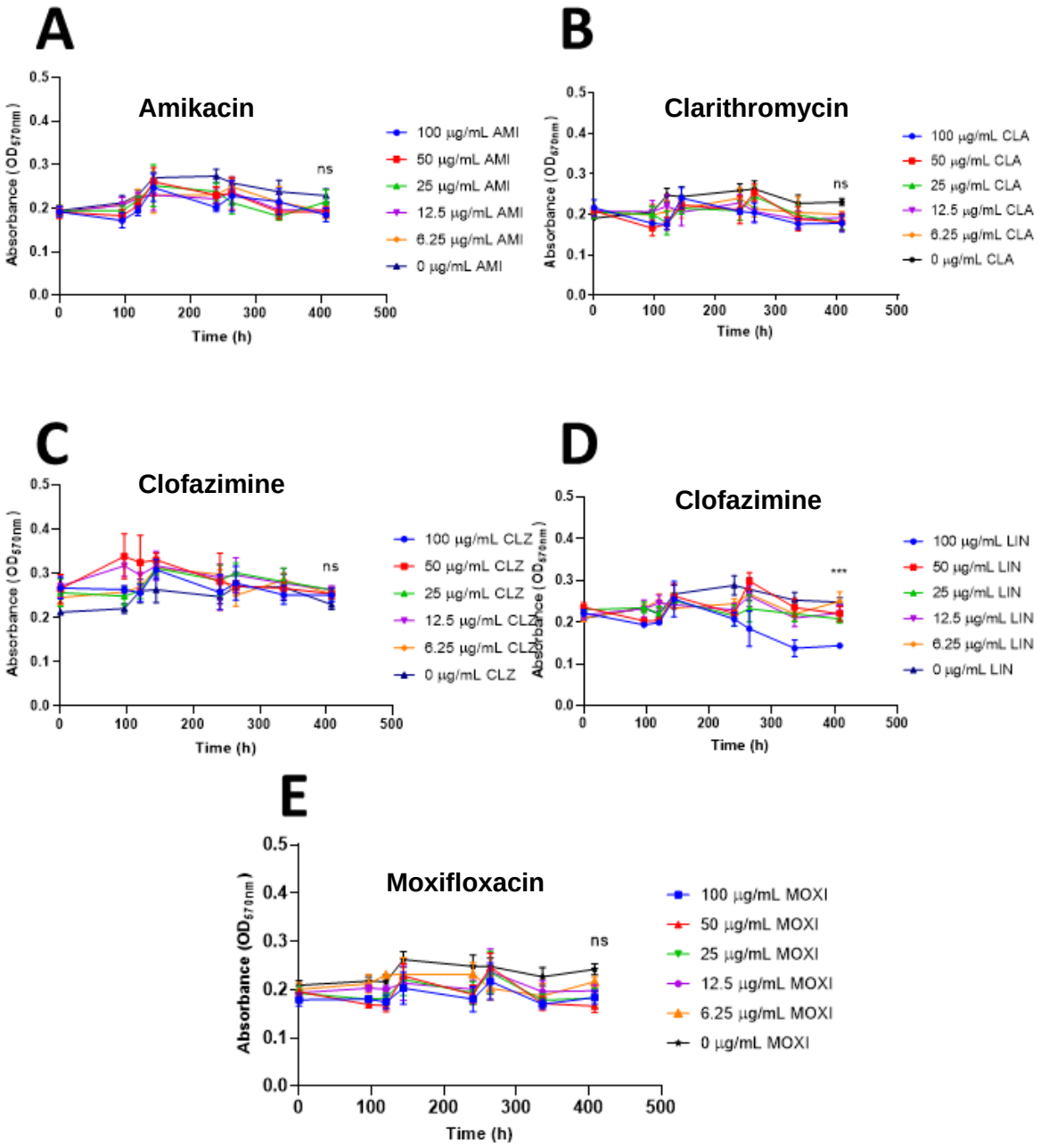

Figure 5.4: **Multi-Stress, Cholesterol NRP Model *M. abscessus* MIC against the antibiotic panel.** (A) shows a serial dilution of Amikacin (AMI) against *M. abscessus.* All cultures remained stationary and relative to the control throughout the experiment with non-significant deviation (p = 0.5876). (B) shows a serial dilution of Clarithromycin (CLA) against *M. abscessus.* All cultures remained stationary and relative to the control throughout the experiment with non-significant deviation (p = 0.3139). (C) shows a serial dilution of Clofazimine (CLZ) against *M. abscessus.* All cultures remained stationary and relative to the control throughout the experiment with non-significant deviation (p= 0.7176). (D) shows a serial dilution of Linezolid (LIN) against *M. abscessus.* All cultures remained stationary until 250 h whereby a slight decline in absorbance is shown by 100 µg/mL which is statistically significant (p = 0.0004). (E) shows a serial dilution of Moxifloxacin (MOXI) against *M. abscessus.* All cultures remained stationary and relative to the control throughout the experiment with non-significant deviation (p = 0.1563). All experiments were conducted in n = 4.

Whilst the treatment for *M. abscessus* infection is commonly prescribed on a case by case basis, CLA is perhaps the most common antimicrobial included in these combination therapies. This is due to the strong antimicrobial activity CLA exhibits against *M. abscessus.* This strong activity is replicated in the aerobic experiments above where CLA gave a MIC of 1 µg/mL, demonstrating why CLA is included in most therapies after *in vitro* testing in biomedical laboratories (Table 5.2). However, despite this strong active antimicrobial activity, the results in the hypoxic NRP model showed a complete lack of antimicrobial activity (Figure 5.3.C). As can be seen in Figure 5.4.B, this complete lack of antimicrobial activity is also seen in the multi-stress, cholesterol model. Over the 400 h of assay, all concentrations of CLA remain identical to the no drug control with no discrepancy for concentration. After statistical analysis, it was found that all concentrations are not statistically significant. Therefore, no concentration of CLA shows antimicrobial activity against *M. abscessus* when NRP under the multi-stress, cholesterol model (Figure 5.4.B). These results represent a dramatic shift in MIC from the active form of *M. abscessus* to both models of NRP.

CLZ has a curious MOA compared to the other antimicrobials tested in this assay. It is a dye that acts as a prodrug that upon activation created ROS (Table 5.1). It isn't quite a frontline drug against *M. abscessus* infection but it is commonly included as a part of combination therapies. Similarly to CLA, it has strong antimicrobial activity against actively replicating *M. abscessus* but failed to show any activity when tested against hypoxic model (Table 5.2, Figure 5.3). Likewise, as can be seen in Figure 5.4.C, under the multi-stress, cholesterol model there is no observable activity at any concentration of CLZ. Throughout the experiment, the absorbance curve of every concentration of CLZ mirrored to the no drug control (0 µg/mL) with no statistically significant deviation (Figure 5.4.C). This would suggest that - comparatively to CLA – despite active microbial activity, CLZ loses efficacy against *M. abscessus* when it is in the NRP state irrespective of the triggering factor.

AMI was one of the antimicrobials tested that retained an MIC against *M. abscessus* once in the NRP state. There was a significant MIC shift from the low aerobic MIC of 16 µg/mL to the

higher hypoxic NRP MIC of 25 µg/mL. AMI remains the only drug recommended by the American Thoracic society for the treatment of *M. abscessus* and is commonly used as a core component of most combination therapies. Therefore, when designing these experiments, establishing what activity, if any, AMI had against NRP *M. abscessus* was important. After AMI was tested against hypoxic model NRP *M. abscessus,* the experiment was repeated but with multi-stress, cholesterol model NRP *M. abscessus* (Figure 5.4.A). Despite the relatively strong antimicrobial activity shown by AMI in hypoxic NRP, there is no MIC when under the cholesterol model (Figure 5.4.A). All absorbance curves remain similar to the no drug control indicating that different concentrations of AMI do not affect the bacteria's "growth". When statistical analysis was conducted on these absorbance curves, none were found to be statistically significant. Indeed, the highest concentration of AMI (100 µg/mL) had the lowest p value at 0.5876.

LIN has proved previously to be a drug of interest due to it being one of the few antimicrobials to remain active in hypoxic model NRP state against both *M. abscessus* and *M. bovis* BCG. The results in the multi-stress, cholesterol model reflect this interest, if not in the way expected. The absorbance curves, for all but the highest concentration of LIN present the pattern that from the previous has become to be expected (Figure 5.4.D). There is no significant deviation away from the absorbance curve of the no drug control (0 µg/mL) allowing the inference that these concentrations of LIN do not exert any antimicrobial on the *M. abscessus*. Despite this, the highest concentration of LIN deviates away from this common thread. For approximately half the assay (200 h), 100 µg/mL follows the trend of the control and the other LIN concentrations. After this time point, the absorbance curve for 100 µg/mL begins to decline away from the control (Figure 5.4.D). This is a clear decline away from the curve of the control, but it is not a steep decline away. In fact, at the lowest point of the absorbance curve, only 0.5 OD_{570nm} is lost from the control. Statistical ANOVA analysis was conducted on this data package to interpret this slight decline better. All concentrations other than 100 µg/mL are thoroughly non-significant with the lowest p value being 0.7732. The p value for 100 µg//mL

proved to be a more insightful result. The ANOVA based p value is 0.0504, which is not statistically significant by 0.0004. This nearly significant p value could be attributed to the observable but slight difference in absorbance curves between 0 µg/mL (no drug control) and 100 µg/mL (Figure 5.4.D). This seems to suggest that at 100 µg/mL, LIN does not quite have a significantly negative effect on the *M. abscessus* culture. However, at a slightly increased concentration, it is possible that the effect seen at 100 µg/mLcould be amplified to become significant.

The final frontline drug tested was MOXI (Figure 5.4.E). MOXI was the only frontline drug tested against hypoxic model NRP *M. abscessus* that mostly retained the aerobic MIC (aerobic MIC =8 µg/mL, hypoxic NRP MIC = 12.5 µg/mL). The strong performance against a classic NRP model is reminiscent of the powerful efficacy of MOXI against hypoxic model *M. tuberculosis*. Despite this when the NRP model was changed to the multi-stress, cholesterol model, MOXI lost all efficacy against *M. bovis* BCG (see section 2.2.6). The results from multi-stress, cholesterol NRP *M. abscessus* reflect and amplify what was observed in NRP *M. bovis* BCG. The absorbance curves throughout the assay do not significantly deviate away from the control in spite of the presence of MOXI. The close grouping of all the absorbance curves including the control shows that differing concentrations of MOXI do not appear to influence *M. abscessus* whilst in the NRP state (Figure 5.4.E). Statistical analysis corroborates this conclusion with all concentrations of MOXI returning a non-significant p value using ANOVA analysis. This is in stark contrast to the high efficacy of MOXI in the hypoxic model of NRP, where all concentrations 12.5 µg/mL and above were shown to have deviated away from the control in a statistically significant manner. Therefore, between the two models of NRP, there is a distinct MIC shift. Indeed, it is challenging to refer to this effect as an MIC shift as that term implies an evident MIC in both models. These results show a culture showing relatively high susceptibility to a drug in one environment and demonstrating total resistance towards the same drug in a heightened environment.

A concise summary of these frontline antibiotic results could be that the hypoxic model of NRP confers on *M. abscessus* a reasonable level of resistance with around half of the drugs tested becoming completely resistant. This level of resistance becomes dramatically heightened when the model of NRP is changed to the multi-stress, cholesterol model. This form of NRP confers total resistance to *M. abscessus* for all of the frontline antimicrobials tested.

5.2.6 Susceptibility of Non-Replicating Persistent *Mycobacterium abscessus* against the sulphone Dapsone

Dapsone (DAP) is an antimicrobial that is part of the antibiotic treatment for Leprosy caused by the infectious agent, *M leprae* (Eichelmann et al., 2013). It was previously thought to work on by competitively inhibiting DHPS, a core protein in the folate acid biosynthesis pathway (Baca et al., 2000). In a previous chapter, it was discussed that DAP appears to have a separate mechanism of action against mycobacteria when in the NRP state. Against active TB, DAP has been previously reported to have minimal but present activity and is occasionally included in MDR-TB treatments.

Due to *M. abscessus* becoming a more prevalent cause of infection and a concerning level of antimicrobial resistance, investigating the antibiotic susceptibility profile of when *M. abscessus* is under the NRP state has clinical importance.

M. abscessus when tested against frontline antimicrobials using two models of NRP showed widespread resistance to all antimicrobials tested in results similar to those found previously against NRP *M. bovis* BCG. Thus, as DAP proved to be highly successful against NRP *M. bovis* BCG when all other antimicrobials were resistant, it was hypothesised that it was possible that NRP *M. abscessus* also to be susceptible to DAP. The below results show the absorbance curves of NRP *M. abscessus* tested against DAP in both models of NRP.

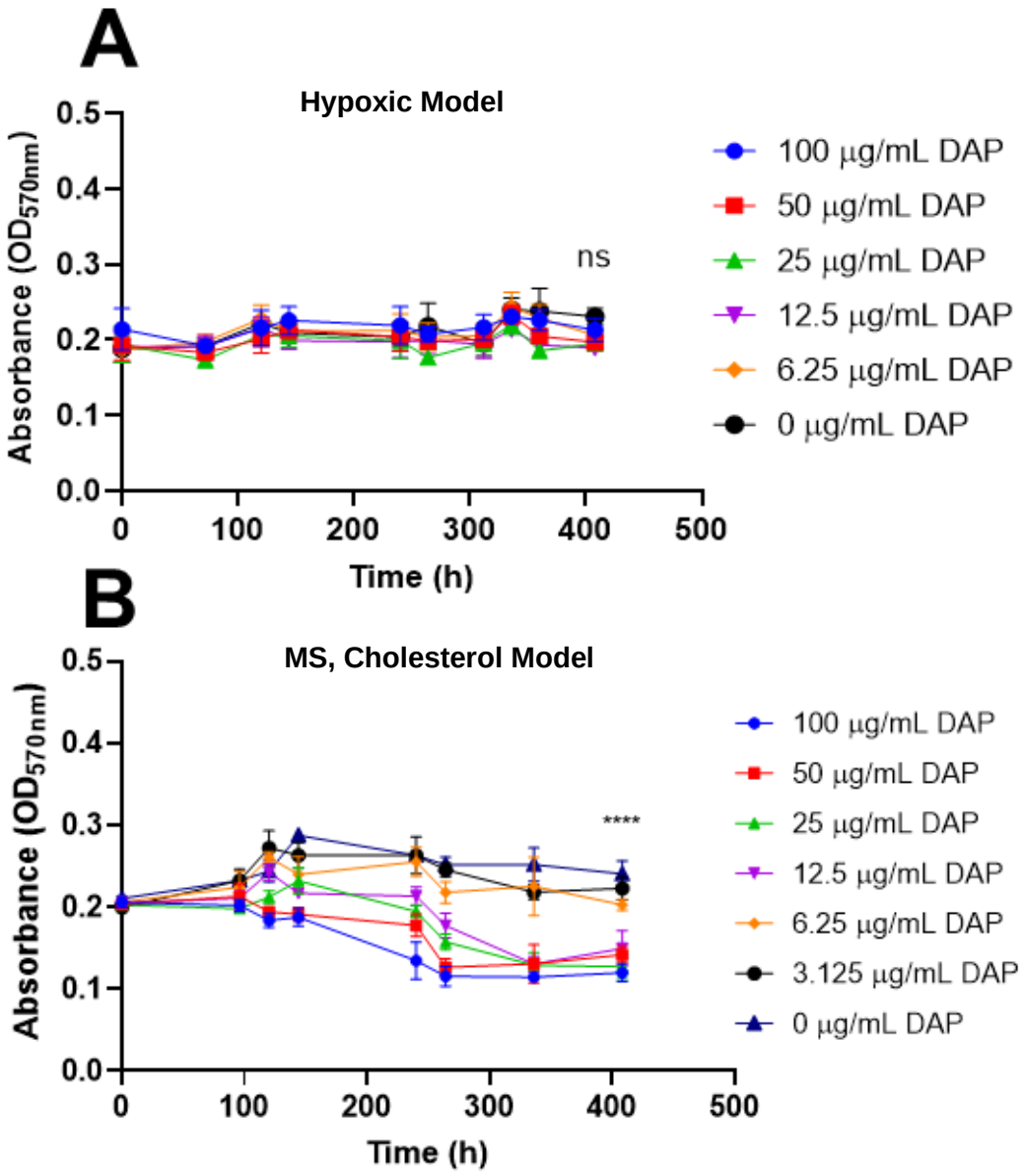

Figure 5.5: **MIC of Dapsone against NRP *M abscessus* using both models of NRP** (A) shows the absorbance curve of DAP challenging Hypoxic model NRP *M. abscessus*. This produced a non significant stationary growth curve (p value = 0.1194). (B) shows the absorbance curve of DAP challenging MS, Cholesterol model NRP *M. abscessus.* This produced a dose dependent response to the four highest concentrations of DAP which was statistically significant (p value = <0.0001). All experiments were conducted in n = 4.

Firstly, the results of the hypoxic model of NRP (Figure 5.5.A). The absorbance curves show all concentrations of DAP over 400 h. They all stay very similar to the no drug control (0 µg/mL) over the full course of the assay. There is no disparity in OD_{570nm} regardless of DAP concentration. Statistical ANOVA analysis of the dosed absorbance curves compared with the no drug control (0 µg/mL) found that no statistical significance. The p values range from 0.1194 at the lowest to 0.7244 at the highest.

These results are in distinct contrast to the results in the multi-stress, cholesterol model NRP model (Figure 5.5.B). There is a clear dose dependant response visible in the absorbance curves that depicts a clear MIC of 12.5 µg/mL. The absorbance curve for 100 µg/mL is the first to break away from the line of the control at approximately 100 h of assay. This decline is quickly followed by the absorbance curve for 50 µg/mL. The absorbance curves for 25 µg/mL and 12.5 µg/mL take approximately 100 h more of incubation before any noteworthy decline away from the control curve occurs (Figure 5.5.B). Whilst a clear decline in OD can be observed for 12.5 µg/mL of DAP, 6.25 µg/mL of DAP mirrors closely the absorbance of the 0 µg/mL line. This allows for the inference that 6.25 µg/mL cannot affect the same activity on the bacteria, thus 12.5 µg/mL of DAP is the MIC in this scenario. Statistical analysis of this assay added credence to the observed dose dependant response. The p value for 100 µg/mL was <0.0001 showing this result to be highly significant. The p values for 50 µg/mL and 25 µg/mL were 0.0002 and 0.0001 which are significant result albeit not quite as low as 100 µg/mL. Finally, 12.5 µg/mL DAP gave a p value of 0.0012 which reflects the weakening of activity at lower concentration and sets the boundary of inhibition. The remaining three concentrations of DAP all were non-significant with p value from 0.2564 and above. This statistical analysis highlights the activity of DAP against NRP *M. abscessus* to the MIC of 12.5 µg/mL which correspond with the absorbance curve.

5.3 Conclusion

M. abscessus was only identified in 1953 making it a comparatively young pathogen however, identification of the complex infection and widespread antibiotic resistance have led to the recognition of *M. abscessus* as an important human pathogen (Moore & Frerichs, 1953; Nessar et al., 2012). The current dogma surrounding mycobacteria is that those species not within the *M. tuberculosis* complex cannot enter the NRP state. Current research has identified the NRP state as a mycobacterium specific virulence factor, as it is arguably the foremost method of survival. There has been little to no research conducted on the capability of NTMs, or non-tuberculous mycobacteria, to have an NRP state. *M. abscessus* has proven to create complex human infections which prove an immense challenge to treat (Griffith, 2019; Nessar et al., 2012). One of the main features of these complex infections are chronic infections, where typically immunocompromised patients have concurrent infections that become increasingly hard to treat (Esther et al., 2010). Clinicians have theorised that the immunocompromised nature of the patients results in sequential, separate infections. Cases of TB are often plagued by chronic infection or “previously treated” infections (Munje et al., 2015; Zignol et al., 2006). This has come to be attributed to latent infection as opposed to reinfection. It stands to reason that *M. abscessus* could have a “latent state” where if conditions became adverse, for example during antibiotic treatment, it could act as a means of survival for the organism until conditions improved the antibiotic challenge is removed.

The results in this chapter firmly establish that *M. abscessus* does have the ability to enter into the Non-Replicating Persistent state akin to *M. tuberculosis.* This clearly has far reaching clinical implications as one of the hallmarks of the NRP state is antimicrobial indifference (Nessar et al., 2012). Whilst this research does not establish whether *M. abscessus* uses the NRP state clinically, it seems likely when considering the previously discussed disparity between *in vitro* testing and clinical observation and the high prevalence of chronic infection (Esther et al., 2010; Jarand et al., 2011; Nessar et al., 2012).

That being said, it would be incorrect to declare that the NRP state for *M. abscessus* is the same as it is in *M. tuberculosis.* The above results established that similarly to *M. bovis* BCG, transition into the NRP state is less stressful under the multi-stress, cholesterol model.

The main difference between the NRP state in *M. tuberculosis* and *M. abscessus* is time. There has been a great deal of research that established that *M. tuberculosis* can stay in the NRP state somewhat indefinitely (Jakkala & Ajitkumar, 2019; Trutneva et al., 2020). There are so many adaptations to the granuloma environment that make that possible. During these experiments with *M. abscessus,* it was firmly established that after 400 h of incubation all cultures would start to decrease in OD regardless of drug concentration. However, this ability should not be dismissed. The capability for a bacterium to enter into a protective state that renders it invulnerable to the majority of antimicrobials, even if for a short amount of time, is a formidable virulence factor. Indeed, this virulence factor could be the main cause of the "chronic" *M. abscessus* infection (Esther et al., 2010).

As previously stated, the major hallmark of the NRP state is drug indifference (Wayne & Sohaskey, 2001). The fascinating thing about these results is the disparity in antibiotic profiles between the two NRP models tested. The hypoxic NRP model used above was designed to be as close to Wayne's model of NRP as possible. There are no restrictions on metabolism in this model, the only environmental stress present in this model is the slow shiftdown into hypoxia. As per the antibiotic profile of NRP *M. tuberculosis, M. abscessus* when under a hypoxic model of NRP shows a high level of antibiotic resistance. The notable exceptions to this resistance are AMI and MOXI. Perhaps the least surprising of the two is MOXI, as MOXI has been notably identified as an antimicrobial that is effective against NRP *M. tuberculosis*. Indeed, MOXI is being included in combination therapies currently in clinical trials partly for its activity against LTBI (de Miranda Silva et al., 2019). Therefore, the retention of activity against *M. abscessus,* even when in the NRP state. It was also encouraging that AMI retained activity against *M. abscessus* as AMI is one of the most commonly prescribed antimicrobials (Huang et al., 2010).

The above results would be concerning to see this high level of drug resistance in an already worryingly resistant pathogen (Nessar et al., 2012). However, all the results talked about above are using the Wayne model (or our version, the hypoxic model) and as previously discussed in this thesis, this model does not fully represent the NRP state. The NRP state is triggered by exposure to a complex and hostile environment composed of several factors (Gibson et al., 2018). If the assumption is made that *M. abscessus* is subjected to the same environment as *M. tuberculosis,* then the assumption that the Wayne model is not the best fit can also be extended. Highlighted with the above assumption, the antibiotic profile for *M. 9abscessus* in the multi-stress, cholesterol model is of grave clinical importance.

Every antimicrobial tested against multi-stress, cholesterol model NRP *M. abscessus* completely lost their activity. The panel of antimicrobials was chosen partly for their high prevalence in combination therapies for *M. abscessus* infection (Novosad et al., 2016). The mere fact that at the highest concentration of 100 µg/mL, these antimicrobials still showed no significant activity against *M. abscessus* clearly shows how important and dangerous this state is. The NRP state appears to act as a safety bunker for *M. abscessus* in terms of high stress. This results in the patient being exposed to a side effect heavy therapy that does not clear the infection. Therefore, when the antibiotic treatment has passed or been lessened, *M. abscessus* can reactivate and begin the infection anew. This then exposes the already weakened patient to a fresh dose of toxic antibiotics. It is unclear how many times *M. abscessus* can enter the NRP state as the process is inherently stressful but even if it can only be entered once a great deal of damage can be dealt to the patient; both from the infection and from an ineffective and strong antibiotic treatment. In addition, the drugs tested in these experiments are not novel compounds that are proposed for *M. abscessus* treatment; these are the current antibiotics of choice for this infection (Esther et al., 2010; Nessar et al., 2012; Novosad et al., 2016). The lack of activity against NRP *M. abscessus* in the NRP state highlights the need for a new approach to *M. abscessus* treatment. A two-pronged approach that can target active and NRP *M. abscessus* could reduce antibiotic treatment periods and prevent chronic infections.

In light of this two-pronged approach, the result of DAP activity is especially poignant. In previous chapters of this thesis, DAP activity on NRP *M. bovis* BCG was researched and discussed. In these chapters, new evidence of novel activity was presented, separate to the previously established activity. Instead of inhibiting DHPS in the folic acid biosynthesis pathway which it is the apparent MOA in aerobic mycobacteria; when in the NRP state, the weak aerobic inhibition appears to be replaced by a far stronger inhibition of DHPS homolog FolP2 (Baca et al., 2000; Gengenbacher et al., 2008; Minato et al., 2015a). *M. abscessus* also has a copy of both *fol*P1 and *fol*P2. Thus, it stands to reason that similarly in *M. bovis* BCG, FolP2 is a part of the hypoxic pathway of cholesterol catabolism in *M. abscessus* (Wilburn et al., 2018). If this is the case, the results would make sense that DAP showed activity in the multi-stress, cholesterol model of NRP but none in the hypoxic model. If *M. abscessus* is metabolising cholesterol in a hypoxic atmosphere, it would need the same “hypoxic bypass”, FolP2. Therefore, DAP inhibition of FolP2 is an exciting and new breakthrough in both *M. bovis* BCG and *M. abscessus*. This discovery of activity could allow for the development of a new combination therapy that would eliminate the safety bunker for *M. abscessus.* As most *in vivo* models of NRP are not truly representative of the NRP state (see section), the activity of DAP would need to be tested in a minipig model (Guirado & Schlesinger, 2013). If the *in vivo* activity of DAP reflects the *in vitro* activity of DAP, as DAP has already been through clinical trials it could be included into a new combination therapy for *M. abcessus* treatment. This combination therapy could result in a major reduction in chronic infection and a decrease in the length of antibiotic therapy.

As seen in the results of this chapter, the phenotype given by these single stress models is worryingly resistant. Additionally, even if a drug has retained activity, there is normally a dramatic MIC shift to accompany it. Using a multi-stress model reveals the full nature of the “drug indifferent” NRP state. Nevertheless, despite total resistance against the frontline drugs tested, the susceptibility to DAP will help to combat this issue.

Chapter 6:
General Discussion

Chapter 6 Discussion

6.1 Discussion of Thesis

(S. H. Cho et al., 2006; Parish et al., 2003; Wayne & Sohaskey, 2001)(Bacon et al., 2014; Betts et al., 2002; Iona et al., 2016; Muñoz-Elías et al., 2006; van der Geize et al., 2007; Wayne & Sohaskey, 2001)It would not be an over exaggeration to say that tuberculosis is the most studied disease of all time (T. M. Daniel, 2006; Hippocrates, 1708; Koch, 1882). This archaic disease is so complex that the Non-Replicating Persistence state is still being defined (Bacon et al., 2014; Betts et al., 2002; Iona et al., 2016; Muñoz-Elías et al., 2006; van der Geize et al., 2007; Wayne & Sohaskey, 2001). The NRP state is intricate in isolation but is further complicated by the unique scenario *M. tuberculosis* in which utilises it (Barry et al., 2009a; Gil et al., 2010; Guirado & Schlesinger, 2013; Sakamoto, 2012; Santucci et al., 2016). Despite the depth of research, what happens to the M. tuberculosis inside the granuloma has remained largely unknown, due to the dangers of tampering with a granuloma in a clinical setting. Indeed, until Wayne identified the NRP state, it was presumed that the cessation of symptoms meant that the TB infection had been cured. In recent years, more details have been discovered about NRP *M. tuberculosis*, the granuloma environment and LTBI as a whole (Bacon et al., 2014; Betts et al., 2002; Esmail et al., 2014; Gopinath et al., 2015; Iona et al., 2016; Muñoz-Elías et al., 2006; Soto-Ramirez et al., 2017). Much of the research has highlighted the presence and importance of hypoxia as a driving factor for NRP, as well as the vast changes to the proteome and morphology caused by hypoxia (S. H. Cho et al., 2006; Parish et al., 2003; Wayne & Sohaskey, 2001). Conversely, there is a great deal of discussion centred around *M. tuberculosis* metabolism within the granuloma and the importance of cholesterol catabolism to *M. tuberculosis* granuloma survival (Griffin et al., 2012; Pandey & Sassetti, 2008; Soto-Ramirez et al., 2017; van der Geize et al., 2007; Wilburn et al., 2018). The above factors are widely accepted as intrinsically important to the initiation, maintenance and function of the NRP state. The crucial element is that despite acknowledgement of the importance of all of these factors, they (particularly hypoxia and cholesterol catabolism) are mutually exclusive towards

each other. Several steps in the cholesterol catabolism pathway have an active oxygen demand, and therefore cannot exist in a completely hypoxic atmosphere in the current elucidated state (Dresen et al., 2010; Wilburn et al., 2018; Wipperman et al., 2014). This contradiction between cholesterol catabolism and hypoxia is enthralling and is what makes the NRP state so interesting.

The novel *in vitro* model of the NRP state set out in this thesis (Multi-Stress, Cholesterol model) combines a hypoxic atmosphere with a nutrient deprived media that solely focuses metabolism onto cholesterol. Throughout the thesis the results of this novel model were contrasted with an adaptation of Wayne's model of NRP (the Hypoxic model) which is the most used *in vitro* model for NRP research (Wayne & Hayes, 1996; Wayne & Sohaskey, 2001). This model exclusively uses hypoxia with the culture medium being the rich 7H9-ADC and thus not the instigator of any stress. That being stated, despite the MS, Cholesterol model containing more limiting factors than the Hypoxic model, it was the bacteria within the Hypoxic model which were obviously stressed. This suggests that the combination of stresses set out in the MS, Cholesterol model actually eases the Mycobacterial culture into the NRP state; whereas, in the Hypoxic model, entry into the NRP state comes as more of a shock. This ease of entry in the MS, Cholesterol model is also reflected at the opposing end of the NRP state, with an ease of resuscitation compared to the Hypoxic model. Indeed, the resuscitation observed in *M. bovis* BCG under the MS, Cholesterol model was effective despite two years of sealed, stationary culture (*see* **section 2.2.8**). Another impactful finding was the complete drug resistance shown by *M. bovis* BCG resuscitating from the NRP state. "Drug Indifference" in reference to Mycobacteria was coined by Wayne and has been thought to be a hallmark of the protective NRP state. A return to active growth should mark a return to the original antibiotic susceptibility profile (Wayne & Sohaskey, 2001). If the MS. Cholesterol model is a more physiologically relevant model, this carried over drug indifference is deeply concerning as resistance was to the frontline antibiotics INH and RIF. If *in vitro* resistance happened clinically it would give the resuscitating infection a temporary shield to gain a foothold in the patient before any treatment

became effective. Indeed, this could be the reason behind the complicated nature of "secondary" or previously treated TB infection.

The NRP state of *M. tuberculosis* has always been associated with widespread antibiotic resistance (Wayne & Sohaskey, 2001). However, subsequent research identified the activity of drugs such as MOXI and PA-824 as active against hypoxic-based NRP models (de Miranda Silva et al., 2019). These drugs have been escalated into clinical trials for the treatment of LTBI (Burki, 2019; Conradie, 2017). Nevertheless, all drug testing has been conducted in single stress *in vitro* models or *in vivo* animal models such as mice, which cannot form a granuloma and cannot reproduce the NRP state. As both drugs are effective against active *M. tuberculosis*, these clinical trials make sense.

All activity against NRP *M. tuberculosis* by any antimicrobial bar one was lost in the MS, Cholesterol model. This resistance was found even in well characterised drugs such as bedaquiline, pretomanid, moxifloxacin and linezolid (de Miranda Silva et al., 2019). There was total resistance found even at high drug concentrations. This resistance was in contrast to the profile in the Hypoxic model, whereby resistance was common but most of the above antimicrobials were active.

This resistance, if consistent with the clinical phenotype, could completely change the way LTBI infection is viewed. If resistance is observed to the new highly active drug, bedaquiline, can LTBI be treated and therefore, should it be treated as a totally drug resistant infection of a similar severity to the ESKAPE pathogens? Coupled with weak diagnostic procedures, this creates a scenario where a large proportion of the world's population are infected with a highly drug resistant pathogen.

As previously mentioned, all antimicrobials bar one proved ineffective against MS, Cholesterol model NRP *M. bovis* BCG. With the backdrop of near total drug resistance, the activity of Dapsone becomes far more impactful. Dapsone is one of the oldest antibiotics still in common use and is thought to be well characterised (Baca et al., 2000; Eichelmann et al., 2013; Faget

& Pogge, 1945; Wozel & Blasum, 2014). Nevertheless, this thesis has highlighted its singular activity against physiologically relevant NRP *M. bovis* BCG with a novel mechanism of action. Dapsone was always considered a weak antimicrobial against *M. tuberculosis*, presumably due to the characterised weak inhibition of DHPS, and therefore, was never previously considered as an antibiotic candidate for LTBI. It is possibly unfair to be surprised at this old drug behaving in a completely novel manner as the main characteristic of Dapsone is disjointed applications (Wozel & Blasum, 2014). In addition to usage as an antibiotic primarily against *M. leprae*, Dapsone is a potent anti-malarial drug, a strong anti-inflammatory with a purported similarity to NSAIDS, an anti-venom against spider bites and is being investigated for anti-cancer properties. With all of these disconnected activities, it makes a strange sense that Dapsone could have two MOA against *M. tuberculosis*; one for active growth (DHPS inhibition) and one against NRP populations (inhibition of the cholesterol catabolism pathway by the inhibtion of FolP2) (Baca et al., 2000; Gengenbacher et al., 2008). Considering Dapsone as a treatment for LTBI, there is clearly strong antimicrobial activity, however, its anti inflammatory activity is already prescribed for the alleviation of skin based granuloma (Martín-Sáez et al., 2008; Van De Kerkhof, 1994). To sterilise a patient of an NRP population is a complex problem, as if the bacteria are within the granuloma, there is a complete lack of vascularistion. Therefore, Dapsone treatment could possibly eradicate this access issue but could come with the risk factor of disrupting the granuloma.

The inhibition of FolP2 by Dapsone has a two-fold impact: firstly, this is an established drug that has been through many clinical trials and has clear inhibitory activity against NRP M. bovis BCG through the inhibition of a novel target; secondly, the use of Dapsone inhibition to highlight the essentiality of FolP2 within the NRP state. FolP2 has long been considered an inactive DHPS ortholog of FolP1. Previous research showed that Dapsone could bind FolP2, but was investigating its activity as a DHPS and did not consider the possibility of another function (Gengenbacher et al., 2008).

The discovery that FolP2 is a hypoxic bypass for the anoxic cholesterol catabolism pathway instead of the folic acid biosynthesis pathway is impactful to tuberculosis research as a whole. Whilst previous literature had described interactions between Dapsone and FolP2, there was no information about what activity FolP2 could have. The only information available was the strong antimicrobial activity within the Multi-Stress, Cholesterol model, but a complete lack of activity within the Hypoxic model. With the main difference between the two models being cholesterol catabolism, that pathway was investigated for a potential fit (Chiang et al., 2008; Wilburn et al., 2018; Wipperman et al., 2014). This investigation leads us back to the initial point of this discussion that the NRP state as currently described is inherently contradictory. The current cholesterol catabolism pathway requires oxygen to function, therefore its presence within a hypoxic atmosphere is unlikely. Therefore, it is possible that those steps that have oxygen demands have hypoxic bypasses. This was the basis for the testing of FolP2 as a replacement for part of the HsaA/HsaB complex (Dresen et al., 2010). This hypothesis proved correct as with 3,4-dMP acting as the substrate 3-HSA, FolP2 reduced FMN. This suggests that FolP2 has an activity, crucial to the NRP state within the Multi-Stress, Cholesterol model. Hence, this activity becomes essential only when anoxic cholesterol catabolism is required (Chiang et al., 2008). This explains why Dapsone activity was seen against the Multi-Stress, Cholesterol model and not the Hypoxic model. However, if FolP2 is active in NRP and is essential, this hints at a hidden proteome with M. tuberculosis that has never previously been identified and, if found, could unlock LTBI treatment and possibly the treatment of chronic TB infection as a whole.

Testing *M. abscessus* in our NRP assays (using both the Hypoxic model and the Multi-Stress, Cholesterol model) provided an insight into the bacteria and its pathogenesis as a whole. *M. abscessus* is a newly emerging pathogen with high levels of drug resistance (Nessar et al., 2012; Shen et al., 2010). A details of *M. abscessus* infection that has confounded physicians and scientist is the presence of reoccurring or chronic infections, whereby a patient who has undergone antimicrobial therapy and been declared sterilised will spontaneously become

reinfected (Esther et al., 2010). This thesis hypothesised that this reinfection was not due to unlucky chance or re-exposure, but as evidence of a protective, asymptomatic latent infection caused by the *M. abscessus* entering the NRP state. Through a variety of testing in both models of NRP, it was established that *M. abscessus* can enter the NRP state and gains the protective, drug indifferent phenotype seen in *M. tuberculosis*. The NCTC strain of *M. abscessus* which was shown to be susceptible to the antibiotic panel chosen gained almost total resistance when in the NRP state. Additionally, Dapsone became active when under the Multi-Stress, Cholesterol model of NRP *M. abscessus*. This activity may indicate that *M. abscessus* also has an anoxic cholesterol catabolism pathway and in this model the hypoxic bypass, FolP2, has become essential (Chiang et al., 2008). The identification of the NRP in *M. abscessus* has a broad clinical impact as the patients most at risk of developing *M. abscess*us infection are those least capable of tolerating the associated intense antibiotic treatment. Commonly, the “chronic” reinfection of *M. abscessus* proves a death sentence. If an NRP-state specific antimicrobial (i.e Dapsone as discovered in this thesis) could be included into the initial treatment, this deadly reinfection pattern could be prevented.

The NRP model detailed in this thesis is the first attempt at combining three highlighted NRP stresses into one model, namely: hypoxia, nutrient deprivation and a limitation of carbon sources to cholesterol. In doing so, the Multi-Stress, Cholesterol model has unveiled a novel uncharacterised phenotype of *M. tuberculosis* with differences in morphology, proteome, antibiotic susceptibility profile and resuscitation. The primary aim of this thesis was to create an *in vitro* model that was more physiologically relevant and could explain some of the contradictions present in the current literature. The novel phenotype displayed by *M. bovis* BCG within this model coupled with a greater stress tolerance and heightened drug resistance is a good indicator that this aim may have been achieved.

The novel phenotype displayed by the Multi-Stress, Cholesterol model highlighted an under researched area of TB. Typically, LTBI is an afterthought in the story of TB. Novel antimicrobials are designed with active *M. tuberculosis* in mind and clinical trials are mainly

based on treating the symptomatic, active infection. If the latent infection is treated as well, it is an added extra, certainly not the focus of the therapy. This thesis identifies the dangers in this philosophy. With around ¼ of the world's population latently infected, the reach of LTBI is inarguable (Houben & Dodd, 2016). *M. abscessus* infection is a difficult to detect, nigh impossible to treat infection that on return to active, symptomatic disease drives drug resistance and complicates the infection by adding a temporary immunity. If TB is ever to be eradicated – which are current methods are not achieving – treating this reservoir has to be the priority and thus removing *M. tuberculosis'* long held sanctuary.

6.2 Future Work

PhDs are started with the view of answering a research question, certainly this one was started with such an aim. As it turns out, the research and discoveries detailed in this thesis have opened far more questions than it solved. Therefore, there is an abundance of work that could be proposed from the findings in this thesis.

Initially, the creation of a multi-stress model using previously defined stresses was theorised to create a crossover phenotype with majorly the same characteristics, however, the phenotype revealed in the Multi-Stress, Cholesterol model, however, appears to be quite distinct. Ideally, future research into elucidating this phenotype would be undertaken. There was an attempt during this thesis to conduct some transcriptomic analysis, however, this was exceptionally challenging due to the small culture volumes, the difficulties of extracting RNA from Mycobacteria and the highly transient nature of RNA. This research is still ongoing and could shed some light on the priorities of *M. bovis* BCG under the Multi-Stress, Cholesterol model. Additionally, proteomic work using mass spectrometry could highlight new drug targets and could reveal the hidden NRP proteome discussed previously. As FolP2 was only expressed under these specific conditions, despite being a highly conserved protein, it stand to reason that other highly conserved proteins that are currently regarded as having no function could also reveal their activity. This activity could be inhibited and could guide antimicrobial design for a library of novel compounds specifically created for the inhibition of NRP M. tuberculosis. Mass spectrometry analysis could be utilised to quantify and examine the expression of RPF factors before entry into the NRP state and detect if this number declines upon resuscitation. This analysis would allow the interrogation of the previously proposed hypothesis that cholesterol catabolism – whilst not being a NRP driving trigger – prepares the cell for entry into the NRP state and thus easing the transition. If cholesterol catabolism upregulated the expression of RPF factors, it would not only make the entry to the NRP state smoother but aid in the resuscitation process. As seen above, resuscitation in the MS, Cholesterol model was faster and conferred a great level of antimicrobial resistance whilst

simultaneously reaching a higher OD by the endpoint. This ease of resuscitation, especially when compared to the NRP state, is potentially caused by a higher pre-NRP state expression of RPF factors.

There was a distinct change in morphology seen between the two models of NRP. In the hypoxic model, the bacteria were thinner and smaller than in the active state but retained thier rod-shape. Whereas, in the MS, Cholesterol model, this rod-shaped physiology was lost and replaced by a cocci like shape. This clearly needs continued investigation by either fluorescence microscopy or scanning electron microscopy to clearly identify the differences in morphology brought about by the change in NRP model.

The identification of the inhibitory activity of Dapsone and the subsequent identification of its drug target (FolP2) followed by the elucidation of FolP2's activity is certainly a highlight of this thesis, however, much of the work to discover the activity of FolP2 is very preliminary. Indeed, the research was aimed at finding proof that FolP2 was active rather than providing a concrete biochemical analysis of this activity. Such analysis would provide better context for understanding this activity. The FMN redox assay should be repeated with the addition of NAPH (and possibly 3-HSA) to create another Michaelis-Menten curve with a more accurate Km to the actual proteomic activity. This would also help with bolstering the proposed activity mechanism. Additionally, while the data strongly suggests that Dapsone can inhibit this activity, elucidating a Ki value with the amended FMN assay detailed above would greatly aid in the knowledge of the interaction between FolP2 and Dapsone. It could also be of value to express and purify HsaA to potentially show HsaA and FolP2 working in complex and examine whether this protein complex will only function in a hypoxic environment.

A key limitation of this thesis is its reliance on *in vitro* models. Whilst many in vivo models of LTBI suffer from the lack of granuloma formation, the minipig model appears a good option to study NRP M. tuberculosis *in vivo*. To that end, it would be crucial to identify if FolP2 and hence Dapsone activity was present in a minipig model. Due to the specificity of FolP2, it is unlikely that it would be expressed in a mouse or even guinea pig model, as neither model contains

the nutrient deprivation caused by encasement within the granuloma. Therefore, if any Dapsone activity is found, it is likely to be inhibiting DHPS (FolP1) in the active MOA seen in M. leprae. However, minipigs have the ability to make and maintain a complex granuloma, similar to humans. Therefore, it would be interesting to see if Dapsone could treat LTBI in this model. In addition, it would be crucial to see what effect Dapsone treatment might have on the granuloma itself due to its anti-inflammatory properties.

Chapter 7:
Methods and Materials

Chapter 7 Methods and Materials

7.1 General Growth Media and Chemical Preparation

All chemicals, reagents and solvents are from Sigma-Aldritch, Merck, Fisher Scientific or Melford unless otherwise stated.

7.1.1 Middlebrook 7H9 Broth Medium

4.6 g of Middlebrook 7H9 broth base, 4 mL of 50% (v/v) glycerol and 2.5 mL of 20% (w/v) Tween 80 were combined in 900 mL of dH2O. This was then autoclaved at 121 ℃ for 15 mins and cooled to below 50 ℃ in a water bath. 100 mL of sterile ADC enrichment, warmed to the same temperature, was then added. The media was stored at 4 ºC.

7.1.2 ADC Enrichment

5 g bovine serum albumin fraction V, 2 g dextrose and 3 g catalase were combined in 100 mL of dH2O. This was then mixed until all components had dissolved and filter sterilised with a 0.22 µm sterile filter. The ADC Enrichment was stored at 4 ºC.

7.1.3 Minimal Cholesterol Broth Medium

4.6 g of Middlebrook 7H9 media was dissolved in 1 L of dH2O. A magnetic stirrer bar was added and the mixture was autoclaved at 121 ℃ for 15 mins. The broth base and the dissolved cholesterol additive were then heated to 65 ℃ in a water bath. The broth base was placed on a hot magnetic stirrer and the additive to the media was added while the media was hot and stirring. The media was then filter sterilised with a 0.22 µm filter into a clean sterile bottle and stored for one month at 4 ℃.

7.1.4 Dissolved Cholesterol Additive

1 mL of Tyloxapol:Ethanol (50:50, v/v) mixture was made. This was mixed until homologous and heated to 65 ℃ in a water bath. 100 mg of cholesterol was then dissolved in the mixture.

7.1.5 Middlebrook 7H11 Agar

20 g of Middlebrook 7H11 agar base and 10 mL of 50% (w/v) glycerol were combined in 900 mL of dH20. This was then autoclaved at 121 ℃ for 15 mins and cooled to below 50 ℃ in a water bath. 100 mL of sterile OADC enrichment that had been warmed to the same temperature was then added. The Agar was stored at 4 ℃.

7.1.6 OADC Enrichment

5 mg oleic acid, 5 g bovine serum albumin fraction V, 2 g dextrose and 3 g catalase was combined in 100 mL of dH2O. This was mixed until all components had dissolved and filter sterilised with a 0.22 µm sterile filter. The OADC Enrichment was stored at 4 ^{o}C .

7.1.7 Nutrient Broth (+/- Kanamycin Supplement)

25 g of Nutrient Broth powder was dissolved in 1L of dH2O and sterilised by autoclaving at 121 ^{o}C for 15 mins. When Kanamycin (Kan) supplement was required for transformation, Kan dissolved in dH2O a final concentration of 50 µg/mL.

7.1.8 Nutrient Agar (+/- Kanamycin Supplement)

28 g of Nutrient Agar powder was dissolved in 1 L of dH2O and sterilised by autoclaving at 121 ^{o}C for 15 mins. When Kanamycin (Kan) supplement was required for transformation, add Kan dissolved in dH2O a final concentration of 50 µg/mL.

7.1.9 Terrific Broth

47.6 g of Terrific Broth powder was dissolved in 1 L of dH2O and4 mL of 100% glycerol (v/v) was added. This was sterilised by autoclaving at 121 ^{o}C for 15 mins.

7.1.10 Transformation Buffers

7.1.10.1 Transformation Buffer 1 (TFB1)

100 mM Rubidium Chloride ($RbCl_2$), 50 mM Manganese Chloride ($MnCl_2$), 30 mM Potassium Acetate (KAc), 10 mM Calcium Chloride ($CaCl_2$) and 15 % glycerol (v/v) was combined and made up to 1 L at pH 5.8.

7.1.10.2 Transformation Buffer 2

10 mM MOPS, 10 mM $RbCl_2$, 75 mM $CaCl_2$ and 15 % glycerol (v/v) was combined and made up to 1 L at pH 6.8.

7.1.11 Phosphate-based Protein Purification Buffer (2x)

100 mM Potassium Phosphate (KH_2PO_4) and 600 mM NaCl was combined and made up to 1 L at pH 7.9.

7.1.12 Phosphate-based Lysis Buffer

50 mM KH_2PO_4, 300 mM NaCl and 20 mM Imidazole was combined and made up to 1 L at pH 7.9.

7.1.13 Phosphate-based Wash Buffer

50 mM KH_2PO_4, 300 mM NaCl and 50 mM Imidazole was combined and made up to 1 L at pH 7.9

7.1.14 Dialysis Buffer

50 mM Tris HCl (pH 7.9) and 200 mM NaCl was combined and made up to 2 L

7.1.15 Tris-based Protein Purification Buffer (2x)

100 mM Tris HCl (pH 8) and 600 mM NaCl was combined.

7.1.16 Tris-based Lysis Buffer

50 mM Tris HCl (pH 8), 300 mM NaCl and 20 mM Imidazole was combined and made up to 1 L at pH 7.9.

7.1.17 Tris-based Wash Buffer

50 mM Tris HCl (pH 8), 300 mM NaCl and 50 mM Imidazole was combined and made up to 1 L at pH 7.9

7.1.18 SDS Loading Dye

2 % SDS, 125 mM Tris pH 6.8, 715 mM β-mercaptoethanol, 20 % glycerol with dH_2O was combined and made up to 1 mL

7.1.19 SDS-PAGE Destain Solution

dH2O, Methanol and Acetic acid was combined in a 50:40:10 ratio

7.1.20 SDS-PAGE Running Buffer (10x)

30.3 g of Tris, 144 g of Glycine and 10 g of SDS were dissolved in dH_2O

7.2 Growth Conditions of Bacterial spp.

7.2.1 Growth of Mycobacterium bovis BCG in ADC Enriched 7H9 Broth

10 mL aliquots of Middlebrook 7H9 media with ADC supplement (*see* **section 2.1.4**) were dispensed into vented culture flasks and inoculate with Mycobacterium bovis BCG from a frozen glycerol stock kept at -80 ^oC. This was incubated for approximately 2 weeks at 37 ^oC with 5% CO_2. Growth was monitored until culture reached a mid-logarithmic phase of growth (OD600nm = 0.6).

7.2.2 Growth of Mycobacterium bovis BCG in Minimal Cholesterol Broth

10 mL aliquots of minimal cholesterol media (*see* **section 2.1.4**) were dispensed into vented culture flasks. The media was inoculated with M. bovis BCG from a frozen glycerol stock kept at -80 ^oC. Then the cultures were incubated for approximately 2 weeks in at 37 ^oC with 5% CO_2. Growth was monitored until culture reached a mid-logarithmic phase of growth (OD600nm = 0.6).

7.2.3 Growth of *Escherichia coli* Top 10

E. coli Top10 cells were grown for the propagation of plasmid DNA. They were grown in nutrient broth or nutrient agar overnight at 37 oC with an approximate incubation time of 16 h.

7.2.4 Growth of Escherichia coli BL21

E. coli BL21 (DE3) cells were used for the overproduction of recombinant protein and were grown in Terrific Broth at 37 °C overnight with an approximate incubation time of 16 h.

7.2.5 Growth of *Mycobacterium abscessus*

Mycbacterium abscessus was grown in ADC enriched 7H9 media (see section) in 10mL aliquots. The media was inoculated from a frozen glycerol stock and was grown for 5 days (approximately 100 h) in an orbital incubator at 37 °C

7.3 Non-Replicating Persistence of Mycobacteria spp.

This is a summary of the methods used to initiate NRP in varying Mycobacteria species. This is not how they are used in assays but instead a detailing of how to incite the entry into NRP to facilitate experiments laid out further down.

7.3.1 Hypoxic Model

7.3.1.1 Initiation into the NRP state

M. bovis BCG culture was aerobically grown to mid log phase and then diluted to an OD600nm of 0.3 in sterilised glass tubes to a total volume of 3 mL using 7H9-ADC media (*see* **section** 7.2.1). 4.5 µL of methylene blue solution (oxygen indicator) was added to each culture tube to reach a final concentration of 1.5 µg/mL. The lids were lefy loose but remained on the culture tube to facilitate controlled gas exchange. These culture tubes were then placed into the anaerobic cabinet for 48-72 h to allow a slow degassing of the cultures to take place. This was noticeable from the decolourisation of the methylene blue.

7.3.1.2 Glass Tube Assay

After the *M. bovis* BCG culture had entered NRP stage I which was visually identified by the decolourisation of methylene blue (*see* **section 7.3.1.1**), the tubes were dosed with chosen antimicrobials. The dosing of cultures tubes cannot happen any earlier than 48 h as the *M. bovis* BCG had not yet entered NRP stage I and gained the antibiotic indifference. The frontline

drug, INH and anaerobic antibiotic MET can be used in this model as negative and positive controls respectively. The screw cap lids were tightened and sealed around the lid and tube with parafilm (parafilm acts as a temporary hypoxic seal). The cultures were then removed from the anaerobic cabinet. Paraffin wax was melted by heating to >70 ^{o}C. The lids were sealed to the tubes with the molten paraffin wax. The sealed culture tubes were incubated in an orbital incubator at 37 ^{o}C with shaking at 100-120 RPM. Cultures were measured by absorbance readings (OD600nm) using an optical density reader every 24 h for 42 days (1000 h). The standard testing is 1000 h, however for some assays this was extended to a period of approximately 20,000 h. To do this, paraffin wax seals were “topped up” every 5000 h to maintain a hypoxic atmosphere. Additionally, absorbance readings for these extended assays became once a week, so approximately every 100 h. If the compound is active, there will be a noticeable decline in OD in a dose dependant fashion. If the compound is inactive, there will be no significant difference in OD between a drug treated culture and a non-drug treated control. Additional validation can be obtained by conducting CFU/mL counts (*see* **section 7.4.1**).

7.3.1.3 Anaerobic Microtitre Plate Assay

Once methylene blue decolourised (*see* **section 7.3.1.1**) after 48-72 h in the anaerobic cabinet, the cultures were normalised to OD600nm = 0.5, using 7H9-ADC media. After this point, the cultures should be in NRP stage I and ready to use. Each well of a 96-well microtitre plate with 1 µL was dosed of either a single shot high throughput screen, a dilution series of a few select compounds, or a checkerboard assay. Inside the anaerobic cabinet, the 96-well plate containing compounds was inoculated with the NRP *mycobacterial* culture. As all compounds are dissolved in DMSO, this dosing is done in a ratio of 1 µL:99 µL compound:culture to be below the toxic level of DMSO. In addition, a no drug control is added to each experiment where 1 µL of DMSO without anything dissolved in it. This is to check that the DMSO is not exerting an antimicrobial effect itself. The cultures were left for 30 mins to ensure that each well contains no residual oxygen. Then, the plate was sealed with an oxygen

impermeable plate seal, ClearVue plate seal (*see* **section 3.2.1**). The plates were incubated in the anaerobic cabinet at 37 ºC for up to 42 days (1000 h). Cultures were measured by absorbance readings (OD600nm) using an optical density reader every 24 h for 42 days (1000 h). The hypoxic seal maintained the hypoxic atmosphere during absorbance readings; additionally, the microtitre plates were briefly stirred before reading to ensure dispersal of microorganisms.

For an MBC count, the *M. bovis* BCG cultures were serially diluted in 7H9-ADC media and spread out onto solid media to conduct an endpoint CFU/mL count (*see* **section 7.4.1**) to check the nature of activity of the compounds. The OADC enriched 7H11 agar plates were incubated in a static incubator at 37 ºC for approximately three weeks or until visible colonies can be observed. The colonies were counted and adjusted to calculate CFU/mL curves.

7.3.2 Multi-Stress, Cholesterol Model

7.3.2.1 Initiation into the NRP state

M. bovis BCG culture was aerobically grown to mid log phase and then diluted to an OD600nm of 0.3 in sterilised glass tubes to a total volume of 3 mL using minimal cholesterol media (*see* **section** 7.2.1). 4.5 µL of methylene blue solution (oxygen indicator) was added to each culture tube to reach a final concentration of 1.5 µg/mL. The lids were lefy loose but remained on the culture tube to facilitate controlled gas exchange. These culture tubes were then placed into the anaerobic cabinet for 48-72 h to allow a slow degassing of the cultures to take place. This was noticeable from the decolourisation of the methylene blue.

7.3.2.2 Glass Tube Assay

After the *M. bovis* BCG culture had entered NRP stage I which was visually identified by the decolourisation of methylene blue (*see* **section 7.3.1.1**), the tubes were dosed with chosen antimicrobials. The dosing of cultures tubes cannot happen any earlier than 48 h as the *M. bovis* BCG had not yet entered NRP stage I and gained the antibiotic indifference. The frontline drug, INH and anaerobic antibiotic MET can be used in this model as negative and positive

controls respectively. The screw cap lids were tightened and sealed around the lid and tube with parafilm (parafilm acts as a temporary hypoxic seal). The cultures were then removed from the anaerobic cabinet. Paraffin wax was melted by heating to >70 ^{o}C. The lids were sealed to the tubes with the molten paraffin wax. The sealed culture tubes were incubated in an orbital incubator at 37 ^{o}C with shaking at 100-120 RPM. Cultures were measured by absorbance readings (OD600nm) using an optical density reader every 24 h for 42 days (1000 h). The standard testing is 1000 h, however for some assays this was extended to a period of approximately 20,000 h. To do this, paraffin wax seals were “topped up” every 5000 h to maintain a hypoxic atmosphere. Additionally, absorbance readings for these extended assays became once a week, so approximately every 100 h. If the compound is active, there will be a noticeable decline in OD in a dose dependant fashion. If the compound is inactive, there will be no significant difference in OD between a drug treated culture and a non-drug treated control. Additional validation can be obtained by conducting CFU/mL counts (*see* **section 7.4.1**).

7.3.2.3 Anaerobic Microtitre Plate Assay

Once methylene blue decolourised (*see* **section 7.3.1.1**) after 48-72 h in the anaerobic cabinet, the cultures were normalised to OD600nm = 0.5, using 7H9-ADC media. After this point, the cultures should be in NRP stage I and ready to use. Each well of a 96-well microtitre plate with 1 µL was dosed of either a single shot high throughput screen, a dilution series of a few select compounds, or a checkerboard assay. Inside the anaerobic cabinet, the 96-well plate containing compounds was inoculated with the NRP *mycobacterial* culture. As all compounds are dissolved in DMSO, this dosing is done in a ratio of 1 µL:99 µL compound:culture to be below the toxic level of DMSO. In addition, a no drug control is added to each experiment where 1 µL of DMSO without anything dissolved in it. This is to check that the DMSO is not exerting an antimicrobial effect itself. The cultures were left for 30 mins to ensure that each well contains no residual oxygen. Then, the plate was sealed with an oxygen

impermeable plate seal, ClearVue plate seal (*see* **section 3.2.1**). The plates were incubated in the anaerobic cabinet at 37 ºC for up to 42 days (1000 h). Cultures were measured by absorbance readings (OD600nm) using an optical density reader every 24 h for 42 days (1000 h). The hypoxic seal maintained the hypoxic atmosphere during absorbance readings; additionally, the microtitre plates were briefly stirred before reading to ensure dispersal of microorganisms.

For an MBC count, the *M. bovis* BCG cultures were serially diluted in 7H9-ADC media and spread out onto solid media to conduct an endpoint CFU/mL count (*see* **section 7.4.1**) to check the nature of activity of the compounds. The OADC enriched 7H11 agar plates were incubated in a static incubator at 37 ºC for approximately three weeks or until visible colonies can be observed. The colonies were counted and adjusted to calculate CFU/mL curves.

7.4 Resuscitation of Non-Replicating Persistent Mycobacteria spp.

7.4.1 Resuscitation of Mycobacterium bovis BCG

7.4.1.1 Resuscitation of M. bovis BCG

The culture tube or 96-well microtitre plate (*see* **section 7.2.1 or 7.2.2**) were removed from the anaerobic cabinet and the hypoxic seal were broken open under aseptic conditions by initial scoring with a scalpel. The opened NRP *M. bovis* BCG cultures were taken transferred into either liquid medium or solid agar. For resuscitation in liquid media, the 500 µL of NRP *m. bovis* BCG from either the Hypoxic model or the MS, Cholesterol cultures were used to inoculate 2.5 mL of either 7H9-ADC media in either a sterile glass culture tube or a vented tissue culture flask. The inoculated glass tube cultures were incubated at 37 ºC in an orbital incubator shaking at 180 rpm. The inoculated tissue cultures flask were incubated in a static incubator at 37 ºC with 5% CO_2. For a resuscitation growth curve, the glass culture tubes were read every 24 h in a spectrophotometer at OD_{600nm}.

For resuscitation on solid medium, 50-100 µL of NRP *M. bovis* BCG was plated out onto 7H11-OADC (*see* **section 7.1.5)**. The inoculated agar plates were incubated in a static incubator at 37 ºC with 5% CO_2. To conduct an endpoint CFU/mL count, the cultures were serially dilute in sterile PBS, typically to 10^{-4}. These dilutions were spread out using minimum aliquot of 50 µL of each dilution. The inoculated agar plates were incubated in a static incubator at 37 ºC with 5% CO_2. After approximately 3 weeks of incubation, growth should be present. Count the colonies at this point. A significant reduction in CFU/mL will indicate activity of test compound

7.4.2 Resuscitation of Mycobacterium abscessus

7.4.2.1 Resuscitation of M. abscessus

The culture tube or 96-well microtitre plate (*see* **section 7.2.1 or 7.2.2**) were removed from the anaerobic cabinet and the hypoxic seal were broken open under aseptic conditions by initial scoring with a scalpel. The opened NRP *M. abscessus* cultures were taken transferred into either liquid medium or solid agar. For resuscitation in liquid media, the 500 µL of *M. abscessus* cultures were used to inoculate 2.5 mL of either 7H9-ADC media or Nutrient Broth in either a sterile glass culture tube or a Falcon tube. The inoculated cultures were incubated at 37 ºC in an orbital incubator shaking at 180 rpm. For a resuscitation growth curve, culture were read every 24 h in a spectrophotometer at OD_{600nm}.

For resuscitation on solid medium, 50-100 µL of NRP *M. abscessus* was plated out onto 7H11-OADC (*see* **section 7.1.5)**. The inoculated agar plates were incubated in a static incubator at 37 ºC with 5% CO_2. To conduct an endpoint CFU/mL count, the cultures were serially dilute in sterile PBS, typically to 10^{-4}. These dilutions were spread out using minimum aliquot of 50 µL of each dilution. The inoculated agar plates were incubated in a static incubator at 37 ºC with 5% CO_2. After approximately 3 weeks of incubation, growth should be present. Count the colonies at this point. A significant reduction in CFU/mL will indicate activity of test compound.

7.5 Preparation of Competent Cells

7.5.1 Escherichia coli chemically competent cells

E. coli cells were grown at 37 °C to OD600 = 0.4-0.5, before incubation on ice for 10 min. Cells were pelleted by centrifugation at 3,300 × g for 15 min and the supernatant was discarded. From this point, pelleted cells were kept on ice and were then re-suspended in 0.4 volume of ice cold TFB1 (*see* **section 7.1.10.1**). The suspension was then incubated on ice for 15 min, before centrifugation at 3,300 × g for 15 min at 4 °C. The supernatant was discarded, and the cells were re-suspended in 0.02 volume of ice cold TFB2 (*see* **section 7.1.10.2**). The suspension was then incubated on ice for 30-60 min, before being aliquoted into microcentrifuge tubes. Each aliquot was then flash frozen in liquid nitrogen (N2) and stored at -80 °C.

7.5.2 Mycobacterium bovis BCG electrocompetent cells

M. smegmatis cells were grown at 37 °C to OD600 = 0.4-0.5, then pelleted by centrifugation at 3,300 × g for 15 min at 4 °C. The supernatant was discarded, and the pellet was re-suspended in 0.5 volume of ice cold 10 % glycerol (v/v). The suspension was then incubated on ice for 132 10 min. Cells were pelleted by centrifugation at 3,300 × g for 15 min at 4 °C, before being resuspended in 0.3 volume of ice cold 10 % glycerol (v/v). The suspension was incubated on ice for 10 min. This trend of centrifugation, resuspension and incubation continued, reducing the volume of 10 % glycerol in each round (0.15 volume, 0.1 volume and 0.04 volume successively). Once the cells had been incubated in 0.04 volume 10 % glycerol (v/v), cells were aliquoted into microcentrifuge tubes. Each aliquot was then flash frozen in liquid N_2 and stored at -80 °C.

7.6 Transformation

7.6.1 Heat Shock Transformation of E. coli

100 µL of chemically competent E. coli (*see* **section 7.5.1**) were added to 1µL of plasmid DNA and placed in ice for 15 mins. The heat shock treatment was commenced by incubating the

cell suspension at 42℃ for 1 min. The cell suspension was then put back on ice for a further 2 mins. After this, cells were rescued by the addition of 250 µL of nutrient broth and then incubated at 37℃ for 1 hr. The mixture was then plated out onto nutrient agar plates containing Kanamycin (*see* **section 7.1.8**) and then incubated at 37 ℃ overnight.

7.6.2 Transformation by electroporation of Mycobacterium bovis BCG

Electrocompetent *M. bovis* BCG cells (*see* **section 7.5.2**) and plasmid DNA were incubated on ice until thawed. After this, 2 µL of plasmid DNA was inserted into a 1 mm electroporation cuvette (Cell Projects) and incubated on ice for 20 min. Then 200 µL of M. smegmatis cells were added to the cuvette and incubated on ice for 30 min. The cuvette was then inserted into an electroporator 2510 (Eppendorf) and pulsed at 1,800 V before incubation on ice for 15 min. Cells were rescued by the addition of 250 µL 7H9-ADC media (*see* **section 7.1.1)** and incubation at 37 °C for 4 h. After 133 incubation, cells were plated onto OADC enriched 7H11 agar plates (supplemented with Kanamycin) and incubated at 37 °C for 2-3 days (*see* **section 7.1.5)**.

7.7 Polymerase Chain Reaction (PCR)

PCR was performed in 20 µL reactions, consisting of 0.5 µM forward primer, 0.5 µM reverse primer, 250 ng genomic DNA (M. tuberculosis), 200 µM dNTP mix, 1.5 mM MgCl2, 3 % dimethyl sulfoxide (DMSO), 1 µL (50 µL reaction) TaqDNA polymerase (New England Biolabs), 1× Phusion 5× GC buffer (New England Biolabs) and made up to 20 µL with nuclease free H2O. Each reaction was then subjected to cycling conditions for gene amplification, inside a PCR amplifier.

7.7.1 Primers used for PCR

The *fol*p1 (Rv3608c) and *fol*p2 (Rv1207) genes from *M. tuberculosis* H37Rv were amplified by polymerase chain reaction. There is 100% identity between *M. bovis* BCG and *M. tuberculosis*. The primers used can be found in Table 7.1 with restriction site underlined (Eurofins Genomics).

Table 7.1: **PCR Primers for the amplification of *fol*P1 and *fol*P2**

Primer	Code
*fol*P1 Forward Primer	AAAAAAGGATCCGTGAGTCCGGCGCCCGTG
*fol*P1 Reverse Primer	AAAAAAAAGCTTGCCATCGCGTTCTATCCT
*fol*P2 Forward Primer	AAAAAAGGATCCGTGCGTTCAACACCGCCG
*fol*P2 Reverse Primer	AAAAAAAAGCTTTGCGAGTCCTCTCACCGT

Amplicons were purified and ligated into pVV16 using BamHI and HinDIII restriction sites and the sequence was confirmed by sequencing (Eurofins genomics). The pVV16-folp1 and pVV16-folP2 constructs, as well as pVV16, were inserted into electrocompetent Mycobacterium bovis BCG by electroporation (2.5 kV, 25 µF and 1000 Ω).

7.8 DNA Electrophoresis

DNA samples were added to Loading Dye (5 % glycerol (v/v), 0.04 % Bromophenol Blue), and loaded onto 1 % TAE (40 mM Tris-acetate, 1 mM EDTA, pH 8.0) agarose gel, alongside 1 kb DNA ladder (New England Biolabs). Gel was run in 1 × TAE buffer at 140 V, 400 mA for 50 min. The gel was then visualised using a Gel Doc (Bio-Rad).

7.8.1 DNA Band Extraction from DNA Electrophoresis

DNA was extracted from agarose gel with the use of QIAquick gel extraction kit (Qiagen). The DNA band was excised from the agarose gel using a scalpel, but by minimising the amount of excess agarose in the slice. The agarose slice was then weighed and 3 volumes of Buffer QG was added to every 1 volume of agarose (3 µL:1 mg). The agarose was then incubated at 50 °C for 10 min, until the agarose had dissolved. The pH of the solution was then checked, by assuring the mixture was yellow in colour (indicator shows pH ≤ 7.5). One gel volume of isopropanol was added to the solution and mixed, before being transferred to a QIAquick spin column. The column was centrifuged at 18,000 × g for 1 min, and the flow through was discarded. This was repeated until all the sample was passed through the spin column. The

spin column was then washed with 500 µL Buffer QG and centrifuged at 18,000 × g for 1 min. The flow through was discarded before 750 µL Buffer PE (Qiagen) was added to the spin column and was centrifuged at 18,000 × g for 1 min. The flow through was discarded and the spin column was again centrifuged at 18,000 × g for 1 min, to extract any residual flow through, which was then also discarded. The spin column was then inserted into a microcentrifuge tube, with 50 µL H_2O being added to the column for 2 min. The tube was then centrifuged at 18,000 × g for 1 min and the DNA in the flow through was retained and stored at -20 °C.

7.8.2 Extracted DNA Clean Up

DNA that contained enzymes and buffers was cleaned by making use of QIAquick gel extraction kit (Qiagen). The DNA sample was mixed with 500 µL Buffer QG (Qiagen) and transferred to a QIAquick spin column. The column was then centrifuged at 18,000 × g for 1 min and the flow through was discarded. The spin column was then washed with 750 µL Buffer PE (Qiagen) by centrifugation at 18,000 × g for 1 min. The flow through was discarded and the spin column was again centrifuged at 18,000 × g for 1 min, to extract any residual flow through, which was then also discarded. The spin column was then inserted into a microcentrifuge tube, with 50 µL H2O being added to the column for 2 min. The tube was then centrifuged at 18,000 × g for 1 min and the cleaned DNA in the flow through was retained and stored at -20 °C.

7.9 Plasmid DNA Extraction

Plasmid DNA was extracted from 5 mL bacterial culture with use of QIAprep spin miniprep kit (Qiagen). Cells were pelleted by centrifugation at 3,300 × g for 15 min and supernatant discarded. Pellets were re-suspended in 250 µL Buffer P1 containing RNAse A (Qiagen) and transferred into microcentrifuge tubes. After this, 250 µL Buffer P2 (Qiagen) was added and mixed by tube inversion, before the addition of 350 µL Buffer N3 (Qiagen) which was also mixed by tube inversion. Mixtures were then centrifuged at 18,000 × g for 10 min, and the supernatant was extracted and transferred into a miniprep spin column (Qiagen). The spin column was centrifuged at 18,000 × g for 1 min and the flow through was discarded. The spin

column was then washed with 500 µL Buffer PB (Qiagen), by centrifugation at 18,000 × g for 1 min and the flow through was discarded. A final wash step of 750 µL Buffer PE (Qiagen) was then added to the spin column and was centrifuged at 18,000 × g for 1 min, with the flow through being discarded. The spin column was again centrifuged at 18,000 × g for 1 min, to extract any residual flow through, which was then discarded. The spin column was then inserted into a microcentrifuge tube, with 50 µL H2O being added to the column for 2 min. The tube was then centrifuged at 18,000 × g for 1 min and the plasmid DNA in the flow through was retained and stored at -20 °C.

7.10 Recombinant Protein Purification

Transformed E. coli BL21 (*see* **7.6.1)** were induced for protein production, once OD600 = 0.5 was reached, by the addition of 1 mL 1 M IPTG (0.1 M final concentration). Cultures were then incubated at 16 °C overnight with shaking. Cells were then harvested from via centrifugation at 6,000 × g for 15 min at 4 °C. The supernatant was discarded and the pellet was resuspended in Phosphate Buffered Saline (PBS). The resuspended cells were then centrifuged at 3,300 × g for 18 min at 4 °C. The supernatant was discarded and the cell pellets were stored at -20 °C. An imidazole gradient was produced from Purification Buffer (2 ×) (Section 5.1.10.) and 2 M Imidazole pH 7.9. Protein containing pellet was defrosted then re-suspended in 20-30 mL 'lysis buffer' (*see* **section 7.1.16**), with a Proteinase Inhibitor Cocktail tablet (Merck) added. The mixture was subsequently sonicated using a sonicator (30 sec on, 30 sec off, 10 cycles). The solution was then centrifuged at 21,000 × g for 40 min at 4 °C, and the supernatant was retained (clarified lysate). Protein was purified using a HisTrap 1 mL column (GE healthcare) charged with 0.1 M NiSO4 (binds to 6x Histidine tag). The clarified lysate/flow-through and imidazole fractions were collected. All fractions were collected. After identification of the protein containing fraction (generally for FolP2, the protein containing fraction is 250 µM). This imidazole fraction is dialysed using dialysis tubing in dialysis buffer (*see* **section 7.1.14**) to purify the protein.

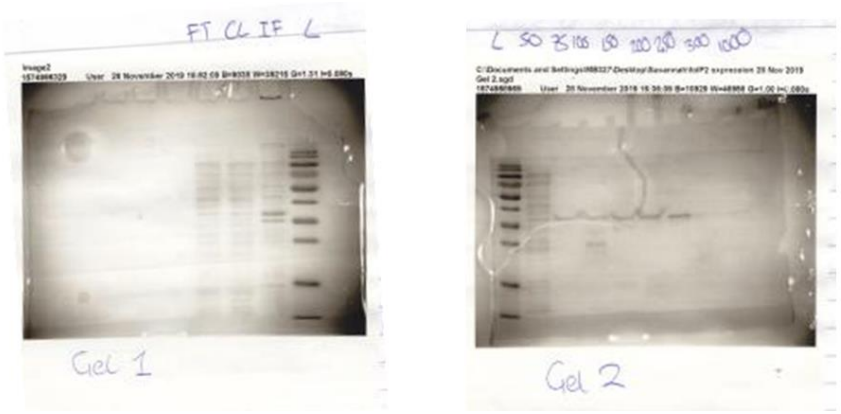

Figure 7.1: SDS-PAGE analysis of imidazole fractions. Gel 1 shows the flow through (FT), clarified lysate (CL) and insoluable fraction (IF). Gel 2 shows the imidazole fractions of the purification. FolP2 appear to elute at 250 μM

7.11 SDS-PAGE

7.11.1 SDS-PAGE Gels

SDS-PAGE (SDS-polyacrylamide gel electrophoresis) was used to separate out protein and have two parts. The running gel (15% SDS) was prepared by adding 2.8 mL ddH2O, 3 mL of 40 % acrylamide/bis-acrylamide, 2 mL of 1.5 M Tris pH 8.8, 80 µL of 10 % SDS, 8 µL of TEMED and 80 µL of 10 % APS. The stacking gel (4% SDS) was prepared by adding 3.1 mL ddH2O, 0.5 mL of 40 % acrylamide/bis-acrylamide, 1.25 mL of 0.5 M Tris pH 6.8, 50 µL of 10 % SDS, 5 µL of TEMED and 50 µL of 10 % APS.

7.11.2 Running SDS-PAGE Gels

Protein fractions were mixed with SDS loading dye (*see* **section 7.1.18**) and incubated at 100 °C for 10 min. Boiled samples, alongside PageRuler (Thermo Scientific) protein marker, were then ran on SDS-PAGE gels (*see* **section 7.11.1**) at 200 V, 50 mA for 30 min in SDS-PAGE Running Buffer (1X) (*see* **section 7.1.20**). Gels were then incubated in Coomassie Blue stain at room temperature with shaking for 24 h and then destained in SDS-PAGE destain solution for 2 h (*see* **section 7.1.19**).

7.12 Intrinisic Tryptophan Fluorescence (ITF)

ITF is used to measure the fluorescence of proteins and measure binding. When ligands bind to the active site, a quenching effect is produced. This ITF assay used a black bottomed 96 well microtitre plate in a fluorometer to measure the fluorescence of the protein. The emission wavelength was 280 nm and the excitation wavelength was 315 nm. The assay was conducted in one of two ways. Firstly, the purified protein (FolP2) was mixed with a serial dilution of riboflavin-5-phosphate (FMN) and a fixed concentration of 3,4-dimethylphenol. Alternatively, the ITF assay was conducted with purified protein (FolP2) and a dilution series of 3,4-dimethylphenol and a fixed concentration of FMN. These mixtures were incubated together for 10 mins and then the fluorescence readings were taken.

7.13 Redox Reaction of Riboflavin-5-Phosphate (FMN) with 3,4-dimethylphenol and FolP2

FMN is a common cofactor in many biological systems. The difference in absorbance between the oxidised form (FMN) and the reduced form (FMNH2) has been widely described. A decline in absorbance indicates a change in absorbance. All experiments were absorbance readings measured at 450 nm. This assay could not be conducted on a fluorometer as the fluorescence of FMN oversaturated the fluorometer. This assay was conducted using black, clear bottomed microtitre plates and were measured as a time course at OD450nm. These assays used a fixed concentration of FMN (500 µM) and a serial dilution of 3,4-dimethylphenol and a fixed concentration of protein (FolP2). These experiments were done in tandem with a control set of experiments where all parameters detailed above are maintained but the protein (FolP2) was replaced with buffer. Therefore, if any decline was seen it was due to protein action. These absorbance data was used to plot a Michaelis-Menten graph to detect protein activity. To additionally test the protein activity, the above redox activity was repeated with the addition of a serial dilution of dapsone (DAP). In this assay, every component but DAP was at a fixed concentration. 3,4-dimethylphenol was fixed at 300 µM and FMN was fixed at 500 µM. As above, this was read as a time course at OD450nm.

7.14 Mass Spectrometry Analysis of acr-1/*hspX*

The coomassie-stained bands present in the gel were excised and tryptic digestion was performed according to Verrastro *et al*., 2016 (Verrastro et al., 2016). The gel pieces were washed with 500 µL of 100 mM NH4HCO3 and then with 100 mM NH4HCO3/50% acetonitrile. 10 µL of 45 mM DTT in 150 µL NH4HCO3 were added to the gel pieces and left incubating at 60 °C for 30 mins for reduction. Cysteine alkylation was performed by adding 10 µL of 100 mM iodoacetamide and left to react at room temperature for 30 min in the dark. The gel pieces were then washed in 100 mM NH4HCO3/50% acetonitrile and incubated in 50 µL of 100% acetonitrile for 10 min. The gel pieces were then dried completely using a vacuum centrifuge

and resuspended in 25 µL of 0.1 µg/µL trypsin prepared in 25 mM ammonium bicarbonate. 25 µL of 25 mM ammonium bicarbonate was added to the trypsin digests and the digestions were incubated overnight at 37 °C. The gel pieces were pelleted by centrifugation and the supernatant was collected into a fresh tube. Further peptide extraction from the gel pieces was performed by adding 20 µL 5% formic acid and incubating at 37 °C for 20 mins, followed by addition of 40 µL acetonitrile and incubation for 20 mins at 37 °C. The gel pieces were pelleted by centrifugation, and the supernatant was removed and combined with the first supernatant. The peptide extracts were dried in a vacuum centrifuge for storage and resuspended in 30 µL H2O/acetonitrile (98:2, %) with 0.1% formic acid prior to MS analysis.

7.14.1 Liquid Chromatography-Tandem Mass Spectrometry (LC-MS/MS) Analysis

Peptides were separated and analysed using an Ultimate 3000 system (Thermo Scientific, Hemel Hempstead, UK) coupled to a 5600 TripleTOF (ABSciex, Warrington, UK). The analysis was performed as previously described by Verrastro (Verrastro et al., 2016). Briefly, the peptide solution was loaded onto a C18 trap column (C18 PepMapTM, 5 µm, 0.5 x 5mm, Thermo Scientific, Hemel Hempstead, UK) before separation on a nano-HPLC column (C18 PepMapTM, 5 µm, 0.075 x 150mm, Thermo Scientific, Hemel Hempstead, UK) at 300 µL/min using a gradient elution running from 2% to 45% aqueous acetonitrile, 0.1% formic acid over

45 minutes. Ionization of the peptides was achieved with spray voltage set at 2.4 kV, a source temperature of 150 ºC, declustering potential of 100V and a curtain gas setting of 25. Survey scans were collected in positive mode from 350 to 2000 Da using high-sensitivity TOF-MS mode. Information-dependent acquisition (IDA) was used to collect MS/MS data using the following criteria: the 10 most intense with +2 to +5 charge states and a minimum intensity of 200 cps were chosen for analysis, using dynamic exclusion for 12 s and standard rolling collision energy settings.

7.15 Proof of the NRP state by Kanamycin challenge

Kanamycin was used at a final concentration of 25 µg/mL as this concentration aerobically provides a fast and strong bactericidal effect on *M. abscessus* NCTC 13031. *M. abscessus* was grown in ADC enriched 7H9 media for the Hypoxic model or minimal cholesterol media for the cholesterol multi stress model to an approximately OD_{600nm} 0.3 (*see* **section 7.2.5).**. Cultures were then set up in 3mL aliquots with methylene blue and placed into the anaerobic cabinet as per the respective model (*see* **section 7.3.1, section 7.3.2**). Kanamycin was added in triplicate to cultures at 0h, 24h, 48h. Decolourisation of methylene blue occurred in both cultures before 24 h of anaerobic incubation. Absorbance readings were taken as were endpoint CFU/mL counts.

7.16 Ziehl-Neelsen (Z/N) Staining

A 10 µL aliquot of *Mycobacteria* culture was taken and heat fixed onto a microscope slide. After heat fixing, the slide was covered in carbol fuschin stain (Fisher) and heated on a bursen burner. The carbol fushcin stain will heat up and was periodically heated until the stain was completely gone. Any excess carbol fuschin was washed away with dH2O. The microscope slide was then cover with 20% Sulfuric acid (v/v) for 30 s. The slide was washed with dH2O to remove excess acid. Finally, the slide was covered with malachite green stain and left for 60 s. The slide was washed with dH2O to remove the excess malachite green stain. The microscope slide was left by a Bunsen burner to dry before visualisation with a microscope.

7.17 Aerobic Antibiotic Testing of *M. abscessus*

96 well microtitre plates were dosed with the appropriate antimicrobials in a 1:99 compound to broth ratio. *M. abscessus* was grown in either 7H9 media or nutrient broth to mid log, approximately OD_{600nm} = 0.6 (*see* **section 7.2.5**). 99 µL of mid log *M. abscessus* culture was used to inoculated with previously dosed 96 well microtitre plates. These plates were sealed with an aerobic plate seal and incubated in a static incubator at 37 ^{o}C with 5% CO_2.

Chapter 8:
Bibliography

Chapter 8 Bibliography

Achtman, M., Zurth, K., Morelli, G., Torrea, G., Guiyoule, A., & Carniel, E. (1999). Yersinia pestis, the cause of plague, is a recently emerged clone of Yersinia pseudotuberculosis. *Proceedings of the National Academy of Sciences of the United States of America*, *96*(24), 14043–14048. https://doi.org/10.1073/pnas.96.24.14043

Anand, A., Verma, P., Singh, A. K., Kaushik, S., Pandey, R., Shi, C., Kaur, H., Chawla, M., Elechalawar, C. K., Kumar, D., Yang, Y., Bhavesh, N. S., Banerjee, R., Dash, D., Singh, A., Natarajan, V. T., Ojha, A. K., Aldrich, C. C., & Gokhale, R. S. (2015). Polyketide Quinones Are Alternate Intermediate Electron Carriers during Mycobacterial Respiration in Oxygen-Deficient Niches. *Molecular Cell*, *60*(4), 637–650. https://doi.org/10.1016/j.molcel.2015.10.016

Ando, H., Kitao, T., Miyoshi-Akiyama, T., Kato, S., Mori, T., & Kirikae, T. (2011). Downregulation of katG expression is associated with isoniazid resistance in Mycobacterium tuberculosis. *Molecular Microbiology*, *79*(6), 1615–1628. https://doi.org/10.1111/j.1365-2958.2011.07547.x

Arbiser, J. L., & Moschella, S. L. (1995). Clofazimine: A review of its medical uses and mechanisms of action. In *Journal of the American Academy of Dermatology* (Vol. 32, Issue 2 PART 1, pp. 241–247). https://doi.org/10.1016/0190-9622(95)90134-5

Argyrou, A., Vetting, M. W., Aladegbami, B., & Blanchard, J. S. (2006). Mycobacterium tuberculosis dihydrofolate reductase is a target for isoniazid. *Nature Structural and Molecular Biology*, *13*(5), 408–413. https://doi.org/10.1038/nsmb1089

Baca, A. M., Sirawaraporn, R., Turley, S., Sirawaraporn, W., & Hol, W. G. J. (2000). Crystal structure of Mycobacterium tuberculosis 6-hydroxymethyl-7,8-dihydropteroate synthase in complex with pterin monophosphate: New insight into the enzymatic mechanism and sulfa-drug action. *Journal of Molecular Biology*, *302*(5), 1193–1212. https://doi.org/10.1006/jmbi.2000.4094

Bacon, J., Alderwick, L. J., Allnutt, J. A., Gabasova, E., Watson, R., Hatch, K. A., Clark, S. O., Jeeves, R. E., Marriott, A., Rayner, E., Tolley, H., Pearson, G., Hall, G., Besra, G. S., Wernisch, L., Williams, A., & Marsh, P. D. (2014). Non-replicating Mycobacterium tuberculosis elicits a reduced infectivity profile with corresponding modifications to the cell wall and extracellular matrix. *PLoS ONE*, *9*(2), e87329. https://doi.org/10.1371/journal.pone.0087329

Ballou, D. P., Entsch, B., & Cole, L. J. (2005). Dynamics involved in catalysis by single-component and two-component flavin-dependent aromatic hydroxylases. In *Biochemical and Biophysical Research Communications* (Vol. 338, Issue 1, pp. 590–598). Academic Press. https://doi.org/10.1016/j.bbrc.2005.09.081

Banerjee, A., Dubnau, E., Quemard, A., Balasubramanian, V., Um, K. S., Wilson, T., Collins, D., De Lisle, G., & Jacobs, W. R. (1994). inhA, a gene encoding a target for isoniazid and ethionamide in Mycobacterium tuberculosis. *Science*, *263*(5144), 227–230. https://doi.org/10.1126/science.8284673

Baptista, R., Fazakerley, D. M., Beckmann, M., Baillie, L., & Mur, L. A. J. (2018). Untargeted metabolomics reveals a new mode of action of pretomanid (PA-824). *Scientific Reports*, *8*(1). https://doi.org/10.1038/s41598-018-23110-1

Barry, C. E. (2001). Interpreting cell wall “virulence factors” of Mycobacterium tuberculosis. In *Trends in Microbiology* (Vol. 9, Issue 5, pp. 237–241). https://doi.org/10.1016/S0966-842X(01)02018-2

Barry, C. E., Boshoff, H., Dartois, V., Dick, T., Ehrt, S., Flynn, J., Schnappinger, D., Wilkinson, R. J., & Young, D. (2009a). The spectrum of latent tuberculosis: rethinking the goals of prophylaxis. *Nat Rev Microbiol*, *7*(12), 845–855. https://doi.org/10.1038/nrmicro2236

Barry, C. E., Boshoff, H. I., Dartois, V., Dick, T., Ehrt, S., Flynn, J. A., Schnappinger, D., Wilkinson, R. J., & Young, D. (2009b). The spectrum of latent tuberculosis: Rethinking

the biology and intervention strategies. In *Nature Reviews Microbiology* (Vol. 7, Issue 12, pp. 845–855). https://doi.org/10.1038/nrmicro2236

Bartek, I. L., Rutherford, R., Gruppo, V., Morton, R. A., Morris, R. P., Klein, M. R., Visconti, K. C., Ryan, G. J., Schoolnik, G. K., Lenaerts, A., & Voskuil, M. I. (2009). The DosR regulon of M. tuberculosis and antibacterial tolerance. *Tuberculosis*, *89*(4), 310–316. https://doi.org/10.1016/j.tube.2009.06.001

Beauregard, K. E., Lee, K. D., Collier, R. J., & Swanson, J. A. (1997). pH-dependent perforation of macrophage phagosomes by listeriolysin O from Listeria monocytogenes. *Journal of Experimental Medicine*, *186*(7), 1159–1163. https://doi.org/10.1084/jem.186.7.1159

Betts, J. C., Lukey, P. T., Robb, L. C., McAdam, R. A., & Duncan, K. (2002). Evaluation of a nutrient starvation model of Mycobacterium tuberculosis persistence by gene and protein expression profiling. *Molecular Microbiology*, *43*(3), 717–731. https://doi.org/10.1046/j.1365-2958.2002.02779.x

Biketov, S., Potapov, V., Ganina, E., Downing, K., Kana, B. D., & Kaprelyants, A. (2007). The role of resuscitation promoting factors in pathogenesis and reactivation of Mycobacterium tuberculosis during intra-peritoneal infection in mice. *BMC Infectious Diseases*, *7*. https://doi.org/10.1186/1471-2334-7-146

Bishop, P. J. (1981). Laennec: A great student of tuberculosis. *Tubercle*, *62*(2), 129–134. https://doi.org/10.1016/0041-3879(81)90021-0

Bonnett, S. A., Dennison, D., Files, M., Bajpai, A., & Parish, T. (2018). A class of hydrazones are active against nonreplicating Mycobacterium tuberculosis. *PLoS ONE*, *13*(10). https://doi.org/10.1371/journal.pone.0198059

Bonnett, S. A., Ollinger, J., Chandrasekera, S., Florio, S., O'Malley, T., Files, M., Jee, J. A., Ahn, J., Casey, A., Ovechkina, Y., Roberts, D., Korkegian, A., & Parish, T. (2016). A

Target-Based Whole Cell Screen Approach to Identify Potential Inhibitors of Mycobacterium tuberculosis Signal Peptidase. *ACS Infectious Diseases*, *2*(12), 893–902. https://doi.org/10.1021/acsinfecdis.6b00075

Boon, C., Li, R., Qi, R., & Dick, T. (2001). Proteins of Mycobacterium bovis BCG induced in the wayne dormancy model. *Journal of Bacteriology*, *183*(8), 2672–2676. https://doi.org/10.1128/JB.183.8.2672-2676.2001

Burki, T. (2019). BPaL approved for multidrug-resistant tuberculosis. *The Lancet. Infectious Diseases*, *19*(10), 1063–1064. https://doi.org/10.1016/S1473-3099(19)30489-X

Buttle, G. A. H., Stephenson, D., Smith, S., Dewing, T., & Foster, G. E. (1937). THE TREATMENT OF STREPTOCOCCAL INFECTIONS IN MICE WITH 4:4'DIAMINODIPHENYLSULPHONE. *The Lancet*, *229*(5936), 1331–1334. https://doi.org/10.1016/S0140-6736(00)75868-5

Cambau, E., & Williams, D. L. (2019). Anti-Leprosy Drugs: Modes of Action and Mechanisms of Resistance in Mycobacterium leprae. *The International Textbook of Leprosy*, *7*, 1–33.

Capuano, S. V., Croix, D. A., Pawar, S., Zinovik, A., Myers, A., Lin, P. L., Bissel, S., Fuhrman, C., Klein, E., & Flynn, J. A. L. (2003). Experimental Mycobacterium tuberculosis infection of cynomolgus macaques closely resembles the various manifestations of human M. tuberculosis infection. *Infection and Immunity*, *71*(10), 5831–5844. https://doi.org/10.1128/IAI.71.10.5831-5844.2003

Capyk, J. K., Casabon, I., Gruninger, R., Strynadka, N. C., & Eltis, L. D. (2011). Activity of 3-ketosteroid 9α-hydroxylase (KshAB) indicates cholesterol side chain and ring degradation occur simultaneously in Mycobacterium tuberculosis. *Journal of Biological Chemistry*, *286*(47), 40717–40724. https://doi.org/10.1074/jbc.M111.289975

Capyk, J. K., D'Angelo, I., Strynadka, N. C., & Eltis, L. D. (2009). Characterization of 3-ketosteroid 9α-hydroxylase, a Rieske oxygenase in the cholesterol degradation pathway

of Mycobacterium tuberculosis. *Journal of Biological Chemistry*, *284*(15), 9937–9946. https://doi.org/10.1074/jbc.M900719200

Carroll, P., Schreuder, L. J., Muwanguzi-Karugaba, J., Wiles, S., Robertson, B. D., Ripoll, J., Ward, T. H., Bancroft, G. J., Schaible, U. E., & Parish, T. (2010). Sensitive detection of gene expression in mycobacteria under replicating and non-replicating conditions using optimized far-red reporters. *PLoS ONE*, *5*(3). https://doi.org/10.1371/journal.pone.0009823

Chaiyen, P., Suadee, C., & Wilairat, P. (2001). A novel two-protein component flavoprotein hydroxylase p-hydroxyphenylacetate hydroxylase from Acinetobacter baumannii. *European Journal of Biochemistry*, *268*(21), 5550–5561. https://doi.org/10.1046/j.1432-1033.2001.02490.x

Chakraborty, S., Gruber, T., Barry, C. E., Boshoff, H. I., & Rhee, K. Y. (2013). Para-aminosalicylic acid acts as an alternative substrate of folate metabolism in Mycobacterium tuberculosis. *Science*, *339*(6115), 88–91. https://doi.org/10.1126/science.1228980

Chiang, Y. R., Ismail, W., Heintz, D., Schaeffer, C., Van Dorsselaer, A., & Fuchs, G. (2008). Study of anoxic and oxic cholesterol metabolism by Sterolibacterium denitrificans. *Journal of Bacteriology*, *190*(3), 905–914. https://doi.org/10.1128/JB.01525-07

Cho, S. H., Goodlett, D., & Franzblau, S. (2006). ICAT-based comparative proteomic analysis of non-replicating persistent Mycobacterium tuberculosis. *Tuberculosis*, *86*(6), 445–460. https://doi.org/10.1016/j.tube.2005.10.002

Cho, S. H., Warit, S., Wan, B., Hwang, C. H., Pauli, G. F., & Franzblau, S. G. (2007). Low-oxygen-recovery assay for high-throughput screening of compounds against nonreplicating Mycobacterium tuberculosis. *Antimicrobial Agents and Chemotherapy*, *51*(4), 1380–1385. https://doi.org/10.1128/AAC.00055-06

Cho, S., Lee, H. S., & Franzblau, S. (2015). Microplate alamar blue assay (MABA) and Low oxygen recovery assay (LORA) for Mycobacterium tuberculosis. *Methods in Molecular Biology*, *1285*, 281–292. https://doi.org/10.1007/978-1-4939-2450-9_17

Cholo, M. C., Mothiba, M. T., Fourie, B., & Anderson, R. (2017). Mechanisms of action and therapeutic efficacies of the lipophilic antimycobacterial agents clofazimine and bedaquiline. *Journal of Antimicrobial Chemotherapy*, *72*(2), 338–353. https://doi.org/10.1093/jac/dkw426

Chua, J., Vergne, I., Master, S., & Deretic, V. (2004). A tale of two lipids: Mycobacterium tuberculosis phagosome maturation arrest. In *Current Opinion in Microbiology* (Vol. 7, Issue 1, pp. 71–77). Elsevier Ltd. https://doi.org/10.1016/j.mib.2003.12.011

Cole, S. T., Brosch, R., Parkhill, J., Garnier, T., Churcher, C., Harris, D., Gordon, S. V., Eiglmeier, K., Gas, S., Barry, C. E., Tekaia, F., Badcock, K., Basham, D., Brown, D., Chillingworth, T., Connor, R., Davies, R., Devlin, K., Feltwell, T., … Barrell, B. G. (1998). Deciphering the biology of mycobacterium tuberculosis from the complete genome sequence. In *Nature* (Vol. 393, Issue 6685, pp. 537–544). Nature. https://doi.org/10.1038/31159

Collins, L. A., & Franzblau, S. G. (1997). Microplate Alamar blue assay versus BACTEC 460 system for high- throughput screening of compounds against Mycobacterium tuberculosis and Mycobacterium avium. *Antimicrobial Agents and Chemotherapy*, *41*(5), 1004–1009. https://doi.org/10.1128/aac.41.5.1004

Conradie, F. (2017). *THE NIX-TB TRIAL OF PRETOMANID, BEDAQUILINE AND LINEZOLID TO TREAT XDR-TB | CROI Conference*. Croi. https://www.croiconference.org/sessions/nix-tb-trial-pretomanid-bedaquiline-and-linezolid-treat-xdr-tb

Conradie, F., Diacon, A. H., Ngubane, N., Howell, P., Everitt, D., Crook, A. M., Mendel, C. M., Egizi, E., Moreira, J., Timm, J., McHugh, T. D., Wills, G. H., Bateson, A., Hunt, R.,

Van Niekerk, C., Li, M., Olugbosi, M., & Spigelman, M. (2020). Treatment of Highly Drug-Resistant Pulmonary Tuberculosis. *New England Journal of Medicine*, *382*(10), 893–902. https://doi.org/10.1056/nejmoa1901814

Conte, M. P., Petrone, G., Longhi, C., Valenti, P., Morelli, R., Superti, F., & Seganti, L. (1996). The effects of inhibitors of vacuolar acidification on the release of Listeria monocytogenes from phagosomes of Caco-2 cells. *Journal of Medical Microbiology*, *44*(6), 418–424. https://doi.org/10.1099/00222615-44-6-418

Corper, H. J., & Cohn, M. L. (1951). The viability and virulence of old cultures of tubercle bacilli. (Studies on 30-year-old broth cultures maintained at 37° C.). *Tubercle*, *32*(11), 232–237. https://doi.org/10.1016/S0041-3879(51)80038-2

Crofton, J., & Mitchison, D. A. (1948). Streptomycin resistance in pulmonary tuberculosis. *British Medical Journal*, *2*(4588), 1009–1015. https://doi.org/10.1136/bmj.2.4588.1009

da Silva, P. E. A., & Palomino, J. C. (2011). Molecular basis and mechanisms of drug resistance in Mycobacterium tuberculosis: Classical and new drugs. In *Journal of Antimicrobial Chemotherapy* (Vol. 66, Issue 7, pp. 1417–1430). https://doi.org/10.1093/jac/dkr173

Dalla Costa, E. R., Ribeiro, M. O., Silva, M. S., Arnold, L. S., Rostirolla, D. C., Cafrune, P. I., Espinoza, R. C., Palaci, M., Telles, M. A., Ritacco, V., Suffys, P. N., Lopes, M. L., Campelo, C. L., Miranda, S. S., Kremer, K., Da Silva, P. E. A., Fonseca, L. D. S., Ho, J. L., Kritski, A. L., & Rossetti, M. L. (2009). Correlations of mutations in katG, oxyR-ahpC and inhA genes and in vitro susceptibility in Mycobacterium tuberculosis clinical strains segregated by spoligotype families from tuberculosis prevalent countries in South America. *BMC Microbiology*, *9*. https://doi.org/10.1186/1471-2180-9-39

Daniel, J., Maamar, H., Deb, C., Sirakova, T. D., & Kolattukudy, P. E. (2011). Mycobacterium tuberculosis uses host triacylglycerol to accumulate lipid droplets and acquires a

dormancy-like phenotype in lipid-loaded macrophages. *PLoS Pathogens*, *7*(6), e1002093. https://doi.org/10.1371/journal.ppat.1002093

Daniel, T. M. (2006). The history of tuberculosis. *Respiratory Medicine*, *100*(11), 1862–1870. https://doi.org/10.1016/j.rmed.2006.08.006

Dawson, R., Diacon, A. H., Everitt, D., Van Niekerk, C., Donald, P. R., Burger, D. A., Schall, R., Spigelman, M., Conradie, A., Eisenach, K., Venter, A., Ive, P., Page-Shipp, L., Variava, E., Reither, K., Ntinginya, N. E., Pym, A., Von Groote-Bidlingmaier, F., & Mendel, C. M. (2015). Efficiency and safety of the combination of moxifloxacin, pretomanid (PA-824), and pyrazinamide during the first 8 weeks of antituberculosis treatment: A phase 2b, open-label, partly randomised trial in patients with drug-susceptible or drug-resistant pul. *The Lancet*, *385*(9979), 1738–1747. https://doi.org/10.1016/S0140-6736(14)62002-X

De Carvalho, L. P. S., Lin, G., Jiang, X., & Nathan, C. (2009). Nitazoxanide kills replicating and nonreplicating Mycobacterium tuberculosis and evades resistance. *Journal of Medicinal Chemistry*, *52*(19), 5789–5792. https://doi.org/10.1021/jm9010719

De Groote, M. A., & Huitt, G. (2006). Infections due to rapidly growing mycobacteria. *Clinical Infectious Diseases*, *42*(12), 1756–1763. https://doi.org/10.1086/504381

de Miranda Silva, C., Hajihosseini, A., Myrick, J., Nole, J., Louie, A., Schmidt, S., & Drusano, G. L. (2019). Effect of Moxifloxacin plus Pretomanid against Mycobacterium tuberculosis in Log Phase, Acid Phase, and Nonreplicating-Persister Phase in an In Vitro Assay. *Antimicrobial Agents and Chemotherapy*, *63*(1). https://doi.org/10.1128/AAC.01695-18

Deb, C., Lee, C. M., Dubey, V. S., Daniel, J., Abomoelak, B., Sirakova, T. D., Pawar, S., Rogers, L., & Kolattukudy, P. E. (2009). A novel in vitro multiple-stress dormancy model for mycobacterium tuberculosis generates a lipid-loaded, drug-tolerant, dormant pathogen. *PLoS ONE*, *4*(6). https://doi.org/10.1371/journal.pone.0006077

Delogu, G., Sali, M., & Fadda, G. (2013). The biology of mycobacterium tuberculosis infection. In *Mediterranean Journal of Hematology and Infectious Diseases* (Vol. 5, Issue 1). Universita Cattolica del Sacro Cuore. https://doi.org/10.4084/mjhid.2013.070

Dermer, J., & Fuchs, G. (2012). Molybdoenzyme that catalyzes the anaerobic hydroxylation of a tertiary carbon atom in the side chain of cholesterol. *Journal of Biological Chemistry*, *287*(44), 36905–36916. https://doi.org/10.1074/jbc.M112.407304

Deshpande, D., Magombedze, G., Srivastava, S., Bendet, P., Lee, P. S., Cirrincione, K. N., Martin, K. R., Dheda, K., & Gumbo, T. (2019). Once-a-week tigecycline for the treatment of drug-resistant TB. *Journal of Antimicrobial Chemotherapy*, *74*(6), 1607–1617. https://doi.org/10.1093/jac/dkz061

Desjardin, L. E., Hayes, L. G., Sohaskey, C. D., Wayne, L. G., & Eisenach, K. D. (2001). Microaerophilic induction of the alpha-crystallin chaperone protein homologue (hspX) mRNA of Mycobacterium tuberculosis. *Journal of Bacteriology*, *183*(18), 5311–5316. https://doi.org/10.1128/JB.183.18.5311-5316.2001

Dessen, A., Quémard, A., Blanchard, J. S., Jacobs, W. R., & Sacchettini, J. C. (1995). Crystal structure and function of the isoniazid target of Mycobacterium tuberculosis. *Science*, *267*(5204), 1638–1641. https://doi.org/10.1126/science.7886450

Dooley, K. E., & Chaisson, R. E. (2009). Tuberculosis and diabetes mellitus: convergence of two epidemics. In *The Lancet Infectious Diseases* (Vol. 9, Issue 12, pp. 737–746). Elsevier. https://doi.org/10.1016/S1473-3099(09)70282-8

Dresen, C., Lin, L. Y. C., D'Angelo, I., Tocheva, E. I., Strynadka, N., & Eltis, L. D. (2010). A flavin-dependent monooxygenase from Mycobacterium tuberculosis involved in cholesterol catabolism. *Journal of Biological Chemistry*, *285*(29), 22264–22275. https://doi.org/10.1074/jbc.M109.099028

Du, P., Sohaskey, C. D., & Shi, L. (2016). Transcriptional and physiological changes during Mycobacterium tuberculosis reactivation from non-replicating persistence. *Frontiers in Microbiology*, *7*(AUG), 1346. https://doi.org/10.3389/fmicb.2016.01346

Dutta, N. K., & Karakousis, P. C. (2014). Latent Tuberculosis Infection: Myths, Models, and Molecular Mechanisms. *Microbiology and Molecular Biology Reviews*, *78*(3), 343–371. https://doi.org/10.1128/mmbr.00010-14

Dyrhol-Riise, A. M., Gran, G., Wenzel-Larsen, T., Blomberg, B., Haanshuus, C. G., & Mørkve, O. (2010). Diagnosis and follow-up of treatment of latent tuberculosis; the utility of the QuantiFERON-TB Gold In-tube assay in outpatients from a tuberculosis low-endemic country. *BMC Infectious Diseases*, *10*(1), 1–9. https://doi.org/10.1186/1471-2334-10-57

Ehlers, S. (2009). Lazy, dynamic or minimally recrudescent? on the elusive nature and location of the mycobacterium responsible for latent tuberculosis. In *Infection* (Vol. 37, Issue 2, pp. 87–95). https://doi.org/10.1007/s15010-009-8450-7

Ehlers, S., & Schaible, U. E. (2012). The granuloma in tuberculosis: Dynamics of a host-pathogen collusion. In *Frontiers in Immunology* (Vol. 3, Issue JAN, p. 411). Frontiers. https://doi.org/10.3389/fimmu.2012.00411

Eichelmann, K., González González, S. E., Salas-Alanis, J. C., & Ocampo-Candiani, J. (2013). Leprosy. An Update: Definition, Pathogenesis, Classification, Diagnosis, and Treatment. *Actas Dermo-Sifiliográficas (English Edition)*, *104*(7), 554–563. https://doi.org/10.1016/j.adengl.2012.03.028

Ernst, J. D. (2012). The immunological life cycle of tuberculosis. In *Nature Reviews Immunology* (Vol. 12, Issue 8, pp. 581–591). https://doi.org/10.1038/nri3259

Ernst, S., Rovida, S., Mattevi, A., Fetzner, S., & Drees, S. L. (2020). Photoinduced monooxygenation involving NAD(P)H-FAD sequential single-electron transfer. *Nature Communications*, *11*(1), 1–11. https://doi.org/10.1038/s41467-020-16450-y

Esmail, H., Barry, C. E., Young, D. B., & Wilkinson, R. J. (2014). The ongoing challenge of latent tuberculosis. In *Philosophical Transactions of the Royal Society B: Biological Sciences* (Vol. 369, Issue 1645). Royal Society. https://doi.org/10.1098/rstb.2013.0437

Esther, C. R., Esserman, D. A., Gilligan, P., Kerr, A., & Noone, P. G. (2010). Chronic Mycobacterium abscessus infection and lung function decline in cystic fibrosis. *Journal of Cystic Fibrosis*, *9*(2), 117–123. https://doi.org/10.1016/j.jcf.2009.12.001

Faget, G. H., & Pogge, R. C. (1945). The Therapeutic Effect of Promin in Leprosy. *Public Health Reports (1896-1970)*, *60*(40), 1165. https://doi.org/10.2307/4585405

Faget, G. H., Pogge, R. C., Johansen, F. A., Dinan, J. F., Prejean, B. M., & Eccles, C. G. (1966). The promin treatment of leprosy. A progress report. *International Journal of Leprosy and Other Mycobacterial Diseases*, *34*(3), 298–310.

Finn, R. D., Basran, J., Roitel, O., Wolf, C. R., Munro, A. W., Paine, M. J. I., & Scrutton, N. S. (2003). Determination of the redox potentials and electron transfer properties of the FAD- and FMN-binding domains of the human oxidoreductase NR1. *European Journal of Biochemistry*, *270*(6), 1164–1175. https://doi.org/10.1046/j.1432-1033.2003.03474.x

Flynn, J. A. L. (2006). Lessons from experimental Mycobacterium tuberculosis infections. In *Microbes and Infection* (Vol. 8, Issue 4, pp. 1179–1188). https://doi.org/10.1016/j.micinf.2005.10.033

Flynn, J. L., Capuano, S. V., Croix, D., Pawar, S., Myers, A., Zinovik, A., & Klein, E. (2003). Non-human primates: A model for tuberculosis research. *Tuberculosis*, *83*(1–3), 116–118. https://doi.org/10.1016/S1472-9792(02)00059-8

Forrellad, M. A., Klepp, L. I., Gioffré, A., García, J. S., Morbidoni, H. R., de la Paz Santangelo, M., Cataldi, A. A., & Bigi, F. (2013). Virulence factors of the mycobacterium tuberculosis complex. In *Virulence* (Vol. 4, Issue 1, pp. 3–66). https://doi.org/10.4161/viru.22329

Fraser, A., Paul, M., Attamna, A., & Leibovici, L. (2006). Treatment of latent tuberculosis in persons at risk for multidrug-resistant tuberculosis: Systematic review. In *International Journal of Tuberculosis and Lung Disease* (Vol. 10, Issue 1, pp. 19–23). International Union Against Tuberculosis and Lung Disease.

Freeman, C. D., Klutman, N. E., & Lamp, K. C. (1997). Metronidazole. A therapeutic review and update. In *Drugs* (Vol. 54, Issue 5, pp. 679–708). Springer International Publishing. https://doi.org/10.2165/00003495-199754050-00003

Frieden, T. R., Sterling, T. R., Munsiff, S. S., Watt, C. J., & Dye, C. (2003). Tuberculosis. *Lancet*, *362*(9387), 887–899. https://doi.org/10.1016/S0140-6736(03)14333-4

Fromm, E., & Wittmann, J. (1908). Derivate des p-Nitrothiophenols. *Berichte Der Deutschen Chemischen Gesellschaft*, *41*(2), 2264–2273. https://doi.org/10.1002/cber.190804102131

Galán, B., Díaz, E., Prieto, M. A., & García, J. L. (2000). Functional analysis of the small component of the 4-hydroxyphenylacetate 3-monooxygenase of Escherichia coli W: A prototype of a new flavin:NAD(P)H reductase subfamily. *Journal of Bacteriology*, *182*(3), 627–636. https://doi.org/10.1128/JB.182.3.627-636.2000

García-Tapia, A., Rodríguez, J. C., Ruiz, M., & Royo, G. (2004). Action of fluoroquinolones and linezolid on logarithmic- and stationary-phase culture of Mycobacterium tuberculosis. *Chemotherapy*, *50*(5), 211–213. https://doi.org/10.1159/000081707

Garton, N. J., Waddell, S. J., Sherratt, A. L., Lee, S. M., Smith, R. J., Senner, C., Hinds, J., Rajakumar, K., Adegbola, R. A., Besra, G. S., Butcher, P. D., & Barer, M. R. (2008).

Cytological and transcript analyses reveal fat and lazy persister-like bacilli in tuberculous sputum. *PLoS Medicine*, *5*(4), 0634–0645. https://doi.org/10.1371/journal.pmed.0050075

Gatfield, J., & Pieters, J. (2000). Essential role for cholesterol in entry of mycobacteria into macrophages. *Science*, *288*(5471), 1647–1650. https://doi.org/10.1126/science.288.5471.1647

Gengenbacher, M., Rao, S. P. S., Pethe, K., & Dick, T. (2010). Nutrient-starved, non-replicating Mycobacterium tuberculosis requires respiration, ATP synthase and isocitrate lyase for maintenance of ATP homeostasis and viability. *Microbiology*, *156*(1), 81–87. https://doi.org/10.1099/mic.0.033084-0

Gengenbacher, M., Xu, T., Niyomrattanakit, P., Spraggon, G., & Dick, T. (2008). Biochemical and structural characterization of the putative dihydropteroate synthase ortholog Rv1207 of Mycobacterium tuberculosis. *FEMS Microbiology Letters*, *287*(1), 128–135. https://doi.org/10.1111/j.1574-6968.2008.01302.x

Gerasimova, A., Kazakov, A. E., Arkin, A. P., Dubchak, I., & Gelfand, M. S. (2011). Comparative genomics of the dormancy regulons in mycobacteria. *Journal of Bacteriology*, *193*(14), 3446–3452. https://doi.org/10.1128/JB.00179-11

Ghazaei, C. (2018). Mycobacterium tuberculosis and lipids: Insights into molecular mechanisms from persistence to virulence. In *Journal of Research in Medical Sciences* (Vol. 23, Issue 1). Wolters Kluwer Medknow Publications. https://doi.org/10.4103/jrms.JRMS_904_17

Gibson, S. E. R., Harrison, J., & Cox, J. A. G. (2018). Modelling a silent epidemic: A review of the in vitro models of latent tuberculosis. In *Pathogens* (Vol. 7, Issue 4). https://doi.org/10.3390/pathogens7040088

Gil, O., Díaz, I., Vilaplana, C., Tapia, G., Díaz, J., Fort, M., Cáceres, N., Pinto, S., Caylà, J., Corner, L., Domingo, M., & Cardona, P. J. (2010). Granuloma encapsulation is a key factor for containing tuberculosis infection in minipigs. *PLoS ONE*, *5*(4). https://doi.org/10.1371/journal.pone.0010030

Gillis, T. P., & Williams, D. L. (2000). Dapsone resistance in Mycobacterium leprae. *Leprosy Review*, *71*(SUPPL.). https://doi.org/10.5935/0305-7518.20000076

Gomez, J. E., & McKinney, J. D. (2004). M. tuberculosis persistence, latency, and drug tolerance. *Tuberculosis*, *84*(1–2), 29–44. https://doi.org/10.1016/j.tube.2003.08.003

Gonçalves, L. C. P., Mansouri, H. R., Bastos, E. L., Abdellah, M., Fadiga, B. S., Sá, J., Rudroff, F., & Mihovilovic, M. D. (2019). Morpholine-based buffers activate aerobic photobiocatalysis: Via spin correlated ion pair formation. *Catalysis Science and Technology*, *9*(6), 1365–1371. https://doi.org/10.1039/c8cy02524j

Goncąlves, L. C. P., Mansouri, H. R., Pourmehdi, S., Abdellah, M., Fadiga, B. S., Bastos, E. L., Sá, J., Mihovilovic, M. D., & Rudroff, F. (2019). Boosting photobioredox catalysis by morpholine electron donors under aerobic conditions. *Catalysis Science and Technology*, *9*(10), 2682–2688. https://doi.org/10.1039/c9cy00496c

Gopinath, V., Raghunandanan, S., Gomez, R. L., Jose, L., Surendran, A., Ramachandran, R., Pushparajan, A. R., Mundayoor, S., Jaleel, A., & Kumar, R. A. (2015). Profiling the proteome of Mycobacterium tuberculosis during dormancy and reactivation. *Molecular and Cellular Proteomics*, *14*(8), 2160–2176. https://doi.org/10.1074/mcp.M115.051151

Goude, R., Amin, A. G., Chatterjee, D., & Parish, T. (2009). The arabinosyltransferase EmbC is inhibited by ethambutol in Mycobacterium tuberculosis. *Antimicrobial Agents and Chemotherapy*, *53*(10), 4138–4146. https://doi.org/10.1128/AAC.00162-09

Govender, L., Abel, B., Hughes, E. J., Scriba, T. J., Kagina, B. M. N., de Kock, M., Walzl, G., Black, G., Rosenkrands, I., Hussey, G. D., Mahomed, H., Andersen, P., & Hanekom, W.

A. (2010). Higher human CD4 T cell response to novel Mycobacterium tuberculosis latency associated antigens Rv2660 and Rv2659 in latent infection compared with tuberculosis disease. *Vaccine*, *29*(1), 51–57. https://doi.org/10.1016/j.vaccine.2010.10.022

Granville, A. B. (1825). XIII. An essay on Egyptian mummies; with observations on the art of embalming among the ancient Egyptians. *Philosophical Transactions of the Royal Society of London*, *115*, 269–316. https://doi.org/10.1098/rstl.1825.0015

Griffin, J. E., Gawronski, J. D., DeJesus, M. A., Ioerger, T. R., Akerley, B. J., & Sassetti, C. M. (2011). High-resolution phenotypic profiling defines genes essential for mycobacterial growth and cholesterol catabolism. *PLoS Pathogens*, *7*(9). https://doi.org/10.1371/journal.ppat.1002251

Griffin, J. E., Pandey, A. K., Gilmore, S. A., Mizrahi, V., McKinney, J. D., Bertozzi, C. R., & Sassetti, C. M. (2012). Cholesterol catabolism by Mycobacterium tuberculosis requires transcriptional and metabolic adaptations. *Chemistry and Biology*, *19*(2), 218–227. https://doi.org/10.1016/j.chembiol.2011.12.016

Griffith, D. E. (2019). Mycobacterium abscessus and Antibiotic Resistance: Same As It Ever Was. In *Clinical Infectious Diseases* (Vol. 69, Issue 10, pp. 1687–1689). https://doi.org/10.1093/cid/ciz071

Guirado, E., & Schlesinger, L. S. (2013). Modeling the Mycobacterium tuberculosis granuloma - the critical battlefield in host immunity and disease. *Frontiers in Immunology*, *4*(APR). https://doi.org/10.3389/fimmu.2013.00098

Gumbo, T., Louie, A., Deziel, M. R., Parsons, L. M., Salfinger, M., & Drusano, G. L. (2004). Selection of a Moxifloxacin Dose That Suppresses Drug Resistance in Mycobacterium tuberculosis, by Use of an In Vitro Pharmacodynamic Infection Model and Mathematical Modeling. *The Journal of Infectious Diseases*, *190*(9), 1642–1651. https://doi.org/10.1086/424849

Gupta, U. D., & Katoch, V. M. (2005). Animal models of tuberculosis. *Tuberculosis*, *85*(5–6), 277–293. https://doi.org/10.1016/j.tube.2005.08.008

Gupte, A. N., Auld, S. C., Checkley, W. N., & Bisson, G. P. (2021). Outcomes for Clinical Trials of Host-Directed Therapies for Tuberculosis. In *Advances in Host-Directed Therapies Against Tuberculosis* (pp. 295–310). Springer International Publishing. https://doi.org/10.1007/978-3-030-56905-1_21

Gutierrez, M. C., Brisse, S., Brosch, R., Fabre, M., Omaïs, B., Marmiesse, M., Supply, P., & Vincent, V. (2005). Ancient origin and gene mosaicism of the progenitor of Mycobacterium tuberculosis. *PLoS Pathogens*, *1*(1), 0055–0061. https://doi.org/10.1371/journal.ppat.0010005

Hampshire, T., Soneji, S., Bacon, J., James, B. W., Hinds, J., Laing, K., Stabler, R. A., Marsh, P. D., & Butcher, P. D. (2004). Stationary phase gene expression of Mycobacterium tuberculosis following a progressive nutrient depletion: A model for persistent organisms? *Tuberculosis*, *84*(3–4), 228–238. https://doi.org/10.1016/j.tube.2003.12.010

Handschin, J. C., & Wehrli, W. (1976). On the Kinetics of the Rifampicin RNA-Polymerase Complex Differences between Crude and Purified Enzyme Fractions. *European Journal of Biochemistry*, *66*(2), 309–317. https://doi.org/10.1111/j.1432-1033.1976.tb10520.x

Harder, J., & Probian, C. (1997). Anaerobic mineralization of cholesterol by a novel type of denitrifying bacterium. *Archives of Microbiology*, *167*(5), 269–274. https://doi.org/10.1007/s002030050442

Hards, K., Robson, J. R., Berney, M., Shaw, L., Bald, D., Koul, A., Andries, K., & Cook, G. M. (2015). Bactericidal mode of action of bedaquiline. *Journal of Antimicrobial Chemotherapy*, *70*(7), 2028–2037. https://doi.org/10.1093/jac/dkv054

Hashimoto, T. (1955). Experimental studies on the mechanism of infection and immunity in tuberculosis from the analytical standpoint of streptomycin-dependent tubercle bacilli. 1. Isolation and biological characteristics of a streptomycin-dependent mutant, and effect of strept. *Kekkaku : [Tuberculosis]*, *30*(1). https://doi.org/10.11400/kekkaku1923.30.4

Hazbón, M. H., Brimacombe, M., Del Valle, M. B., Cavatore, M., Guerrero, M. I., Varma-Basil, M., Billman-Jacobe, H., Lavender, C., Fyfe, J., García-García, L., León, C. I., Bose, M., Chaves, F., Murray, M., Eisenach, K. D., Sifuentes-Osornio, J., Cave, M. D., De León, A. P., & Alland, D. (2006). Population genetics study of isoniazid resistance mutations and evolution of multidrug-resistant Mycobacterium tuberculosis. *Antimicrobial Agents and Chemotherapy*, *50*(8), 2640–2649. https://doi.org/10.1128/AAC.00112-06

Hedges, R. E. M., Pettitt, P. B., Ramsey, C. B., & Van Klinken, G. J. (1997). Radiocarbon dates from the Oxford AMS System: Archaeometry datelist 23. *Archaeometry*, *39*(1), 247–262. https://doi.org/10.1111/j.1475-4754.1997.tb00803.x

Heifets, L., Simon, J., & Pham, V. (2005). Capreomycin is active against non-replicating M. tuberculosis. *Annals of Clinical Microbiology and Antimicrobials*, *4*. https://doi.org/10.1186/1476-0711-4-6

Hernández-Pando, R., Jeyanathan, M., Mengistu, G., Aguilar, D., Orozco, H., Harboe, M., Rook, G. A. W., & Bjune, G. (2000). Persistence of DNA from Mycobacterium tuberculosis in superficially normal lung tissue during latent infection. *Lancet*, *356*(9248), 2133–2138. https://doi.org/10.1016/S0140-6736(00)03493-0

Hertzberg, R. P., & Pope, A. J. (2000). High-throughput screening: New technology for the 21st century. In *Current Opinion in Chemical Biology* (Vol. 4, Issue 4, pp. 445–451). https://doi.org/10.1016/S1367-5931(00)00110-1

Hippocrates. (1708). *Aphorisms of Hippocrates and the Sentences of Celsus: With Explanations and References to the Most Considerable Writers in Physick and*

Philosophy, Both Ancient and Modern : to which are Added, Aphorisms Upon the Small-pox, Measles, and Other Distempers, N.

Hoff, D. R., Caraway, M. L., Brooks, E. J., Driver, E. R., Ryan, G. J., Peloquin, C. A., Orme, I. M., Basaraba, R. J., & Lenaerts, A. J. (2008). Metronidazole lacks antibacterial activity in guinea pigs infected with Mycobacterium tuberculosis. *Antimicrobial Agents and Chemotherapy*, *52*(11), 4137–4140. https://doi.org/10.1128/AAC.00196-08

Honaker, R. W., Leistikow, R. L., Bartek, I. L., & Voskui, M. I. (2009). Unique roles of DosT and DosS in DosR regulon induction and Mycobacterium tuberculosis dormancy. *Infection and Immunity*, *77*(8), 3258–3263. https://doi.org/10.1128/IAI.01449-08

Houben, R. M. G. J., & Dodd, P. J. (2016). The Global Burden of Latent Tuberculosis Infection: A Re-estimation Using Mathematical Modelling. *PLoS Medicine*, *13*(10). https://doi.org/10.1371/journal.pmed.1002152

Hu, Y., & Coates, A. (2018). A method to evaluate persistent Mycobacterium tuberculosis in vitro and in the cornell mouse model of tuberculosis. In *Methods in Molecular Biology* (Vol. 1736, pp. 157–166). Humana Press Inc. https://doi.org/10.1007/978-1-4939-7638-6_15

Hu, Y., & Coates, A. R. M. (1999). Transcription of two sigma 70 homologue genes, sigA and sigB, in stationary-phase Mycobacterium tuberculosis. *Journal of Bacteriology*, *181*(2), 469–476. https://doi.org/10.1128/jb.181.2.469-476.1999

Huang, Y. C., Liu, M. F., Shen, G. H., Lin, C. F., Kao, C. C., Liu, P. Y., & Shi, Z. Y. (2010). Clinical Outcome of Mycobacterium abscessus Infection and Antimicrobial Susceptibility Testing. *Journal of Microbiology, Immunology and Infection*, *43*(5), 401–406. https://doi.org/10.1016/S1684-1182(10)60063-1

Hugh, R., & Leifson, E. (1953). The taxonomic significance of fermentative versus oxidative metabolism of carbohydrates by various gram negative bacteria. *Journal of Bacteriology*, *66*(1), 24–26. https://doi.org/10.1128/jb.66.1.24-26.1953

Iona, E., Pardini, M., Mustazzolu, A., Piccaro, G., Nisini, R., Fattorini, L., & Giannoni, F. (2016). Mycobacterium tuberculosis gene expression at different stages of hypoxia-induced dormancy and upon resuscitation. *Journal of Microbiology*, *54*(8), 565–572. https://doi.org/10.1007/s12275-016-6150-4

J Libardo, M. D., Boshoff, H. I., & Barry, C. E. (2018). The present state of the tuberculosis drug development pipeline. In *Current Opinion in Pharmacology* (Vol. 42, pp. 81–94). Elsevier Ltd. https://doi.org/10.1016/j.coph.2018.08.001

Jakkala, K., & Ajitkumar, P. (2019). Hypoxic Non-replicating Persistent Mycobacterium tuberculosis Develops Thickened Outer Layer That Helps in Restricting Rifampicin Entry. *Frontiers in Microbiology*, *10*. https://doi.org/10.3389/fmicb.2019.02339

Jankute, M., Cox, J. A. G., Harrison, J., & Besra, G. S. (2015). Assembly of the Mycobacterial Cell Wall. *Annual Review of Microbiology*, *69*(1), 405–423. https://doi.org/10.1146/annurev-micro-091014-104121

Jarand, J., Levin, A., Zhang, L., Huitt, G., Mitchell, J. D., & Daley, C. L. (2011). Clinical and microbiologic outcomes in patients receiving treatment for Mycobacterium abscessus pulmonary disease. *Clinical Infectious Diseases*, *52*(5), 565–571. https://doi.org/10.1093/cid/ciq237

Johnson, K. A., & Goody, R. S. (2011). The original Michaelis constant: Translation of the 1913 Michaelis-Menten Paper. *Biochemistry*, *50*(39), 8264–8269. https://doi.org/10.1021/bi201284u

Kana, B. D., Gordhan, B. G., Downing, K. J., Sung, N., Vostroktunova, G., Machowski, E. E., Tsenova, L., Young, M., Kaprelyants, A., Kaplan, G., & Mizrahi, V. (2008). The

resuscitation-promoting factors of Mycobacterium tuberculosis are required for virulence and resuscitation from dormancy but are collectively dispensable for growth in vitro. *Molecular Microbiology*, *67*(3), 672–684. https://doi.org/10.1111/j.1365-2958.2007.06078.x

Kashino, S. S., Napolitano, D. R., Skobe, Z., & Campos-Neto, A. (2008). Guinea pig model of Mycobacterium tuberculosis latent/dormant infection. *Microbes and Infection*, *10*(14–15), 1469–1476. https://doi.org/10.1016/j.micinf.2008.08.010

Kassardjian, M., Patel, M., Shitabata, P., & Horowitz, D. (2015). Management of Periocular Granuloma Annulare Using Topical Dapsone. *The Journal of Clinical and Aesthetic Dermatology*, *8*(7), 48–51.

Klinkenberg, L. G., Sutherland, L. A., Bishai, W. R., & Karakousis, P. C. (2008). Metronidazole Lacks Activity against Mycobacterium tuberculosis in an In Vivo Hypoxic Granuloma Model of Latency. *The Journal of Infectious Diseases*, *198*(2), 275–283. https://doi.org/10.1086/589515

Knechel, N. A. (2009). Tuberculosis: Pathophysiology, clinical features, and diagnosis. *Critical Care Nurse*, *29*(2), 34–43. https://doi.org/10.4037/ccn2009968

Knol, J., Bodewits, K., Hessels, G. I., Dijkhuizen, L., & Van Der Geize, R. (2008). 3-Keto-5α-steroid Δ1-dehydrogenase from Rhodococcus erythropolis SQ1 and its orthologue in Mycobacterium tuberculosis H37Rv are highly specific enzymes that function in cholesterol catabolism. *Biochemical Journal*, *410*(2), 339–346. https://doi.org/10.1042/BJ20071130

Koch, R. (1882). Die Aetiologie der Tuberculose. *Deutsche Medizinische Wochenschrift*, *8*(20), 283. https://doi.org/10.1055/s-0029-1196567

Koh, W. J., Jeon, K., Lee, N. Y., Kim, B. J., Kook, Y. H., Lee, S. H., Park, Y. K., Kim, C. K., Shin, S. J., Huitt, G. A., Daley, C. L., & Kwon, O. J. (2011). Clinical significance of

differentiation of Mycobacterium massiliense from Mycobacterium abscessus. *American Journal of Respiratory and Critical Care Medicine*, *183*(3), 405–410. https://doi.org/10.1164/rccm.201003-0395OC

Lavollay, M., Dubée, V., Heym, B., Herrmann, J. L., Gaillard, J. L., Gutmann, L., Arthur, M., & Mainardi, J. L. (2014). In vitro activity of cefoxitin and imipenem against Mycobacterium abscessus complex. *Clinical Microbiology and Infection*, *20*(5). https://doi.org/10.1111/1469-0691.12405

Lee, B. Y., Hefta, S. A., & Brennan, P. J. (1992). Characterization of the major membrane protein of virulent Mycobacterium tuberculosis. *Infection and Immunity*, *60*(5), 2066–2074. https://doi.org/10.1128/iai.60.5.2066-2074.1992

Lee, M. R., Sheng, W. H., Hung, C. C., Yu, C. J., Lee, L. N., & Hsueh, P. R. (2015). Mycobacterium abscessus complex infections in humans. *Emerging Infectious Diseases*, *21*(9), 1638–1646. https://doi.org/10.3201/eid2109.141634

Lee, S. H. (2016). Tuberculosis infection and latent tuberculosis. In *Tuberculosis and Respiratory Diseases* (Vol. 79, Issue 4, pp. 201–206). Korean National Tuberculosis Association. https://doi.org/10.4046/trd.2016.79.4.201

Leung, E. T. Y., Ho, P. L., Yuen, K. Y., Woo, W. L., Lam, T. H., Kao, R. Y., Seto, W. H., & Yam, W. C. (2006). Molecular characterization of isoniazid resistance in Mycobacterium tuberculosis: Identification of a novel mutation in inhA. *Antimicrobial Agents and Chemotherapy*, *50*(3), 1075–1078. https://doi.org/10.1128/AAC.50.3.1075-1078.2006

Li, Q., Ge, F., Tan, Y., Zhang, G., & Li, W. (2016). Genome-wide transcriptome profiling of Mycobacterium smegmatis MC2 155 cultivated in minimal media supplemented with cholesterol, androstenedione or glycerol. *International Journal of Molecular Sciences*, *17*(5). https://doi.org/10.3390/ijms17050689

Li, Y. J., Petrofsky, M., & Bermudez, L. E. (2002). Mycobacterium tuberculosis uptake by recipient host macrophages is influenced by environmental conditions in the granuloma of the infectious individual and is associated with impaired production of interleukin-12 and tumor necrosis factor alpha. *Infection and Immunity*, *70*(11), 6223–6230. https://doi.org/10.1128/IAI.70.11.6223-6230.2002

Lin, P. L., & Flynn, J. L. (2010). Understanding Latent Tuberculosis: A Moving Target. *The Journal of Immunology*, *185*(1), 15–22. https://doi.org/10.4049/jimmunol.0903856

Liu, T., Wang, B., Guo, J., Zhou, Y., Julius, M., Njire, M., Cao, Y., Wu, T., Liu, Z., Wang, C., Xu, Y., & Zhang, T. (2015). Role of folP1 and folP2 genes in the action of sulfamethoxazole and trimethoprim against mycobacteria. *Journal of Microbiology and Biotechnology*, *25*(9), 1559–1567. https://doi.org/10.4014/jmb.1503.03053

Livermore, D. M. (2003). Linezolid in vitro: Mechanism and antibacterial spectrum. In *Journal of Antimicrobial Chemotherapy* (Vol. 51, Issue SUPPL. 2, pp. 9–16). https://doi.org/10.1093/jac/dkg249

Loebel, R. O., Shorr, E., & Richardson, H. B. (1933a). The Influence of Adverse Conditions upon the Respiratory Metabolism and Growth of Human Tubercle Bacilli. *Journal of Bacteriology*, *26*(2), 167–200. https://doi.org/10.1128/jb.26.2.167-200.1933

Loebel, R. O., Shorr, E., & Richardson, H. B. (1933b). The Influence of Foodstuffs upon the Respiratory Metabolism and Growth of Human Tubercle Bacilli. *Journal of Bacteriology*, *26*(2), 139–166. https://doi.org/10.1128/jb.26.2.139-166.1933

Lopeman, R. C., Harrison, J., Desai, M., & Cox, J. A. G. (2019). Mycobacterium abscessus: Environmental bacterium turned clinical nightmare. *Microorganisms*, *7*(3). https://doi.org/10.3390/microorganisms7030090

Loudon, R. G., Bumgarner, L. R., Lacy, J., & Coffman, G. K. (1969). Aerial transmission of mycobacteria. *American Review of Respiratory Disease*, *100*(2), 165–171. https://doi.org/10.1164/arrd.1969.100.2.165

Lowe, J. (1950). Treatment of Leprosy. In *The Lancet* (Vol. 255, Issue 6599, p. 325). https://doi.org/10.1016/S0140-6736(50)92025-3

Macdonald, A. (1914). the Etiology of Leprosy. In *The Lancet* (Vol. 184, Issue 4764, pp. 1436–1437). https://doi.org/10.1016/S0140-6736(00)86350-3

MacMicking, J. D., Taylor, G. A., & McKinney, J. D. (2003). Immune Control of Tuberculosis by IFN-γ-inducible LRG-47. *Science*, *302*(5645), 654–659. https://doi.org/10.1126/science.1088063

Maggi, N., Pasqualucci, C. R., Ballotta, R., & Sensi, P. (1966). Rifampicin: a new orally active rifamycin. *Chemotherapy*, *11*(5), 285–292. https://doi.org/10.1159/000220462

Mahajan, R. (2013). Bedaquiline: First FDA-approved tuberculosis drug in 40 years. *International Journal of Applied and Basic Medical Research*, *3*(1), 1. https://doi.org/10.4103/2229-516x.112228

Mahapatra, S., Scherman, H., Brennan, P. J., & Crick, D. C. (2005). N glycolylation of the nucleotide precursors of peptidoglycan biosynthesis of Mycobacterium spp. is altered by drug treatment. *Journal of Bacteriology*, *187*(7), 2341–2347. https://doi.org/10.1128/JB.187.7.2341-2347.2005

Mahmoud, D. B., Shitu, Z., & Mostafa, A. (2020). Drug repurposing of nitazoxanide: can it be an effective therapy for COVID-19? In *Journal of Genetic Engineering and Biotechnology* (Vol. 18, Issue 1). Springer. https://doi.org/10.1186/s43141-020-00055-5

Mamo, G., Mihret, A., Taffesse, M., Gebru, G., Afework, M., Yamuah, L. K., Wassie, L., Abebe, M., Aseffa, A., & Parida, S. K. (2014). T cell response to alpha crystallin and Mycobacterium tuberculosis specific antigens using ex-vivo ELISPOT assay for

detecting latent tuberculosis infection in Addis Ababa, Ethiopia. *Ethiopian Medical Journal*, *1*(SUPPL. 1), 15–22.

Manganelli, R., Dubnau, E., Tyagi, S., Kramer, F. R., & Smith, I. (1999). Differential expression of 10 sigma factor genes in Mycobacterium tuberculosis. *Molecular Microbiology*, *31*(2), 715–724. https://doi.org/10.1046/j.1365-2958.1999.01212.x

Manjunatha, U., Boshoff, H. I. M., & Barry, C. E. (2009). The mechanism of action of PA-824. *Communicative and Integrative Biology*, *2*(3), 215–218. https://doi.org/10.4161/cib.2.3.7926

Marimuthu, Y., Nagappa, B., Sharma, N., Basu, S., & Chopra, K. K. (2020). COVID-19 and tuberculosis: A mathematical model based forecasting in Delhi, India. *Indian Journal of Tuberculosis*. https://doi.org/10.1016/j.ijtb.2020.05.006

Mariscal, A., Caldarone, L., Tikkanen, J., Nakajima, D., Chen, M., Yeung, J., Cypel, M., Liu, M., & Keshavjee, S. (2018). Pig lung transplant survival model. *Nature Protocols*, *13*(8), 1814–1828. https://doi.org/10.1038/s41596-018-0019-4

Marques, M. A. M., Berrêdo-Pinho, M., Rosa, T. L. S. A., Pujari, V., Lemes, R. M. R., Lery, L. M. S., Silva, C. A. M., Guimarães, A. C. R., Atella, G. C., Wheat, W. H., Brennan, P. J., Crick, D. C., Belisle, J. T., & Pessolani, M. C. v. (2015). The essential role of cholesterol metabolism in the intracellular survival of Mycobacterium leprae is not coupled to central carbon metabolism and energy production. *Journal of Bacteriology*, *197*(23), 3698–3707. https://doi.org/10.1128/JB.00625-15

Marrakchi, H., Lanéelle, M. A., & Daffé, M. (2014). Mycolic acids: Structures, biosynthesis, and beyond. In *Chemistry and Biology* (Vol. 21, Issue 1, pp. 67–85). Cell Press. https://doi.org/10.1016/j.chembiol.2013.11.011

Martin, C. J., Carey, A. F., & Fortune, S. M. (2016). A bug's life in the granuloma. In *Seminars in Immunopathology* (Vol. 38, Issue 2, pp. 213–220). Springer Verlag. https://doi.org/10.1007/s00281-015-0533-1

Martín-Sáez, E., Fernández-Guarino, M., Carrillo-Gijón, R., Muñoz-Zato, E., & Jaén-Olasolo, P. (2008). Efficacy of Dapsone in Disseminated Granuloma Annulare: A Case Report and Review of the Literature. *Actas Dermo-Sifiliográficas (English Edition)*, *99*(1), 64–68. https://doi.org/10.1016/s1578-2190(08)70196-3

Martins-Filho, P. R., Barreto-Alves, J. A., & Fakhouri, R. (2020). Potential role for nitazoxanide in treating SARS-CoV-2 infection. In *American Journal of Physiology - Lung Cellular and Molecular Physiology* (Vol. 319, Issue 1, pp. L35–L36). American Physiological Society. https://doi.org/10.1152/ajplung.00170.2020

Mayr, L. M., & Bojanic, D. (2009). Novel trends in high-throughput screening. In *Current Opinion in Pharmacology* (Vol. 9, Issue 5, pp. 580–588). https://doi.org/10.1016/j.coph.2009.08.004

McClure, W. R., & Cech, C. L. (1978). On the mechanism of rifampicin inhibition of RNA synthesis. *Journal of Biological Chemistry*, *253*(24), 8949–8956.

MCCUNE, R. M., & TOMPSETT, R. (1956). Fate of Mycobacterium tuberculosis in mouse tissues as determined by the microbial enumeration technique. I. The persistence of drug-susceptible tubercle bacilli in the tissues despite prolonged antimicrobial therapy. *The Journal of Experimental Medicine*, *104*(5), 737–762. https://doi.org/10.1084/jem.104.5.737

McDermott, W., & Tompsett, R. (1954). Activation of pyrazinamide and nicotinamide in acidic environments in vitro. *American Review of Tuberculosis*, *70*(4), 748–754. https://doi.org/10.1164/art.1954.70.4.748

McKenna, L., & Furin, J. (2019). Are pretomanid-containing regimens for tuberculosis a victory or a victory narrative? In *The Lancet Respiratory Medicine* (Vol. 7, Issue 12, pp. 999–1000). https://doi.org/10.1016/S2213-2600(19)30363-7

McNeil, M., Wallner, S. J., Hunter, S. W., & Brennan, P. J. (1987). Demonstration that the galactosyl and arabinosyl residues in the cell-wall arabinogalactan of Mycobacterium leprae and Myobacterium tuberculosis are furanoid. *Carbohydrate Research*, *166*(2), 299–308. https://doi.org/10.1016/0008-6215(87)80065-4

Mehra, S., Foreman, T. W., Didier, P. J., Ahsan, M. H., Hudock, T. A., Kissee, R., Golden, N. A., Gautam, U. S., Johnson, A. M., Alvarez, X., Russell-Lodrigue, K. E., Doyle, L. A., Roy, C. J., Niu, T., Blanchard, J. L., Khader, S. A., Lackner, A. A., Sherman, D. R., & Kaushal, D. (2015). The DosR Regulon Modulates Adaptive Immunity and Is Essential for Mycobacterium tuberculosis Persistence. *American Journal of Respiratory and Critical Care Medicine*, *191*(10), 1185–1196. https://doi.org/10.1164/rccm.201408-1502OC

Mendel, R. R. (2013). The molybdenum cofactor. In *Journal of Biological Chemistry* (Vol. 288, Issue 19, pp. 13165–13172). American Society for Biochemistry and Molecular Biology. https://doi.org/10.1074/jbc.R113.455311

Middlebrook, G. (1954). Isoniazid-resistance and catalase activity of tubercle bacilli; a preliminary report. *American Review of Tuberculosis*, *69*(3), 471–472. https://doi.org/10.1164/art.1954.69.3.471

Middlebrook, G., & Cohn, M. L. (1958). Bacteriology of tuberculosis: laboratory methods. *American Journal of Public Health*, *48*(7), 844–853. https://doi.org/10.2105/ajph.48.7.844

Migliori, G. B., Centis, R., D'Ambrosio, L., Spanevello, A., Borroni, E., Cirillo, D. M., & Sotgiu, G. (2012). Totally drug-resistant and extremely drug-resistant tuberculosis: The same

disease? In *Clinical Infectious Diseases* (Vol. 54, Issue 9, pp. 1379–1380). Oxford Academic. https://doi.org/10.1093/cid/cis128

Migliori, G. B., Loddenkemper, R., Blasi, F., & Raviglione, M. C. (2007). 125 years after Robert Koch's discovery of the tubercle bacillus: The new XDR-TB threat. Is "science" enough to tackle the epidemic? In *European Respiratory Journal* (Vol. 29, Issue 3, pp. 423–427). https://doi.org/10.1183/09031936.00001307

Mikušová, K., Mikuš, M., Besra, G. S., Hancock, I., & Brennan, P. J. (1996). Biosynthesis of the linkage region of the mycobacterial cell wall. *Journal of Biological Chemistry*, *271*(13), 7820–7828. https://doi.org/10.1074/jbc.271.13.7820

Miller, J. L., Velmurugan, K., Cowan, M. J., & Briken, V. (2010). The type I NADH dehydrogenase of Mycobacterium tuberculosis counters phagosomal NOX2 activity to inhibit TNF-α-mediated host cell apoptosis. *PLoS Pathogens*, *6*(4), 1–14. https://doi.org/10.1371/journal.ppat.1000864

Minato, Y., Thiede, J. M., Kordus, S. L., McKlveen, E. J., Turman, B. J., & Baughn, A. D. (2015). Mycobacterium tuberculosis folate metabolism and the mechanistic basis for para-aminosalicylic acid susceptibility and resistance. In *Antimicrobial Agents and Chemotherapy* (Vol. 59, Issue 9, pp. 5097–5106). https://doi.org/10.1128/AAC.00647-15

Minnikin, D. (1982). Lipids: Complex lipids, their chemistry, biosynthesis, and roles. The Biology of the Mycobacteria, eds Ratledge C. *Stanford Academic*.

Minnikin, D. E., Kremer, L., Dover, L. G., & Besra, G. S. (2002). The methyl-branched fortifications of Mycobacterium tuberculosis. In *Chemistry and Biology* (Vol. 9, Issue 5, pp. 545–553). Cell Press. https://doi.org/10.1016/S1074-5521(02)00142-4

Miyazaki, E., Chaisson, R. E., & Bishai, W. R. (1999). Analysis of rifapentine for preventive therapy in the Cornell mouse model of latent tuberculosis. *Antimicrobial Agents and Chemotherapy*, *43*(9), 2126–2130. https://doi.org/10.1128/aac.43.9.2126

Modongo, C., Sobota, R. S., Kesenogile, B., Ncube, R., Sirugo, G., Williams, S. M., & Zetola, N. M. (2014). Successful MDR-TB treatment regimens including Amikacin are associated with high rates of hearing loss. *BMC Infectious Diseases*, *14*(1). https://doi.org/10.1186/1471-2334-14-542

Moghazeh, S. L., Pan, X., Arain, T., Stover, C. K., Musser, J. M., & Kreiswirth, B. N. (1996). Comparative antimycobacterial activities of rifampin, rifapentine, and KRM-1648 against a collection of rifampin-resistant Mycobacterium tuberculosis isolates with known rpoB mutations. *Antimicrobial Agents and Chemotherapy*, *40*(11), 2655–2657. https://doi.org/10.1128/aac.40.11.2655

Moore, M., & Frerichs, J. B. (1953). An unusual acid-fast infection of the knee with subcutaneous, abscess-like lesions of the gluteal region; report of a case with a study of the organism, Mycobacterium abscessus, n. sp. *The Journal of Investigative Dermatology*, *20*(2), 133–169. https://doi.org/10.1038/jid.1953.18

Mugumbate, G., Abrahams, K. A., Cox, J. A. G., Papadatos, G., Van Westen, G., Lelièvre, J., Calus, S. T., Loman, N. J., Ballell, L., Barros, D., Overington, J. P., & Besra, G. S. (2015). Mycobacterial dihydrofolate reductase inhibitors identified using chemogenomic methods and in vitro validation. *PLoS ONE*, *10*(3), e0121492. https://doi.org/10.1371/journal.pone.0121492

Munje, R., Deshmukh, R., & Tumane, K. (2015). Multidrug-resistant TB among previously treated TB cases: A retrospective study in Nagpur, India. *Indian Journal of Tuberculosis*, *62*(4), 207–210. https://doi.org/10.1016/j.ijtb.2015.11.002

Muñoz-Elías, E. J., & McKinney, J. D. (2005). Mycobacterium tuberculosis isocitrate lyases 1 and 2 are jointly required for in vivo growth and virulence. *Nature Medicine*, *11*(6), 638–644. https://doi.org/10.1038/nm1252

Muñoz-Elías, E. J., Upton, A. M., Cherian, J., & McKinney, J. D. (2006). Role of the methylcitrate cycle in Mycobacterium tuberculosis metabolism, intracellular growth, and

virulence. *Molecular Microbiology*, *60*(5), 1109–1122. https://doi.org/10.1111/j.1365-2958.2006.05155.x

Murugasu-Oei, B., & Dick, T. (2000). Bactericidal activity of nitrofurans against growing and dormant Mycobacterium bovis BCG. *Journal of Antimicrobial Chemotherapy*, *46*(6), 917–919. https://doi.org/10.1093/jac/46.6.917

Muttucumaru, D. G. N., Roberts, G., Hinds, J., Stabler, R. A., & Parish, T. (2004). Gene expression profile of Mycobacterium tuberculosis in a non-replicating state. *Tuberculosis*, *84*(3–4), 239–246. https://doi.org/10.1016/j.tube.2003.12.006

Nakata, N., Kai, M., & Makino, M. (2011). Mutation analysis of the Mycobacterium leprae folP1 gene and dapsone resistance. *Antimicrobial Agents and Chemotherapy*, *55*(2), 762–766. https://doi.org/10.1128/AAC.01212-10

Neijssel, O. M., & Tempest, D. W. (1976). Bioenergetic aspects of aerobic growth of Klebsiella aerogenes NCTC 418 in carbon-limited and carbon-sufficient chemostat culture. *Archives of Microbiology*, *107*(2), 215–221. https://doi.org/10.1007/BF00446843

Nesbitt, N. M., Yang, X., Fontán, P., Kolesnikova, I., Smith, I., Sampson, N. S., & Dubnau, E. (2010). A thiolase of Mycobacterium tuberculosis is required for virulence and production of androstenedione and androstadienedione from cholesterol. *Infection and Immunity*, *78*(1), 275–282. https://doi.org/10.1128/IAI.00893-09

Nessar, R., Cambau, E., Reyrat, J. M., Murray, A., & Gicquel, B. (2012). Mycobacterium abscessus: A new antibiotic nightmare. *Journal of Antimicrobial Chemotherapy*, *67*(4), 810–818. https://doi.org/10.1093/jac/dkr578

Ng, V. H., Cox, J. S., Sousa, A. O., MacMicking, J. D., & McKinney, J. D. (2004). Role of KatG catalase-peroxidase in mycobacterial pathogenisis: Countering the phagocyte oxidative burst. *Molecular Microbiology*, *52*(5), 1291–1302. https://doi.org/10.1111/j.1365-2958.2004.04078.x

Nguyen, L., & Pieters, J. (2005). The Trojan horse: Survival tactics of pathogenic mycobacteria in macrophages. In *Trends in Cell Biology* (Vol. 15, Issue 5, pp. 269–276). Elsevier Ltd. https://doi.org/10.1016/j.tcb.2005.03.009

Niederweis, M., Danilchanka, O., Huff, J., Hoffmann, C., & Engelhardt, H. (2010). Mycobacterial outer membranes: in search of proteins. In *Trends in Microbiology* (Vol. 18, Issue 3, pp. 109–116). Elsevier Current Trends. https://doi.org/10.1016/j.tim.2009.12.005

Novosad, S. A., Beekmann, S. E., Polgreen, P. M., Mackey, K., & Winthrop, K. L. (2016). Treatment of mycobacterium abscessus infection. *Emerging Infectious Diseases*, *22*(3), 511–514. https://doi.org/10.3201/eid2203.150828

Nunn, J. F., & Tapp, E. (2000). Tropical diseases in Ancient Egypt. *Transactions of the Royal Society of Tropical Medicine and Hygiene*, *94*(2), 147–153. https://doi.org/10.1016/s0035-9203(00)90252-9

Ohno, H., Koga, H., Kohno, S., Tashiro, T., & Hara, K. (1996). Relationship between rifampin MICs for and rpoB mutations of Mycobacterium tuberculosis strains isolated in Japan. In *Antimicrobial Agents and Chemotherapy* (Vol. 40, Issue 4, pp. 1053–1056). https://doi.org/10.1128/aac.40.4.1053

Oprian, D. D., & Coon, M. J. (1982). Oxidation-reduction states of FMN and FAD in NADPH-cytochrome P-450 reductase during reduction by NADPH. *Journal of Biological Chemistry*, *257*(15), 8935–8944. https://doi.org/10.1016/s0021-9258(18)34223-6

Orme, I. M. (2003). The mouse as a useful model of tuberculosis. *Tuberculosis*, *83*(1–3), 112–115. https://doi.org/10.1016/S1472-9792(02)00069-0

Pandey, A. K., & Sassetti, C. M. (2008). Mycobacterial persistence requires the utilization of host cholesterol. *Proceedings of the National Academy of Sciences of the United States of America*, *105*(11), 4376–4380. https://doi.org/10.1073/pnas.0711159105

Parish, T. (2020). In vitro drug discovery models for Mycobacterium tuberculosis relevant for host infection. In *Expert Opinion on Drug Discovery* (Vol. 15, Issue 3, pp. 349–358). Taylor and Francis Ltd. https://doi.org/10.1080/17460441.2020.1707801

Parish, T., & Stoker, N. G. (1999). Mycobacteria: Bugs and bugbears (two steps forward and one step back). In *Applied Biochemistry and Biotechnology - Part B Molecular Biotechnology* (Vol. 13, Issue 3, pp. 191–200). Humana Press. https://doi.org/10.1385/MB:13:3:191

Parish, T., Stoker, N. G., & Wayne, L. G. (2003). In Vitro Model of Hypoxically Induced Nonreplicating Persistence of Mycobacterium tuberculosis. In *Mycobacterium Tuberculosis Protocols* (pp. 247–269). Humana Press. https://doi.org/10.1385/1-59259-147-7:247

Park, H. D., Guinn, K. M., Harrell, M. I., Liao, R., Voskuil, M. I., Tompa, M., Schoolnik, G. K., & Sherman, D. R. (2003). Rv3133c/dosR is a transcription factor that mediates the hypoxic response of Mycobacterium tuberculosis. *Molecular Microbiology*, *48*(3), 833–843. https://doi.org/10.1046/j.1365-2958.2003.03474.x

Parveen, U., Sultana, S., Heba, S. F., Rafi, R., Begum, A., & Fatima, N. (2020). Pretomanid: A novel therapeutic paradigm for treatment of drug resistant tuberculosis. In *Indian Journal of Tuberculosis*. https://doi.org/10.1016/j.ijtb.2020.09.005

Patel, K., Jhamb, S. S., & Singh, P. P. (2011). Models of Latent Tuberculosis: Their Salient Features, Limitations, and Development. *Journal of Laboratory Physicians*, *3*(02), 075–079. https://doi.org/10.4103/0974-2727.86837

Pietersen, R. D., du Preez, I., Loots, D. T., van Reenen, M., Beukes, D., Leisching, G., & Baker, B. (2020). Tween 80 induces a carbon flux rerouting in Mycobacterium tuberculosis. *Journal of Microbiological Methods*, *170*. https://doi.org/10.1016/j.mimet.2019.105795

Pontali, E., Raviglione, M. C., Migliori, G. B., Akkerman, O. W., Alffenaar, J. W., Blanc, F. X., Borisov, S., Cirillo, D. M., Dalcolmo, M., Dheda, K., Kritski, A. L., Lienhardt, C., Olliaro, P., Tadolini, M., Tiberi, S., & Udwadia, Z. (2019). Regimens to treat multidrug-resistant tuberculosis: Past, present and future perspectives. In *European Respiratory Review* (Vol. 28, Issue 152). https://doi.org/10.1183/16000617.0035-2019

Prasad, R. (2010). Multidrug and extensively drug-resistant TB (M/XDR-Tb): Problems and solutions. *Indian Journal of Tuberculosis*, *57*(4), 180–191.

Ramakrishnan, L. (2012). Revisiting the role of the granuloma in tuberculosis. In *Nature Reviews Immunology* (Vol. 12, Issue 5, pp. 352–366). Nature Publishing Group. https://doi.org/10.1038/nri3211

Raymond, J. B., Mahapatra, S., Crick, D. C., & Pavelka, M. S. (2005). Identification of the namH gene, encoding the hydroxylase responsible for the N-glycolylation of the mycobacterial peptidoglycan. *Journal of Biological Chemistry*, *280*(1), 326–333. https://doi.org/10.1074/jbc.M411006200

Regev, O., & Zana, R. (1999). Aggregation behavior of tyloxapol, a nonionic surfactant oligomer, in aqueous solution. *Journal of Colloid and Interface Science*, *210*(1), 8–17. https://doi.org/10.1006/jcis.1998.5776

Rhoades, E. R. (1997). Progression of chronic pulmonary tuberculosis in mice aerogenically infected with virulent Mycobacterium tuberculosis. *Tubercle and Lung Disease*, *78*(1), 57–66. https://doi.org/10.1016/S0962-8479(97)90016-2

Rozwarski, D. A., Grant, G. A., Barton, D. H. R., Jacobs, W. R., & Sacchettini, J. C. (1998). Modification of the NADH of the isoniazid target (InhA) from Mycobacterium tuberculosis. *Science*, *279*(5347), 98–102. https://doi.org/10.1126/science.279.5347.98

Russell, D. G., Cardona, P. J., Kim, M. J., Allain, S., & Altare, F. (2009a). Foamy macrophages and the progression of the human tuberculosis granuloma. In *Nature*

Immunology (Vol. 10, Issue 9, pp. 943–948). NIH Public Access. https://doi.org/10.1038/ni.1781

Russell, D. G., Cardona, P. J., Kim, M. J., Allain, S., & Altare, F. (2009b). Foamy macrophages and the progression of the human tuberculosis granuloma. In *Nature Immunology* (Vol. 10, Issue 9, pp. 943–948). Nature Publishing Group. https://doi.org/10.1038/ni.1781

Rustad, T. R., Sherrid, A. M., & Sherman, D. R. (2017). Molecular Mechanisms of Dormancy and Resuscitation. In *Handbook of Tuberculosis* (pp. 287–306). Wiley-VCH Verlag GmbH & Co. KGaA. https://doi.org/10.1002/9783527611614.ch13

Sakamoto, K. (2012). The Pathology of Mycobacterium tuberculosis Infection. In *Veterinary Pathology* (Vol. 49, Issue 3, pp. 423–439). SAGE PublicationsSage CA: Los Angeles, CA. https://doi.org/10.1177/0300985811429313

Sala, C., Dhar, N., Hartkoorn, R. C., Zhang, M., Ha, Y. H., Schneider, P., & Cole, S. T. (2010). Simple model for testing drugs against nonreplicating Mycobacterium tuberculosis. *Antimicrobial Agents and Chemotherapy*, *54*(10), 4150–4158. https://doi.org/10.1128/AAC.00821-10

Santucci, P., Bouzid, F., Smichi, N., Poncin, I., Kremer, L., De Chastellier, C., Drancourt, M., & Canaan, S. (2016). Experimental models of foamy macrophages and approaches for dissecting the mechanisms of lipid accumulation and consumption during dormancy and reactivation of tuberculosis. In *Frontiers in Cellular and Infection Microbiology* (Vol. 6, Issue OCT). Frontiers Media S.A. https://doi.org/10.3389/fcimb.2016.00122

Santucci, P., Johansen, M. D., Point, V., Poncin, I., Viljoen, A., Cavalier, J. F., Kremer, L., & Canaan, S. (2019). Nitrogen deprivation induces triacylglycerol accumulation, drug tolerance and hypervirulence in mycobacteria. *Scientific Reports*, *9*(1). https://doi.org/10.1038/s41598-019-45164-5

Sarker, S. D., Nahar, L., & Kumarasamy, Y. (2007). Microtitre plate-based antibacterial assay incorporating resazurin as an indicator of cell growth, and its application in the in vitro antibacterial screening of phytochemicals. *Methods*, *42*(4), 321–324. https://doi.org/10.1016/j.ymeth.2007.01.006

Sassetti, C. M., Boyd, D. H., & Rubin, E. J. (2003). Genes required for mycobacterial growth defined by high density mutagenesis. *Molecular Microbiology*, *48*(1), 77–84. https://doi.org/10.1046/j.1365-2958.2003.03425.x

Savvi, S., Warner, D. F., Kana, B. D., McKinney, J. D., Mizrahi, V., & Dawes, S. S. (2008). Functional characterization of a vitamin B12-dependent methylmalonyl pathway in Mycobacterium tuberculosis: Implications for propionate metabolism during growth on fatty acids. *Journal of Bacteriology*, *190*(11), 3886–3895. https://doi.org/10.1128/JB.01767-07

Schaible, U. E., Sturgill-Koszycki, S., Schlesinger, P. H., & Russell, D. G. (1998). Cytokine activation leads to acidification and increases maturation of Mycobacterium avium-containing phagosomes in murine macrophages. *Journal of Immunology (Baltimore, Md. : 1950)*, *160*(3), 1290–1296.

Schatz, A., Bugle, E., & Waksman, S. A. (1944). Streptomycin, a Substance Exhibiting Antibiotic Activity Against Gram-Positive and Gram-Negative Bacteria. *Proceedings of the Society for Experimental Biology and Medicine*, *55*(1), 66–69. https://doi.org/10.3181/00379727-55-14461

Schatz, A., & Waksman, S. A. (1944). Effect of Streptomycin and Other Antibiotic Substances upon Mycobacterium tuberculosis and Related Organisms. *Proceedings of the Society for Experimental Biology and Medicine*, *57*(2), 244–248. https://doi.org/10.3181/00379727-57-14769

Schecter, G. F., Scott, C., True, L., Raftery, A., Flood, J., & Mase, S. (2010). Linezolid in the treatment of multidrug-resistant tuberculosis. *Clinical Infectious Diseases*, *50*(1), 49–55. https://doi.org/10.1086/648675

Schoonmaker, M. K., Bishai, W. R., & Lamichhanea, G. (2014). Nonclassical transpeptidases of Mycobacterium tuberculosis alter cell size, morphology, the cytosolic matrix, protein localization, virulence, and resistance to β-lactams. *Journal of Bacteriology*, *196*(7), 1394–1402. https://doi.org/10.1128/JB.01396-13

Schuurbiers, M. M. F., Bruno, M., Zweijpfenning, S. M. H., Magis-Escurra, C., Boeree, M., Netea, M. G., van Ingen, J., van de Veerdonk, F., & Hoefsloot, W. (2020). Immune defects in patients with pulmonary Mycobacterium abscessus disease without cystic fibrosis. *ERJ Open Research*, *6*(4), 00590–02020. https://doi.org/10.1183/23120541.00590-2020

Shen, G. H., Wu, B. Da, Hu, S. T., Lin, C. F., Wu, K. M., & Chen, J. H. (2010). High efficacy of clofazimine and its synergistic effect with amikacin against rapidly growing mycobacteria. *International Journal of Antimicrobial Agents*, *35*(4), 400–404. https://doi.org/10.1016/j.ijantimicag.2009.12.008

Sherman, D. R., Voskuil, M., Schnappinger, D., Liao, R., Harrell, M. I., & Schoolnik, G. K. (2001). Regulation of the mycobacterium tuberculosis hypoxic response gene encoding α-crystallin. *Proceedings of the National Academy of Sciences of the United States of America*, *98*(13), 7534–7539. https://doi.org/10.1073/pnas.121172498

Shigyo, K., Ocheretina, O., Merveille, Y. M., Johnson, W. D., Pape, J. W., Nathan, C. F., & Fitzgerald, D. W. (2013). Efficacy of nitazoxanide against clinical isolates of Mycobacterium tuberculosis. *Antimicrobial Agents and Chemotherapy*, *57*(6), 2834–2837. https://doi.org/10.1128/AAC.02542-12

Siu, G. K. H., Zhang, Y., Lau, T. C. K., Lau, R. W. T., Ho, P. L., Yew, W. W., Tsui, S. K. W., Cheng, V. C. C., Yuen, K. Y., & Yam, W. C. (2011). Mutations outside the rifampicin

resistance-determining region associated with rifampicin resistance in Mycobacterium tuberculosis. *Journal of Antimicrobial Chemotherapy*, *66*(4), 730–733. https://doi.org/10.1093/jac/dkq519

Slayden, R. A., & Barry, C. E. (2000). The genetics and biochemistry of isoniazid resistance in Mycobacterium tuberculosis. In *Microbes and Infection* (Vol. 2, Issue 6, pp. 659–669). https://doi.org/10.1016/S1286-4579(00)00359-2

Smith, C. S., Aerts, A., Saunderson, P., Kawuma, J., Kita, E., & Virmond, M. (2017). Multidrug therapy for leprosy: a game changer on the path to elimination. In *The Lancet Infectious Diseases* (Vol. 17, Issue 9, pp. e293–e297). https://doi.org/10.1016/S1473-3099(17)30418-8

Snewin, V. A., Gares, M. P., Ó Gaora, P., Hasan, Z., Brown, I. N., & Young, D. B. (1999). Assessment of immunity to mycobacterial infection with luciferase reporter constructs. *Infection and Immunity*, *67*(9), 4586–4593. https://doi.org/10.1128/iai.67.9.4586-4593.1999

Sohaskey, C. D. (2008). Nitrate enhances the survival of Mycobacterium tuberculosis during inhibition of respiration. *Journal of Bacteriology*, *190*(8), 2981–2986. https://doi.org/10.1128/JB.01857-07

Somoskovi, A., Parsons, L. M., & Salfinger, M. (2001). The molecular basis of resistance to isoniazid, rifampin, and pyrazinamide in Mycobacterium tuberculosis. In *Respiratory Research* (Vol. 2, Issue 3, pp. 164–168). https://doi.org/10.1186/rr54

Soto-Ramirez, M. D., Aguilar-Ayala, D. A., Garcia-Morales, L., Rodriguez-Peredo, S. M., Badillo-Lopez, C., Rios-Muñiz, D. E., Meza-Segura, M. A., Rivera-Morales, G. Y., Leon-Solis, L., Cerna-Cortes, J. F., Rivera-Gutierrez, S., Helguera-Repetto, A. C., & Gonzalez-y-Merchand, J. A. (2017). Cholesterol plays a larger role during Mycobacterium tuberculosis in vitro dormancy and reactivation than previously suspected. *Tuberculosis*, *103*, 1–9. https://doi.org/10.1016/j.tube.2016.12.004

Spigelman, M., & Gillespie, S. (2006). Tuberculosis drug development pipeline: Progress and hope. In *Lancet* (Vol. 367, Issue 9514, pp. 945–947). https://doi.org/10.1016/S0140-6736(06)68388-8

Spotts, C. R., & Stanier, R. Y. (1961). Mechanism of streptomycin action on bacteria: A unitary hypothesis. *Nature*, *192*(4803), 633–637. https://doi.org/10.1038/192633a0

Sreevatsan, S., Stockbauer, K. E., Pan, X., Kreiswirth, B. N., Moghazeh, S. L., Jacobs, W. R., Telenti, A., & Musser, J. M. (1997). Ethambutol resistance in Mycobacterium tuberculosis: Critical role of embB mutations. *Antimicrobial Agents and Chemotherapy*, *41*(8), 1677–1681. https://doi.org/10.1128/aac.41.8.1677

Strouhal, E. (1976). Tumors in the remains of Ancient Egyptians. *American Journal of Physical Anthropology*, *45*(3), 613–620. https://doi.org/10.1002/ajpa.1330450328

Sumitani, M., Takagi, S., Tanamura, Y., & Inoue, H. (2004). Oxygen indicator composed of an organic/inorganic hybrid compound of methylene blue, reductant, surfactant and saponite. *Analytical Sciences*, *20*(8), 1153–1157. https://doi.org/10.2116/analsci.20.1153

Sutherland, L., Singleton, J., Sessions, J., Hanauer, S., Krawitt, E., Rankin, G., Summers, R., Mekhjian, H., Greenberger, N., Kelly, M., Levine, J., Thomson, A., Alpert, E., & Prokipchuk, E. (1991). Double blind, placebo controlled trial of metronidazole in Crohn's disease. *Gut*, *32*(9), 1071–1075. https://doi.org/10.1136/gut.32.9.1071

Szaleniec, M., Wojtkiewicz, A. M., Bernhardt, R., Borowski, T., & Donova, M. (2018). Bacterial steroid hydroxylases: enzyme classes, their functions and comparison of their catalytic mechanisms. In *Applied Microbiology and Biotechnology* (Vol. 102, Issue 19, pp. 8153–8171). Springer Verlag. https://doi.org/10.1007/s00253-018-9239-3

Tak, J. D. (1942). On bacteria decomposing cholesterol. *Antonie van Leeuwenhoek*, *8*(1), 32–40. https://doi.org/10.1007/BF02272764

Takayama, K., & Kilburn, J. O. (1989). Inhibition of synthesis of arabinogalactan by ethambutol in Mycobacterium smegmatis. *Antimicrobial Agents and Chemotherapy*, *33*(9), 1493–1499. https://doi.org/10.1128/AAC.33.9.1493

Takei, S., Ihara, H., Togo, S., Nakamura, A., Fujimoto, Y., Watanabe, J., Kurokawa, K., Shibayama, K., Sumiyoshi, I., Ochi, Y., Iwai, M., Okabe, T., Chonan, M., Misawa, S., Ohsaka, A., & Takahashi, K. (2020). The synergetic effect of Imipenem-clarithromycin combination in the Mycobacteroides abscessus complex. *BMC Microbiology*, *20*(1). https://doi.org/10.1186/s12866-020-02000-5

Takeuchi, O., Hoshino, K., Kawai, T., Sanjo, H., Takada, H., Ogawa, T., Takeda, K., & Akira, S. (1999). Differential roles of TLR2 and TLR4 in recognition of gram-negative and gram-positive bacterial cell wall components. *Immunity*, *11*(4), 443–451. https://doi.org/10.1016/S1074-7613(00)80119-3

Taneja, N. K., & Tyagi, J. S. (2007). Resazurin reduction assays for screening of anti-tubercular compounds against dormant and actively growing Mycobacterium tuberculosis, Mycobacterium bovis BCG and Mycobacterium smegmatis. *Journal of Antimicrobial Chemotherapy*, *60*(2), 288–293. https://doi.org/10.1093/jac/dkm207

Teasley, D. G., Olson, M. M., Gebhard, R. L., Gerding, D. N., Peterson, L. R., Schwartz, M. J., & Lee, J. T. (1983). PROSPECTIVE RANDOMISED TRIAL OF METRONIDAZOLE VERSUS VANCOMYCIN FOR CLOSTRIDIUM-DIFFICILE-ASSOCIATED DIARRHOEA AND COLITIS. *The Lancet*, *322*(8358), 1043–1046. https://doi.org/10.1016/S0140-6736(83)91036-X

Telenti, A., Imboden, P., Marchesi, F., Matter, L., Schopfer, K., Bodmer, T., Lowrie, D., Colston, M. J., & Cole, S. (1993). Detection of rifampicin-resistance mutations in Mycobacterium tuberculosis. *The Lancet*, *341*(8846), 647–651. https://doi.org/10.1016/0140-6736(93)90417-F

Telenti, A., Philipp, W. J., Sreevatsan, S., Bernasconi, C., Stockbauer, K. E., Wieles, B., Musser, J. M., & Jacobs, W. R. (1997). The emb operon, a gene cluster of Mycobacterium tuberculosis involved in resistance to ethambutol. *Nature Medicine*, *3*(5), 567–570. https://doi.org/10.1038/nm0597-567

Timmins, G. S., & Deretic, V. (2006). Mechanisms of action of isoniazid. In *Molecular Microbiology* (Vol. 62, Issue 5, pp. 1220–1227). John Wiley & Sons, Ltd. https://doi.org/10.1111/j.1365-2958.2006.05467.x

Tomas Vert, F., Medina Casamayor, P., Olba Torrent, A., & Monzo Mansanet, I. S. (1987). The fluorescence and phosphorescence spectra of dimethylphenol at 77 K. *Journal of Photochemistry*, *40*(1), 59–65. https://doi.org/10.1016/0047-2670(87)87044-2

Trutneva, K. A., Shleeva, M. O., Demina, G. R., Vostroknutova, G. N., & Kaprelyans, A. S. (2020). One-Year Old Dormant, “Non-culturable” Mycobacterium tuberculosis Preserves Significantly Diverse Protein Profile. *Frontiers in Cellular and Infection Microbiology*, *10*. https://doi.org/10.3389/fcimb.2020.00026

Tuomanen, E., Cozens, R., Tosch, W., Zak, O., & Tomasz, A. (1986). The rate of killing of Escherichia coli by β-lactam antibiotics is strictly proportional to the rate of bacterial growth. *Journal of General Microbiology*, *132*(5), 1297–1304. https://doi.org/10.1099/00221287-132-5-1297

Ursing, B., & Kamme, C. (1975). METRONIDAZOLE FOR CROHN’S DISEASE. *The Lancet*, *305*(7910), 775–777. https://doi.org/10.1016/S0140-6736(75)92438-1

van Andel, J. G., Zoutberg, G. R., Crabbendam, P. M., & Breure, A. M. (1985). Glucose fermentation by Clostridium butyricum grown under a self generated gas atmosphere in chemostat culture. *Applied Microbiology and Biotechnology*, *23*(1), 21–26. https://doi.org/10.1007/BF02660113

van Berkel, W. J. H., Kamerbeek, N. M., & Fraaije, M. W. (2006). Flavoprotein monooxygenases, a diverse class of oxidative biocatalysts. In *Journal of Biotechnology* (Vol. 124, Issue 4, pp. 670–689). Elsevier. https://doi.org/10.1016/j.jbiotec.2006.03.044

Van De Kerkhof, P. C. M. (1994). On the efficacy of dapsone in granuloma faciale. *Acta Dermato-Venereologica*, *74*(1), 61–62. https://doi.org/10.2340/00015555746162

van der Geize, R., Yam, K., Heuser, T., Wilbrink, M. H., Hara, H., Anderton, M. C., Sim, E., Dijkhuizen, L., Davies, J. E., Mohn, W. W., & Eltis, L. D. (2007). A gene cluster encoding cholesterol catabolism in a soil actinomycete provides insight into Mycobacterium tuberculosis survival in macrophages. *Proceedings of the National Academy of Sciences of the United States of America*, *104*(6), 1947–1952. https://doi.org/10.1073/pnas.0605728104

Vandal, O. H., Nathan, C. F., & Ehrt, S. (2009). Acid resistance in Mycobacterium tuberculosis. In *Journal of Bacteriology* (Vol. 191, Issue 15, pp. 4714–4721). American Society for Microbiology Journals. https://doi.org/10.1128/JB.00305-09

Veatch, A. V., & Kaushal, D. (2018). Opening Pandora's Box: Mechanisms of Mycobacterium tuberculosis Resuscitation. In *Trends in Microbiology* (Vol. 26, Issue 2, pp. 145–157). https://doi.org/10.1016/j.tim.2017.08.001

Velayati, A. A., Farnia, P., Masjedi, M. R., Zhavnerko, G. K., Merza, M. A., Ghanavi, J., Tabarsi, P., Farnia, P., Poleschuyk, N. N., & Ignatyev, G. (2011). Sequential adaptation in latent tuberculosis bacilli: Observation by atomic force microscopy (AFM). *International Journal of Clinical and Experimental Medicine*, *4*(3), 193–199.

Velmurugan, K., Chen, B., Miller, J. L., Azogue, S., Gurses, S., Hsu, T., Glickman, M., Jacobs, W. R., Porcelli, S. A., & Briken, V. (2007). Mycobacterium tuberculosis nuoG Is a virulence gene that inhibits apoptosis of infected host cells. *PLoS Pathogens*, *3*(7), 0972–0980. https://doi.org/10.1371/journal.ppat.0030110

Verrastro, I., Tveen-Jensen, K., Woscholski, R., Spickett, C. M., & Pitt, A. R. (2016). Reversible oxidation of phosphatase and tensin homolog (PTEN) alters its interactions with signaling and regulatory proteins. *Free Radical Biology and Medicine*, *90*, 24–34. https://doi.org/10.1016/j.freeradbiomed.2015.11.004

Vilchèze, C., & Jacobs, Jr., W. R. (2007). The Mechanism of Isoniazid Killing: Clarity Through the Scope of Genetics. *Annual Review of Microbiology*, *61*(1), 35–50. https://doi.org/10.1146/annurev.micro.61.111606.122346

Vla, L. E., Frattl, R. A., McFalone, M., Pagán-Ramos, E., Deretic, D., & Deretic, V. (1998). Effects of cytokines on mycobacterial phagosome maturation. *Journal of Cell Science*, *111*(7), 897–905.

Voskuil, M. I., Visconti, K. C., & Schoolnik, G. K. (2004). Mycobacterium tuberculosis gene expression during adaptation to stationary phase and low-oxygen dormancy. *Tuberculosis*, *84*(3–4), 218–227. https://doi.org/10.1016/j.tube.2004.02.003

Walker, G. C., & Nicholas, D. J. D. (1961). Nitrite reductase from Pseudomonas aeruginosa. *BBA - Biochimica et Biophysica Acta*, *49*(2), 350–360. https://doi.org/10.1016/0006-3002(61)90134-2

Wayne, L. G. (1994). Dormancy of Mycobacterium tuberculosis and latency of disease. In *European Journal of Clinical Microbiology & Infectious Diseases* (Vol. 13, Issue 11, pp. 908–914). Springer-Verlag. https://doi.org/10.1007/BF02111491

Wayne, L. G., & Hayes, L. G. (1996). An in vitro model for sequential study of shiftdown of Mycobacterium tuberculosis through two stages of nonreplicating persistence. *Infection and Immunity*, *64*(6), 2062–2069. https://doi.org/10.1128/iai.64.6.2062-2069.1996

Wayne, L. G., & Hayes, L. G. (1998). Nitrate reduction as a marker for hypoxic shiftdown of Mycobacterium tuberculosis. *Tubercle and Lung Disease*, *79*(2), 127–132. https://doi.org/10.1054/tuld.1998.0015

Wayne, L. G., & Sohaskey, C. D. (2001). Nonreplicating Persistence of Mycobacterium Tuberculosis. *Annual Review of Microbiology*, *55*(1), 139–163. https://doi.org/10.1146/annurev.micro.55.1.139

Wayne, L. G., & Sramek, H. A. (1994). Metronidazole is bactericidal to dormant cells of Mycobacterium tuberculosis. *Antimicrobial Agents and Chemotherapy*, *38*(9), 2054–2058. https://doi.org/10.1128/AAC.38.9.2054

Wehrli, W. (1983). Rifampin: Mechanisms of action and resistance. *Reviews of Infectious Diseases*, *5*, S407–S411. https://doi.org/10.1093/clinids/5.Supplement_3.S407

Wehrli, W., Knüsel, F., Schmid, K., & Staehelin, M. (1968). Interaction of rifamycin with bacterial RNA polymerase. *Proceedings of the National Academy of Sciences of the United States of America*, *61*(2), 667–673. https://doi.org/10.1073/pnas.61.2.667

White, R. E. (2000). High-throughput screening in drug metabolism and pharmacokinetic support of drug discovery. In *Annual Review of Pharmacology and Toxicology* (Vol. 40, pp. 133–157). https://doi.org/10.1146/annurev.pharmtox.40.1.133

WHO. (2017). Treatment of Tuberculosis: Guidelines for treatment of drug-susceptible tuberculosis and patient care. 2017 update. In *WHO*.

WHO. (2020). WHO | Global tuberculosis report 2019. *WHO*.

Wilburn, K. M., Fieweger, R. A., & VanderVen, B. C. (2018). Cholesterol and fatty acids grease the wheels of Mycobacterium tuberculosis pathogenesis. In *Pathogens and disease* (Vol. 76, Issue 2, p. 21). Oxford Academic. https://doi.org/10.1093/femspd/fty021

Williams, D. L., Spring, L., Harris, E., Roche, P., & Gillis, T. P. (2000). Dihydropteroate synthase of Mycobacterium leprae and dapsone resistance. *Antimicrobial Agents and Chemotherapy*, *44*(6), 1530–1537. https://doi.org/10.1128/AAC.44.6.1530-1537.2000

Wipperman, M. F., Sampson, N. S., & Thomas, S. T. (2014). Pathogen roid rage: Cholesterol utilization by Mycobacterium tuberculosis. In *Critical Reviews in Biochemistry and Molecular Biology* (Vol. 49, Issue 4, pp. 269–293). Informa Healthcare. https://doi.org/10.3109/10409238.2014.895700

Wolf, A. J., Linas, B., Trevejo-Nuñez, G. J., Kincaid, E., Tamura, T., Takatsu, K., & Ernst, J. D. (2007). Mycobacterium tuberculosis Infects Dendritic Cells with High Frequency and Impairs Their Function In Vivo. *The Journal of Immunology*, *179*(4), 2509–2519. https://doi.org/10.4049/jimmunol.179.4.2509

World Health Organization. (1999). What is DOTS ? A Guide to Understanding the WHO-recommended TB Control Strategy Known as DOTS. In *Prevention and Control*.

World Health Organization. (2012). WHO Expert Committee on Leprosy. In *World Health Organization technical report series* (Issue 968).

World Health Organization. (2015). Implementing the End TB Strategy: The Essentials. *Who*, 1–130. https://doi.org/10.1017/CBO9781107415324.004

World Health Organization. (2019). Consolidated Guidelines on Tuberculosis Treatment. *WHO*.

Wozel, G., & Blasum, C. (2014). Dapsone in dermatology and beyond. In *Archives of Dermatological Research* (Vol. 306, Issue 2, pp. 103–124). https://doi.org/10.1007/s00403-013-1409-7

Xu, H. B., Jiang, R. H., & Xiao, H. P. (2012). Clofazimine in the treatment of multidrug-resistant tuberculosis. *Clinical Microbiology and Infection*, *18*(11), 1104–1110. https://doi.org/10.1111/j.1469-0691.2011.03716.x

Yeware, A., & Sarkar, D. (2018). Novel red fluorescence protein based microplate assay for drug screening against dormant Mycobacterium tuberculosis by using paraffin. *Tuberculosis*, *110*, 15–19. https://doi.org/10.1016/j.tube.2018.02.008

Yuan, Y., Crane, D. D., Simpson, R. M., Zhu, Y., Hickey, M. J., Sherman, D. R., & Barry, C. E. (1998). The 16-kDa α-crystallin (Acr) protein of Mycobacterium tuberculosis is required for growth in macrophages. *Proceedings of the National Academy of Sciences of the United States of America*, *95*(16), 9578–9583. https://doi.org/10.1073/pnas.95.16.9578

Zedelius, J., Rabus, R., Grundmann, O., Werner, I., Brodkorb, D., Schreiber, F., Ehrenreich, P., Behrends, A., Wilkes, H., Kube, M., Reinhardt, R., & Widdel, F. (2011). Alkane degradation under anoxic conditions by a nitrate-reducing bacterium with possible involvement of the electron acceptor in substrate activation. *Environmental Microbiology Reports*, *3*(1), 125–135. https://doi.org/10.1111/j.1758-2229.2010.00198.x

Zenno, S., Koike, H., Kumar, A. N., Jayaraman, R., Tanokura, M., & Saigo, K. (1996). Biochemical characterization of NfsA, the Escherichia coli major nitroreductase exhibiting a high amino acid sequence homology to Frp, a Vibrio harveyi flavin oxidoreductase. *Journal of Bacteriology*, *178*(15), 4508–4514. https://doi.org/10.1128/jb.178.15.4508-4514.1996

Zhang, Y., Heym, B., Allen, B., Young, D., & Cole, S. (1992). The catalase - Peroxidase gene and isoniazid resistance of Mycobacterium tuberculosis. *Nature*, *358*(6387), 591–593. https://doi.org/10.1038/358591a0

Zhang, Y., Shi, W., Zhang, W., & Mitchison, D. (2015). Mechanisms of Pyrazinamide Action and Resistance. In *Molecular Genetics of Mycobacteria* (pp. 479–491). ASM Press. https://doi.org/10.1128/9781555818845.ch24

Zhang, Y., Wade, M. M., Scorpio, A., Zhang, H., & Sun, Z. (2003). Mode of action of pyrazinamide: Disruption of Mycobacterium tuberculosis membrane transport and energetics by pyrazinoic acid. *Journal of Antimicrobial Chemotherapy*, *52*(5), 790–795. https://doi.org/10.1093/jac/dkg446

Zhu, Y. I., & Stiller, M. J. (2001). Dapsone and sulfones in dermatology: Overview and update. *Journal of the American Academy of Dermatology*, *45*(3), 420–434. https://doi.org/10.1067/mjd.2001.114733

Zignol, M., Hosseini, M. S., Wright, A., Weezenbeek, C. L., Nunn, P., Watt, C. J., Williams, B. G., & Dye, C. (2006). Global Incidence of Multidrug-Resistant Tuberculosis. *The Journal of Infectious Diseases*, *194*(4), 479–485. https://doi.org/10.1086/505877

Zignol, M., Wright, A., Jaramillo, E., Nunn, P., & Raviglione, M. C. (2007). Patients with Previously Treated Tuberculosis No Longer Neglected. *Clinical Infectious Diseases*, *44*(1), 61–64. https://doi.org/10.1086/509328

Zink, A., Haas, C. J., Reischl, U., Szeimies, U., & Nerlich, A. G. (2001). Molecular analysis of skeletal tuberculosis in an ancient egyptian population. *Journal of Medical Microbiology*, *50*(4), 355–366. https://doi.org/10.1099/0022-1317-50-4-355

Zweijpfenning, S., Hoefsloot, W., & van Ingen, J. (2018). Nontuberculous mycobacteria. *ERS Monograph*, *2018*(9781849841009), 399–413. https://doi.org/10.1183/2312508X.10022717

Chapter 9:

Appendices

Chapter 9 Appendices

ASNP Code	Compound	ASNP Code	Compound
AS1	Ampicillin	AS43	Quinacrine
AS2	Amoxicillin	AS45	Sulfanilamide
AS4	Cetylpyridinium chloride	AS46	Salicin
AS11	Cloxacillin	AS47	Sulfamethoxazole
AS12	Cefazolin	AS48	Thiomersal
AS14	Cephaloridine	AS49	Tetrecycline
AS15	Cefotaxime	AS51	Trimethoprim
AS16	Carbenicillin	AS52	Potassium clavulanate
AS18	Colistin	NP1	Raspberry
AS19	Cetylpyridinium chloride [S]	NP2	Turmeric
AS20	Chloromercuribenzoic acid	NP3	Basil
AS21	Doxycycline	NP4	Parsley
AS25	Isonicatinic acid	NP5	Cumin
AS26	Formic Acid	NP6	Red Grape
AS27	Minocycline	NP7	Lemon
AS29	Novobiocin	NP8	Lime
AS30	Neomycin	NP9	Beetroot
AS32	Nisin	NP10	Cucumber
AS33	Nitrofurantoin	NP11	Coffee
AS34	Oxytetracycline	NP12	Tea
AS35	Oxolinic Acid	NP13	Almond
AS36	Oxacillin	NP14	Carrot
AS37	Phenylmercuric	NP15	Broccoli
AS38	Phenyl-mercury	NP16	Green Cabbage
AS39	Phosphomycin	NP17	Garam Massala
AS41	Piperacillin	NP18	Mint
AS42	Penicillin	NP19	Coriander

Appendix A

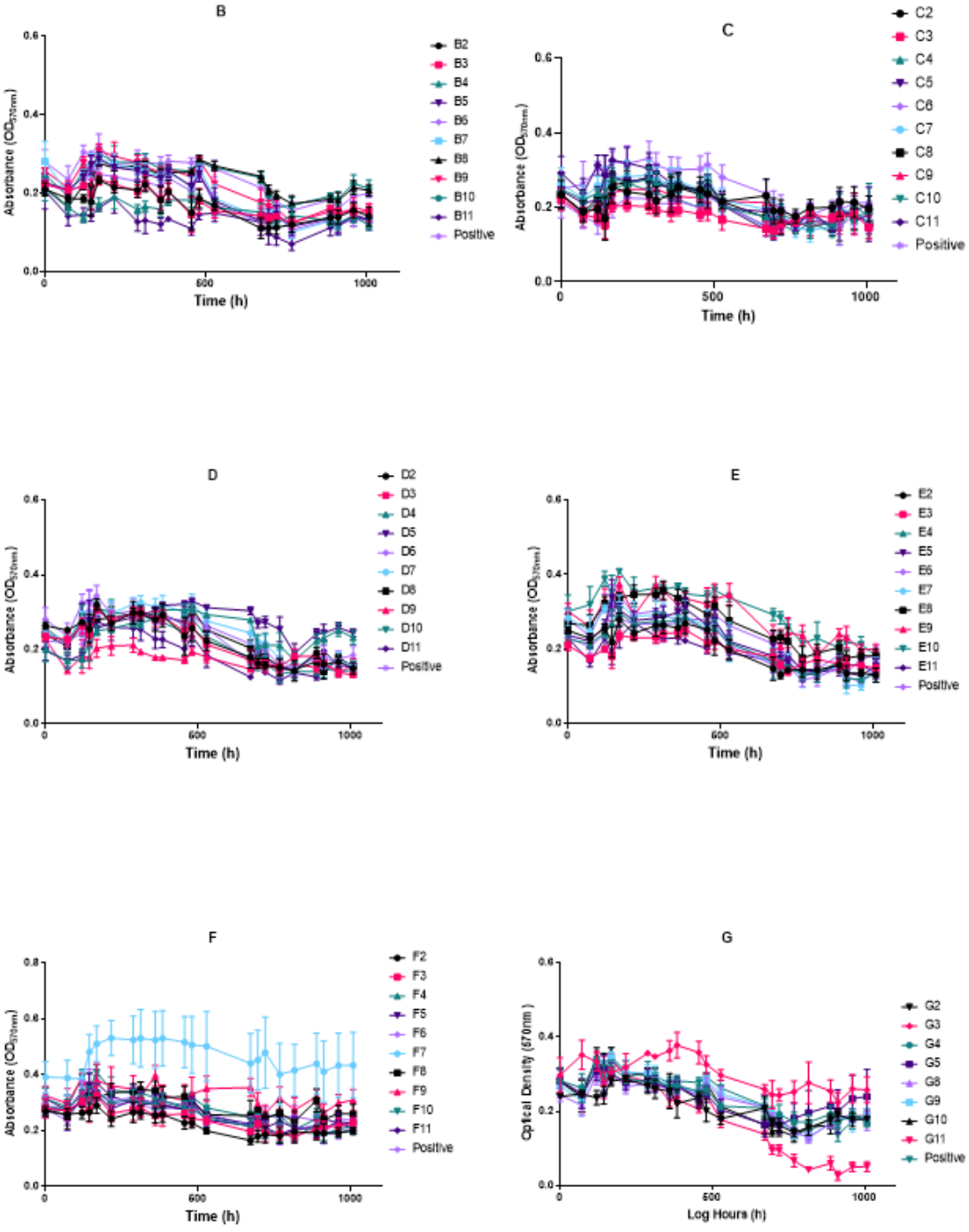
B
Absorbance (OD570nm)
Time (h)
B2
B3
B4
B5
B6
B7
B8
B9
B10
B11
Positive
C
C2
C3
C4
C5
C6
C7
C8
C9
C10
C11
Positive
D
D2
D3
D4
D5
D6
D7
D8
D9
D10
D11
Positive
E
E2
E3
E4
E5
E6
E7
E8
E9
E10
E11
Positive
F
F2
F3
F4
F5
F6
F7
F8
F9
F10
F11
Positive
G
Optical Density (670nm)
Log Hours (h)
G2
G3
G4
G5
G8
G9
G10
G11
Positive

Appendix B

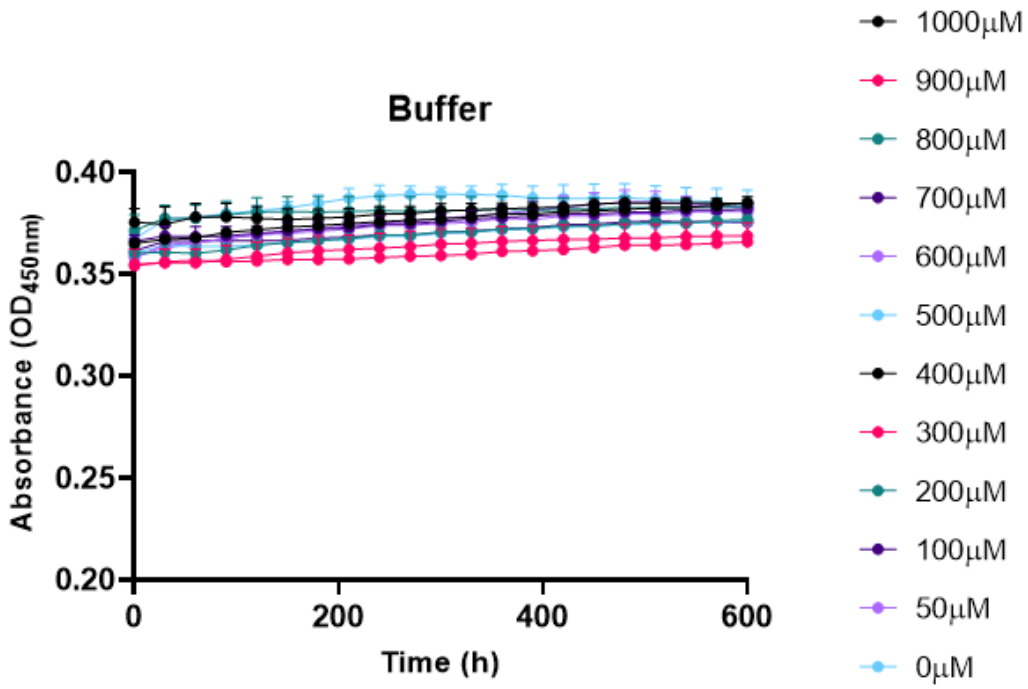
Buffer
Absorbance (OD450nm)
0.40
0.35
0.30
0.25
0.20
0
200
400
600
Time (h)
1000μM
900μM
800μM
700μM
600μM
500μM
400μM
300μM
200μM
100μM
50μM
0μM

Appendix C